CORE
Metadata, citation and similar papers at core.ac.uk
Provided by ScholarBank@NUS

HIGH CAPACITY HIGH SPECTRAL EFFICIENCY TRANSMISSION TECHNIQUES IN WIRELESS BROADBAND SYSTEMS

ZHOU KAINAN

NATIONAL UNIVERSITY OF SINGAPORE

2006

HIGH CAPACITY HIGH SPECTRAL EFFICIENCY TRANSMISSION TECHNIQUES IN WIRELESS BROADBAND SYSTEMS

ZHOU KAINAN

(*B. Eng., Beijing University of Posts and Telecommunications., P. R. China*)

A THESIS SUBMITTED

FOR THE DEGREE OF DOCTOR OF PHILOSOPHY

DEPARTMENT OF ELECTRICAL AND COMPUTER ENGINEERING

NATIONAL UNIVERSITY OF SINGAPORE

2006

Acknowledgements

Firstly, the author would like to express sincere thanks to her supervisor, Dr. Chew Yong Huat, for his excellent guidance and continuous support during her study and thesis making. He encouraged me when I was depressed; he enlightened me when I was confused; he shared his own study experiences with me when I lost motivation– He could always give good advices on courses, research as well as other aspects in university life. Moreover, his enthusiasm and preciseness in work have also influenced and benefited me.

Next, I would like to thank my former labmate, Long Hai, for his collaboration work in MC-DS-CDMA. Special thanks go to Dr. Li Yuan, for the discussions and cooperations on Turbo coded modulation. Thank Dr. Chai Chin Choy for the discussions about some common research topics.

My thanks also go to the Department of Electrical and Computer Engineering in National University of Singapore (NUS) and the Institute for Infocomm Research (I^2R) for giving me the opportunity to study here.

Sincerely, I want to thank my friends in NUS and (I^2R), who have given me much care and help in research as well as in life. Without them, my life in Singapore would not have been so colorful and memorable. Especially, Ronghong, Cao Wei,

Xiaoyu, Wang Jia and Jianxin helped me a lot to pull through the most difficult period in the Ph.D study. Moreover, it has been my luck to get to know Sebastian, Mahani, Vineet, and Lux, who have rendered great kindness and friendship to me.

Great encouragement also comes from my other friends around the world, Gao Xuan, Li Chuxiang, Wang Mingshu, Yue Lin and Liu Xinyu, who have inspired me to go further on the completion of thesis.

Last but not least, I am deeply indebted to my family for their continuous care and support. They have been standing by my side whatever difficulty I had during these years of study. With all the love and appreciation in my heart, I thank them for their understandings and devotions at every step of my way.

Contents

Summary

The objective of this thesis is to look into some potential techniques to achieve the high capacity high spectral efficiency transmission in the wireless broadband systems, as the next generation wireless communication (NextG) urges on high quality high data rate transmissions.

Some advanced techniques to improve the spectral utilization of the wireless communication systems is discussed, and a literature summary in these areas is provided. Some minor contributions on turbo coding and quantifying the achievable diversity gain in multiuser OFDM systems are given in Chapter 3.

More major contributions follow with two different methodologies: one is to improve the spectral efficiency with fixed spectrum, while the other one is dynamic spectrum assignment. Both, however, aim to improve spectral utilization.

We first propose a power control scheme for the transmit power of the mobile users on the uplink transmission in a slotted DS-CDMA system. Cross layer design methodology is used to obtain the optimal performance. Based on the proposed power control techniques, we derive the maximum number of users the system could support, subject to the delay and outage probability constraints imposed on the two service categories (voice and data). Both our simulation results and theoretical

derivations prove that the system capacity is enhanced with the proposed power control scheme.

In the next few chapters, we focus on the subcarrier-and-bit allocation problems for multicarrier systems. Multiclass multiuser OFDM system is firstly explored, where the *exact* optimal solution for the adaptive subcarrier-and-bit allocation is derived with the BER and data rate constraints met. Based on the benchmark provided by the optimal scheme, two suboptimal schemes are proposed to speed up the computation. The study is then extended to the three class system. When the best effort service is added to the system, the objective function is accordingly modified to the maximization of the system revenue. The optimal solution for this case is also obtained, with all the QoS constraints achieved.

When we consider the adaptive subcarrier allocations in MC-DS-CDMA system, the effect of multiple access interference (MAI) cannot be ignored. We design two suboptimal algorithms to adaptively assign the subcarriers so that the BER performance will be optimized with MAI considered. Some advanced optimization tools are used to find the optimum and great improvement is shown by the results, compared with the scheme in the literature without MAI consideration.

Finally we address another issue about dynamic spectrum assignment. We design a centralized system to perform the spectrum allocation among OFDM and CDMA users. Scenarios with and without primary users are investigated to obtain the optimal solution to maximize the system utility. We also propose a suboptimal algorithm to reduce the computation complexity when the number of users and subcarriers increases. This simple treatment models the spectrum allocations in

multiple radio systems.

Abbreviations

2D FFT:	Two Dimensional Fast Fourier Transform
AWGN:	Additive White Gaussian Noise
BER:	Bit Error Rate
BS:	Base Station
CDD:	Cyclic Delay Diversity
CDMA:	Code Division Multiple Access
CIR:	Channel Impulse Response
CNR:	Carrier-to-Noise Ratio
CP:	Cyclic Prefix
CSI:	Channel State Information
DFT:	Discrete Fourier Transform
DSSS:	Direct Sequence Spread Spectrum
DS-CDMA:	Direct Sequence Code Division Multiple Access
FFT:	Fast Fourier Transform
FDMA:	Frequency Division Multiple Access
GSM:	Global System for Mobile communication
ICI:	Interchannel Interference
IDFT:	Inverse Discrete Fourier Transform
IF:	Intermediate Frequency
IP:	Integer Programming
IFFT:	Inverse Fast Fourier Transform
ISI:	Intersymbol Interference
LMS:	Least Mean Square
LOS:	Line Of Sight
LP:	Linear Programming

MAC:	Medium Access Control
MAI:	Multiple Access Interference
MINLP:	Mixed Integer Nonlinear Programming
MLSE:	Maximum Likelihood Sequence Estimation
MMSE:	Minimum Mean Square Error
MS:	Mobile Station
NextG:	Next Generation Wireless Communication
NLP:	Nonlinear Programming
OFDM:	Orthogonal Frequency Division Multiplexing
PAR:	Peak-to-Average Ratio
PDF:	Probability Density Function
PG:	Processing Gain
QAM:	Quadrature Amplitude Modulation
QP:	Quadratic Programming
RF:	Radio Frequency
RX:	Receiver
SBA:	Subcarrier-and-Bit Allocation
SC:	Single Carrier
SDR:	Software-Defined Radio
SFM:	Spectral Flatness Measurement
SNR:	Signal to Noise Ratio
SIR:	Signal to Interference Ratio
SQP:	Sequential Quadratic Programming
STBC:	Space-Time Block-Coding / Space-Time Block-Coded
SU-RLS:	Subsampled-Updating RLS
TCM:	Trellis-Coded Modulation
TDMA:	Time Division Multiple Access
TX:	Transmitter

List of Figures

List of Tables

Notations

Scalar variables in this thesis are expressed as plain lower-case letters, vectors as bold face low-case letters and matrices as bold-face upper-case letters. Other notations used in the thesis are listed below with spacings between different chapters (Chapter 2∼7):

$D_\tau^{(1)}$: Channel average delay
$D_\tau^{(2)}$: Channel delay spread
$p(\tau)$: Power delay profile
f_d : Doppler Spread
N_0 : Power spectral density (PSD) of the white Gaussian noise
E_b/N_0 : Signal-to-noise ratio (SNR)
R : Data rate
P_e : Bit error probability
J : Number of path
$\mathrm{E}\{\cdot\}$: Statistical expectation
$\{\cdot\}^*$: Conjugate
J_0 : Bessel function of the first kind
δ_r : Unit impulse function at r
T_s : Sample duration

M : The size of signal set

ω_c : Code rate

N : Number of subcarriers in OFDM system

c : Constellation size

$Q(x)$: Error function

$H_{k,n}$: Channel frequency response on the nth subcarrier for the kth user

$s_{k,n}$: Binary subcarrier allocation indicator for the nth subcarrier of the kth user

$c_{k,n}$: Number of bits assigned on the nth subcarrier of the kth user

P : Transmit power

χ : Subcarrier correlation coefficent

P_0 : Power floor

P_a : Average transmit power

S_P : Constant receive power with perfect power control

β : Pass loss exponent

$Q_v\,(Q_d)$: Processing gain of voice (data) users

$n_v\,(n_d)$: Number of voice (data) users

N_u : Total number of users within a cell

$\alpha_v\,(\alpha_d)$: Voice (data) activity factor

L_d : Data packet length

λ_d : Average arrival rate of new data packets

p_{r_d} : Retransmission probability of data users

R_c : Chip Rate in CDMA systems

$\Psi_v\,(\Psi_d)$: SIR threshold for voice (data) users

$p_{f_v}\,(p_{f_d})$: Probability of packet failure for voice (data) users

P_{out_v} : Outage probability

D : Average delay for the data service

D_{th} : Delay threshold

C : User capacity

U : Throughput (Chapter 4 & 5)

$\lfloor x \rfloor$: The nearest integer less than or equal to x

r : Distance from mobile to base station

F_m : Interference Correction Factor

R_{eq} : Equivalent circular radius of a cell

I_{oc} : Interference from outer cell

I_h : Interference from home cell

η : Density of mobile users

δ : Power control profile index

m_v (σ_v^2) : Logarithmic mean (variance) of the received power from a single voice user

m_d (σ_d^2) : Logarithmic mean (variance) of the received power from a single data user without power constraint

μ_d (D_d^2) : Arithmetic mean (variance) of the received power from a single data user without power constraint

$\bar{\mu}_d$ $\left(\bar{D}_d^2\right)$: Arithmetic mean (variance) of the average received power from a single data user with power constraint

$(\cdot)_{vt}$: Mean or variance of the total interference from voice users

$(\cdot)_{dt}$ $((\cdot)'_{dt})$: Mean or variance of the total interference from data users without (with) power constraint

$(\cdot)_I$: Mean or variance of the total interference from both services without power constraint

$(\cdot)'_I$: Mean or variance of the total interference from both services with power constraint

$K_1\,(K_2, K_3)$: Number of Class 1 (2,3) users

$R_1\,(R_2)$: Data rate requirement of Class 1 (2) users

Δ : System revenue

π_1, π_2, π_3 : Scaling constants for the revenue function

b_k : Data stream of the kth user

a_k : kth user's signature sequence

E_{c_k} : Received energy per chip for the kth MS

μ_0 : Additional energy gain allocated to pilot signal

a_0 : Spreading code for the pilot signal

$C_{k,j}$: Cross correlation between CDMA users k and j

$T\,(T_c)$: Symbol (chip) period in CDMA system

$\alpha_{k,n}$: Amplitude of channel gain on the nth subcarrier seen by the kth MS

ω : Carrier angular frequency

$\phi_{k,n}$: Phase shift on the nth subcarrier for the kth MS

L_c : Number of subcarriers assigned to each CDMA user

$\{\cdot\}^T$: Transpose of a matrix or a vector

$\mathbf{v}$: Frequency bin allocation vector for primary users

N_T : Total number of frequency bins

L : Number of frequency bins allocated to OFDM user in cognitive radio

K : Number of CDMA users in cognitive radio

Chapter 1

Introduction

The next generation wireless communication (NextG) systems are making a major move towards supporting high-quality wireless multimedia services for users of different mobility.

1.1 Technology Evolution of Telecommunication Networks

The first-generation wireless mobile telecommunication services date back to more than 20 years ago, when analog frequency modulation (FDM)/frequency division multiple access (FDMA) was used as the key technology. Today, the mobile communication systems are mostly based on global system for mobile communications (GSM), IS-95 or personal digital cellular (PDC), which are known as the second generation wireless mobile communication systems. The third generation (3G) wireless mobile systems aim at providing high quality service simultaneously for

voice, data and multimedia traffics. Although the services have just begun to take off, wireless telecommunication researchers and engineers have already started groping for the new technologies suitable for the next generation wireless communication systems (NextG).

In the first and second generation wireless mobile systems, technical interests were mainly focused on increasing system capacity for voice services. However, there are increasing demands recently for multimedia services including voice, data, image and video, thus, more and more attention has been paid to develop high-speed reliable wireless multimedia systems rather than merely voice systems. 3G systems are able to support multiclass services but the guarantee for service QoS remains to be a challenging problem. CDMA is used as the multiple access technique in current 3G system due to its flexibility in producing scalable transmission rate, and other distinct features such as soft capacity and soft handover. The future mobile wireless systems are expected to have higher and more intelligent channel adaptability to provide high-speed multimedia services with the quality-of-service (QoS) requirements for every service category fulfilled.

Although 3G is still waiting to take off, design for next generation of high speed network is in the pipeline. The main focus is to research and develop advanced high-speed spectrally efficient wireless technologies for next generation cellular systems, wireless broadband networks and mobile devices. For the cellular mobile systems, there have been global interests in NextG with target transmission rate ranging from 20Mbps to 100Mbps and to support users of different mobility. However, the technology that NextG will adopt remains an open question. CDMA remains to

be one of the potential candidates for the air interface because it has been widely adopted and technically it is more mature. However, the success of using multicarrier technology in telephone network and wireless local area network has made orthogonal frequency division multiplexing (OFDM) attracting more attentions by the research committee. The merging of multicarrier and CDMA technologies into multicarrier CDMA offers another potential candidate, whose main attractions are the high spectral efficiency and the ease to operate in multiuser environment.

1.2 Spectral Efficiency and Dynamic Spectrum Allocation

With the transmission going wideband, the received signal suffers greatly from the multipath dispersions, as will be described in the next chapter. In turn, the transmission link becomes hostile and the quality degradation becomes intolerable. Thus, effective anti-multipath measures shall be taken to mitigate the fading effect in order to improve the system performance. One possible way is to perform equalization. However, when the system bandwidth increases and so does the effect of intersymbol interference (ISI), equalizers would need more and more delay taps, which will inevitably result in higher complexity and longer processing delay. Another option is to use multicarrier modulations. Among these, OFDM is an attractive countermeasure to combat multipath fading as it can transmit the data stream in multiple parallel channels of narrower bandwidth so that each parallel channel only undergos flat fading. By using OFDM, the effect of ISI can be

easily compensated through frequency domain equalization. Multicarrier CDMA, the merging of multicarrier techniques and CDMA, is, in principle, still another multicarrier transmission scheme from the implementation point of view.

The high-rate data transmission in NextG requires more and more spectrum which is limited and already scarce with the current situations depicted by ITU. Therefore, researchers have been motivated to find ways to optimize the spectrum usage. Firstly, some of the design issues are common for all the multiple access schemes, e.g., in general, spectral efficiency can be enhanced by the techniques such as coded modulations, multiple-input-multiple-output (MIMO) antennas, joint detections, etc. Secondly, more specific approaches can be applied to respective multiple access schemes. For example, in CDMA networks, spectral efficiency can be improved by proper power control and management to minimize the amount of interference imposed on other users. For multicarrier networks, adaptive subcarrier-and-bit allocations can be exploited to enhance the spectral efficiency.

As the technologies progress and the development for reconfigurable devices become feasible, future communications devices will be able to detect their favorable spectrums, and to find the best transmission schemes according to the service standard while preventing additional interference to other users. One possible way to achieve this flexibility and adaptability is cognitive radio which could be integrated as an important feature in NextG communication devices. The motivation of such development is that normally not all the spectrum bands allocated to the service providers are fully utilized. This development, distinct from the approaches discussed above, provides a second method to improve the spectrum utilization

through dynamically assigning spectrum bands to secondary radio systems which demand for bandwidth.

In this thesis, it is not our intention to give any recommendation on which of the wireless transmission techniques will be the best for the NextG communications, since it is expected that in the future, various radio systems adopting different technologies are going to coexist together. Rather, our main focus is to look into techniques to improve spectral efficiency of CDMA systems through power control and multicarrier systems through adaptive subcarrier-and-bit allocation. Simple treatment on dynamic spectrum allocation for multi-radio systems to improve spectrum utilization is also given.

1.3 Thesis Outline

This thesis gives extensive study on the high capacity high spectral efficiency transmission techniques in wireless broadband systems supporting multiclass services.

In Chapter 2, we begin with the introduction of mobile channel characteristics, and then we review the three popular multiple access techniques to improve the spectral efficiency and enhance the system capacity, i.e. OFDMA, CDMA, MC-CDMA. They are attractive techniques for the next generation wireless wideband transmission, and in each of those systems, there are still some open issues which need further exploration to reveal more potentials or to facilitate implementations.

Next, some advanced techniques to improve the spectral efficiency in the systems discussed in Chapter 2 are reviewed, such as Turbo coded modulation, power

control and subcarrier-and-bit allocation. Also, the achievable performance gain in multiuser OFDM systems by the optimal subcarrier-and-bit allocation is investigated in Chapter 3. Besides, general overviews on cross layer design and cognitive radio are presented.

In Chapter 4, we zoom into the power control issues in DS-CDMA system and present our research on the constrained power control profile. An uplink slotted DS-CDMA system is considered and the capacity of the proposed power control scheme is compared with the conventional power control.

We carry on with our study in multiuser OFDM systems supporting multiple service classes. The adaptive subcarrier and bit allocation schemes are discussed and the optimal solution to minimize the transmit power is derived. Furthermore, two heuristic algorithms are proposed based on the optimal scheme, to reduce the computation complexity but maintain certain accuracy. Their performance is presented and compared with the optimal results. The three class case is also studied, with the system revenue maximized.

Extending our research to another system, multicarrier DS-CDMA (MC-DS-CDMA), the next chapter, i.e., Chapter 6, focuses on the the subcarrier allocations in MC-DS-CDMA system where multiple access interference (MAI) limits the system performance and thus has to be taken into account in the subcarrier assignments. Two suboptimal schemes are proposed by which the overall BER performance of the system is greatly improved, compared to that of the other subcarrier allocation schemes.

With the results and revelations from the previous work in this thesis, we

develop a model for the cognitive radio where adaptive spectrum allocation across multiple radio systems is employed. Both OFDM and CDMA systems are included and the spectrum allocation is optimized to achieve the best spectrum utilization.

Finally, conclusions are drawn in Chapter 8 to summarize the thesis.

1.4 Contributions

In Chapter 2, the theoretical treatment for the interchannel interference (ICI) in OFDM system is presented. It is shown that the ICI in OFDM system remains unchanged if the total bandwidth increases with constant subcarrier bandwidth. Also in this system setting, our simulation results show that there exists a maximum usable bandwidth for the OFDM system if a given BER requirement is to be guaranteed. This maximum bandwidth is a function of the channel parameters such as Doppler spread or power delay profile. These results show that there could be a limit in OFDM system bandwidth which would be a barrier to achieve high transmission rate while trying to support a given mobility group.

In Chapter 3, the amount of tolerable SNR mismatch is investigated in a turbo decoder using higher order constellations. Past research only presented the SNR sensitivity for the turbo codes with BSPK. However, in our work, the turbo coded system with 16-QAM is simulated and the result shows that the denser constellation causes a narrower tolerance range for the SNR mismatch. It suggests the need for more accurate SNR estimation for the turbo decoder combined with higher order constellations.

Although adaptive subcarrier-and-bit allocation is not new in the literature, past work was dealing with instantaneous channel conditions and there is a lack of knowledge on the average performance gain that is attainable. In our work, the diversity gain in a multiuser OFDM system is quantified using spectral flatness measurements (SFM), subcarrier correlation coefficients χ and RMS delay spread $D_{\tau}^{(2)}$. Firstly, the probability density function (PDF) of the SFM is presented. Next, the optimal solution for the adaptive subcarrier-and-bit allocation in a multiuser OFDM system is obtained, and the results are used to obtain the relationship between the transmit power and SFM, χ and $D_{\tau}^{(2)}$, for a given number of users and subcarriers. From these relationships, we see that the average transmit power P_a can be minimized at an optimum delay spread for a certain number of subcarriers. This developed approach could be also useful for the designers to fully exploit the channel diversity gain.

In Chapter 4, a constrained power control scheme is proposed, where the voice users adopt perfect power control, while the transmit power of the data users is imposed by some constraints governed by the profile index. Several power control profiles for data users are suggested to reduce interference imposed on both its own and neighboring cells. It has been recognized that the total received power from voice and data users by the conventional scheme follows a log-normal distribution, and with our proposed scheme, the simulation results also show that the sum of the received power at the base station can still be approximated by a log-normal distribution, whose mean and variance can be evaluated analytically. In the sequel, the interference correction factor is derived as a closed form function of the path

loss exponent as well as the profile index of the proposed scheme, as the widely used value $F_m = 0.326$ (for path loss exponent $\beta = 4$) is not valid anymore in the new power scheme. The value of the interference correction factor is then used to obtain the PDF of the signal-to-noise ratio (SIR) for the voice and data users, which can be further used to derive the capacity subject to certain delay and outage constrains. Notably in our approach, the retransmission rate is successfully introduced to the evaluation of outage probability and thus enables the evaluation of theoretical capacity. Our results show that the constrained power control scheme can enhance the capacity, compared to the conventional scheme, if proper profile index is chosen for the transmit power of the data users. Moreover, the effects of the data activity factor and the data packets arrival rate on the system performance are also discussed.

The subcarrier-and-bit allocation problems are extensively investigated in Chapter 5 for multiclass multiuser OFDM systems. The constrained power optimization problem for the uplink OFDM transmission supporting 2 service classes is formulated and the optimal solution to minimize the transmit power is obtained with all the service QoS constraints satisfied. It is noteworthy that our solution is the *exact* optimal solution without any assumption or relaxation, which is novel in the literature. Thus, the theoretical framework and the optimal solution provided in this chapter can be used as a benchmark for other suboptimal solutions. Two heuristic algorithms are proposed to speed up the computation without significant performance penalty. The quadratic fitting scheme can give a good approximation to the optimal scheme, as shown in the simulation results; and the two-step ap-

proach contributes for the lower bound of the minimum transmit power. Further, the problem is extended into a three class multiuser system with presence of best effort service. The objective function is revised to maximize the overall revenue. The optimal solution is obtained and the revenue, throughput and the transmit power are presented over changing channel conditions.

Two suboptimal subcarrier allocation schemes are proposed in Chapter 6 to improve the spectral efficiency of a MC-DS-CDMA system in the presence of multiple access interference (MAI). An iterative algorithm is developed in the first scheme to search for the optimal subcarrier allocations to simultaneously minimize the average BER over each subcarrier. Our second approach aims to assign each user with the subcarrier on which the fading gain for this user is maximized after excluding the interference to other users. The performance of these two schemes is presented and compared with Kim's method [2], i.e., the subcarrier allocation algorithm without MAI considerations. And it is shown that with MAI taken account of, our second approach gives general BER improvement over the other two schemes, while the first approach also performs well above the Kim's method except when the subcarrier sharing rate is low.

Finally, a simple treatment of cognitive radio is discussed in Chapter 7. The spectrum allocation to the cognitive radios is performed in the proposed centralized model. There are two categories of users, using either OFDM or CDMA radios, each of which has its respective spectrum requirement. The optimal solution for the adaptive allocation of the frequency bins is then derived with the system utility maximized, with or without the presence of primary users. Moreover, a suboptimal

approach is proposed to reduce the computation time when the number of users or the frequency bins increases. The OFDM spectrum is firstly assigned and then the CDMA users are attended. The simulation results are presented and compared with the optimal solution. It can be observed that the heuristic algorithm only gives minimal penalty from the optimal scheme, if it does not provide the optimum.

Chapter 2

Mobile Radio Channels and High Rate Data Transmissions

One major challenge which the NextG high data rate system designers have to handle is the hostile channel conditions resulted from the fading effects of mobile radio channels. In this chapter, we address the basics of the fading characteristics in the wireless link, and then proceed to introduce the techniques used in the mobile receiver which deal with the fading impairments to recover the transmit information from the received signal. On the other hand, how to provide service to more users at their required transmission quality is also a problem the system designers try to solve, because more efficient use of spectrum resources will convert into higher revenues. Therefore, the countermeasures to meet these challenges in the wideband wireless transmissions attract a lot of interests. In this chapter, three multiple access techniques for the high data rate transmissions are introduced, namely, orthogonal frequency division multiple access (OFDMA), code division multiple

access (CDMA) and multicarrier code division multiple access (MC-CDMA). Literature survey is conducted and their major technical considerations are addressed.

2.1 Mobile Radio Channels

In wireless communications, the signal transmissions are not only affected by a constant attenuation and a constant delay like in AWGN channel, however, the performance will also be constrained by fading effects. *Fading*, in a general sense, is caused by the propagation environment referred to as *multipath* and the relative movement of transmitter and receiver leading to time variations of the channel.

2.1.1 Large-Scale Fading and Small-Scale Fading

There are two types of fading effects that characterize mobile communications: large-scale and small-scale fading. Large-scale fading represents the average signal power attenuation or path loss due to motion over large areas. Small-scale fading includes Rayleigh fading and Rician fading. If the multiple reflective paths are large in number and there is no line-of-sight signal component, the envelope of the received signal is statistically described by a Rayleigh probability density function (PDF). When there is a dominant non-fading signal component present, such as a line-of sight propagation path, the small-scale fading envelope is described by a Rician PDF. A mobile radio roaming over a large area must process signals that experience both types of fading: small-scale fading superimposed on large-scale fading.

The small-scale fading has two manifestations: signal time-delay spread and the Doppler-frequency spread.

2.1.2 Time Delay Spreading

The signal components arriving from the various paths (direct and indirect) with different delays combine to produce a distorted version of the transmitted signal (Figure 2.1). This effect is known as multipath propagation. Due to the multipath propagation, the received signal consists of an infinite sum of attenuated, delayed, and phase-shifted replicas of the transmitted signal, each influencing each other.

$$r(t) = \sum_{k=0}^{M-1} h_k(t)s(t - \tau_k(t))e^{j\theta_k(t)}, \tag{2.1}$$

where $h_k(t)$, $\tau_k(t)$ and $\theta_k(t)$ are the kth path amplitudes, delays, and phases, respectively. $s(t)$ is the input signal, $r(t)$ is the output signal deteriorated by the multipath fading. Depending on the phase of the signal on each path, the superposition can be constructive or destructive. This delay spreading results in intersymbol interference (ISI) which causes time dispersion and frequency-selective fading, i.e., different frequency components of the signal endure different distortions.

The multipath fading channel is usually characterized by *delay power profile*, which shows the power distribution of different path delays. There are two important quantities describing the characteristics of multipath power delay profiles. One is the average delay $D_\tau^{(1)}$, and the other is the delay spread $D_\tau^{(2)}$. If we denote the power delay profile as $p(\tau)$, these two quantities could be obtained as:

$$D_\tau^{(1)} = \int_0^\infty \tau p(\tau) \mathrm{d}\tau \tag{2.2}$$

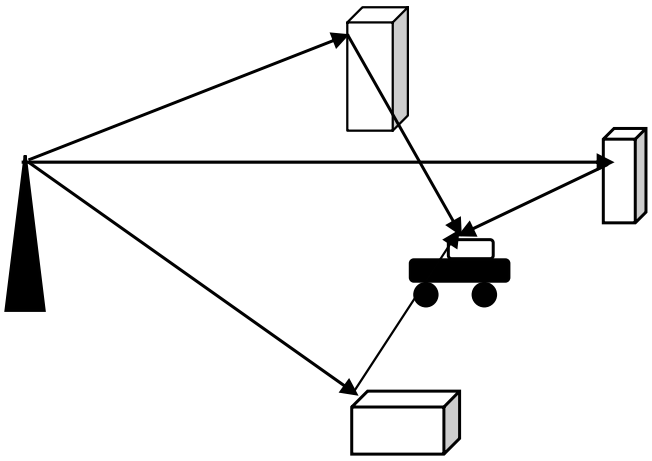

Figure 2.1: Illustration of the multipath physical environment.

$$D_{\tau}^{(2)} = \sqrt{\int_0^{\infty} \left(\tau - D_{\tau}^{(1)}\right)^2 p(\tau)\mathrm{d}\tau} \tag{2.3}$$

The distortions caused by multipath propagation are linear and have to be compensated for at the receiver side, for example, by a time domain or frequency domain equalizer, Rake receiver, etc.

2.1.3 Doppler-Frequency Spread

Besides the multipath propagation, the *Doppler effect* also has an impact on the transmission characteristics of the mobile radio channels. Due to the movement of the mobile unit, the Doppler effect causes a frequency shift on the signal from each of the incoming paths. The power spectrum of the received signal is the sum of these paths. The *angle of arrival* α_n, which is defined by the direction of arrival of the nth path and the direction of motion of the mobile unit as shown in Figure 2.2, determines the *Doppler frequency (frequency shift)* of the nth path according

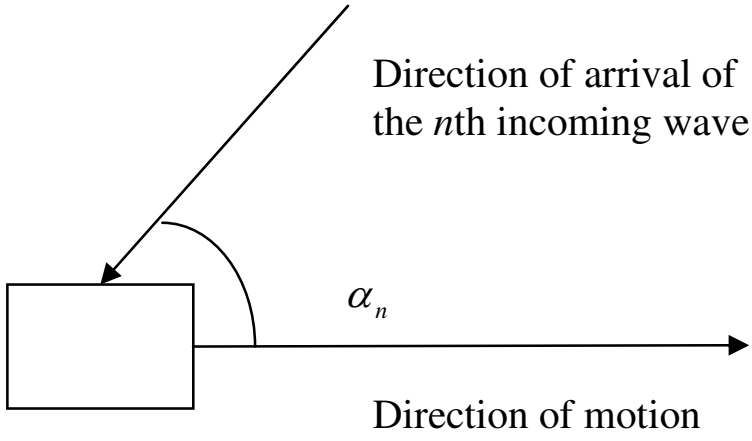

Figure 2.2: Doppler frequency effect.

to the relation

$$f_n = f_d \cos \alpha_n. \tag{2.4}$$

In this case, f_d is the *Doppler Spread* related to the speed of the mobile unit v, the speed of light c_0, and the carrier frequency f_0 by the equation

$$f_d = \frac{v}{c_0} f_0 = \frac{v}{\lambda}, \tag{2.5}$$

where λ is the wavelength.

This Doppler effect causes frequency dispersion and time-selective fading, which means the channel characteristics are time-variant and different time components of the signal endures different attenuations. When the channel changes its characteristics during signal propagation, frequency dispersion occurs, in the form of an increase of the bandwidth occupancy of a signal. To quantify this dispersion, the *Doppler spread* is defined as the difference between the largest and the smallest among the frequency shifts of the various paths.

2.1.4 Degradation Categories

Let B_x, B_c, T_x, T_c, f_d denote the bandwidth of the transmitted signal, the coherence bandwidth of the channel, the duration of a transmitted pulse, the coherence time, and the Doppler spread of the channel, respectively, where $T_c = 1/f_d$.

- If $B_x \ll B_c$, there is no frequency-selective fading, and hence no time dispersion. The channel transfer function looks constant, and the channel is called flat (or non-selective) in frequency.
- If $T_x \ll T_c$, there is no time-selective fading, and the channel is called flat (or non-selective) in time, or we can call it slow fading.
- If $B_x > B_c$, the channel is called frequency-selective fading.
- If $T_x > T_c$, or $B_x < f_d$, the channel is called fast fading.

It was shown that due to signal dispersion, the coherence bandwidth, B_c, sets an upper limit on the signaling rate which can be used without suffering frequency-selective distortion. Similarly, the channel fading rate f_d sets a lower limit on the signaling rate that can be used without suffering fast fading distortion. In this thesis, unless otherwise stated, we are dealing with slow frequency-selective fading channel.

2.2 Wireless Communication Systems

In the more advanced system, there has been an increasing demand for efficient and reliable wireless communication systems. The major concern of system designers

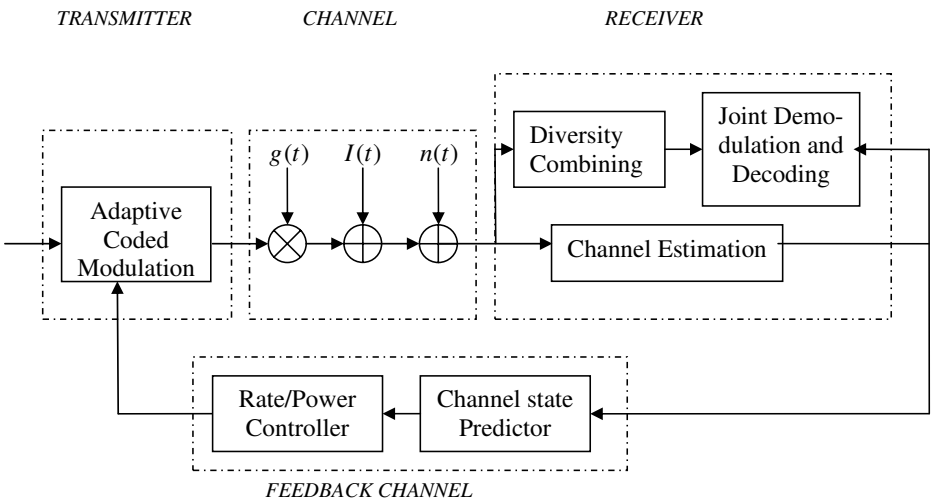

Figure 2.3: Block diagram of an advanced mobile communication system.

is to minimize the error probability at the receiver end by making wise use of the power and bandwidth resources, while keeping the system complexity reasonable to reduce cost.

2.2.1 Composition of a Mobile Receiver

A block diagram of a typical receiver structure in a mobile communication system is shown in Figure 2.3.

Channel coding with interleaving is a good way of achieving the necessary transmission fidelity with the available transmitter and receiver resources, such as power, bandwidth, and modulation techniques. And the digital modulator is used to transform the binary data into a continuous-time waveform suitable for transmission. Yet the advanced mobile communication systems take the privilege of the combination of the two techniques, namely, coded-modulation, which we will

discuss in detail in the next chapter.

The waveform resulted in the coded modulation is sent over the physical channel. The transmitted signal will be contaminated in a random manner by, e.g., the additive thermal noise $n(t)$ generated by the electronic devices or the multiplicative noise $g(t)$ caused by the fading effects of the mobile radio channels. Also, multiple access interference (MAI) $I(t)$ caused by other users in a multiuser environment is another major impairment of the transmitted signal. More about the fading and interference and their countermeasures will be discussed in the following chapters.

Adaptive algorithms will be used to adapt the transceiver to the changes of the channel conditions to provide the required QoS. Channel state information is obtained through employing channel estimation techniques, and is deployed to facilitate the adaptive control of the code rate of the encoder or constellation size of the modulator.

On the other hand, the estimated channel gain is also input into the demodulator and decoder to compensate the deterioration of the physical channel. With this, the demodulator and decoder process the corrupted waveform and produce the estimation of the transmitted signal. Moreover, joint detection might be required to enhance the overall system performance in presence of multiple users and the resulted MAI. With the added block of subcarrier-and-bit allocation, the receiver structure is also suitable for multicarrier modulation systems.

2.2.2 Spectral and Energy Efficiency

The rapid development of wireless communications results in the increasing demands for total transmission bandwidth and efficient digital communication systems. In this section, we introduce the two essential criterions for efficient communication systems, namely, spectral efficiency and energy efficiency.

With the increasing bandwidth, the symbol duration of the system becomes smaller, which, in turn, will lead to increasing ISI due to the channel distortions and increasing difficulties in performing signal recovery and symbol synchronization. So it is critical for us to come up with the wise schemes so that the system could retain good performance while increasing bandwidth is used.

When it comes to fixed transmission bandwidth, our concern is to achieve high spectral efficiency and high energy efficiency. Spectral efficiency of a transmission system is defined as the ratio of data rate R to bandwidth W

$$\eta_B = R/W. \tag{2.6}$$

This means the data rate transmitted on a unit bandwidth. The unit for η_B is bits/s/Hz. And those systems with higher η_B use bandwidth more efficiently than others.

Energy efficiency, however, is defined as

$$\eta_E = E_b/N_0|_{P_e=10^{-5}}, \tag{2.7}$$

where E_b is the bit energy, and N_0 is the noise power spectral density. P_e denotes the bit error probability. If some type of modulation achieves the same P_e at *lower*

power than others, we say this modulation is more energy efficient. Thus, small η_E suggests high energy efficiency.

Most of the times, we have to trade between the spectral efficiency and energy efficiency. For example, M-ary modulation can send multiple bits per symbol, which means it has higher spectral efficiency compared with binary modulation, but it is more vulnerable to errors as well and hence much larger transmit energy is required to maintain the bit error rate. In case of error correction coding, the inserted redundant bits improve bit error rate, but at the same time increase bandwidth. This problem could be solved by suitably combining error control coding and modulation to achieve high spectral efficiency as well as high energy efficiency. Another example can be taken for the CDMA systems. As more and more users share the same spectrum, the spectral efficiency is improved, in the sense that the system accommodates more users; yet on the other hand, the interference between the users also mounts up. To a certain extent, the detector may not be able to recover the desired user signal from interference any more if the transmit power is not accordingly increased. This means the energy efficiency is reduced if no other measures are taken. However, the transmit power is usually restricted, which makes the power control schemes and joint detection become necessary in CDMA systems to minimize the inter-user interference in order to obtain the best tradeoff between energy and spectral efficiency. Unfortunately, in some scenarios, when the performance exhibits error floor such as due to the presence of phase error, an increase in energy may not even bring any improvement on the system throughput.

2.3 Technical Challenges and our Resorts

In the NextG systems, as we go to the higher data rates, the channels become truly broadband where multipath fading is a major limitation for performance of the wireless transmission if it is not managed properly for diversity gain. Therefore, some advanced processing has to be considered in the design of NextG communication systems to mitigate the fading effect and at the same time utilize the diversity effect from the resolvable paths. CDMA gives us the possible solution to nicely enhance the system capacity while exploiting the multipath diversity, by the use of orthogonal spreading codes and Rake receivers. Besides, multicarrier transmission techniques become more and more attractive as bandwidth and data rates grow, since it can better handle larger numbers of resolvable paths by transmitting many narrow band signals in parallel at orthogonal subcarrier frequencies, and hence allow for adaptive access of the subcarriers. In the next section of this chapter, we will give brief overview of CDMA, OFDMA as well as MC-CDMA to introduce the three systems used in this thesis.

2.4 A General Review of Code Division Multiple Access (CDMA)

2.4.1 Multiple Access Schemes

There are several schemes to accommodate multiple users in a wireless communications system. The users can transmit at different time slots, which is called

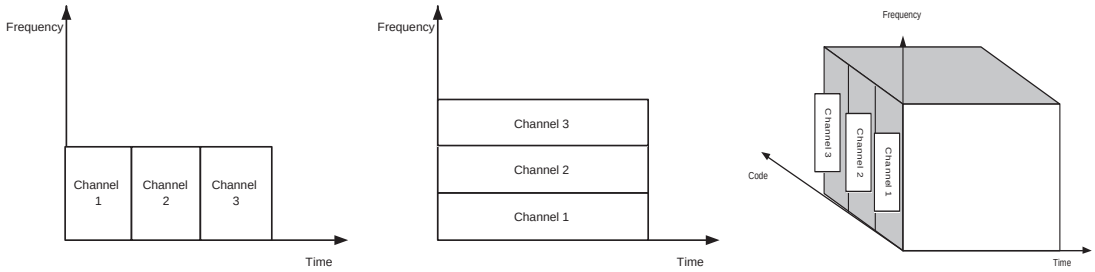

(a) TDMA (b) FDMA (c) CDMA

Figure 2.4: Multiple access schemes.

time division multiple access (TDMA)(Figure. 2.4 (a)). Alternatively, the spectrum is divided into frequency channels which are distributed among the system users, and this is called frequency division multiple access (FDMA)(Figure 2.4 (b)). Otherwise, different users can transmit signals on the same frequency bands but distinguish themselves using some signature codes. Thus, it is called CDMA(Figure 2.4 (c)). Recently, there also evolves another multiple access scheme, space division multiple access (SDMA), which differentiates each user by its location or signal direction.

FDMA scheme was used in the first generation mobile communications, where the whole spectrum was divided into several frequency channels and each channel could only be assigned to one user. Because the bandwidth is fixed, it has less flexibility to provide scalable data rate services. TDMA is employed in the GSM system, namely, the second generation mobile communications (2G). However, the high data rate resulted from the time slotted signals leads to the severe ISI, which brings the poor BER performance in a multipath environment. CDMA allows different users to share the spectrum simultaneously with orthogonal access codes,

which renders its scalability to support services of different data rates, through changing the processing gain. Furthermore, with Rake receiver, the received signals from different paths can be combined, and thus the multipath diversity is exploited. Besides, CDMA also has other attractive features such as soft-handover, narrow band interference elimination, which have made it the major technique in 3G systems.

Research and innovations are still ongoing to search for the best combination of multiple access scheme, modulation, and coding. NextG adaptability would involve optimizing the selected hybrid scheme dynamically based on its system performance metrics such as BER. In all cases, fast adaptation to the channel and traffic conditions is the key to provide the needed QoS.

There are three possible ways to realize the CDMA principle. Firstly, we can multiply the original signal with the spreading code sequence whose symbol duration is much shorter. Each user is assigned one unique code which is used to distinguish one user from another. At the receiver, the same code is used to detect the original information from the intended transmitter. The spreading codes used in the CDMA systems have to possess good orthogonality between each other in order to minimize the amount of MAI. This scheme is called direct sequence CDMA (DS-CDMA). In frequency hopping (FH) CDMA, the instantaneous transmission frequency is defined by a pseudo-noise sequence. The bandwidth at a certain moment is small, but the whole bandwidth over a symbol period is large. Also, the transmission moment can also defined by the time hopping sequences, and the resulted spread spectrum signal can be classified as time-hopping CDMA (TH-

CDMA).

2.4.2 Key Technical Considerations of CDMA systems

Code Selection

The chip rate of the spreading code should be much higher than the user information rate, so that the signal is spread to a much larger bandwidth. The spreading codes assigned to the users are required to have sufficiently low cross correlations between each other, in order that the user signals can be separated with low MAI after despreading at the receiver. Besides, the autocorrelation function of the codes should have a small preferable zero value at non-zero shift to work well under multipath environment. The type, the code length and the chip rate of the spreading sequences are of great importance for the system capacity. A review for some commonly adopted codes in CDMA networks can be found in [3].

Multiuser Detection (MUD)

In CDMA systems, multiple users share the same frequency spectrum which inevitably leads to MAI. However, this interference is different from random noise as it is possible to be removed once other users' recovered bits can be correctly decoded and known by the intended receiver. Such receivers which jointly recover the information bits of all users are known as multiuser detectors.

Power Control

In a cellular CDMA system, if all users use constant power for signal transmission, due to the path loss, the received power at the base station will be greater from those mobile users (MSs) near BS than that from MSs at the cell boundary. Therefore, the received signal from the users far from BS will be marked by the stronger signals from nearer users. This is the so-called *near far effect*. The idea of power control is to set the transmission power of each user in the CDMA system so that the signal from each user is appropriately detected without excessive interference to the other users. Power control has been proved to be an effective way to suppress both intracell interference and intercell interference and thus to enhance the system capacity. Detailed survey on power control schemes in CDMA systems will be provided in the next chapter.

Soft Handover

Since all the users in a CDMA system transmit their signals on the same frequency band, no hard handover from one frequency to another is needed when the user moves from one cell to another. Furthermore, the use of Rake receiver facilitates the users to make soft handover, since a mobile user is capable to simultaneously communicate with more surrounding base stations through different fingers and perform combining before a hard decision is made.

Soft Capacity

In a CDMA system, if the number of users is less than the nominal value, an enhancement in signal-to-interference ratio (SIR) is observed and it is directly reflected in an improvement in bit error rate. This improvement can be transferred back to users by lowering their battery consumption after reducing their transmit power. On the other hand, if the number of active users exceeds the nominal value, providing services to all users are still possible except that the signal quality for all users will be slightly degraded. This phenomenon is called soft capacity. Hence, CDMA is unlike FDMA/TDMA systems which cannot support users beyond the nominal number.

2.5 Overview of Multicarrier Transmissions

The higher data rates expected in NextG will necessitate modulations and codings which are suitable for wideband transmissions with the capability of multipath mitigation and signal recovery. OFDM and related modulation and multiple access schemes are emerging as a possibly preferred set of technologies.

The basic idea of multicarrier transmission has been proposed in some literature in 1960s [4] [5] [6]. Yet in these classical frequency-division multiplexing (FDM) or multi-tone systems were based on the filter banks, which made the realization impractical due to high complexity and large processing delay, and the spectral efficiency was rather low. OFDM, which employs multiple carriers overlapping in the frequency domain, was pioneered by Chang [7], [8]. Later, the use of

the discrete Fourier transform (DFT) to replace the banks of sinusoidal generators and the demodulators suggested by Weinstein and Ebert [9] in 1971 significantly reduce the implementation complexity of OFDM modems. Also, the use of the fast Fourier transform (FFT) makes it possible to design OFDM systems with a large number of subcarriers and low implementation complexity. A few years later, Cimini [10] provided early seminal results on the performance of OFDM modems both over flat fading channels and frequency selective channels. As shown in [11], OFDM is included in the digital video broadcasting standards. Besides, it has also been chosen as the key transmission technique wireless LAN standards. More recent advances in OFDM transmission are presented in the impressive state-of-art collection of works edited by Fazel and Fettweis [12].

The basic idea of OFDM is to divide the available spectrum into several orthogonal subchannels (subcarriers). By making all subchannels narrow band, they experience almost flat fading, which makes equalization very simple. OFDM reduces the effect of ISI by making the signal period of subcarriers much larger than the delay spread of the channel. In addition, a cyclic prefix (CP) will also be inserted in the guard time to eliminate ISI.

Variations of OFDM include multicarrier CDMA (MC-CDMA) and other coded OFDM schemes. MC-CDMA applies a spreading sequence in the frequency domain, whose schemes will be discussed later on. In presence of deep fades, some subcarriers will suffer greatly, while others will not. In order to achieve favorable performance in such cases, it is necessary to incorporate a channel coding scheme in the system design to introduce a link between bits transmitted on dif-

ferent subcarriers. The signal transmitted on the badly distorted subcarriers could be recovered more easily due to the coding link with other subcarriers. Thus, in coded OFDM (COFDM), multiple subcarriers are modulated and coded to ensure that encoded bits can be decoded even if some of the subcarriers have a very low signal-to-interference+noise ratio (SINR).

2.5.1 Advantages and Disadvantages

OFDM technique has many attractive features. OFDM transmissions over mobile communications channels can alleviate the problem of multipath propagation. And since OFDM systems transmit data on parallel subcarriers with lower transmission rate, they have longer symbol intervals, reducing the sensitivity to impulse noise. Besides, the subcarrier spectrum overlapping leads to high spectral efficiency. More interestingly, OFDM signaling provides adaptive access in the frequency domain. The system performance can be improved through the adaptation to the channel conditions on each subcarrier during transmission, i.e., the subcarriers have the option to choose the modulation and coding schemes according to their respective subcarrier channel environments. Unlike OFDM, when integrated with CDMA, multiple users' accessing the same subcarrier becomes possible. More details addressing the adaptive subcarrier-and-bit allocations in OFDM as well as MC-CDMA systems can be found in Chapter 5 and 6, respectively.

Multicarrier transmissions show many advantages over other techniques over time-dispersive radio channels, and that is why it is a very promising candidate for the 4G communications. However, recent research efforts have focused on solv-

ing a set of inherent difficulties regarding OFDM, namely, on reducing the peak-to-average-power ratio (PAPR), on time and frequency synchronization and on mitigation of the effects of interchannel interference (ICI).

OFDM is an *orthogonal* multicarrier transmission technique, yet the Doppler spread and the ISI between two neighboring OFDM symbols will cause loss of orthogonality between subcarriers, which, in turn, leads to ICI. As indicated in [13], ICI degrades the performance of OFDM systems seriously. The loss of orthogonality due to ISI can be removed by the use of CP, whilst the effect of doppler spread within a OFDM symbol duration is generally not easy to track and compensated for. Recently, much work has also been done [13] [14] to obtain the expressions for the ICI of an OFDM signal resulting from Doppler spread.

2.5.2 OFDM System Description

A schematic diagram for a point-to-point OFDM system model is shown in Figure 2.5, in which coding block is optional. When coding is included, the input signal is firstly encoded, and then mapped to the symbols before they are inverse Fourier transformed. And the CPs are added to preserve the orthogonality between subcarriers. After that, the transmitted signal is exposed to the multipath fading channel. At the receiver, inverse operations are performed.

The input symbols to OFDM block c_n (whether coded or uncoded) are assumed independent, identically distributed and possibly coded. c_n are modulated into different subcarriers using N-point IFFT. After guard intervals are added, the

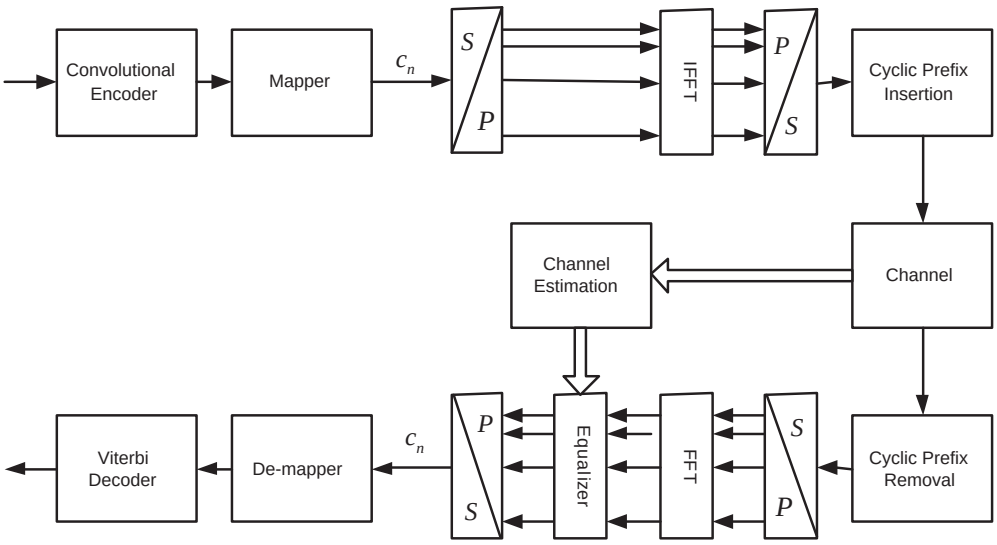

Figure 2.5: Schematic model of the OFDM system.

symbols could be expressed as

$$X_k^g = \frac{1}{\sqrt{N}} \sum_{n=0}^{N-1} c_n \exp\left(j\frac{2\pi nk}{N}\right) \quad 0 \leq k \leq N+G-1 \tag{2.8}$$

where X_k is the output sequence of the IFFT, $X_k^g = X_{(k)_N}$ is the sequence with guard interval, and $(k)_N$ is the residue of k modulo N.

For our work on OFDM systems concerned in this chapter, two channel models are used. The first channel model is specified by the power delay profile shown in Figure 2.6, which simulates a situation in an open terrain where there are only a few distinct multipaths. The relative delays and the normalized power for the 6 paths are listed in Table 2.1. The second channel model is an uniform delay power profile which is more likely to happen in urban area. We assume that the power delay profile will not change with the increase in the signal bandwidth and this is quite reasonably correct especially in the first scenario. Moreover, the signal of each path is Rayleigh faded and exhibits maximum doppler spread of f_d.

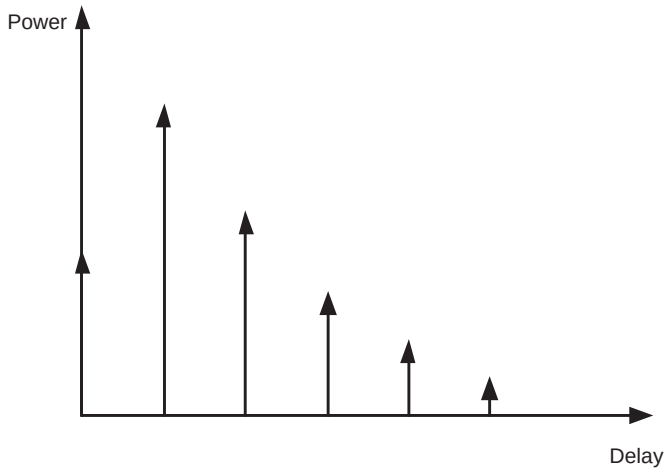

Figure 2.6: Power delay profile of the multipath channel.

Table 2.1: Power distribution of the different path.

Delay	0.0	1.953	3.906	5.859	7.812	9.765
Power	0.190	0.379	0.239	0.095	0.060	0.037

The received signal then has the form

$$R_k^g = \sum_{m=0}^{M-1} h_{m,k} X_{k-m}^g \quad 0 \leq k \leq N+G-1 \tag{2.9}$$

where $h_{m,k}$ is the value of the channel impulse response at position m (normalized to sample period) and instant k. This way of generating the channel gains at each sample of the OFDM symbols will take into account the time selectivity of the channel. After removal of the guard interval and FFT transformation, the demodulated signal could be written as

$$Z_l = \sum_{n=0}^{N-1} \sum_{m=0}^{M-1} c_n \Phi_m(n-l) \exp\left(-j\frac{2\pi nm}{N}\right) \quad 0 \leq l \leq N-1 \tag{2.10}$$

where

$$\Phi_m(n-l) = \frac{1}{N} \sum_{k=0}^{N-1} h_{m,G+(k-G)_N} \exp\left(j\frac{2\pi k}{N}(n-l)\right) \tag{2.11}$$

Frequency domain equalization is then applied before the signal is demapped and detected to make decisions on the transmitted data. The tap coefficients of the equalizer are updated at the beginning of each OFDM symbol, and these values are computed from the channel gains of each multipath at the beginning of each OFDM symbol which assumed to be known.

2.5.3 ICI for Uncoded OFDM System

When the total bandwidth of the signal is fixed, the increase of FFT size would lead to increased ICI [13], so the performance deteriorates as the FFT size increases. On the other hand, if the FFT size remains small to reduce the effect of ICI, the overhead due to transmission of CP will increase. Therefore, there exists an optimal FFT size that can maximize the system performance. However, such a design approach sometimes may not be desirable. In order to have a time nonselective OFDM symbol to ensure it can support a given mobility group, it would be better to keep the subcarrier bandwidth constant. In the following discussions, we present our study on the effect of ICI on the performance of OFDM when the total bandwidth increases while the subcarrier bandwidth remains constant. The system model described in the last section is used.

To evaluate the amount of ICI, the expression of the ICI terms can be obtained by rewriting (2.8) as

$$Z_l = \eta_l c_l + \rho_l \tag{2.12}$$

where $\eta_l = \sum_{m=0}^{M-1} \Phi_m(0) \exp\left(-j\frac{2\pi lm}{N}\right)$ is the multiplicative noise term and

$$\rho_l = \sum_{n \neq l} \sum_{m=0}^{M-1} c_n \Phi_m(n-l) \exp\left(-j\frac{2\pi nm}{N}\right) \tag{2.13}$$

is the ICI term. In the sequel, we can get the autocorrelation of ρ_l in the uncoded and coded system, assuming signal and the channel are independent and $\sum_{m=0}^{M-1} \mathbf{E}\left[|h_{m,k}|^2\right] = 1$.

$$\begin{aligned} \mathbf{E}\left[\rho_l \rho_{l+r}^*\right] &= E_s \sum_{n \neq l, l+r} \sum_{m=0}^{M-1} \mathbf{E}\left[\Phi_m(n-l)\Phi_m^*(n-l-r)\right] \\ &= E_s\delta_r - \frac{E_s}{N^2} \sum_{k=0}^{N-1} \sum_{k'=0}^{N-1} J_0\left(2\pi f_d T_s(k-k')\right) \cdot \\ &\quad \left[\exp\left(j\frac{2\pi k'r}{N}\right) + (1-\delta_r)\exp\left(j\frac{2\pi kr}{N}\right)\right] \end{aligned} \tag{2.14}$$

where T_s denotes the sample duration. If we let $r = 0$, we can get the ICI variance as follows

$$\mathbf{E}\left[|\rho_l|^2\right] = E_s - \frac{E_s}{N^2}\left\{N + 2\sum_{i=1}^{N-1}(N-i)J_0(2\pi f_d T_s i)\right\} \tag{2.15}$$

When the FFT size keeps increasing, the total bandwidth increases proportionately if the subcarrier bandwidth remains constant. Thus the sample duration T_s of the OFDM symbols decreases in proportion with the bandwidth. However, the ICI variance keeps constant, which means there is no performance degradation due to ICI when the total bandwidth becomes greater with fixed subcarrier bandwidth. This can be observed in the numerical results shown in Figure 2.7, where we calculate the ICI variance according to (2.15) when the FFT size increases from N to $2N$, for different N. The curve uses cross markers in the figure denotes the ICI variance for the FFT size of N and sample duration of T_s, while the curve uses circle markers denotes the ICI variance for the FFT size of $2N$ and sample

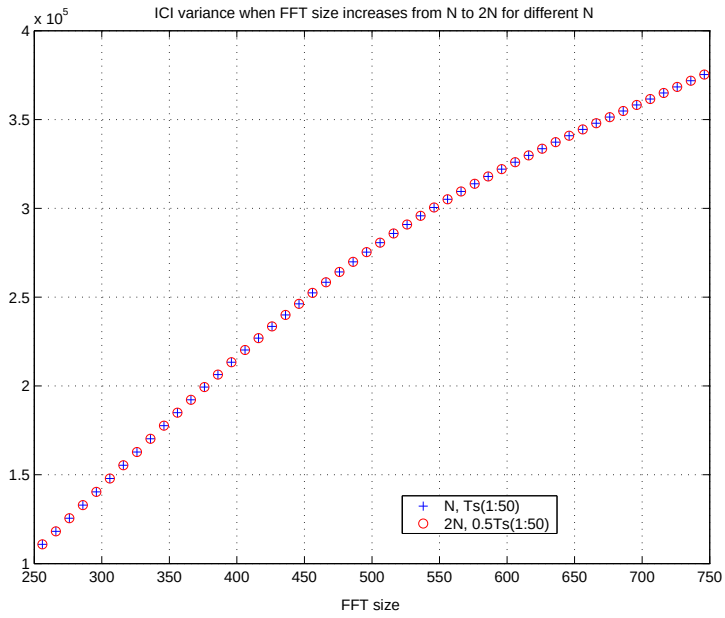

Figure 2.7: ICI variance when FFT size increases from N to $2N$ for different N.

duration of $0.5T_s$. We can see that for different N, the ICI variance for (N, T_s) and $(2N, 0.5T_s)$ agree well with each other. Similar results could be obtained if FFT size increases from N to other multiples of N, which means the ICI variance will remain the same as the total bandwidth increases in uncoded OFDM system, if the subcarrier bandwidth remains constant.

2.5.4 Maximum Bandwidth of Uncoded/Coded OFDM Systems

In this section, we will focus on studying the effect of the frequency selective fading on the performance of OFDM system in such a case that the total bandwidth of the signal keeps increasing while the subcarrier bandwidth remains constant. In other words, we will increase FFT size with fixed subcarrier bandwidth. The objective to

this study is to answer the following question: in the future, while services require higher and higher transmission rate, will there be a limiting bandwidth that OFDM cannot go beyond, for a fading channel of given time selectivity?

We still use the system model described above. For uncoded OFDM system, BPSK modulation is used; yet for coded OFDM system, a convolutional code of rate 1/2 and constraint length 7 is used before the signal is mapped onto QPSK symbols. The carrier-to-noise ratio (CNR) of the received signal is defined as:

$$CNR = \varrho \frac{E_s}{N_0} \tag{2.16}$$

where $\varrho = N/(N+G)$ stands for the normalization factor to compensate for the bandwidth increase due to CP, and hence it indicates the spectral efficiency of the system. E_s is the symbol energy; N_0 is the noise spectral density. In our simulation, the curves of BER versus Carrier-to-Noise-Ratio (CNR) are developed for different FFT sizes both in the uncoded and coded OFDM systems to see how the total bandwidth could affect the system performance and to further identify whether maximum bandwidth exists to ensure certain system performance.

The subcarrier bandwidth in use is 32kHz, and the Doppler frequency spread is kept at some constant values, namely, $f_d = 200$Hz. The BER vs. CNR curve for the uncoded system using the discrete multipath channel model is displayed in Figure 2.8, where we can see the BER curves are different for different FFT sizes. This shows there is performance degradation when FFT size increases in uncoded systems. Hence there exists an maximum usable bandwidth, which means if we keep increasing the total bandwidth, there will be a state where the BER

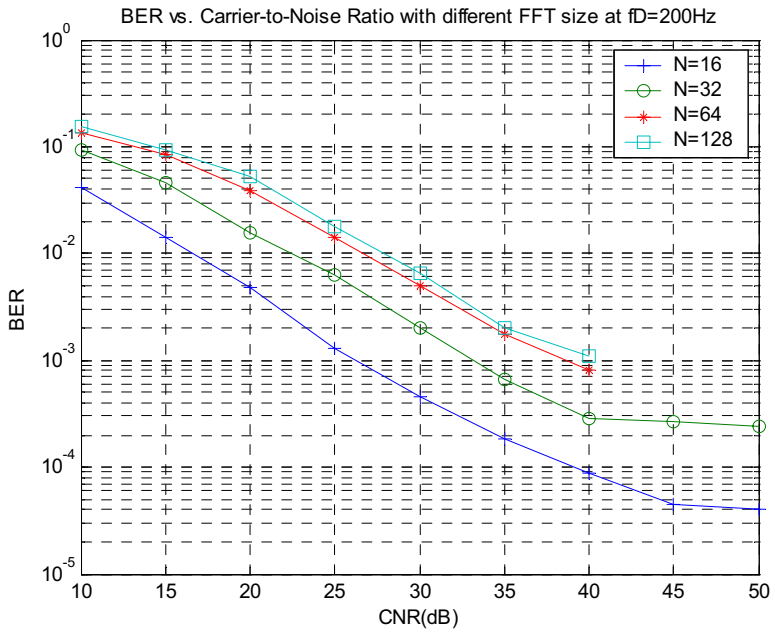

Figure 2.8: BER vs. CNR in the 6-path channel with different FFT sizes, $f_d = 200$Hz.

requirement will no longer be fulfilled. Notice that from last section, the effect of ICI for different OFDM bandwidth but same subcarrier bandwidth is the same for a given maximum doppler spread, this degrade in performance is mainly due to the more severe frequency selective fading and hence more CPs are needed. Figure 2.8 shows that to ensure a BER of 10^{-4}, only 16 subcarriers can be used, which means the maximum bandwidth is $16 \times 32 = 512$kHz.

In Figure 2.9, we reduce the number of multipath to 2, with average power of 0.6 and 0.4. Results show that we roughly can have a maximum bandwidth of $64 \times 32 = 2048$kHz.

To illustrate further, we change the maximum Doppler spread f_d to 100Hz, and the result is shown in Figure 2.10. It can be seen that the maximum bandwidth

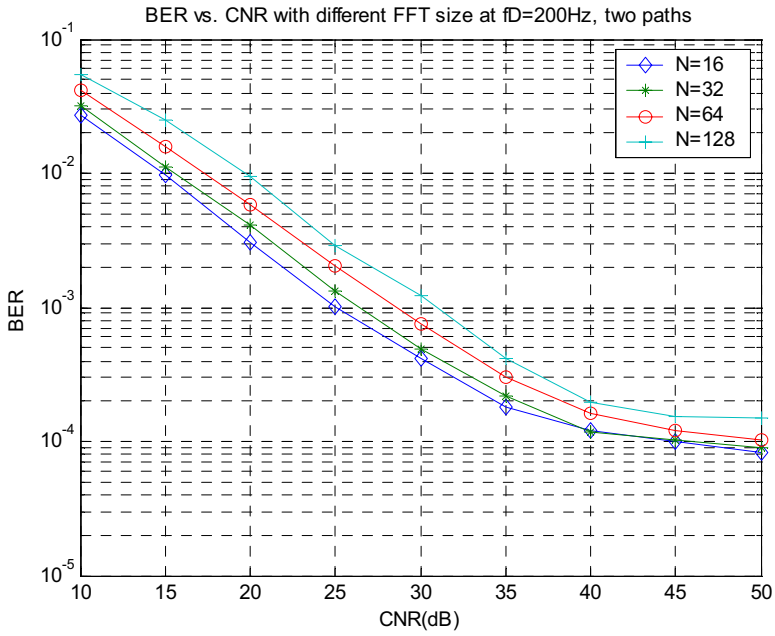

Figure 2.9: BER vs. CNR in the 2-path channel with different FFT sizes, $f_d = 200$Hz, path average energy $60\% : 40\%$

to ensure a performance of 10^{-4} can be $64 \times 32 = 2048$kHz for $f_d = 100$Hz, over the 6-path channel.

Similarly, the performance curves of BER versus CNR for *coded* OFDM system in 6-path channel model are also shown in Figure 2.11. Once again, the performance of the coded OFDM system exhibits the same behavior indicating that there exists a maximum usable bandwidth.

Results show that this maximum transmission bandwidth is a function of channel conditions such as maximum Doppler spread and power delay profile. This part of work addresses a problem that might need to look into: there exists a maximum usable bandwidth in uncoded and coded OFDM system if the subcarrier bandwidth remains constant to ensure a given time selectivity (in order to support a given mobility group). This indicates that OFDM can support up to a maximum

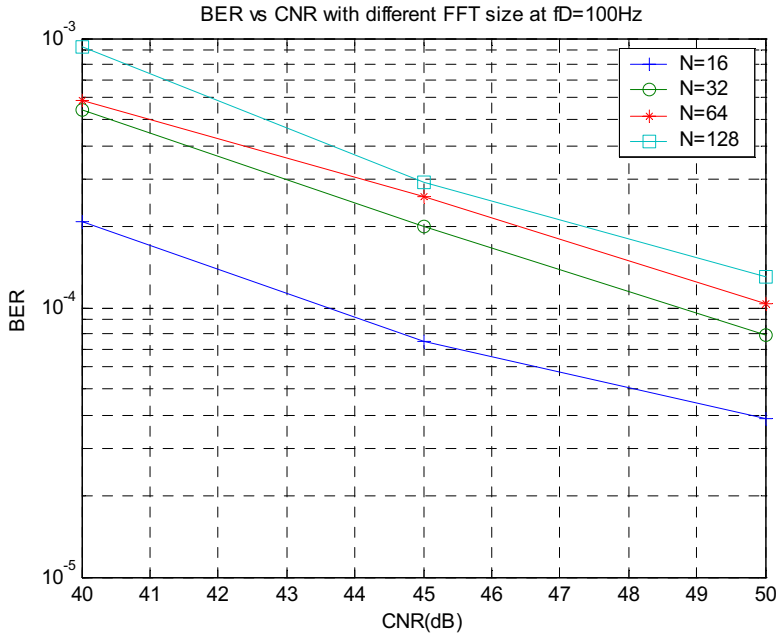

Figure 2.10: BER vs. CNR in the 6-path channel with different FFT sizes, $f_d = 100$Hz.

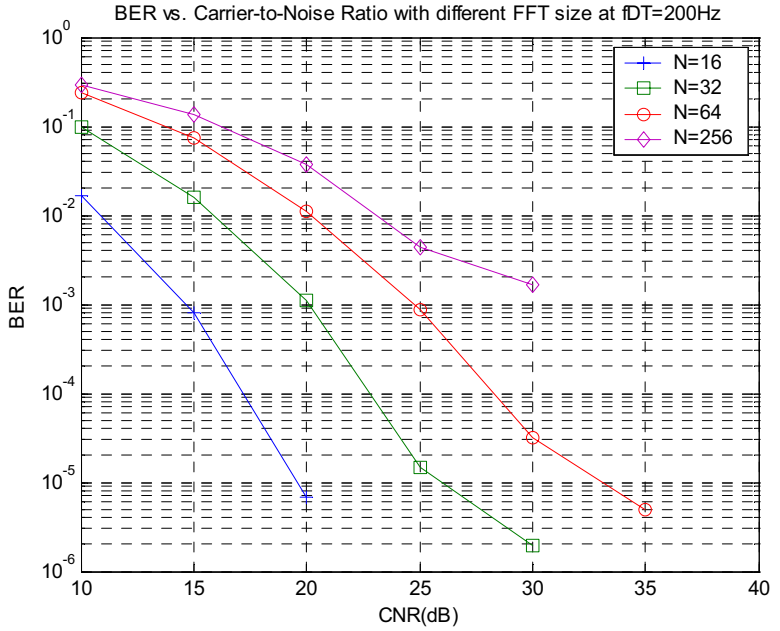

Figure 2.11: BER vs. CNR in the 6-path channel for coded OFDM system with different FFT sizes, $f_d = 200$Hz.

transmission rate if a given BER is to be guaranteed.

2.6 Multicarrier CDMA (MC-CDMA)

Combining OFDM transmissions with CDMA allows us to exploit the inherent channel frequency diversity by spreading each symbol across multiple subcarriers. This technique has been pioneered by Yee et al. [15], by Chouly et al. [16], and by Fettweis et al. [17]. Fazel and Papke [18] investigated convolutional coding in conjunction with OFDM/CDMA. Prasad and Hara [19] compared various methods of combining the two techniques, identifying three different structures, namely MC-CDMA, MC-DS-CDMA [20] [21], and MT-CDMA [22]. These three MC-CDMA schemes will be introduced in the following.

The MC-CDMA technique has some attractive features like high spectral efficiency, easy implementation, robustness against multipath, etc, yet at the same time, it inherits some drawbacks from CDMA and OFDM, such as sensitivity to frequency offset, high PAPR and MAI.

2.6.1 MC-CDMA spread in Frequency domain

In this design, the incoming bit stream is copied to N symbols. These N symbols are each modulated onto a different orthogonal carrier frequency. However, the spreading of the symbol is done in the frequency domain before modulating to the carrier frequencies. Each carrier is spread with a chip from the spreading sequence belonging to the user who sends the data. This is equivalent to performing a N-

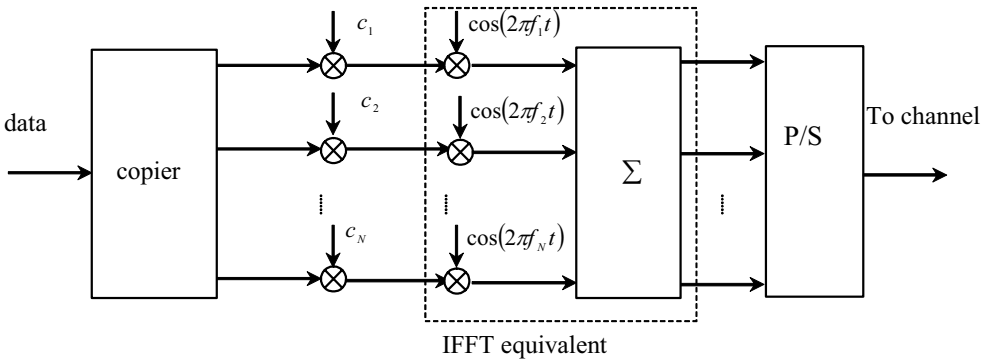

Figure 2.12: MC-CDMA transmitter.

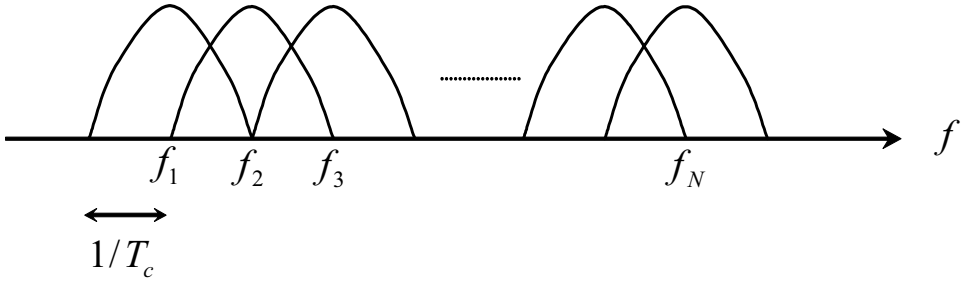

Figure 2.13: Frequency spectrum of transmitted MC-CDMA signal.

point serial to parallel (S/P) conversion after a data stream has been spread by the spreading sequence. All the N modulated signals are summed together and transmitted. The transmitter structure is shown in Figure 2.12. The modulation operation shown in the dashed box of Figure 2.12 is equivalent to the IFFT operation, which leads to a simplified MC-CDMA system by replacing the modulators with the IFFT operation.

The frequency spectrum of the MC-CDMA signal is shown in Figure 2.13. Suppose the processing gain of the system is G and the incoming data duration for one bit is T_s , the chip duration on each subcarrier is then $T_c = T_s N/G$. The required bandwidth for this MC-CDMA scheme is $(N+1)G/(T_s N)$.

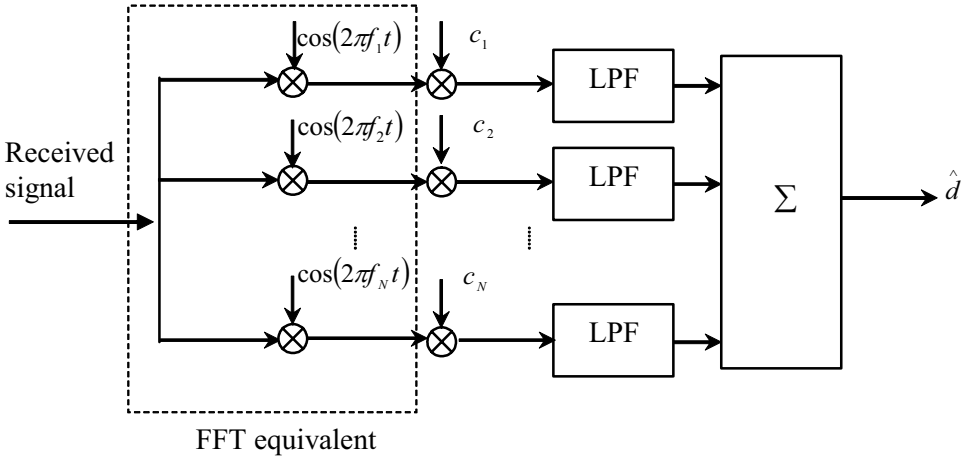

Figure 2.14: MC-CDMA receiver.

The receiver reverses the operation of the transmitter. First, the received signal is demodulated, equivalent to multiplying this signal with the N orthogonal carrier frequencies and then low pass filtered the resulted signals. The demodulated signals are each multiplied with the same spreading sequence used at the transmitter. Next, the receiver will attempt to detect the transmitted data symbols from the despread signals. Figure 2.14 shows the receiver design of the MC-CDMA.

2.6.2 MC-DS-CDMA

This scheme is the combination of time domain spreading and multicarrier modulation. The transmitter spreads the S/P converted data streams using a given spreading code in the time domain so that the resulting spectrum of each subcarrier can satisfy the orthogonal condition with the minimum frequency separation, as shown in Figure 2.15. The symbols modulated on the N subcarriers are summed together before being transmitted over the channel. The N subcarriers can overlap

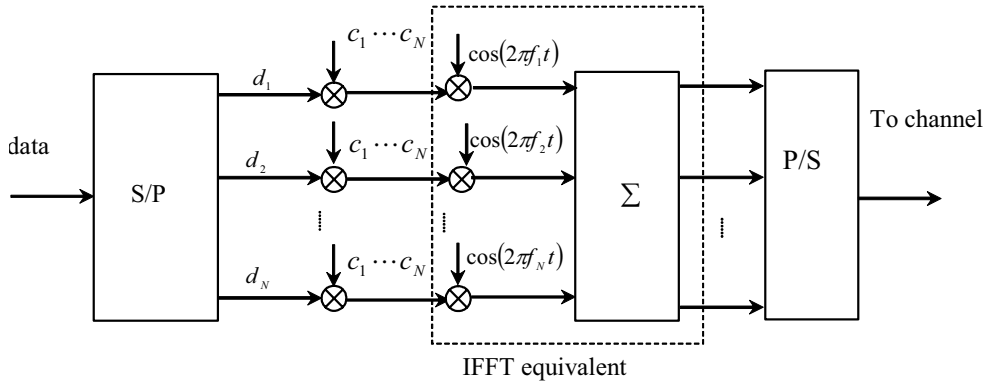

Figure 2.15: MC-DS-CDMA transmitter.

as in the conventional OFDM. For the overlapping case, the adjacent subcarriers are separated by $1/T_c$, where $T_c = T_s N/G$. The frequency spectrum is the same as Figure 2.13.

At the receiver, the signals are demodulated by the N carriers and despread with the user's spreading sequence. The receiver design is shown in Figure 2.16. It is important to note that each symbol in the MC-DS-CDMA is spread in time by the same spreading sequence per carrier while in the MC-CDMA, each symbol is spread by a spreading sequence in frequency but one chip per carrier.

In Chapter 6 of this thesis, we will provide a more detailed treatment on a multiple user MC-DS-CDMA system.

2.6.3 MT-CDMA

Transmitter MT-CDMA is similar to the MC-DS-CDMA with the incoming bit stream divided into N different bit streams, after which the spreading of each stream is done in time with a long spreading sequence aiming at maintaining a

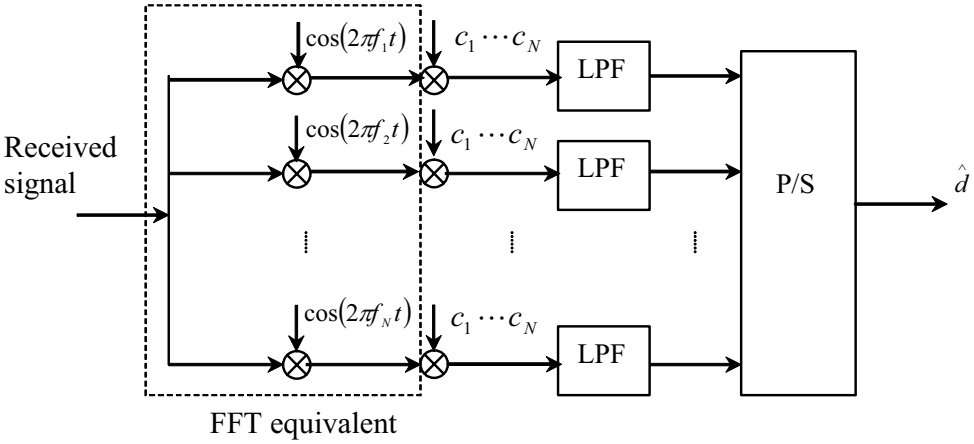

Figure 2.16: MC-DS-CDMA receiver.

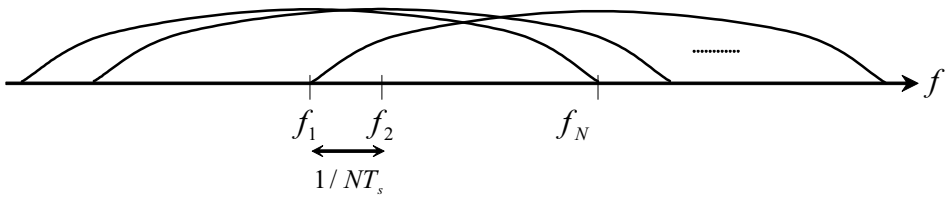

Figure 2.17: Frequency spectrum of transmitted MT-CDMA signal.

constant bandwidth for each of the subcarriers. The ratio of the length of spreading codes to the number of subcarriers, r, is kept constant. The relationship is $r/N = G$, where G has been previously denoted as the processing gain of the MC-CDMA and MC-DS-CDMA systems.

The MT-CDMA transmitter has the same structure as that of MC-DS-CDMA. Its only difference from MC-DS-CDMA is that the spectrum of each subcarrier prior to the spreading operation satisfies the orthogonal condition which subsequently loses the orthogonal quality after spreading. Loss of orthogonality results in ICI. The frequency domain spectrum is shown in Figure 2.17.

The transmitter design is performed using the same data mapping and spread-

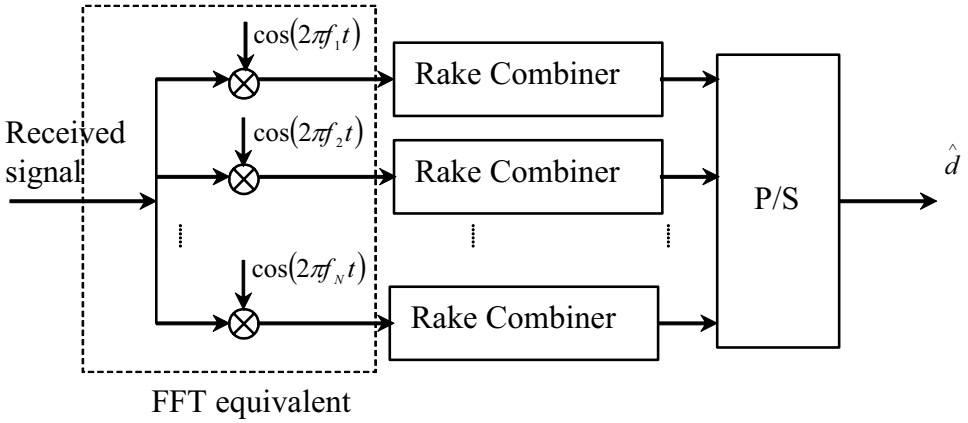

Figure 2.18: MT-CDMA receiver.

ing (in time) as in the MC-DS-CDMA except that longer codes are used to spread each subcarrier signal so that it experiences frequency selective fading. Therefore, a Rake receiver or other multiuser detector can be used at the receiver side. It is important to note that the N modulators/demodulators in the transmitter/receiver can also be implemented by the IFFT/FFT. The receiver design is shown in Figure 2.18.

2.7 Summary and Contribution

In the area of wireless communications, most of the efforts the researchers have made aim to find the ways to overcome the impairments resulted from the channel fading and interference.

In this chapter, we showed that mobile fading channels can impose impact on the achievable OFDM bandwidth. It was also illustrated that it is impractical to keep increasing the number of subcarriers if the subcarrier bandwidth remains

constant, as there exists a maximum bandwidth for OFDM transmission, beyond which the system performance degrades. Moreover, the maximum bandwidth was observed as a function of channel delay spread and the given Doppler shift.

However, in the next few chapters, we will show that in a multiuser environment, channel impairments like frequency selectivity can also be suitably exploited to achieve the diversity gain.

Chapter 3

High Performance Physical Layer

NextG is expected to provide data rate of 20-100Mb/s or as high as 1 Gb/s, so the demand for more spectrum never abates. As a result, the dynamic spectrum allocation to increase spectrum reusability or channel adaptive signal processing techniques have become the main focus to achieve both high spectral efficiency and better QoS under given spectral and capacity restrictions.

This chapter discusses about some of the commonly used techniques to improve the spectral efficiency of CDMA and multicarrier systems. Besides, our contributions in some of these areas are also given. It is our objective to investigate on how these techniques can enhance the system performance, but not to give any recommendation on any of these technologies. Literature reviews to these mentioned techniques are given in the next few sections.

We first look into Turbo coding which is generic and can be applied to any systems. Near-Shannon capacity limit can be achieved with moderate complexity decoding. We make a simple contribution to investigate the SNR mismatch sen-

sitivity of Turbo decoder when using higher order signal constellation, while the past work only focused on smaller constellation sizes.

Later in the Section 3.2, power control in CDMA systems is discussed. Conventional power control is to compensate for the propagation path loss and also the amount of interference imposed by inter-cell and intra-cell users in the uplink or surrounding base stations in the downlink. Because CDMA systems are interference limited, those users close to cell boundary are expected to introduce large interference power if conventional power control technique is used. It is therefore reasonable to think of reducing interference power through more complicated power control profiles. The disadvantage is user location awareness might be required in these techniques. Such a system will be further investigated in Chapter 4 and only survey review is made in this chapter.

Water filling based and heuristic subcarrier-and-bit allocation algorithms for OFDM systems have been studied to minimize energy usage under fixed system throughput or maximize spectral efficiency under fixed system energy. But it seems that there is no attempt to quantify the amount of gain that can be achieved through the use of subcarrier-bit-allocation. In Section 3.3, a review is made by looking into the earlier work which has been reported in the literature. And in Section 3.4, the platform to study the relationships between the performance gain and the channel parameters, e.g., channel delay spread, subcarrier correlation coefficient and spectral flatness measurement, is proposed. The work is then extended to multiclass rate adaptive OFDM systems in Chapter 5, and single class MC-DS-CDMA systems in Chapter 6. Both chapters aim to solve their unique technical

challenges and thus contribute differently. In Chapter 5, nonlinear objective function and nonlinear constraints are generally resulted from the rate adaptivity in multiclass environment. Whilst in Chapter 6, the subcarrier allocation process in MC-DS-CDMA systems becomes complicated in the presence of the interference between users who are sharing the same subcarrier.

The concept of cross layer design is given in Section 3.5. Because the channel undergoes frequency selective fading, its instantaneous capacity actually varies over time. In the traditional approach where design is carried out at segregated layers, if ergodic capacity, which is the average capacity over a long period of time, is used in the design, it may not be able to support delay sensitive services because there could be unacceptable delay at some period of time when the channel is in deep fade. On the other hand, if worst channel capacity is used in the design, the spectrum could be under utilized most of the time. A better approach is to jointly consider the higher layer QoS requirements and physical layer channel conditions together in the process of optimizing resource allocation, so that we can exploit the statistical behavior between the performance metrics in various layers. The work in Chapter 4 can be treated as an example for the simple application of cross layer design, as the performance optimization involves the physical layer parameter BER, the data link layer parameters SIR and outage probability, as well as the network layer parameters like information on user locations, delay and throughput.

Finally, the progress in dynamic spectrum allocation among different radio systems, also known as cognitive radio, is discussed.

3.1 Brief Overview of Turbo Coded Modulation

Turbo coding has received considerable attention by the researchers since its birth in 1993 [23]. It is an ideal option to provide highly efficient transmission for the delay-insensitive services in NextG.

Just as mentioned in Chapter 2, adaptability is a very important factor in the selection of transmission techniques since, in all cases, fast adaptation to the channel and traffic conditions is the key to achieve the needed QoS. Thus it is natural to know how well turbo coding could be adapted to the channel and the accuracy of channel estimation. Goff [24] demonstrated that Turbo coding could be combined with bandwidth efficient modulations such as high order quadrature amplitude modulation (QAM) to get good performance both over AWGN channel and over Rayleigh fading channel, which, in turn, provides such adaptability to use different constellations over different channels or OFDM subcarriers.

In [23] [24], we can see that turbo decoding needs channel information to detect the transmitted data from the distorted received data, which we will go into details below. In case this channel information is absent at the receiver's end, a fixed value of it will be given [1], or in some algorithms developed, no SNR information is needed at the receiver [25]. However, this requires the detector to operate constructively without channel information. Some research is performed to find how turbo coding combined with different constellations is related to the accuracy of channel estimation. Such a study is important since it reveals how practical to apply high order constellation in conjunction with turbo coding for

delay-insensitive services in the NextG communication systems.

3.1.1 Development of Coded Modulation

Coded modulation has become one of the most active topics since 1974, when Massey [26] in the seminal paper formally suggested the notion of improving system performance by looking at modulation and coding as a combined entity.

Perhaps the most significant contribution toward carrying out Massey's thoughts was the invention of trellis-coded modulation (TCM) as described by Ungerboeck in his classic paper in 1982 [27]. The primary advantage of TCM over modulation schemes employing traditional error-correction coding was the ability to achieve increased energy efficiency without the customary expansion of bandwidth introduced by the coding process. Thus, channels that were power-limited and bandwidth-limited were an ideal application for TCM.

The innovative aspect of TCM is the concept that convolution encoding and modulation should not be treated as separate entities, but rather, as a unique operation [27] [28]. The input bits are first convolutional encoded, then mapped into a signal set using a certain constellation. It has been shown that optimally designed trellis codes mapped into conventional signal sets can provide a significant coding gain in the order of 3-4dB without bandwidth expansion when compared to the uncoded conventional signal sets [29].

Lately, the increasing interest for mobile radio channels has led to the consideration of coded modulation for fading channels [30]. Multiple trellis-coded modulation (MTCM), which was first introduced by Divsalar and Simon in 1988 [31],

showed prominent performance gain over fading channel. The main advantage of MTCM is its allowing more than one output channel symbol per trellis branch so that it is able to provide an additional degree of freedom for designing a code to meet the optimization criteria on the fading channel. In particular, we are able to achieve diversities larger than those achievable with conventional trellis codes having the same number of trellis states [31]. Further, Simon and Divsalar evaluated the performance of trellis-coded multilevel differential phase shift keying (DPSK) over AWGN channel and slow Rician fading [32].

A notable departure from Ungerboeck's paradigm was followed by Zehavi [33], who recognized that the code diversity could be further improved by making it equal to the smallest number of distinct bits (rather than channel symbols) along any error event. This is achieved by bit-wise interleaving the encoder output and by using an appropriate soft-decision bit metric as an input to the Viterbi decoder. This idea was elaborated by Caire [34], in whose paper the theory underlying bit-interleaved coded modulation (BICM) was presented and general information-theoretical frame-work for this concept was provided. This analysis also yielded tools for evaluating the performance of BICM (with bounds to error probabilities tighter than those previously known) as well as guidelines for its design.

Another significant contribution was the invention of turbo coding.

Turbo coding is a class of convolutional codes proposed by Berrou, Glavieux and Thitimajshima [23] whose performances in terms of BER are very close to Shannon's limit. Since its proposal, turbo coding has become a part of the mainstream telecommunication theory and practice. Moreover, the turbo decoding principles

have found widespread applications not only in error control, but in detection, interference suppression and equalization.

Since the introduction of turbo codes, some successful attempts have been undertaken to combine these codes with multilevel modulations to design bandwidth-efficient coding schemes. Goff [24] was one of the pioneers. He combined turbo codes with bandwidth-efficient modulation, such as high order QAM to get a better performance both over AWGN channel and over Rayleigh fading channel. The combination of turbo codes with bandwidth-efficient modulation, termed turbo-coded modulation, outperforms the classical TCM scheme by Ungerboeck [27] in terms of the bit error rate (BER).

Another successful attempt was made by Robertson [35], who combined TCM with turbo coding to get a bandwidth-efficient channel coding scheme that has an overall structure similar to binary turbo codes, but employs TCM codes (including multidimensional codes) as a component codes. The combination of turbo codes with powerful bandwidth-efficient component codes leads to a straightforward encoder structure, and allows iterative decoding in analogy to the binary turbo decoder. However, the iterative decoder needs to be adapted to the decoding of the component TCM codes. This scheme is proved to be very powerful compared with the traditional TCM as well as turbo codes with Gray mapping, yet of modest complexity since simple component codes are used.

More recently, Goff [36] combined turbo coding with BICM using high order QAM modulations, which he named as bit-interleaved turbo-coded modulation (BITCM). This scheme was proved to be particularly attractive on Rayleigh fading

channels.

3.1.2 Turbo Coding and SNR Mismatch

Turbo codes and other similar constructions have captured the fancy of error control coding community in that performance quite near the Shannon capacity limit is attainable with moderate complexity decoding [23]. These codes are built from the parallel concatenation of two *recursive systematic convolutional* (RSC) codes with separate decoders processing each code to estimate the *a posteriori* probability of the various message bits. These estimates become prior information to the other decoder(s), which further update the *a posteriori* estimates. Upon iteration between decoders, it is found that error probability in the range of 10^{-5} is attainable at signal-to-noise ratio (SNR) within 1dB of channel capacity over AWGN channel.

Maximum likelihood decoding is the optimum decoding scenario for turbo codes. Since it requires high computational costs, some suboptimum iterative decoding scenarios are proposed in [37–40]. Several optimum and suboptimum soft-in/soft-out decoding algorithms were derived in order to achieve close to optimal performance with acceptable decoding effort. In the meantime, the iterative philosophy itself was embedded in many other environments such as combined equalization and decoding [41].

Detector Structure and Effects of SNR Mismatch

For turbo detection, the optimal SISO algorithm (in the sense of minimum bit error rate) to be used for equalization/decoding is the MAP (Maximum *a Posteriori*)

algorithm, with which we can estimate *a posteriori* probabilities. In practice, this algorithm is implemented in logarithmic domain, in order to reduce the numerical computation problems. The resulting algorithm is called Log-MAP.

Log-MAP algorithm derives its advantage over other algorithms for greater encoder memory lengths. However, the knowledge of the channel SNR for a Gaussian noise channel is needed to supply the proper combination of prior bit statistics. These statistics are obtained from raw channel measurement, which are Gaussian random variables, and *a posteriori* data from previous iterations. Since the MAP algorithm requires an SNR parameter to produce the correct MAP estimates, it is crucial for us to study how sensitive the decoder error rate is to the mismatch of this parameter.

Some research work has been conducted to find out the SNR sensitivity of the turbo decoder [1] [25] using lower order constellations, such as BPSK [1]. One example is shown in [1], where BPSK was assumed. However, it is also notable that turbo coded modulation can be combined with higher order constellations to give higher spectral efficiency, yet the SNR sensitivity of the turbo detector in this case remains an open issue in this area.

SNR Mismatch with Higher Order Constellation

In order to find out about the sensitivity of turbo decoding to SNR mismatch for the system using higher order constellation, we extend the research in the system with 16-QAM. The block diagram used in our simulation is shown in Figure 3.1.

The input information is firstly encoded, where the turbo encoder consists of

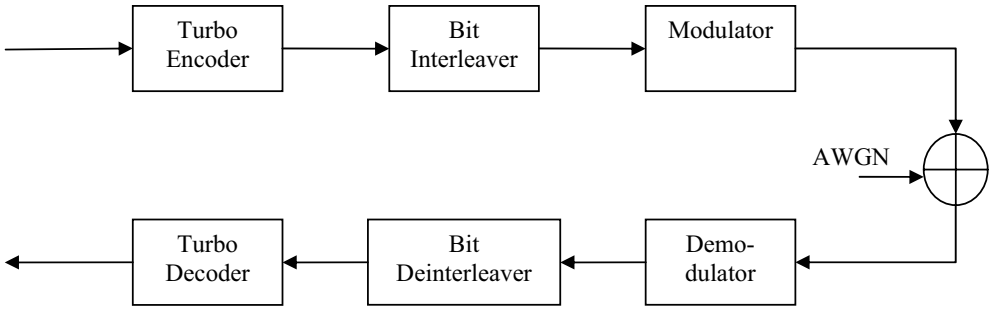

Figure 3.1: BITCM over AWGN channel.

two identical convolutional codes with rate 1/2, memory order 4 and generator [1 35/23]. Then the coded bits are interleaved using a 3GPP interleaver. 16-QAM with Graying mapping is used for modulation. The simulations are done over AWGN channels. In the receiver's side, the log-MAP turbo detector is used.

The block diagram of the turbo-detector employed at the receiver is shown in Figure 3.2. Firstly a soft-input soft-output (SISO) equalizer tries to remove the ISI; the soft outputs of this equalizer which are in the form of LLR (*Logarithm Likelihood Ratio*) are then used to feed a SISO decoder, which decodes the RSC channel coding made at transmitter. In the next iteration, profiting from the information at the decoder output, the equalizer tries to equalize the initial received symbols better. In this way, the equalizer, in fact, can profit from the redundancy added in the transmitted data by channel encoding. The procedure of equalization and decoding is repeated for several iterations. Each time, the extrinsic LLR's at the output of SISO block are delivered to the other one, which uses them as a priori information. Passing extrinsic information between equalizer and decoder ensures that the *a priori* information used by them is de-correlated with the other

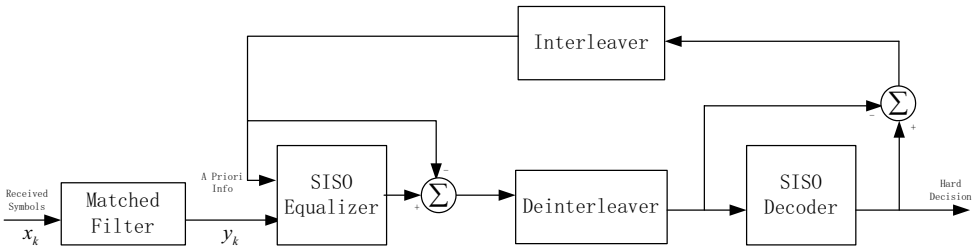

Figure 3.2: Block diagram of the turbo-detector.

information (observations) that they receive.

The Discrete signal received by the demodulator is

$$y_k = x_k + n_k, \tag{3.1}$$

where $x_k \in C$ is the transmitted signal chosen from a set of designed constellation (16-QAM) following the Gray mapping with $\mathbf{E}[x_k^2] = 1$, and $n_k = n_k^I + jn_k^Q$ is the complex Gaussian noise with variance $2\sigma_n^2$, where σ_n^2 is the variance of n_k^I and n_k^Q. Note that given E_b/N_0 in dB, σ_n^2 is calculated by

$$\sigma_n^2 = \frac{1}{2M\omega_c 10^{(E_b/N_0)/10}}, \tag{3.2}$$

where M is the size of the signal set (16 in 16-QAM), and ω_c is the code rate. The demodulator calculates the LLR for the ith bit in the kth signal as

$$\lambda^i(y_k) = \log \frac{\sum\limits_{x_j \in \Phi^+} p_n(y_k|x_j)}{\sum\limits_{x_j \in \Phi^-} p_n(y_k|x_j)}, \tag{3.3}$$

where $p_n(\cdot)$ is the distribution of additive noise, Φ^+ and Φ^- are the subset of signal constellation whose ith bit equals to 1 and 0, respectively. Because n_k is complex Gaussian noise,

$$p_n(y_k|x_k) = \exp\left(-\frac{||y_k - x_k||^2}{2\sigma_n^2}\right). \tag{3.4}$$

Thus we can see that σ_n^2 is definitely needed in the process of LLR estimation. If we obtain this information from channel estimation, we have to make sure the estimation error will not have a destructive effect for the performance of the turbo detector. Or if we want to fix an estimation value in the detection, we also need to know the region where the value could be safely located. Therefore, our aim is to find out the effects of σ_n^2 offsets, or the SNR mismatch on the BER of the system.

In the previous literature [1], BPSK constellation was assumed. And the log-MAP turbo decoder with a rate- 1/3, 16-state $(37, 21)$ encoder was used. The simulations were performed at various true SNRs, while varying assessments of SNR from -6 to $+6$dB relative to the true SNR. In Figure 3.3, error probability is plotted versus mismatch of SNR. Notice the interesting qualitative effect of mismatch: 1dB and perhaps 2dB under-estimation is rather tolerable, but degradation becomes large for greater mismatch. Over-estimation of SNR is less detrimental than under-estimation, tolerating a mismatch of several decibels without significant degradation. Obviously, when the actual received SNR is very poor, the system is not usable because of very high BER. On the other hand, for SNR in the region where iterative decoding provides good performance, SNR mismatch approximately from -3 to $+6$ dB could be tolerated. In this case, fixed estimated SNR values could be given within the tolerable offset region [1], or simple estimation is done to supply the MAP statistics in the decoding procedure.

For our system using 16-QAM, the simulation results are shown in Figure 3.4, where the true SNR is fixed to be 4 dB, and the SNR mismatch varies from -6 dB to $+6$ dB. BER curves for iterations from 1 to 5 are denoted with different

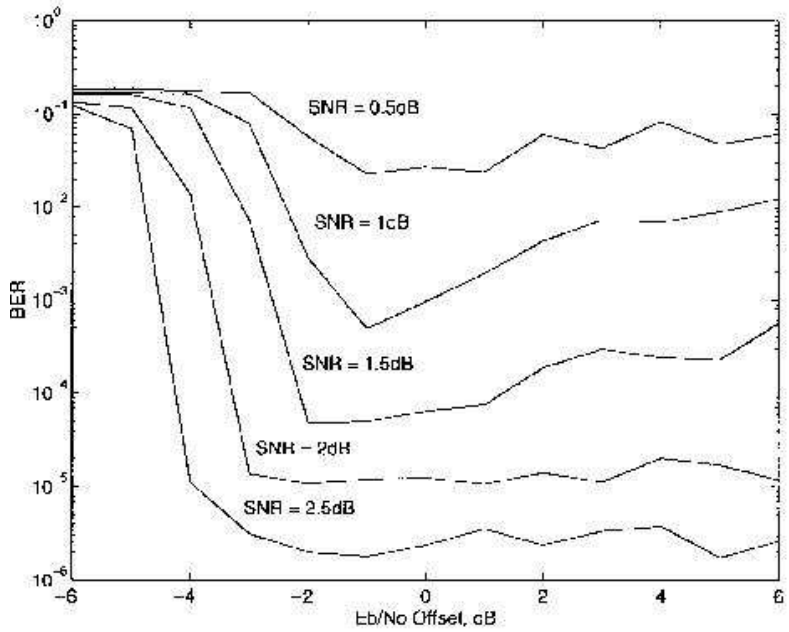

Figure 3.3: Error probability versus mismatch for several true SNR values, extracted from [1].

marks. Comparing with the curves in Figure 3.3, we can see that the range over which the SNR mismatch would be tolerable is narrower for the system using 16-QAM than that using BPSK. In other words, the SNR sensitivity is greater in the system using higher order QAM than that using lower order constellation. One possible reason for that observation is the higher order constellation has a denser arrangement. Thus neighboring points are closer to each other, which leads to the greater sensitivity of the soft turbo decoder to the SNR offsets.

Similarly as in Figure 3.3, we can see from Figure 3.4 that the tolerance for the positive offsets is still relatively greater than that for the negative ones. The result suggests that turbo decoder with higher constellations is more sensitive to SNR mismatch, and hence it imposes a need to apply more accurate channel estimation techniques.

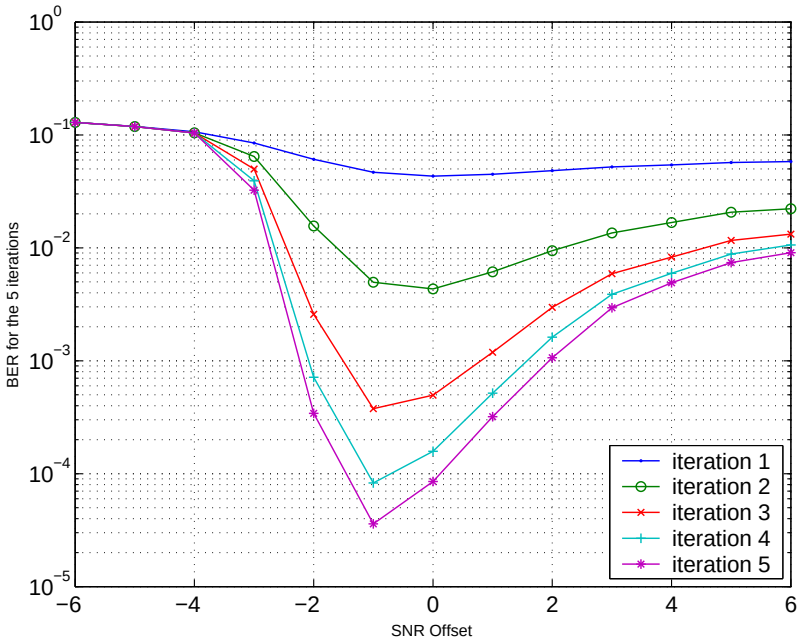

Figure 3.4: BER vs. SNR offsets in different iterations, true SNR = 4dB.

3.2 Power Control in CDMA systems

CDMA, as discussed in the previous chapter, has been widely explored as a main technology for mobile communication systems of 3G and beyond. The CDMA system performance is interference limited, and MAI becomes the major performance limitation. As the cellular mobile communication evolves, more and more users are expected to share the spectrum. Yet the interference from the users inside the cell and from other neighboring cells greatly affects the system performance. Besides, in a cellular CDMA system, if all users use constant power for signal transmission, due to the path loss (as stated in Chapter 2), the received power from those mobile users near base station will be greater than that from users at the cell boundary. Therefore, the received signal from the users far from base station will be marked by the stronger signals from nearer users. This is the so-called *near far effect*.

The idea of power control is to set the transmission power of each user in the CDMA system so that the signal from each user is appropriately detected without excessive interference to the other users. Power control has been proved to be an effective method to keep both intracell interference and intercell interference at their minimum and indirectly maximize the system capacity.

Power control schemes, in general, can be classified into different groups according to different criteria. For example, open-loop and closed-loop power control are distinguished by the SINR information in use for the transmission power adjustment in different transmission links [42–44]. A mobile station can determine its uplink transmission power according to its downlink-received SINR and a base station can update its downlink transmission power based on its received SINR in the uplink. This is called open-loop power control. While in closed-loop power control, the power levels are controlled according to the actual channel conditions in separate links. Centralized and distributed algorithms are another possible classification of power control schemes. Centralized power control (CPC) requires the knowledge of all the radio link gains in the system. It gives the optimal solution for the power control problem and this solution can become a performance measurement criterion for the distributed power control algorithms (DPC). Contrast to CPC, in DPC schemes, each link measures autonomously its current SIR/SINR or received interference and link gain and then updates its transmission power based on these local measurements. Moreover, according to whether transmitters are subject to maximum or minimum power constraints, power control schemes can also be divided into constrained and unconstrained. In constrained power control,

the range of adjusting the power levels cannot exceed the maximum and minimum limits.

Early work aimed at keeping the received power of the desired link at some constant level [45] [46]. This scheme has the advantage that the requirements on the receiver dynamic range are smaller which results in better adjacent channel protection, but analytical investigation showed that the constant received power control has only limited ability to reduce co-channel interference. Then, SIR-balancing power control scheme was proposed in [47–49] to find a power vector to achieve the same SIR at the receiver from all desired communication links. This power control algorithm belongs to CPC and hence may not be applicable in practice due to the high complexity; however, it serves as a tool to derive upper bounds on the performance of power control schemes and becomes an important basis for the later research on power control. Moreover, with the SIR-balancing transmitter power control scheme, there are cases when the required SIR cannot be achieved. Therefore, stepwise removal algorithms were proposed in [47] [50] to remove some transmitters from the system step by step in order that the SIR threshold is finally attained. Besides the basic functions of link QoS maintenance and interference suppression, power control schemes were further designed to realize some key network operations such as resource allocation, handoff and admission control. In [51–54], the joint minimum power assignment and base station allocation scheme was introduced. Moreover, these joint schemes were extended to asynchronous communication case in [52] and constraint power control case in [52, 55, 56]. Problems related to power control and QoS provisioning of either a single-class or two-class

services have been widely studied [57–62]. However, in general, their focuses were to increase capacity with QoS provisioning by using more accurate traffic models, joint layer optimization [58] [59] or call admission policies [61] [62], by assuming either constant received SIR or constant received power of mobiles regardless of its locations in the cell.

Our focus on power control in this thesis is different from all the above works. We want to optimize the resource allocation to enhance the user capacity while maintaining the QoS requirements for a system supporting multiple services. In a system providing multi-service, every service class is associated with its own outage and delay requirements. In general, it is acceptable as long as non real-time data traffics can be transmitted within a certain delay bound, therefore retransmission is normally allowed for data services. If all data users who are further away from the base station can transmit at lower power while achieving their respective service requirements, the resulted lower inter-cell and intra-cell interference will be less detrimental and a higher overall system throughput could be achieved. However, if their transmitted power is too low, more frequent retransmission may result in a waste of radio resources due to increase in delay and poor user capacity. This gives room to exploit the statistical multiplexing gain between the throughput and delay through joint layer optimization. The main focus of our study in Chapter 4 is: by controlling a mobile's transmit power differently based on its distance from the base station and its service requirement, we want to explore possible improvement in the user capacity of a system supporting real-time (such as voice) and non real-time services (such as data).

3.3 Subcarrier-and-Bit Allocation (SBA)

NextG is featured by providing high rate, high quality data transmission. The system should be able to support multiclass services with the satisfaction of individual quality-of-service (QoS) requirements; this, in turn, demands more and more of the limited spectrum and calls for the wise use of system resources. Therefore, adaptive resource allocation has become an essential topic in NextG system design.

OFDM technique is a very attractive candidate for NextG, not only because it can exploit frequency diversity to combat multipath fading, and thus enhance the system capacity, but also because of its capability of flexible frequency access to facilitate adaptive resource allocation. It can assign more bits on those better subcarriers which have higher SNR and less bits on worse subcarriers or simply switch it off, i.e., no data is transmitted on those subcarriers. This concept is generally called "water-filling". For multiuser OFDM, system can even dynamically distribute subcarriers among different users according to their respective channel conditions rather than allocate fixed groups of subcarriers to a certain user. In this way, multiuser diversity is exploited, which is why adaptive subcarrier-and-bit allocation is able to achieve higher spectral efficiency in the multiuser environment, compared with either the fixed subcarrier and bit allocation scheme or the rate-adaptive scheme without dynamic subcarrier selection.

Recently, many subcarrier-and-bit allocation algorithms for multiuser OFDM system were proposed. In [63], Wong aimed to minimize the overall transmit power with given QoS requirements. The integer constraints were relaxed and an assump-

tion of time-sharing subcarriers was made. Then, a Lagrangian-based algorithm was proposed to solve the modified problem to give the lower bound of the minimum transmit power. In order to reduce computational complexity of this algorithm, a heuristic subcarrier allocation scheme was proposed in [64], with the assumption of fixed modulation modes. Later in [65], Zhang proposed another reduced-complexity subcarrier-bit-and-power allocation algorithm to maximize the overall system throughput. Equal power distribution over the subcarriers was assumed so that subcarrier-and-bit allocation problems can be decoupled, and therefore the modified problem could be easily solved through linear integer programming (IP). Some other adaptive subcarrier-and-bit allocation algorithms were developed in a grouped manner, which allocate the subcarriers in groups instead of considering each subcarrier individually to reduce the complexity. These examples can be found in [66–68], where different schemes were employed to group the subcarriers and update the allocations to improve the system capacity.

These algorithms and those reported elsewhere [69] [70], however, only gave the suboptimal solutions to the original problems with certain assumptions or relaxations. For example, some algorithms avoided IP by relaxing integer solutions to real numbers [63] and allowing subcarrier sharing [63] [69]; some avoided nonlinear programming by converting the nonlinear objective function into a linear one based on some assumptions [64] [65]; still some used a two-step adaptation to decouple the combinatorial problem [70] [71]. Although suboptimal solutions were shown to be efficient to reduce the computational complexity for realtime implementation, the optimal solution has yet been given so far. Moreover, variety of

service classes was not taken into consideration in the previous literature, which restricted the application of these algorithms in only single-class case. This could be mainly attributed to the computation challenges resulted from the non-convex objective function and nonlinear constraints involved in the optimal formulation.

In Chapter 5, we will discuss further about subcarrier-and-bit allocations and present a unified analysis of adaptive subcarrier-and-bit allocation for multiclass multiuser OFDM systems. The constrained power optimization is formulated as a mixed integer nonlinear programming (MINLP) problem. The optimal solution to this problem is derived, i.e., the instantaneous total system revenue is maximized with the QoS in terms of data rate and bit error rate of each class guaranteed. The optimized system performance is compared with the rate-adaptive scheme without multiuser diversity and a simple subcarrier-and-bit allocation scheme. The framework presented in this work, based on the optimal solution, can be used as a benchmark for future developed heuristic algorithm.

Since complexity to the exact solution is generally high and involves solving the nonlinear objective function and constraints, two suboptimal approaches to this problem are suggested based on the optimal scheme. The objective functions as well as nonlinear constraints are simplified and the computation complexity is greatly reduced. The first approach uses a quadratic approximation to the objective function; while in the second approach, a two-step algorithm is developed to obtain the suboptimal solution. The solution is first relaxed to real numbers with some constraints removed before the integer solutions are obtained. The accuracy and complexity of these two approaches are compared with each other as well as with

the optimal solution.The results will show that the two suboptimal algorithms give good approximations to the optimal solution with easier implementation.

The idea of subcarrier-and-bit allocation is extended to MC-DS-CDMA systems to improve the spectral efficiency–the multiuser MC-DS-CDMA system also has the ability to allocate subcarriers adaptively based on the instantaneous channel information of all users, so that more efficient use of radio resources is realized. Chen et al. [72] proposed a subcarrier allocation scheme for uplink transmission. In this scheme, every subcarrier has constant rate, yet users can use a different number of subcarriers up to a maximum number of N. The hopping pattern in the proposed system is adaptively determined by channel fading conditions. Although MAI has been included in the model, the developed water-filling based algorithm failed to address this issue. In [2], a simple adaptive subcarrier allocation scheme was proposed for MC-DS-CDMA systems. The mobile estimates its channel gains of all subcarriers and feeds back the index of subcarriers to the base station (BS). With the index information, the BS assigns subcarriers so that each user transmits on the subcarrier on which it has the largest channel gain. The performance when random codes are used whereby MAI is present was computed. However, such a scheme may not necessarily result in the optimal solution. Indeed, it has been pointed out in [73] that a near optimal allocation policy is obtained by averagely distributing the users over all subcarriers. This is because by avoiding multiple users' from transmitting on the same subcarrier, the system performance is improved due to the MAI reduction, although some users may not be transmitting on their best subcarriers. Furthermore, the authors of [73] set a predetermined

threshold for the channel gains so as to identify those candidate subcarriers of all users. In this way, the number of subcarriers considered was reduced.

To support higher data rate transmission, the work has been extended in [74] to the case where BS selects L subcarriers for a mobile to transmit data out of a total of N subcarriers (L/N system). To simplify the allocation process, priority among users was assumed. Moreover, subcarrier grouping method is also used in MC-DS-CDMA systems. In [75], Tabulo et al. proposed a subcarrier grouping and allocation approach for a MC-DS-CDMA system, on the basis of linear programming. To make the algorithm more practical, Al-susa et al. proposed an efficient fast-converging algorithm [76] based on priority swapping allocation. More adaptive subcarrier allocation algorithms were proposed in [77] [78] [79] for discrete multi-tone or OFDM systems, which can also be useful references for developing algorithms for MC-DS-CDMA systems.

From the literature review above, most of the existing schemes [73]- [76] have not considered the effect of MAI in the decisions of subcarrier allocation. However, this consideration is critical in real system design, since MAI is a major performance limitation in MC-DS-CDMA systems. On the other hand, for the scheme in [2], although BER performance is derived in the presence of MAI, those derivations are only performed after subcarrier allocation; while during the allocation process, MAI was not jointly considered. Therefore, our aim in this chapter is to design subcarrier allocation schemes for MC-DS-CDMA system with MAI taken into consideration. A general perception reveals that MAI computations add to the complexity of subcarrier allocation process, since the BER calculations before sub-

carrier allocations will become more complicated. Furthermore, the search space increases as the number of subcarriers and the number of users increases, which will possibly make the optimal solution infeasible. This, in turn, has motivated us to investigate suboptimal algorithms to tradeoff performance and complexity.

In Chapter 6 of our thesis, the subcarrier allocations in MC-DS-CDMA systems will be extensively investigated, with the assumption of fixed modulation. Two novel suboptimal schemes are proposed, in which the MAI effect is dealt with in the allocation process. The first algorithm is to minimize the BER of respective users rather than minimize the overall system BER. Each user performs channel estimation, orders subcarrier channel gains and feeds back an index vector to the BS. BS uses these index vectors (and not channel gains) from all the users, together with subcarrier allocation coefficients of the previous updating stage, to adaptively generate subcarrier allocation coefficients of the current updating stage so that the BER performance is optimized. However, since the assignment process depends on the previous allocation coefficients of other users, once a discrepancy is generated in the allocation process, it will also propagate to the next stage. In our second approach, the problem is formulated using Quadratic Programming (QP), and a single objective function is used to optimize the overall system BER. The algorithm uses the actual values of channel gains and does not depend on any information from the previous updating stage. Thus, the discrepancy propagation is avoided. We use Kuhn-Tucker conditions to convert the formulated QP to a linear programming (LP) problem, and the solution can be obtained using standard LP solvers.

3.4 On the Achievable Diversity Gain

In multiuser OFDM systems, performance gain in terms of reduction in total power consumption is made possible if subcarrier-and-bit allocation algorithm is used to exploit the time-frequency selectivity. However, most of these work are focused on developing heuristic algorithms, and no attention has been paid to quantify the achievable multiuser diversity gain. In some of the recent developed techniques, such as cyclic delay diversity (CDD) [80], spatial diversity is intentionally introduced to OFDM signal through the use of multiple antennas each with different cyclic delays. This basically transformed a multiple-input system into a single-input system with increased frequency selectivity, i.e., spatial diversity is transformed into frequency diversity, so that multiple users can exploit adaptively among the time-frequency bins to achieve diversity gain. This gives rise to a question of how much spatial diversity can be brought into the signals and whether there is a limit on the gain we can achieve. The objective of this section is to show that it is possible to quantify the achievable multiuser diversity gains in terms of the channel parameters such as spectral flatness measurement, channel delay spread and subcarrier correlation coefficient. Our example shows that there exists a maximum allowable diversity gain that can be brought into the OFDM signals, and beyond this point performance gain is degraded.

In this section, we propose an approach to quantify the achievable multiuser diversity gain when applying optimal subcarrier-and-bit allocation algorithm. We first define spectral flatness measurement (SFM) [81] which is used to measure the

spectral flatness of the channel frequency response, and its technical manifestation is explained. The statistical distributions of SFM under different number of multipath and power delay profile are presented. We then formulate a subcarrier allocation problem to minimize the total power consumption in a multiuser single-class OFDM system. The total transmit power is minimized with the fulfillment of data rate requirement of each user. Simulation results are presented, in which the normalized average power is obtained as a function of channel delay spread or subcarrier correlation coefficient. Furthermore, the relationships between the total system power and SFM, channel delay spread and subcarrier correlation coefficient are obtained.

3.4.1 Channel Parameters

Spectral Flatness Measurement

Consider transmission over a frequency selective fading channel which can be described by a tapped delay line. The maximum delay spread (normalized to $T_s = 1/B$, where B is the OFDM system bandwidth) is J=2, 4, 8, 16 which is equal to the number of taps. We assume two types of power delay profiles: (1) uniform (2) exponential. The ith tap is assumed to have gains following Rayleigh distribution with variance equal to $1/J$ for uniform power delay profile and $Ae^{-i/J}$ for exponential power delay profile, where A is a positive constant used for power normalization.

From the FFT of the instantaneous tap coefficients, we can obtain the chan-

nel frequency response. Zeros are padded when necessary so that the subcarrier frequency spectral gain H_n can be obtained directly through taking the FFT.

$$H_n = \frac{1}{\sqrt{N}} \sum_{k=0}^{J-1} h_k \exp\left(-j\frac{2\pi nk}{N}\right) \quad n = 1, 2, \ldots, N \tag{3.5}$$

where h_k are the channel tap coefficient for the kth path, and N is the total number of subcarriers used in the OFDM. The instantaneous SFM of the channel frequency response is defined as:

$$SFM = \frac{\frac{1}{N}\sum_{n=1}^{N} |H_n|^2}{\left[\prod_{n=1}^{N} |H_n|^2\right]^{\frac{1}{N}}} \tag{3.6}$$

Eq. (3.6) gives the ratio between the arithmetic mean and geometric mean of the channel frequency response, and is a common adopted way to describe the spectral flatness. This ratio is greater than one and the larger it is, the more variation in the instantaneous power spectral. However, it is worthwhile to mention here that SFM does not provide an indication to the correlation between any two neighboring subcarriers. We shall show later that with the same SFM but different subcarrier correlation, the achievable gain can be significantly different.

The multipath multiuser channel was randomly generated for 50000 times and the SFM values for each user are calculated on each snapshot. With the assumption of independent user channels, the samples from all the users were collected and put together to generate the probability distributions of the SFM, and its probability density function (PDF, denoted as $f(S_{fm})$) is obtained and shown in Figure 3.5(a) and Figure 3.5(b) for uniform and exponential power delay profile, respectively. Each curve comprises 3200000 samples in a system with 64 users. As expected, as the number of paths increases, the PDF is more Gaussian-like. The probability of

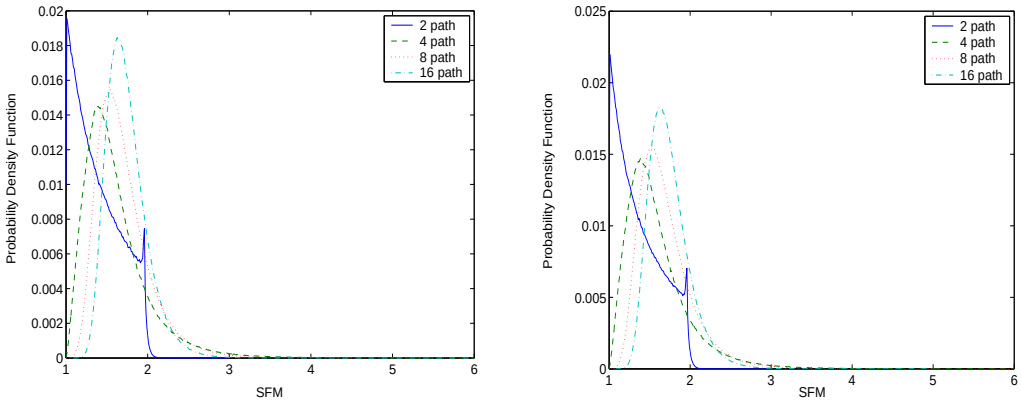

(a) uniform power delay profile (b) exponential power delay profile

Figure 3.5: Probability density function of the SFM for different number paths. $N = 64$**.**

having high SFM is kept maximum at 4 paths and reduces subsequently, whilst the probability of having low SFM will decrease tremendously as the number of paths increases.

Channel delay spread and subcarrier correlation coefficient

The RMS delay spread of the channel is calculated according to (2.2) and (2.3), for each of the number of paths, and it is normalized by the OFDM symbol length ($N = 64$). Thus, the RMS delay spreads for the number of path $J = 2, 4, 8, 16$ for both uniform and exponential power delay profile are shown in Table 3.1.

The subcarrier correlation coefficient between the n_1th and n_2th subcarriers is defined in [82] as:

$$\chi_{n_1,n_2} = \frac{(1+\lambda_{n_1,n_2})\,\tilde{\mathrm{E}}\left\{\dfrac{2\sqrt{\lambda_{n_1,n_2}}}{1+\lambda_{n_1,n_2}}\right\} - \dfrac{\pi}{2}}{2-\dfrac{\pi}{2}} \tag{3.7}$$

Table 3.1: RMS delay spread vs. No. of path. for uniform and exponential power delay profile.

J	Uniform	Exponential
2	0.0078125	0.0075746
4	0.017469	0.017017
8	0.035801	0.034916
16	0.072028	0.070268

where $\tilde{\mathrm{E}}$ is the complete elliptic integral of the second kind, and

$$\lambda_{n_1,n_2} = \frac{1}{\sqrt{1 + \left[2\pi \left(n_1 - n_2\right) D_\tau^{(2)}\right]}} \tag{3.8}$$

with $D_\tau^{(2)}$ denoting the RMS channel delay spread normalized by the number of subcarriers.

So the corresponding subcarrier correlation coefficients can be obtained for each RMS delay spread. For example, the correlation coefficients between the neighboring subcarriers are respectively, 0.9458, 0.8855,0.7872 and 0.6367 for 2,4,8 and 16 paths under the uniform power delay profile with 64 subcarriers.

In the next section, we will set up the mathematical model to optimize the power transmission using the subcarrier-and-bit allocation in a single class multiuser OFDM system under given users' channel conditions.

3.4.2 Achievable Power Gain in Single Class OFDM Systems

Assuming that there is only one service class with K users in the OFDM system. Each user should be assigned at least one subcarrier which transmits signal using 16-QAM. The N subcarriers are allocated among the K users in such a way that the total system transmit power is minimized. We assume that inter-symbol interference and inter-carrier interference have been properly taken care of. The received power and the BER requirement should satisfy the relationship in [63]:

$$f(c) \approx \frac{N_0}{3}\left[Q^{-1}\left(\frac{P_e}{4}\right)\right]^2 (2^c - 1) \tag{3.9}$$

where

$$Q(x) = \frac{1}{\sqrt{2\pi}}\int_x^\infty e^{-t^2/2}\mathrm{d}t \tag{3.10}$$

and c is the order of the constellation used. For 16-QAM, $c = 4$. N_0 denotes the power spectral density (PSD) of the additive white Gaussian noise (AWGN) for all subcarriers and all users. Also, P_e is the target BER defined in the QoS requirement of the concerned service class. Further, we let $s_{k,n}$ denote the assignment indicator, i.e., if the nth subcarrier is assigned to the kth user, $s_{k,n} = 1$; otherwise $s_{k,n} = 0$. In our system, no subcarrier can be assigned to more than one user. Therefore, if $s_{k,n} = 1$, $s_{k',n} = 0$ for all $k' \neq k$.

Assuming user k observes a frequency power spectral of $H_{k,n}$, the assigned

power at the transmitter for the kth user on the nth subcarrier is

$$\begin{aligned} P_{k,n} &= f(c)/|H_{k,n}|^2 \\ &\approx \frac{N_0}{3}\left[Q^{-1}\left(\frac{P_e}{4}\right)\right]^2 (2^c-1)/|H_{k,n}|^2 \end{aligned} \tag{3.11}$$

on the condition that the nth subcarrier is assigned to the kth user, i.e., $s_{k,n}=1$; otherwise, $P_{k,n}=0$.

Our objective is to minimize the overall transmit power while satisfying all the data rate and BER constraints for all the K users. Referring to (3.11) and its condition, the problem can be numerically formulated as below:

$$\min_{s_{k,n}} \sum_{k=1}^{K}\sum_{n=1}^{N} \rho(2^{s_{k,n}c}-1)/|H_{k,n}|^2 \tag{3.12}$$

subject to

$$1 \le \sum_{n=1}^{N} s_{k,n} \le N, \quad k=1,2,\ldots,K \tag{3.13}$$

$$\sum_{k=1}^{K} s_{k,n} = 1, \quad n=1,2,\ldots,N \tag{3.14}$$

and

$$s_{k,n} \in \{0,1\} \tag{3.15}$$

where $\rho = \frac{N_0}{3}\left[Q^{-1}\left(\frac{P_e}{4}\right)\right]^2$ are constants related to the QoS requirement. Eq. (3.13) are linear inequality constraints which indicate that each user should choose at least one subcarrier among the N subcarriers to transmit data. Eq. (3.14), however, exclude the subcarrier sharing.

The objective function defined by (3.12) can be further reduced to a linear function of $s_{k,n}$, given that $s_{k,n}$ are binary variables. Thus, the mixed integer linear problem can be solved by MIP solver using branch and bound algorithm.

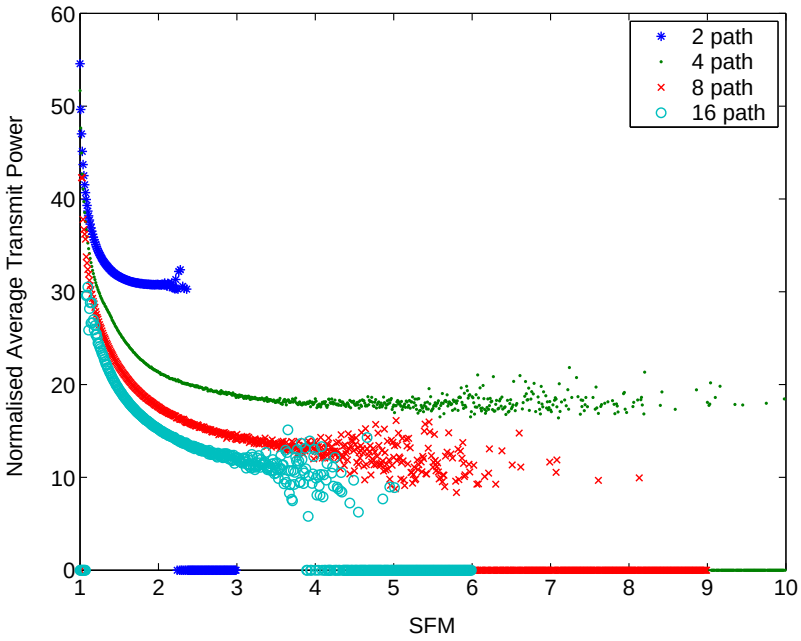

Figure 3.6: Transmit power as a function of SFM with uniform power delay profile. $N = 64, K = 64$**.**

We conducted simulations in a system of 64 users and 64 subcarriers with 50000 random trials. As the SFM is user-sensitive and the users are independent from each other, we sequence the individual transmit power and the corresponding SFM values of all users and display their relationship in Figure 3.6 for different number of multipath. Note that the power is normalized by multiplying the average channel frequency response ($|H_f|^2 = (1/N)\sum_{n=1}^{N}|H_n|^2$). Such normalization is necessary because (1) we find that it will help to obtain a neat relationship between the RMS delay spread and the normalized transmit power, and (2) such normalization provide the performance with respect to system with power control, so that all the users will have about the same amount of received power and none will be in deep fade. From the resource allocation point of view, it provides a much better fairness to all users.

The first observation is that the normalized transmit power decreases with the increase of SFM values regardless of the number of paths. At high SFM, the channel gains exhibit significant variations at different frequencies, hence the users in the system have a greater potential to exploit the frequency diversity gain through adaptive subcarrier allocations. The second observation is for a given SFM, the normalized transmit power is lower as the channel delay spread increases. This means that correlation coefficient between neighboring subcarriers has an impact on the achievable gain through subcarrier allocation. One thing worth of mentioning is channel delay spread also contributes to the distribution of PDF of SFM, as have been shown in Figure 3.5. The study of SFM is mainly to deal with instantaneous achievable gain, i.e., under a given delay spread, whilst for the other case, we are concerned about the average achievable gain. Therefore, we shall discuss the results on these two observations separately.

Average Transmit Power

We define the average transmit power, P_a, as the normalized transmit power averaged over different SFM. Mathematically,

$$P_a = \int_1^{\infty} P_n\left(S_{fm}\right) f\left(S_{fm}\right) dS_{fm} \tag{3.16}$$

where $P_n\left(S_{fm}\right)$ denotes the normalized transmit power at each SFM, as shown on the vertical axis in Figure 3.6, and $f\left(S_{fm}\right)$ is the PDF of the SFM which has been discussed in the previous section. The average transmit power for various channel delay spread are computed and shown in Figure 3.7, for both uniform

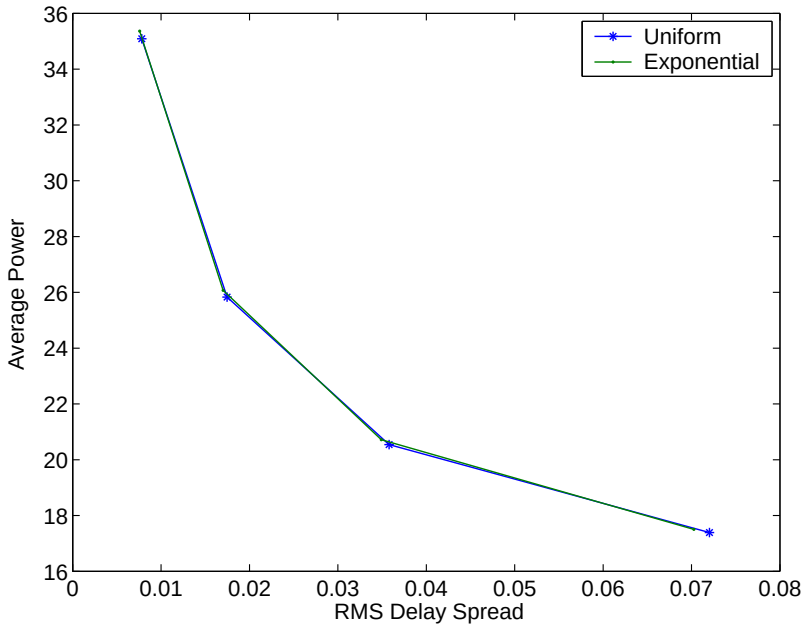

Figure 3.7: Average transmit power as a function of SFM under uniform and exponential power delay profile. $N = 64, K = 64$**.**

and exponential power delay profile. It is worth noting that the relationship for average power versus RMS delay spread is independent of power delay profiles, as shown in our simulation results that only negligible difference is observed in the function of P_a vs. $D_\tau^{(2)}$ for uniform and exponential power delay profile. Figure 3.7 illustrates the transmit power decay along with the increasing delay spread, which manifest the potential average diversity gain which we can exploit with the optimal subcarrier-and-bit allocations.

As mentioned above, the diversity gain is partially governed by the subcarrier correlations, we proceed to highlight the relationship between the average transmit power and the subcarrier correlation coefficient. According to (3.7), the subcarrier correlation coefficient χ can be calculated given a delay spread. Therefore from the observations in Figure 3.7, we can easily obtain the relationship between P_a and χ,

and it is displayed in Figure 3.8. Also, curve fitting is used to interpolate at other correlation coefficients and thus, an empirical function can be defined for P_a versus χ:

$$P_a = \frac{10^{\theta_{c,a,\chi}}}{(1-\chi)^{\theta_{m,a,\chi}}} \tag{3.17}$$

where $\theta_{c,a,\chi} = 1.1329$ and $\theta_{m,a,\chi} = 0.28927$. In the theoretical curve and the simulated points displayed in Figure 3.8,we can observe very good approximation. Therefore, (3.17) can also be used to quantify the achievable diversity gains under different channel conditions. It indicates the minimum transmit power which can be achieved when the subcarriers are uncorrelated ($\chi = 0$ or $D_\tau^{(2)} \to \infty$). If we denote that minimum power as P_{uc}, we can read its value in Figure 3.8 at $\chi = 0$, and it shows $P_{uc} = 13.58$. Conversely, if the subcarriers show strong correlations, chances are great for them to simultaneously suffer deep fade, which will inevitably lead to high average transmit power, given fixed QoS requirements.

Furthermore, curve fitting can also be employed to interpolate the curve for uniform power delay profile in Figure 3.7, and the resulted curve is presented in Figure 3.9, by which we can obtain the following function of the average power P_a versus the RMS delay spread $D_\tau^{(2)}$.

$$P_a - P_{uc} = \frac{10^{\theta_{c,a,D}}}{\left[D_\tau^{(2)}\right]^{\theta_{m,a,D}}} \tag{3.18}$$

where $\theta_{c,a,D}$ and $\theta_{m,a,D}$ are the two constants to define the relationship between P_a and $D_\tau^{(2)}$, and $\theta_{c,a,D} = -0.1933$ and $\theta_{m,a,D} = 0.71988$ by using our simulation results. Thus, the power gain can be possibly quantified at different channel delay spread.

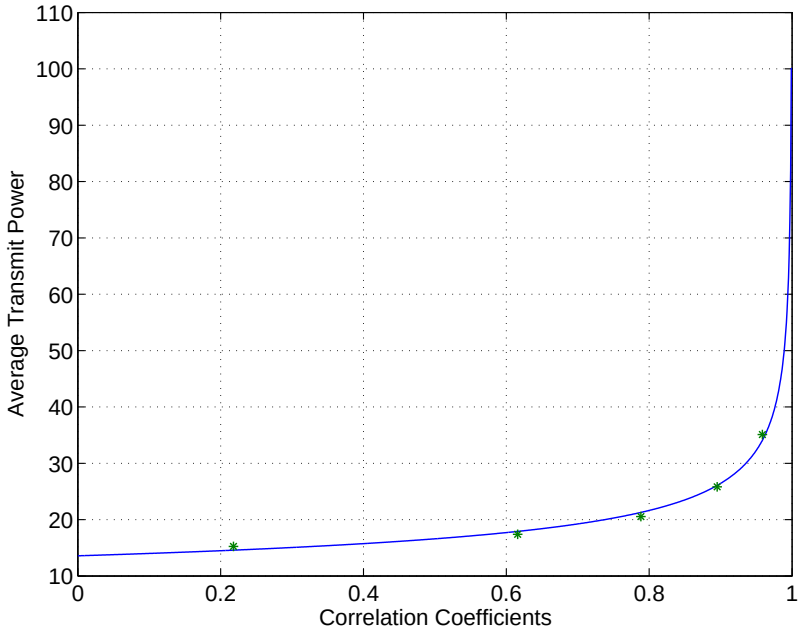

Figure 3.8: Empirical function between the average transmit power and subcarrier correlation coefficient for uniform power delay profile. $N = 64, K = 64$**.**

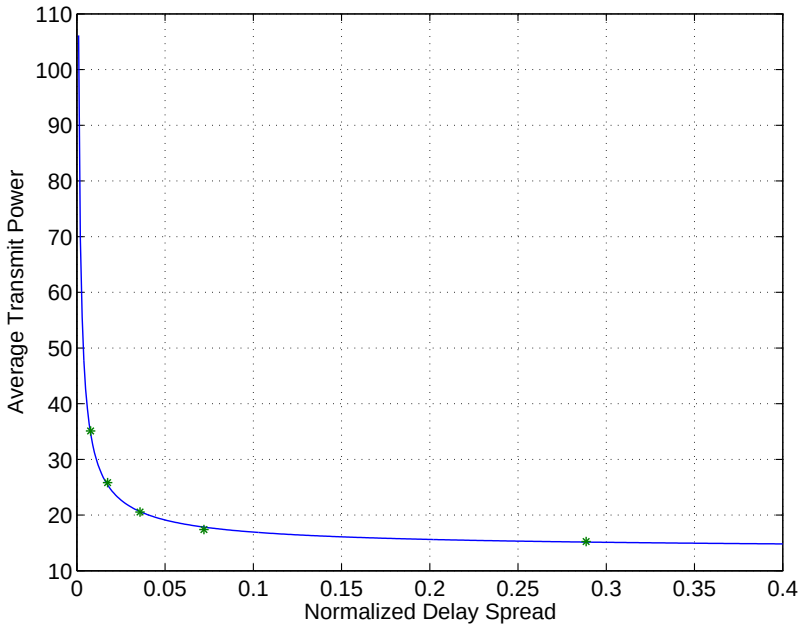

Figure 3.9: Empirical function between the average transmit power and RMS delay spread for uniform power delay profile. $N = 64, K = 64$**.**

Performance as a function of SFM

In previous part of the section, we consider the average transmit power over a long period of observation time. In this part, we deal with instantaneous normalized transmit power, i.e., normalized power in one snapshot with its spectrum described by SFM. We see from Figure 3.6 that the improvement in transmit power tends to diminish, i.e., it will not decrease any more after a certain threshold. This power floor (denoted as P_0 hereafter) shows the minimum power the adaptive subcarrier-and-bit allocation can achieve for a certain given number of paths undergoing Rayleigh fading.

With the same number of subcarriers, the delay spread of a multipath channel is directly proportional to the number of paths. Thus, according to Figure 3.6, the power floor P_0 drops with the increase of the delay spread. Using the data obtained from our simulation, the subcarrier correlation coefficients χ are computed based on different delay spread. Again, curve fitting performed shows that there exist a relationship between χ and P_0, as shown in Figure 3.10. Mathematically this relationship is given by

$$P_0 = \frac{10^{\theta_{c,0,\chi}}}{(1-\chi)^{\theta_{m,0,\chi}}} \tag{3.19}$$

where $\theta_{c,0,\chi} = 0.89062$ and $\theta_{m,0,\chi} = 0.41541$.

In the sequel, the incremental transmit power is obtained by subtracting the corresponding power floor from the power values displayed in Figure 3.6. And after changing the Y-axis to log scale, the resulted power values are presented in Figure 3.11, which demonstrates a linear relationship between the incremental power and

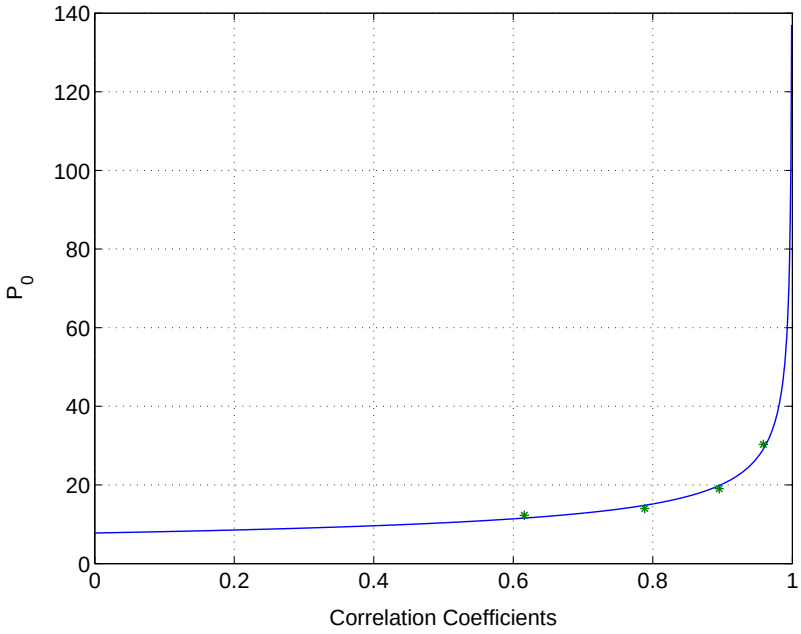

Figure 3.10: Power floor vs. subcarrier correlation coefficient under uniform power delay profile. $N = 64, K = 64$**.**

the SFM for each number of paths.

As seen from the above results, both SFM and channel delay spread contribute to the achievable power gain of the optimal subcarrier-and-bit allocation. Therefore, an empirical function is suggested to denote the relationship between the minimum transmit power, $D_\tau^{(2)}$ and SFM:

$$P = P_0 + \alpha 10^{-\Gamma(D_\tau^{(2)})\, SFM} \tag{3.20}$$

where α is a constant independent of the multipath channel. $D_\tau^{(2)}$ stands for the RMS delay spread and $\Gamma(D_\tau^{(2)})$ is a function of $D_\tau^{(2)}$ which decides the gradient of the curves in Figure 3.11. For different number of paths J under uniform power delay profile, the values of $\Gamma(D_\tau^{(2)})$ are listed in Table. 3.2.

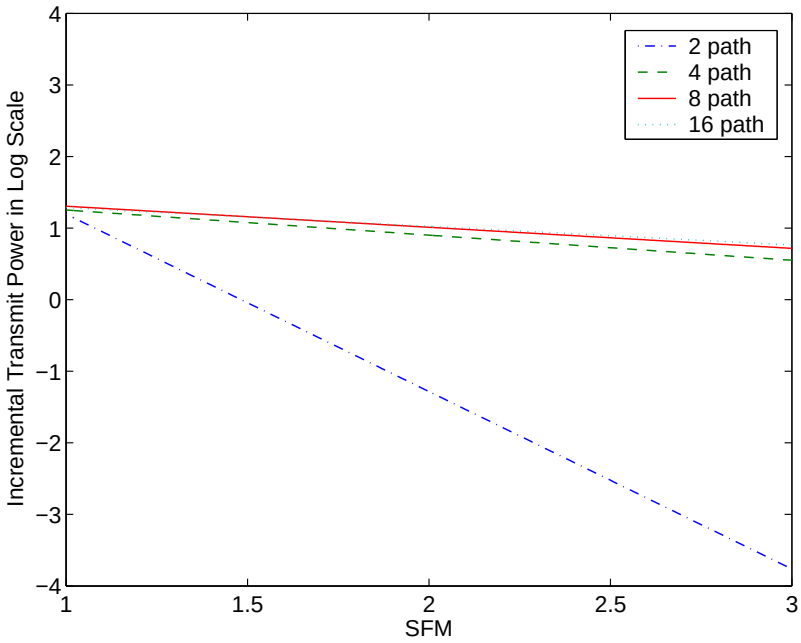

Figure 3.11: Incremental transmit power as a function of SFM with different No. of paths under uniform power delay profile. $N = 64, K = 64$.

Table 3.2: Function of delay spread and power gradient vs. No. of paths.

J	2	4	8	16
$\Gamma(D_\tau^{(2)})$	2.4795	0.3512	0.2943	0.2616

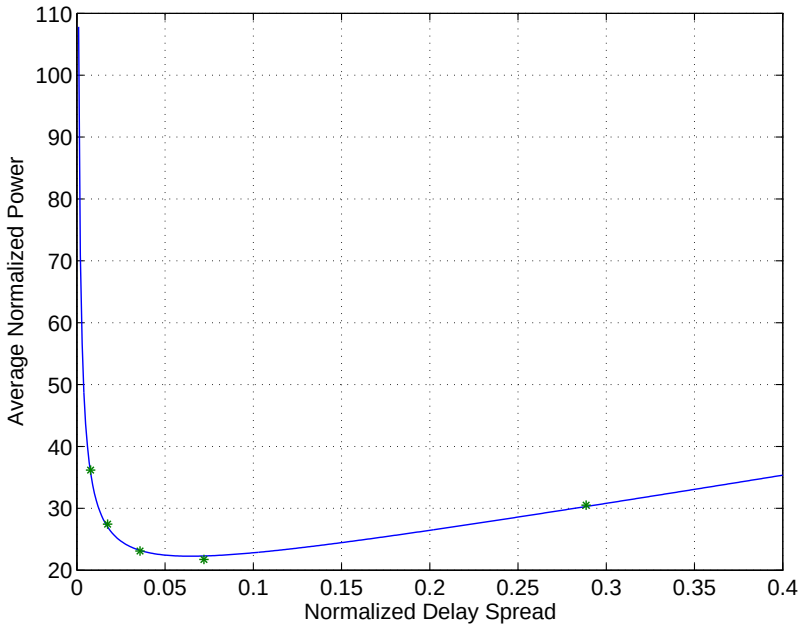

Figure 3.12: Cyclic-prefix-normalized average power as a function of RMS delay spread under uniform power delay profile. $N = 64, K = 64$**.**

Practical consideration

In practice, cyclic prefix needs to be added to remove the effect of ICI and ISI. In this section, the work in previous subsection will be modified to take this effect into consideration.

When cyclic prefix is added in the OFDM symbol, the average transmit power has to be adjusted by $(1 + J/N)$. After this normalization to compensate for the extra bandwidth used, the average transmit power in Figure 3.9 is re-plotted against the power delay spread in Figure 3.12. It can be seen that the normalized transmit power achieves the minimum value 22.2640 at the point of $D_\tau^{(2)} = 0.0650$.

3.4.3 Conclusion

Our results show that for a given multipath channel, the amount of gain achievable through subcarrier-and-bit allocation increases with the instantaneous SFM of the channel and the RMS delay spread. We have shown that there is a clear relationship between the optimal total power and the channel delay spread as well as the SFM, as indicated by (3.20). Hence we provide a quantitative justification on the potential performance gain achievable through exploiting the multiuser diversity. Furthermore, our approach could be useful for the investigations on the achievable gain in the CDD OFDM system.

3.5 Cross Layer Design

Past research has been focused on segregated design, e.g., how to reduce the bit error rate of data transmission to optimize the physical layer performance or how to use admission control to regulate the traffic in order that the QoS requirements such as packet loss probability and maximum delay are fulfilled separately. These motivations have brought about many novel techniques for performance optimization on either physical layer or network layer. Yet NextG systems vision for flexible transmission adapted to the wireless link and traffic loads, the optimization of system performance needs to take account of different layer performance metrics jointly. The reason is easily understood– momentarily long unreliable transmission period in physical layer may result in an intolerable delay on the network layer and thus violate the QoS requirements, but this will not be reflected if only average capacity

is given to the network layer. Besides, fairness is another network layer issue that is easily ignored by the single layer approaches, since optimal spectrum allocations tend to assign spectrum to those users who are in favorable transmission conditions, thus some users may not get any chance for transmission in their durations of deep fades. Therefore, only joint optimization across different layers could make the best of the system resources to meet service requirements in the scenario of changing environments. The approach enables joint considerations of the statistical behavior of all the performance metrics at different layers, so as to avoid the momentarily QoS dissatisfaction by over-admitting of users or the resources waste by under-admitting of users.

There have been many reports on cross layer schemes which involves different layers. Some techniques focus on creating new interfaces between layers, while some realize the joint design by layer couplings, i.e., taking the other layers' parameters during the design process of the current layer. In [83], a rate-adaptive MAC protocol was proposed to allow various rates adapted to the channel condition in high-rate wireless personal area network. The data rate for the next transmission is selected according to the channel prediction based on the current frame and are informed to the sender by some acknowledgement frame. Therefore, the system throughput is greatly improved compared to the traditional MAC protocol without rate adaptivity. Other work on adaptive modulations in the multiuser environment can be also found in [84] where transmission power and constellation sizes are chosen adaptively according to the buffer and channel conditions. Most recent research in cross layer design can refer to [85] [86].

In our thesis, the two important issues, i.e., power control schemes in DS-CDMA systems and subcarrier-and-bit allocation in multiuser OFDM systems are addressed, and they can be simple examples of cross layer design. For the power control proposals which will be presented in Chapter 4, the factors such as delay, throughput, capacity in network layer, retransmission rate, outage probability in data link layer, and SIR, BER in physical layer are considered jointly. Moreover, the defined power control profiles involve the knowledge of user locations, which could be obtained from network or through the measurement at physical layer. In subcarrier-and-bit allocation algorithms, in the MAC layer, the system should decide how to assign subcarriers to different users according to the instantaneous channel conditions seen by each user; while in the physical layer, the decisions of how many bits should be assigned on each subcarrier are made.

3.6 Cognitive Radio

This section is related to the second approach to improve the spectrum utilization through dynamic spectrum allocation, as mentioned previously in Chapter 1.

Typical channel measurements are performed in some locations, and the results indicate low utilization in some of the frequency bands over the investigated spectrum. This conclusion is also recognized by FCC's Spectrum Policy Task Force in their report [87]. Cognitive radios aim to introduce secondary users (of lower priority) into the spectrum which has been allocated to primary users. In a certain way, secondary users can make use of frequency bands which are not occupied by

primary users (also known as "white space") for transmission and these frequency bands are assigned in a dynamic way. By doing this, we hope to achieve better spectrum access and utilization. As defined in [88], cognitive radio is an intelligent wireless communication system that is aware of its environment and uses the methodology of understanding-by-building to learn from the environment and adapt to statistical variations in the input stimuli, with two primary objectives in mind: (a) highly reliable communication whenever and wherever needed; (b) efficient utilization of the radio spectrum. Software-defined radio (SDR), which will be introduced next, is the enabling technology of the cognitive radio. In this section, the concept of SDR is described first, and then the major techniques involved in cognitive radio are explained.

3.6.1 Software-Defined Radio

With the coexistence of multiple networks and multiple access schemes in the current and future mobile wireless communications, service providers and network users need to adjust themselves in order to have seamless network access even if the communication standards and frequency bands of different communication networks vary. One solution is to simultaneously provide different infrastructures for different networks and standards. This is direct but it will bring a great waste of equipments. The other possible way is to embed the standard specifications and relevant techniques on software. Software-Defined Radio (SDR) is the technology capable of flexible changing of frequencies and communication methods by software. The main technical prospective of SDR is a versatile reconfigurable platform

providing interoperability. Whichever service is on request, the corresponding software modules will be loaded to the platform. Yet all the processing is transparent to the users.

To achieve service and application adaptation, distributed intelligence is the best stake such that every wireless element can control how best to use its resources. To this end, the highly adaptive physical layer and joint optimization together with other layers, e.g., MAC, make it possible to adjust the transmission techniques to meet different QoS requirements of service categories and users as the traffic density and channel conditions change.

Besides, advanced digital signal processing (DSP) and field programmable gate array (FPGA) technologies are essentials to design general-purpose programmable devices. Radio frequency (RF) and intermediate frequency (IF) processing techniques are also key techniques enabling software-defined radio (SDR).

3.6.2 Major Progress of Cognitive Radio

Since cognitive radio aims at providing highly reliable and highly efficient radio communications, there are several main tasks to complete. Firstly, the system should obtain the relevant transmission environment, identifying the noise and interference in the multiuser scenario. Secondly, channel estimations are needed to provide knowledge about the wireless channels. Besides, effective measures have to be employed to detect the spectrum holes, in order that the users are aware of the available resources. Furthermore, the transmit power control and dynamic spectrum management are the necessary techniques to optimize the resource allocation

based on the traffic loads, QoS needs, market price, channel conditions and other factors.

Specifically, there are many system level implementation challenges in the design of cognitive radios. A very good summary on this can be found in [88]. In general, each secondary user has to sense its channel over the defined spectrum and use this information to opportunistically obtain frequency bands which can meet its own requirements, either in terms of capacity or performance. Some of the proposed spectrum sensing techniques can be found in [89]. In [90], an adaptive radio which exploits the unused frequency bands for transmission was proposed. Design aspects to maintain the transmission quality in a changing environment and to minimize interference to surrounding systems were discussed. The performance of a cognitive radio which uses a notch filter, so that its signal spectral excludes the used frequency bands, was studied in [91]. A simple testbed has also been reported in [92], where an adaptive controller module with genetic algorithm is built to select the optimized radio frequency band to operate on. In [93], a concept to change the radio parameters of a cognitive radio based on learning was suggested.

In most of these reported works, point to point radio link is considered. There are two ways the unused frequency band can be used for transmission: either the user hops from one spectrum (which is unused) to another with the signal bandwidth remains unchanged [94], or it transmits in all unused frequency bands through waveform shaping [91] [94]. These discussed systems are generally distributed, i.e., each transmission pair only concerns their surroundings primary users and interferers during decision making [95]. For these systems, the inter-

ference from the surrounding transmission pairs could be obtained, for example, through the use of beacon transmissions [96].

In Chapter 7, a simple treatment of cognitive radio is studied and some preliminary results are presented. We propose a *centralized model*, where a powerful base station can reconfigure itself to support communications with secondary users of different transmission technologies and dynamically assign their transmission frequency, assuming the channel state information is correctly fed back to the transmitter. We set up a nonlinear binary integer programming model to optimally allocate frequency bands to all users, both in the presence or absence of primary users. We then convert it to a quadratic integer programming problem with linear constraints to compute the optimal solution. Finally, a suboptimal heuristic approach is proposed.

3.7 Summary and Contribution

In this chapter, the key techniques to enable high performance physical layer were discussed and some of the contributions were presented. Firstly, the development of coded modulations was reviewed, and especial focus was given on turbo coded modulation. The SNR sensitivity of turbo detector with high order constellations was examined to study the accuracy the channel estimations needed to obtain for an effective turbo detector. The tolerance range for the SNR mismatch was shown to become narrower as the constellation order increases. Thus, it is recommended to apply more accurate channel estimations for the turbo codes combined with

higher order constellations.

In the multiuser environment, in order to enhance the capacity of the CDMA systems, the power control schemes have to be employed. In our discussions, the power control schemes were classified and the major literatures were reviewed. Our focus on the work of power control was illustrated and the proposed power control profile was highlighted. The scheme and its results will be unfolded in the later chapter.

In the sequel, an overview for adaptive subcarrier-and-bit allocation in OFDM and MC-DS-CDMA systems was given and the spectral flatness measurement (SFM) was investigated as a way to quantify the diversity gains attainable for the adaptive subcarrier-and-bit allocations schemes. The relationships between the performance gain and the channel parameters, e.g. SFM, RMS delay spread and subcarrier correlation coefficients, were finally quantified in Eq. (3.17)-(3.20).

Finally, more advanced techniques such as cross layer design were also discussed which needs the cooperation from the different transmission layers. Cognitive radio is likely to be a feature of NextG, as it enables the adaptive spectrum allocation across multiple radio systems. A simple model of cognitive radio was presented in Chapter 7 as the extension of the subcarrier-and-bit allocation problems in OFDM and CDMA systems.

Chapter 4

Constrained Power Control Scheme for DS-CDMA Systems

As reviewed in the last chapter, power control is a necessity in DS-CDMA systems to overcome the near-far effect and to enhance the system capacity. In this chapter, we propose a constrained power control scheme aiming to increase the number of users that can be supported (so-called user capacity) by slotted DS-CDMA cellular systems. In the proposed scheme, a power constraint is imposed on the transmitters of data users, while voice users are adopting the conventional power control scheme. We show that with such power range constraint, although it may result in some retransmissions when users are close to the cell boundary, the reduction in interference is more likely to increase the overall user capacity. For given delay and outage probability requirements, we study the effects of such a constrained power control scheme on the user capacity of a DS-CDMA system, when compared to the system in which both types of users are subject to conventional power control.

A few possible power control profiles are suggested and comparisons in achievable capacity are made.

Another contribution of this work is in deriving a distribution model for the total received power from voice and data users under imperfect power control. In the conventional power control scheme, the total received power, including the desired signal and the total interference, from both services under imperfect power control can be modeled by a log-normal distribution [97] [98]. However, the validity of this log-normal model for the total received power is in question when a constraint is imposed on the transmit power. Firstly, we evaluate the distribution of a sum of the received power with constraint theoretically and testify the result through simulations. In addition, we also derive new and general expressions for the the ratio of average inter-cell interference to intra-cell interference, the so-called interference correction factor for cellular systems employing the constrained power control scheme. The new formulae for the interference correction factor is then used to derive the PDF of the SIR for voice and data users, which can be used to analyze the user capacity subject to constrained power control. In addition, the retransmission rate is successfully introduced to the evaluation of outage probability and thus enables the theoretical solution.

This chapter is organized as follows. In Section 4.1, the model for a DS-CDMA system supporting voice and data services is presented. In Section 4.2, we derive the interference correction factor for various constrained power control profiles. In Section 4.3, we evaluate the PDF of the SIR for voice and data users. In Section 4.4, simulation and analytical results on the performance of the proposed power

control scheme are presented and compared with the conventional scheme. Effects of different power range constraints on the overall user capacity are also studied and highlighted. Concluding remarks are drawn in Section 4.5.

4.1 Power Control and System Model

We consider a slotted packet DS-CDMA cellular system in the uplink, where the data signal is spread over the entire system bandwidth. Next, we describe our proposed power control scheme for a system supporting voice/data services.

4.1.1 Proposed Constrained Power Control Scheme

To compensate for the path loss, the conventional power control scheme is applied to all voice users. The transmitted power of the voice users follows

$$P_{T_v}(r) = S_P r^{\beta} \tag{4.1}$$

where S_P is the constant power received at the base station from each mobile user under perfect power control. r is the distance from the mobile to the base station. β is the path-loss exponent, which has the value of 2 in free space and between 3 and 5 for celluar mobile radio systems.

A power constraint is imposed on all data users, as shown in Figure 4.1. Data users located at $0 < r < r_{max}$ are subject to the power control profile associated with (4.1), where r_{max} is a range constraint to be chosen appropriately. For data users located outside the circle of $r = r_{max}$, i.e. $r > r_{max}$, a constraint is imposed on the transmitted power. We propose to use a parameter δ as the profile index

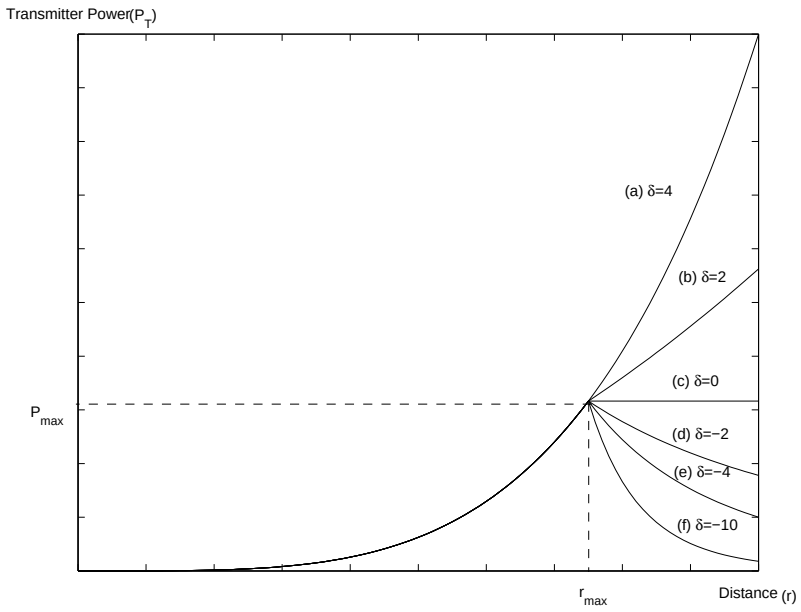

Figure 4.1: Proposed constrained power control scheme with various profile index δ. $\beta = 4$.

to describe the transmitted power profile. In this case, the transmitted power of a data user is a function of the distance r, r_{max} and δ,

$$P_{T_d}(r) = \begin{cases} S_P r^{\beta}, & 0 < r \leq r_{max} \\ P_{max}\left(\frac{r}{r_{max}}\right)^{\delta}, & r_{max} < r \leq R_{eq} \end{cases} \tag{4.2}$$

where $\delta \leq \beta$. The profile with $\delta = \beta$ corresponds to the conventional power control (see curve (a) in Figure 4.1). While with $\delta = 0$, the transmitted power of the data users beyond r_{max} is kept to the maximum value of P_{max}. In our following discussion, five values of $\delta = 2, 0, -2, -4, -10$ will be considered. The power control profiles associated with these values are displayed as curves b, c, d, e, f in Figure 4.1, respectively, for $\beta = 4$.

The received power at the desired base station from a mobile user located at

a distance r is modeled as

$$P_R(r) = P_T(r)\, r^{-\beta} \tag{4.3}$$

Due to imperfect power control, we assume that the received power at the base station from each user is a log-normal process [99]. Using (4.3), and taking account of the power control error, the received power at the base station is

$$P_R(r) = P_T(r) r^{-\beta} 10^{\xi/10} \tag{4.4}$$

where ξ is a zero-mean Gaussian random variable which models the power control error.

The conventional power control strategy is just a special case of (4.2) with $r_{max} = R_{eq}$, where the transmitted power of both voice and data users equals to

$$P_T(r) = S_P r^{\beta} \tag{4.5}$$

4.1.2 System Model and Capacity Evaluation

We consider the reverse link of a slotted DS-CDMA system supporting n_v voice users and n_d data users within each cell, where each user is allowed to transmit packets only at slotted time instants. In our system, the transmission time is divided into slots with duration equal to the transmission time of a packet. Voice and data packets are assumed to have the same fixed packet length. Each service is to meet its own BER or delay requirements. To meet certain BER requirements, a user must have a minimum SIR of $SIR_{th} = (E_b/N_0)_{th}/Q$ before correlation [99], where $(E_b/N_0)_{th}$ can be either $(E_b/N_0)_{th_v}$ (for voice service) or $(E_b/N_0)_{th_d}$ (for data

service). The processing gain Q of voice and data services are denoted by Q_v and Q_d, respectively.

Traffic Models

Assuming that each voice user generates an exponential ON-OFF traffic, the probability that k_v packets are generated by n_v voice users, denoted by $p_1(k_v)$, is described by the binomial distribution

$$p_1(k_v) = \binom{n_v}{k_v} \alpha_v^{k_v} (1-\alpha_v)^{n_v - k_v} \tag{4.6}$$

where α_v is the voice activity factor. For simplicity, we assume that the data packet arrivals follow a Poisson process. Let α_d denote the activity factor of the data users. The probability that k_d data packets are transmitted by n_d data users, $p_2(k_d)$, is described by

$$p_2(k_d) = \binom{n_d}{k_d} \alpha_d^{k_d} (1-\alpha_d)^{n_d - k_d} \tag{4.7}$$

Note here the data activity factor α_d includes the effect of retransmission, as will be illustrated soon. Assuming each data user generates a sequence of fixed-length packets containing L_d symbols. The average arrival rate of the newly generated data packets, λ_d, is related to α_d as [100],

$$\alpha_d = \frac{\lambda_d L_d Q_d}{R_c(1-p_{r_d})} \tag{4.8}$$

where R_c is the common chip rate of all voice and data users in the CDMA system, and p_{r_d} denotes the retransmission probability of data users.

We assume that all erroneous data packets are retransmitted until they are received correctly. We also assume perfect interleaving such that each user's activity

factor is independent from symbol to symbol. The retransmission probability p_{r_d} is,

$$p_{r_d} = 1 - (1 - p_{e_d})^{L_d} \tag{4.9}$$

where p_{e_d} is the BER of data users.

BER of Data Users and Outage Probability of Voice Users

The BER curve decays monotonically with the increase in SIR. For many modulation and coding schemes, the BER can be approximated by the expectation of an exponential function of SIR,

$$p_{e_d} = \mathrm{E}_{SIR_d}\{\Theta(SIR_d)\} = \mathrm{E}_{SIR_d}\left\{\kappa e^{-\rho SIR_d}\right\} \tag{4.10}$$

The function $\Theta(\cdot)$, or the parameters κ and ρ, are determined by the coding scheme used in the data traffic. Note that the choice of $\Theta(\cdot)$ does not influence our analytical results. The expectation in (4.10) is derived with respect to the distribution of the SIR for the data user, SIR_d.

Given i voice users and j data users, the probabilities of packet failure for voice users and data users are, respectively, evaluated as

$$p_{f_v}(i,j) = \Pr(SIR_v \leq \Psi_v) \tag{4.11}$$

$$p_{f_d}(i,j) = \Pr(SIR_d \leq \Psi_d) \tag{4.12}$$

where $\Psi_v = (1/Q_v)(E_b/N_0)_{thv}$ and $\Psi_d = (1/Q_d)(E_b/N_0)_{thd}$ are, respectively, the SIR threshold for voice and data users. The expressions for SIR_v and SIR_d will

be given shortly. The average outage probability of voice users is evaluated as

$$P_{out_v} = \sum_{i=1}^{n_v} \sum_{j=0}^{n_d} p_{fv}(i,j) p_1(i) p_2(j) \tag{4.13}$$

In Section 4.2, the analytical PDF of SIR_v and SIR_d are evaluated. Let D denote the average delay for the data service, with D_{th} as its delay threshold. For voice service, we assume retransmission is not allowed, and there is no delay. The user capacity C with the requirements of $P_{out_v} \leq 0.01$ and $D \leq D_{th}$ is defined as the maximum number of voice and data users that can be supported by the system,

$$C = \{\max(n_v, n_d) | P_{out_v} \leq 0.01, D \leq D_{th}\} = \{(n_v^*, n_d^*)\} \tag{4.14}$$

Note that n_d^* depends on λ_d for a given n_v^* when we calculate C.

Delay and Throughput of Data Users

In the event that a data packet is lost due to packet failure or outage, the mean of the retransmission delay, which depends on the retransmission scheme, is given by [100],

$$\mathrm{E}(\tau) = \frac{1}{1 - p_{r_d}} \tag{4.15}$$

The average data delay, D, is defined as the average time between the generation and successful reception of a data packet. It can be expressed as [101],

$$D = 1.5 + \left[\frac{T}{U} - 1\right] (\lfloor \mathrm{E}(\tau) + 1 \rfloor + 1) \tag{4.16}$$

where U is the data throughput and $T = \alpha_d \, n_d$ is the offered data traffic including retransmissions, $\lfloor x \rfloor$ represents the nearest integer less than or equal to x. The delay in (4.16) has been normalized to the packet interval.

With n_v active voice users and n_d active data users in a cell, the average number of data bits that is successfully transmitted per second, i.e., the overall data throughput U is

$$U = \sum_{j=1}^{n_d} j[1 - \bar{p}_{fd}(j)]p_2(j) \tag{4.17}$$

where

$$\bar{p}_{fd}(j) = \sum_{i=0}^{n_v} p_{fd}(i,j)p_1(i), \tag{4.18}$$

and $p_2(j)$ is the probability of j data packets transmitted by n_d data users, as described in Eq. (4.7).

Interference Correction Factor

The overall capacity of a CDMA system is limited by multi-user interference which composes of both inter-cell and intra-cell interferences. Consider a hexagonal cell shape cellular CDMA system. We want to evaluate the average total interference received at the desired base station from all adjacent cell tiers. The interference correction factor F_m, is defined as the ratio of the average total interference power received from the outer cells (I_{oc}) to the average total interference power generated by users in the home cell (I_h),

$$F_m \hat{=} \frac{I_{oc}}{I_h} = \frac{I_{oc}}{(N_u - 1)S_P} \tag{4.19}$$

where N_u is the number of users per cell, and S_P is the constant received power from a user with perfect power control. The I_{oc} depends on the path loss exponent β and the number of cell tiers. Under the assumption that there is a large number of users ($N_u \gg 1$), and all users are uniformly distributed, the ratio F_m is a

constant because I_{oc} is proportional to N_u. The result of $F_m = 0.326$ has been found analytically for the channels without shadowing and confirmed by the results presented in [99]. However, for our proposed constrained power control scheme, this value of $F_m = 0.326$ is no longer valid, and as far as we know, no result has been published on this topic. In the following section, by considering several number of cell tiers around the home cell, we derive new formulae for the interference correction factor F_m as a function of the path loss exponent β and as well as the constrained profile index δ (for the constrained power control).

Evaluation of SIR for Voice and Data Services

If k_v out of n_v voice users and k_d out of n_d data users are active, the total number of busy channels at time instance t is given by $k_v + k_d$. The total received power at the base station is given by

$$S_t = \sum_{i=1}^{k_v} S_{v,i} + \sum_{j=1}^{k_d} S_{d,j} \tag{4.20}$$

where $S_{v,i}$ is the received signal from i^{th} voice user and $S_{d,j}$ is the received signal from j^{th} data user. Each of the $S_{v,i}$ and $S_{d,j}$ is log-normally distributed.

For a voice user, the SIR at the base station is

$$\begin{aligned} SIR_v &= \frac{S_{v,i}}{I_h + I_{oc} + n_0} \\ &\approx \frac{S_{v,i}}{I_h\,(1 + F_m)} \\ &= \frac{S_{v,i}}{I_{h_v}\,(1 + F_{m_v}) + I_{h_d}\,(1 + F_{m_d})} \end{aligned} \tag{4.21}$$

where F_{m_v} and F_{m_d} stand for the interference correction factor for voice users and data users, respectively. n_0 denotes the AWGN. We assume that the AWGN is

negligible in our analysis. Similarly, for a data user, the SIR is

$$\begin{aligned} SIR_d &= \frac{S_{d,i}}{I_h + I_{oc} + n_0} \\ &\approx \frac{S_{d,i}}{I'_{h_v}(1 + F_{m_v}) + I'_{h_d}(1 + F_{m_d})} \end{aligned} \tag{4.22}$$

The interference from the voice and data users has to be computed separately for our proposed constrained power control scheme. In the next two sections, we derive new expressions for: (i) the interference correction factor F_m by assuming perfect power control and (ii) the PDF of the SIR for both voice and data services by considering imperfect power control. These analytical results are new and will be used to compute outage probabilities given in (4.11) and (4.12) for a multi-service system subject to constrained power control.

4.2 Evaluation of Interference Correction Factor F_m

Our objective is to derive analytical expression of F_m. For analytical simplicity, the hexagonal grid cellular structure is approximated by circular cellular structure, where each cell is approximated by a circle of radius R_{eq}. The transmitted power of each mobile user in the home cell H and its neighboring cell O is controlled by the respective base station. We assume perfect power control, i.e., no power control error is considered.

By assuming that N_u users are uniformly distributed in a circular cell of radius

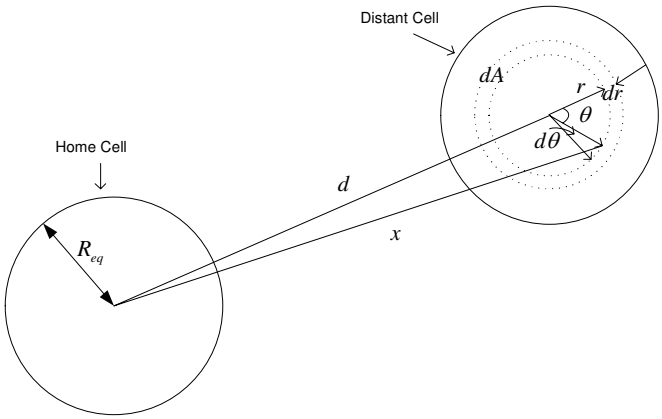

Figure 4.2: Interference from mobile terminals in a distant cell.

R_{eq}, the density of mobile users η is,

$$\eta = \frac{N_u}{\pi R_{eq}^2} \tag{4.23}$$

By referring to Figure 4.2, the total average received interference power at the desired base station, denoted by $S_{RB}(d)$, from mobile users in another cell at distance d from the desired base station, can be obtained by averaging the received signal over the cell area A

$$S_{RB}(d) = \int_A P_T(r) x^{-\beta} \eta \, \mathrm{d}A \tag{4.24}$$

where $P_T(r)$ is the transmitted power of the mobile users and

$$x = \sqrt{d^2 + r^2 + 2dr\cos\theta} \tag{4.25}$$

4.2.1 Computation of Data User's F_m for the Proposed Scheme in Terms of r_{max}

With the proposed power control scheme, the radius r_{max} divides the cell into two regions as shown in Figure 4.3, where the transmitted power of data users, P_{T_d},

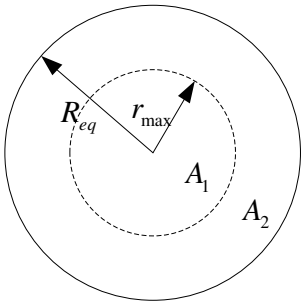

Figure 4.3: A cell coverage area with two power control regions divided by a range constraint r_{max}.

follows two separate rules. According to Figure 4.1 and Eq. (4.2), if the user is located within region A_1, i.e., $r \leq r_{max}$, P_{T_d} follows the conventional power control profile which is dependent on the path loss exponent β. If the user is in region A_2, P_{T_d} is dependent on δ and β.

Average Interference Power from Other Cells

Since the transmitted power is a function of the distance r, the average power can be evaluated by averaging the $P_{T_d}(r)$ over these two regions divided by r_{max}. By integrating $P_{T_d}(r)$ over r, the average received interference power from mobile data users in another outer cell can be evaluated as

$$\begin{aligned} S_{RB}(d) &= \frac{2\,n_d\,S_P}{\pi R_{eq}^2}\left[\int_0^{r_{max}} r^{\beta+1}\mathrm{d}r \int_0^{\pi} \frac{\mathrm{d}\theta}{(d^2+r^2+2dr\cos\theta)^{\beta/2}}\right. \\ &\quad \left. + \int_{r_{max}}^{R_{eq}} r_{max}^{\beta-\delta} r^{\delta+1}\mathrm{d}r \int_0^{\pi} \frac{\mathrm{d}\theta}{(d^2+r^2+2dr\cos\theta)^{\beta/2}}\right] \end{aligned} \tag{4.26}$$

where n_d is the number of data users per cell. From (4.26), we obtain a closed form expression for the average interference power for $\beta = 4$,

$$\begin{aligned} S_{RB}(d) &= n_d S_P \left\{ \frac{4}{L_3} \ln\left(\frac{L_1}{L_1-1}\right) - \frac{4L_1^2 - 6L_1 + 1}{L_2(L_1-1)^2} + \right. \\ &+ \frac{2}{L_1 L_2} \left[\frac{L_3 L_2^{\frac{\delta}{2}}}{2+\delta} H\left(1+\frac{\delta}{2}, 3, 2+\frac{\delta}{2}, \frac{R_{eq}^2}{d^2}\right) \right. \\ &+ \frac{L_3^2 L_2^{\frac{\delta}{2}}}{4+\delta} H\left(2+\frac{\delta}{2}, 3, 3+\frac{\delta}{2}, \frac{R_{eq}^2}{d^2}\right) \\ &- \frac{1}{L_1(2+\delta)} H\left(1+\frac{\delta}{2}, 3, 2+\frac{\delta}{2}, \frac{r_{max}^2}{d^2}\right) \\ &\left. \left. - \frac{1}{L_1^2(4+\delta)} H\left(2+\frac{\delta}{2}, 3, 3+\frac{\delta}{2}, \frac{r_{max}^2}{d^2}\right) \right] \right\} \end{aligned} \tag{4.27}$$

where

$$H(a,b,c,z) = \sum_{k=0}^{\infty} \frac{a_k b_k z^k}{c_k k!} \tag{4.28}$$

is the hypergeometric function, and

$$a_k = \begin{cases} 1, & k = 0 \\ a(1+a)(2+a)\ldots(k-1+a), & k \geq 1 \end{cases} \tag{4.29}$$

$$L_1 = \left(\frac{d}{r_{max}}\right)^2; \quad L_2 = \left(\frac{R_{eq}}{r_{max}}\right)^2; \quad L_3 = \left(\frac{R_{eq}}{d}\right)^2 \tag{4.30}$$

For individual values of δ, simple expressions can be found. For example, for $\delta = 2$, (4.27) is reduced to

$$\begin{aligned} S_{RB}(d) &= \frac{4\, n_d\, S_P}{L_3} \ln\left(\frac{L_1}{L_1-1}\right) - \frac{n_d\, S_P}{L_2} \left[\frac{4L_1^2 - 6L_1 + 1}{(L_1-1)^2} \right. \\ &\left. + \frac{(L_2-1)(3L_3 + L_1 - 2L_2 - 2)}{(1-L_3)^2(L_1-1)^2} + \ln\left(\frac{L_1 - L_2}{L_1 - 1}\right) \right] \end{aligned} \tag{4.31}$$

For a given cell, we refer to the cells immediately contiguous to it as tier-1 cells, and those contiguous to tier-1 cells as tier-2 cells, and so on. Assuming each

CDMA cell has N_u active mobile terminals, the total interference power from outer cells is the sum of the power from mobiles within the cells of every tier. From the hexagonal cellular geometry, the n^{th} tier consists of $6n$ cells. Let the distance from the base station of a n^{th} tier cell to that of the home cell be denoted by $x_{n,i}$, where $i = 1, 2, \ldots, n$. It can be shown that $x_{n,i} = 2R_{eq}\sqrt{n^2 + i^2 - ni}$.

The total interference from other cells, I_{oc}, can be derived as,

$$I_{oc} = \sum_{n=1}^{\infty}\sum_{i=1}^{n} 6S_{RB}(2R_{eq}\sqrt{n^2 + i^2 - ni}) \tag{4.32}$$

By defining

$$d_{n,i} = 4(n^2 + i^2 - ni) = \left(\frac{x_{n,i}}{R_{eq}}\right)^2 \tag{4.33}$$

and using (4.30)-(4.41), the I_{oc} for power control scheme with $\beta = 4, \delta = 2$ can be expressed as a function of L and $d_{n,i}$.

$$\begin{aligned} I_{oc} &= \sum_{n=1}^{\infty}\sum_{i=1}^{n} 6\, n_d\, S_P \left\{ 4d_{n,i} \ln\left(\frac{Ld_{n,i}}{Ld_{n,i}-1}\right) - \frac{1}{L}\left[\frac{4L^2d_{n,i}^2 - 6Ld_{n,i} + 1}{(Ld_{n,i}-1)^2}\right.\right. \\ &\quad \left.\left. + \frac{(L-1)\left(3 + Ld_{n,i}^2 - 2Ld_{n,i} - 2d_{n,i}\right) d_{n,i}}{(d_{n,i}-1)^2 (Ld_{n,i}-1)^2} + \ln\left(\frac{Ld_{n,i}-L}{Ld_{n,i}-1}\right)\right]\right\} \\ &= \sum_{n=1}^{\infty}\sum_{i=1}^{n} 6\, n_d\, S_P\, G_{\delta=2}\,(L, d_{n,i}) \end{aligned} \tag{4.34}$$

where

$$L = L_2 = \left(\frac{R_{eq}}{r_{max}}\right)^2 \tag{4.35}$$

$$\begin{aligned} G_{\delta=2}\,(L, d_{n,i}) &= 4d_{n,i} \ln\left(\frac{Ld_{n,i}}{Ld_{n,i}-1}\right) - \frac{1}{L}\left[\frac{4L^2d_{n,i}^2 - 6Ld_{n,i} + 1}{(Ld_{n,i}-1)^2}\right. \\ &\quad \left. + \frac{(L-1)\left(3 + Ld_{n,i}^2 - 2Ld_{n,i} - 2d_{n,i}\right) d_{n,i}}{(d_{n,i}-1)^2 (Ld_{n,i}-1)^2} + \ln\left(\frac{Ld_{n,i}-L}{Ld_{n,i}-1}\right)\right] \end{aligned} \tag{4.36}$$

Average Interference Power from Home Cell

The average interference power from the home cell is the sum of the average transmitted power from other data users in the desired cell,

$$\begin{aligned} I_h &= \frac{n_d - 1}{\pi R_{eq}^2}\left[\int_0^{2\pi}\int_0^{r_{max}} S_P r^{\beta} r^{-\beta} r \mathrm{d}r\mathrm{d}\theta + \int_0^{2\pi}\int_{r_{max}}^{R_{eq}} S_P \left(\frac{r_{max}}{r}\right)^{\beta-\delta} r\mathrm{d}r\mathrm{d}\theta\right] \\ &= \frac{(n_d-1)\,S_P}{(\delta-\beta+2)L}\left(\delta-\beta+2L^{\frac{\delta-\beta+2}{2}}\right) \end{aligned} \tag{4.37}$$

For the special case of $\delta = 2, \beta = 4$, we have

$$\begin{aligned} I_h &= \lim_{\delta-\beta\to-2} \frac{(n_d-1)\,S_P}{(\delta-\beta+2)L}\left(\delta-\beta+2L^{\frac{\delta-\beta+2}{2}}\right) \\ &= \frac{(n_d-1)\,S_P}{L}\left(1+\ln L\right) \end{aligned} \tag{4.38}$$

where $\lim_{\delta-\beta\to-2}(\cdot)$ denotes the limit as $\delta-\beta$ approaches -2.

Hence, the interference correction factor of data users for this case is,

$$\begin{aligned} F_{m_d} &= \frac{I_{oc}}{I_h} \\ &= \frac{\sum_{n=1}^{\infty}\sum_{i=1}^{n} 6\,n_d\,S_P\,L\,G_{\delta=2}\left(L,d_{n,i}\right)}{(n_d-1)\,S_P\left(1+\ln L\right)} \\ &= \frac{6L}{1+\ln L}\sum_{n=1}^{\infty}\sum_{i=1}^{n} G_{\delta=2}\left(L,d_{n,i}\right) \end{aligned} \tag{4.39}$$

where (4.39) is valid for $n_d \gg 1$.

The corresponding expressions for the F_{m_d} for various power control profiles associated with different δ can be derived similarly. New expressions of F_{m_d} with $\beta = 4$ are tabulated in Table 4.1, and the expressions of $G\left(L,d_{n,i}\right)$ for different δ are given in Appendix II. By substituting (4.33) and (4.35) into the equations listed in Table 4.1, the F_{m_d} can be calculated numerically and the results are tabulated in Table 4.2, for two examples of $r_{max}/R_{eq} = 0.5$ and 0.75.

Table 4.1: Expressions for Interference Correction Factor of Data Users (F_{m_d}) as a Function of δ, $\beta = 4$.

δ	F_{m_d}
2	$\frac{6L}{1+\ln L}\sum_{n=1}^{\infty}\sum_{i=1}^{n} G_{\delta=2}\left(L, d_{n,i}\right)$
0	$\frac{6}{2L^{-1}-L^{-2}}\sum_{n=1}^{\infty}\sum_{i=1}^{n} G_{\delta=0}\left(L, d_{n,i}\right)$
-2	$\frac{12}{3L^{-1}-L^{-3}}\sum_{n=1}^{\infty}\sum_{i=1}^{n} G_{\delta=-2}\left(L, d_{n,i}\right)$
-4	$\frac{18}{4L^{-1}-L^{-4}}\sum_{n=1}^{\infty}\sum_{i=1}^{n} G_{\delta=-4}\left(L, d_{n,i}\right)$
-10	$\frac{36}{7L^{-1}-L^{-7}}\sum_{n=1}^{\infty}\sum_{i=1}^{n} G_{\delta=-10}\left(L, d_{n,i}\right)$

Table 4.2: Values of Interference Correction Factor of Data Users (F_{m_d}) as Function of r_{max}/R_{eq}, $\beta = 4$.

δ	$r_{max}/R_{eq} = 0.5$	$r_{max}/R_{eq} = 0.75$
2	0.1881	0.2679
0	0.0998	0.2222
-2	0.0552	0.1875
-4	0.0349	0.1618
-10	0.0187	0.1189

4.2.2 Interference Correction Factor for Conventional Power Control

When $r_{max}/R_{eq} = 1$ and $\delta = 4$, Eq. (4.27) can be reduced to

$$S_{RB}(d) = 2N_u S_P \left[2k^2 \ln\left(\frac{k^2}{k^2-1}\right) - \frac{4k^4 - 6k^2 + 1}{2(k^2-1)^2}\right] \tag{4.40}$$

where $k = d/R_{eq}$.

Therefore the total interference power from other cells for the conventional power control is,

$$\begin{aligned} I_{oc} &= \sum_{n=1}^{\infty}\sum_{i=1}^{n} 6S_{RB}(2R_{eq}\sqrt{n^2+i^2-ni}) \\ &= 12NS_P \sum_{n=1}^{\infty}\sum_{i=1}^{n} G(d_{n,i}) \end{aligned} \tag{4.41}$$

where

$$G(d_{n,i}) = 2d_{n,i} \ln\left(\frac{d_{n,i}}{d_{n,i}-1}\right) - \frac{4d_{n,i}^2 - 6d_{n,i} + 1}{2(d_{n,i}-1)^2} \tag{4.42}$$

Using (4.19), (4.42) and (4.41), we obtain the known result for the interference correction factor for the conventional power control for $\beta = 4$,

$$F_m = 12 \sum_{n=1}^{\infty}\sum_{i=1}^{n} G\left(d_{n,i}\right) \tag{4.43}$$

In Table 4.3, we tabulate the numerical values for the interference correction factor F_m and the path loss exponent β, by considering various number of cell tiers around the home cell. Note that the interference correction factor for both services is the same for the conventional power control. For $\beta = 4$, no significant difference was found between the numerical values for F_m when more than 10 cell tiers are considered. This is because larger β causes interference from the outer cells to

Table 4.3: Values of Interference Correction Factor F_m as a Function of Path Loss Exponent β.

No. of tiers	$\beta = 2$	$\beta = 3$	$\beta = 4$	$\beta = 5$
1	0.904	0.471	0.284	0.191
2	1.365	0.579	0.312	0.199
3	1.669	0.625	0.319	0.200
5	2.079	0.667	0.323	0.201
10	2.665	0.701	0.326	0.201
15	3.018	0.714	0.326	0.201

decrease more rapidly with the increase in number of cell tiers. In cases where 10 or 15 tiers are considered, the F_m converges to 0.326 for a hexagon geometry cell, which is a widely known result in the literatures.

To sum up the results for both the proposed and conventional power control schemes, a more complete illustration is presented in Figure 4.4 where F_{m_d} is plot against r_{max}/R_{eq} for different power control profiles. As mentioned above, the F_{m_d} can be reduced by either decreasing r_{max} or decreasing δ. When r_{max}/R_{eq} equals to 1, all the values of F_{m_d} under different profiles converge to 0.326, which is simply the known result for the conventional power control where no constraint is imposed on the transmitted power.

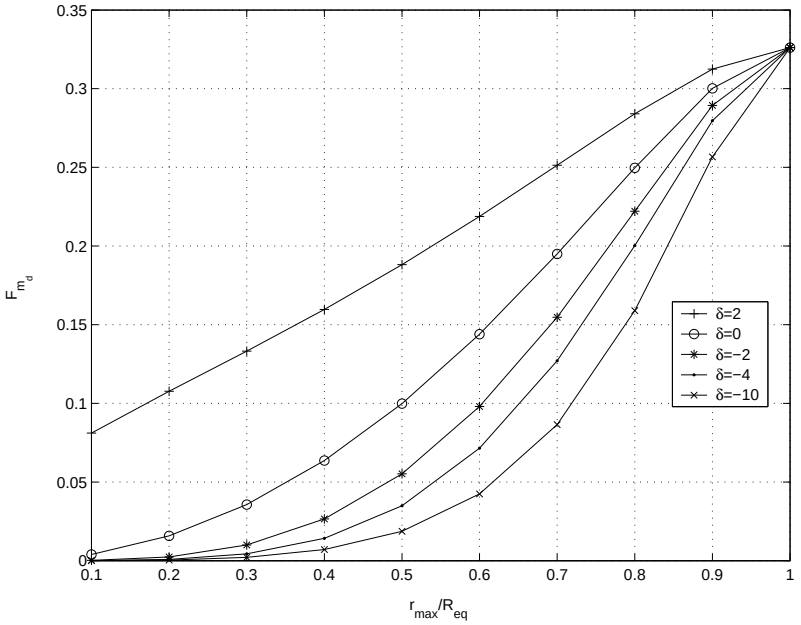

Figure 4.4: Interference correction factor F_{m_d} versus r_{max}/R_{eq} for various constrained power control profiles, with path loss exponent $\beta = 4$.

4.3 Evaluation of SIR for Voice and Data Users

4.3.1 Distribution of a Sum of Log-Normal Variables

Numerical convolution of log-normal distributions can be used to show that the distribution of a sum of log-normal variables can be approximated very well using the log-normal distribution. Therefore, we can assume the distribution of the sum of two (or more) log-normal variables can be approximated by another log-normal distribution. We want to find the approximate log-normal distribution which has the same moments as the exact sum-distribution. Fortunately, as shown by Fenton [97], the moments of the log-normal distribution can be exactly calculated using fairly simple formulae. In our analysis, only the first and second moment is considered.

Consider n Gaussian random variables $\{X_i\}$, $i = 1, 2, \ldots n$, each with means $\{m_i\}$ and variances $\{\sigma_i^2\}$. The means and variances of these corresponding n log-normal distributions $\left\{e^{X_i}\right\}$ are, respectively, given by $\{\mu_i\}$ and $\{D_i^2\}$. In the following analysis, $\{\mu_i\}$ and $\{D_i^2\}$ are called respectively as the arithmetic mean and variance of the given log-normal distribution, while $\{m_i\}$ and $\{\sigma_i^2\}$ are called respectively as the logarithmic mean and variance. The relationships of these parameters are governed by (4.44),

$$\mu = e^m e^{\sigma^2/2}; \quad D^2 = e^{2m} e^{\sigma^2}(e^{\sigma^2} - 1) \tag{4.44}$$

After μ_j and D_j^2 are determined for the distributions of each log-normal components, the arithmetic mean μ and variance D^2 for the distribution of the sum of log-normal components are, respectively, given by [97]

$$\mu = \sum_{j=1}^{n} \mu_j = \mu_1 + \mu_2 + \ldots + \mu_j + \ldots + \mu_n \tag{4.45}$$

$$D^2 = \sum_{j=1}^{n} D_j^2 = D_1^2 + D_2^2 + \ldots + D_j^2 + \ldots + D_n^2 \tag{4.46}$$

The above formulae are useful for computation of the equivalent log-normal distribution based on the first and second moments of a sum of n log-normal variables for arbitrary m and σ. For most practical purposes, this approximation is sufficient.

The logarithmic mean and variance for the summation of K independent and identically distributed (i.i.d) log-normal random variables have been derived as [97]

$$f_\sigma(K, \sigma) = \sigma_K^2 = \ln\left(\frac{1}{K} e^{\sigma^2} + \frac{K-1}{K}\right) \tag{4.47}$$

$$f_m(K, m, \sigma) = m_K = \ln(K) + m + \frac{\sigma^2}{2} - \frac{1}{2}\ln\left(\frac{1}{K} e^{\sigma^2} + \frac{K-1}{K}\right) \tag{4.48}$$

Next, we apply the above principle to derive the PDF of the SIR for power control schemes with and without power constraint.

4.3.2 Case 1: PDF of SIR without Power Constraint

In the following, PDFs of SIR for the voice and data services will be derived separately. The symbols used in the computations of the SIR for voice users are hatted in order to differentiate from those for data users. We use subscript "d" to denote the symbols of data users, and subscript "v" to denote the symbols of voice users. Assume that $k_v = i$ voice users and $k_d = j$ data users are active within one time slot. For a voice user, $i-1$ other voice users and j data users are the interferers. The sum of interference power from the other voice users is log-normally distributed with variance $\hat{\sigma}_{v_t}^2$ and mean $\hat{m}_{v_t}$. The sum of interference power from data users is log-normally distributed with variance $\hat{\sigma}_{d_t}^2$ and mean $\hat{m}_{d_t}$. Therefore, we have $\hat{\sigma}_{v_t}^2 = f_\sigma(i-1, \sigma_v)$, $\hat{m}_{v_t} = f_m(i-1, m_v, \sigma_v)$, $\hat{\sigma}_{d_t}^2 = f_\sigma(j, \sigma_d)$ and $\hat{m}_{d_t} = f_m(j, m_d, \sigma_d)$, where m_v (or m_d) and σ_v^2 (or σ_d^2) denote, respectively, the logarithmic mean and variance of the received power from a single voice (or data) user under conventional power control. The logarithmic mean and variance of the sum of total interference from both services can be evaluated using the result of [97] as,

$$\hat{\sigma}_I^2 = \ln\left[\frac{e^{2\hat{m}_{v_t}+2\hat{\sigma}_{v_t}^2} + 2e^{\hat{m}+\hat{\sigma}^2/2} + e^{2\hat{m}_{d_t}+2\hat{\sigma}_{d_t}^2}}{e^{2\hat{m}_{v_t}+\hat{\sigma}_{v_t}^2} + 2e^{\hat{m}+\hat{\sigma}^2/2} + e^{2\hat{m}_{d_t}+\hat{\sigma}_{d_t}^2}}\right] \tag{4.49}$$

$$\hat{m}_I = \ln\left(e^{\hat{m}_{v_t}+\hat{\sigma}_{v_t}^2/2} + e^{\hat{m}_{d_t}+\hat{\sigma}_{d_t}^2/2}\right) - 0.5\hat{\sigma}_I^2 \tag{4.50}$$

where $\hat{m} = \hat{m}_{v_t} + \hat{m}_{d_t}$, $\hat{\sigma}^2 = \hat{\sigma}_{v_t}^2 + \hat{\sigma}_{d_t}^2$.

For a data user, the interference comes from i voice users and $j-1$ other data users. The parameters for these two interference components are denoted, respectively, by m_{v_t}, $\sigma_{v_t}^2$ (for voice users) and m_{d_t}, $\sigma_{d_t}^2$ (for data users). Similarly, we have $\sigma_{v_t}^2 = f_\sigma(i, \sigma_v)$, $m_{v_t} = f_m(i, m_v, \sigma_v)$, $\sigma_{d_t}^2 = f_\sigma(j-1, \sigma_d)$, $m_{d_t} = f_m(j-1, m_d, \sigma_d)$. The logarithmic variance and mean of the total interference for the data packet, σ_I^2 and m_I, can be obtained in the similar form as (4.49) and (4.50). Now we have the log-normal distribution parameters of the total interference, as well as the desired signal. By referring to (4.21) and (4.22), the PDFs of SIR for a voice user, $f_{SIR_v}(r_{ij})$, and for a data user, $f_{SIR_d}(r_{ij})$, can be written as,

$$f_{SIR_v}(r_{ij}) = \frac{1}{\sqrt{2\pi\,(\hat{\sigma}_I^2 + \sigma_v^2)}\, r_{ij}} \exp\left[-\frac{(\ln r_{ij} - m_v + \hat{m}_I)^2}{2\,(\hat{\sigma}_I^2 + \sigma_v^2)}\right] \tag{4.51}$$

$$f_{SIR_d}(r_{ij}) = \frac{1}{\sqrt{2\pi\,(\sigma_I^2 + \sigma_d^2)}\, r_{ij}} \exp\left[-\frac{(\ln r_{ij} - m_d + m_I)^2}{2\,(\sigma_I^2 + \sigma_d^2)}\right] \tag{4.52}$$

The outage probabilities of voice users, $p_{fv}(i,j)$ and data users, $p_{fv}(i,j)$, can be evaluated respectively as,

$$p_{fv}(i,j) = \int_0^{\Psi_v} f_{SIR_v}(r_{ij}) \mathrm{d}r_{ij} \tag{4.53}$$

$$p_{fd}(i,j) = \int_0^{\Psi_d} f_{SIR_d}(r_{ij}) \mathrm{d}r_{ij} \tag{4.54}$$

After some mathematical manipulations, we have

$$p_{fv}(i,j) = \frac{1}{2} + \frac{1}{2}\mathrm{erf}\left(\left[\ln \Psi_v - m_v + \hat{m}_I\right] / \sqrt{2(\hat{\sigma}_I^2 + \sigma_v^2)}\right) \tag{4.55}$$

$$p_{fd}(i,j) = \frac{1}{2} + \frac{1}{2}\mathrm{erf}\left(\left[\ln \Psi_d - m_d + m_I\right] / \sqrt{2(\sigma_I^2 + \sigma_d^2)}\right) \tag{4.56}$$

where $\Psi_v = SIR_{th_v} = (1/Q_v)\,(E_b/N_0)_{th_v}$, $\Psi_d = SIR_{th_d} = (1/Q_d)\,(E_b/N_0)_{th_d}$, and $\mathrm{erf}(\cdot)$ denotes the error function.

4.3.3 Case 2: PDF of SIR with Power Constraint

With our proposed constrained power control scheme, the transmitted power of the data users becomes distance-dependent. As a result, the PDF of SIR for both services shown in (4.51) and (4.52) are no longer valid and new PDF expressions have to be derived accordingly.

By assuming path loss exponent $\beta = 4$, the interference correction factor for conventional power control scheme ($F_{m_v} = 0.326$) is still valid for the voice users. For the data service, new formula for F_{m_d} has been derived as functions of the power control profile index δ and the ratio r_{max}/R_{eq} as listed in Table 4.1.

Average Total Received Power from Data Users

The received power from a data user is not a constant, but depends on its distance from the base station. In order to evaluate the SIR, we need to derive the first and second moments, which are denoted by μ_t and D_t^2 respectively, of the average total received power from data users.

Firstly, the user density η of mobile data users is defined as the average number of data users per unit area. We assume all data users are uniformly distributed within the cell area, therefore,

$$\eta = \frac{n_d}{\pi R_{eq}^2} \tag{4.57}$$

The total received power at the base station from each user is log-normally distributed due to imperfect power control. According to the theory of Fenton [97], the total received power at the base station from a sum of these users follows

another log-normal distribution. The total average received power from n_d data users, $\bar{P}_d$, is evaluated by averaging the received power over the cell coverage area. The whole cell area can be divided into two power control regions A_1 and A_2 by a circle of radius $r = r_{max}$ as shown in Figure 4.3.

$$\begin{aligned} \bar{P}_d &= \oint_A E\left[P_{R_d}(r)\right] \eta \, \mathbf{d}A \\ &= \oint_{A_1} E\left[P_{R_d}(r)\right] \frac{n_d}{\pi R_{eq}^2} \, \mathbf{d}A_1 + \oint_{A_2} E\left[P_{R_d}(r)\right] \frac{n_d}{\pi R_{eq}^2} \, \mathbf{d}A_2 \end{aligned} \tag{4.58}$$

where $P_{R_d}(r) = P_{T_d}(r) r^{-\beta}$ and $P_{T_d}(r)$ is given in (4.2).

By dividing (4.58) with n_d, the mean value of the average received power from a single data user $\bar{\mu}_d$ equals to,

$$\begin{aligned} \bar{\mu}_d &= \bar{P}_d / n_d \\ &= \oint_{A_1} E\left[P_{R_d}(r)\right] \frac{1}{\pi R_{eq}^2} \, \mathbf{d}A_1 + \oint_{A_2} E\left[P_{R_d}(r)\right] \frac{1}{\pi R_{eq}^2} \, \mathbf{d}A_2 \\ &= \int_0^{r_{max}} \int_0^{2\pi} \mu_d \frac{1}{\pi R_{eq}^2} \, r \, \mathrm{d}r \, \mathrm{d}\theta + \int_{r_{max}}^{R_{eq}} \int_0^{2\pi} \mu_d \left(\frac{r_{max}}{r}\right)^{\beta-\delta} \frac{1}{\pi R_{eq}^2} \, r \, \mathrm{d}r \, \mathrm{d}\theta \\ &= \begin{cases} \frac{\mu_d}{L}\left(1 + \ln L\right), & \delta = 2 \\ \frac{\mu_d}{L}\left(1 - \frac{2}{\delta - \beta + 2}\right) + \frac{2\mu_d}{\delta - \beta + 2} L^{\frac{\delta-\beta}{2}}, & \text{otherwise} \end{cases} \end{aligned} \tag{4.59}$$

where L is defined in (4.35).

Similarly, the variance of the average received power from a single data user

D_t^2 can be evaluated as,

$$\begin{aligned}
\bar{D}_d^2 &= \oint_{A_1} E\left[S_R(r)\right]^2 \frac{1}{\pi R_{eq}^2}\,\mathbf{d}A_1 + \oint_{A_2} E\left[S_R(r)\right]^2 \frac{1}{\pi R_{eq}^2}\,\mathbf{d}A_2 - \bar{\mu}_d^2 \\
&= \int_0^{r_{max}} \int_0^{2\pi} \left(\mu_d^2 + D_d^2\right) \frac{1}{\pi R_{eq}^2}\, r\,\mathrm{d}r\,\mathrm{d}\theta \\
&\quad + \int_{r_{max}}^{R_{eq}} \int_0^{2\pi} \left(\mu_d^2 + D_d^2\right) \left(\frac{r_{max}}{r}\right)^{2\beta-2\delta} \frac{1}{\pi R_{eq}^2}\, r\,\mathrm{d}r\,\mathrm{d}\theta - \bar{\mu}_d^2 \\
&= \frac{(\mu_d^2 + D_d^2)}{L}\left(1 - \frac{1}{\delta - \beta + 1}\right) + \frac{(\mu_d^2 + D_d^2)}{\delta - \beta + 1} L^{\delta-\beta} - \bar{\mu}_d^2 \qquad (4.60)
\end{aligned}$$

where μ_d and D_d^2 are, respectively, the arithmetic mean and variance of the received power from the data user under conventional power control. The μ_d and D_d^2 are related to m_d and σ_d^2 as,

$$\mu_d = e^{m_d} e^{\sigma_d^2/2}; \quad D_d^2 = e^{2m_d} e^{\sigma_d^2}(e^{\sigma_d^2} - 1) \qquad (4.61)$$

Both $\bar{\mu}_d$ and $\bar{D}_d^2$ are functions of the ratio r_{max}/R_{eq}, the path loss exponent β and the constrained power control profile index δ. In Figure 4.5 and Figure 4.6, we illustrate $\bar{\mu}_d$ and $\bar{D}_d^2$ respectively as a function of r_{max}/R_{eq} under different power control profiles with $\beta = 4$. As expected, we observe that with a smaller r_{max} or a smaller δ, the average received interference power from the data user is weaker.

PDF of SIR for a Voice User

Suppose i voice users and j data users are active within one time slot. We want to derive the PDF of the SIR of the voice user, SIR_v. The received power of the desired signal is log-normally distributed with the logarithmic mean m_v and variance σ_v^2. The interference caused by other voice users follows another log-normal

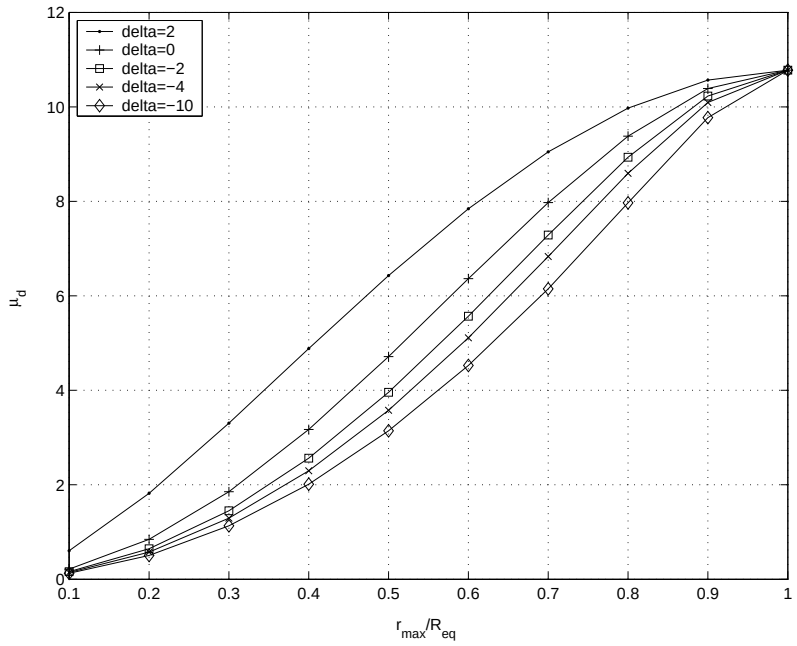

Figure 4.5: The arithmetic mean value of the average received power versus r_{max}/R_{eq} from a single data user. $\beta = 4$**,** $m_v = 0\,\mathrm{dB}, m_d = 2\,\mathrm{dB}, \sigma_v = \sigma_d = 1\,\mathrm{dB}$**.**

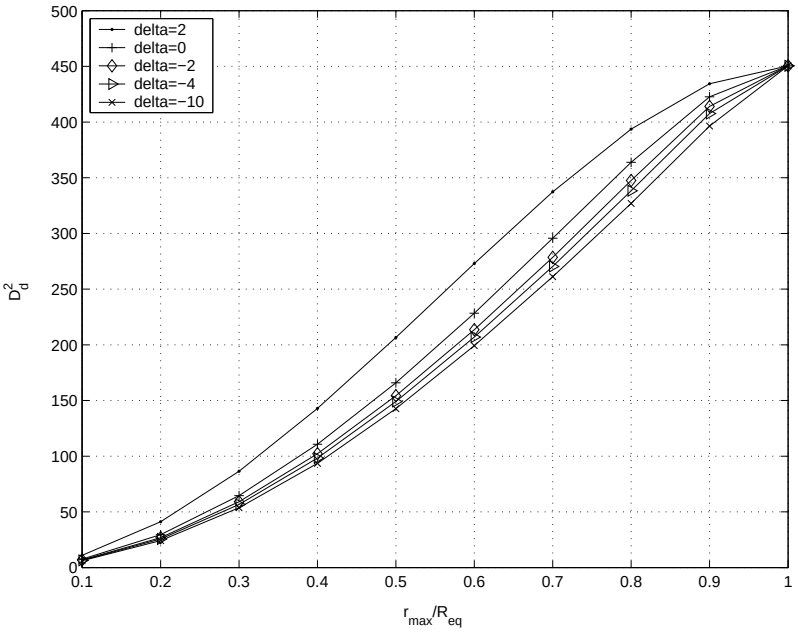

Figure 4.6: The arithmetic variance of the average received power versus r_{max}/R_{eq} from a single data user. $\beta = 4$**,** $m_v = 0\,\mathrm{dB}, m_d = 2\,\mathrm{dB}, \sigma_v = \sigma_d = 1\,\mathrm{dB}$**.**

distribution whose mean and variance is determined by,

$$\hat{m}_{v_t} = f_m(i-1, m_v, \sigma_v); \quad \hat{\sigma}^2_{v_t} = f_\sigma(i-1, \sigma_v) \tag{4.62}$$

where f_m and f_σ are defined in (4.47) and (4.48). The corresponding arithmetic mean and variance are obtained by,

$$\hat{\mu}_{v_t} = e^{\hat{m}_{v_t}} e^{\hat{\sigma}^2_{v_t}/2}; \quad \hat{D}^2_{v_t} = e^{2\hat{m}_{v_t}} e^{\hat{\sigma}^2_{v_t}} (e^{\hat{\sigma}^2_{v_t}} - 1) \tag{4.63}$$

Since all data users are governed by the constrained power control scheme, the mean and variance of the interference from data users, however, is evaluated as,

$$\hat{\mu}'_{d_t} = j\bar{\mu}_d; \quad \hat{D}'^2_{d_t} = j\bar{D}^2_d \tag{4.64}$$

The sum of total interference (which includes all intra-cell and inter-cell interference) also follows a log-normal distribution with mean $\hat{\mu}'_I$ and variance $\hat{D}'^2_I$ given by,

$$\hat{\mu}'_I = (1 + F_{m_v})\,\hat{\mu}_{v_t} + (1 + F_{m_d})\,\hat{\mu}'_{d_t} \tag{4.65}$$

$$\hat{D}'^2_I = (1 + F_{m_v})^2\,\hat{D}^2_{v_t} + (1 + F_{m_d})^2\,\hat{D}'^2_{d_t} \tag{4.66}$$

The corresponding logarithmic mean and variance are obtained by,

$$\hat{\sigma}'^2_I = \ln\left(\frac{\hat{D}'^2_I}{\hat{\mu}'^2_I} + 1\right); \quad \hat{m}'_I = \ln\hat{\mu}'_I - \frac{\hat{\sigma}'^2_I}{2}; \tag{4.67}$$

Finally, by referring to (4.21), the PDF of the SIR for the voice user is

$$f_{SIR_v}(r_{ij}) = \frac{1}{\sqrt{2\pi\,(\hat{\sigma}'^2_I + \sigma^2_v) r_{ij}}} \exp\left[-\frac{(\ln r_{ij} - m_v + \hat{m}'_I)^2}{2\left(\hat{\sigma}'^2_I + \sigma^2_v\right)}\right] \tag{4.68}$$

PDF of SIR for a Data User

The procedure to evaluate the PDF of SIR for the data user, SIR_d, is similar to the case of voice user. But now the desired signal is coming from the data user, whereas the interference is coming from all i voice users and the other $j-1$ data users. The logarithmic mean and variance of the interference from all i voice users are,

$$m_{v_t} = f_m(i, m_v, \sigma_v); \quad \sigma_{v_t}^2 = f_\sigma(i, \sigma_v) \tag{4.69}$$

The corresponding arithmetic mean and variance are obtained by,

$$\mu_{v_t} = e^{m_{v_t}} e^{\sigma_{v_t}^2/2}; \quad D_{v_t}^2 = e^{2m_{v_t}} e^{\sigma_{v_t}^2} (e^{\sigma_{v_t}^2} - 1) \tag{4.70}$$

The arithmetic mean and variance of the interference from all other $j-1$ data users are,

$$\mu'_{d_t} = (j-1)\bar{\mu}_d; \quad D'^2_{d_t} = (j-1)\bar{D}_d^2 \tag{4.71}$$

The arithmetic mean and variance of the total interference can then be evaluated as,

$$\mu'_I = (1 + F_{m_v})\, \mu_{v_t} + (1 + F_{m_d})\, \mu'_{d_t} \tag{4.72}$$

$$D'^2_I = (1 + F_{m_v})^2\, D_{v_t}^2 + (1 + F_{m_d})^2\, D'^2_{d_t} \tag{4.73}$$

Finally, the corresponding logarithmic mean and variance of total interference for the desired data user under the constrained power control scheme can be evaluated as,

$$\sigma'^2_I = \ln\left(\frac{D'^2_I}{\mu'^2_I} + 1\right); \quad m'_I = \ln \mu'_I - \frac{\sigma'^2_I}{2}; \tag{4.74}$$

The PDF of SIR_d in this case is shown as,

$$f_{SIR_d}(r_{ij}) = \frac{1}{\sqrt{2\pi\left(\sigma_I'^2 + \sigma_v^2\right) r_{ij}}} \exp\left[-\frac{\left(\ln r_{ij} - m_v + m_I'\right)^2}{2\left(\sigma_I'^2 + \sigma_v^2\right)}\right] \tag{4.75}$$

4.4 Results and Discussion

4.4.1 Log-Normal Distribution of the Sum of Received Power under Constrained Power Control Scheme

In previous section, we have derived the parameters for the distribution of a sum of received signal power with power control error for cases with and without power constraint, based on the principle proposed by Fenton in [97]. The validity of this log-normal approximation has also been shown in [102] for systems subject to conventional power control. However, when power constraint is imposed on the component transmit power, the validity and the accuracy of this approximation needs to be verified. With this objective in mind, we use simulation to compare and verify our above analytical results.

We simulate a single micro-cell supported by one base station with omni-directional antenna. Circular cell shape with radius of $200m$ is assumed. 20 data users are randomly located in each cell with a uniform density. All users' coordinates (locations) are first generated independently and uniformly within the cell area. The transmit power of data users is allocated according to the proposed power control scheme. The received power from different data users is then collected at the base station and the histogram of the total received power is drawn.

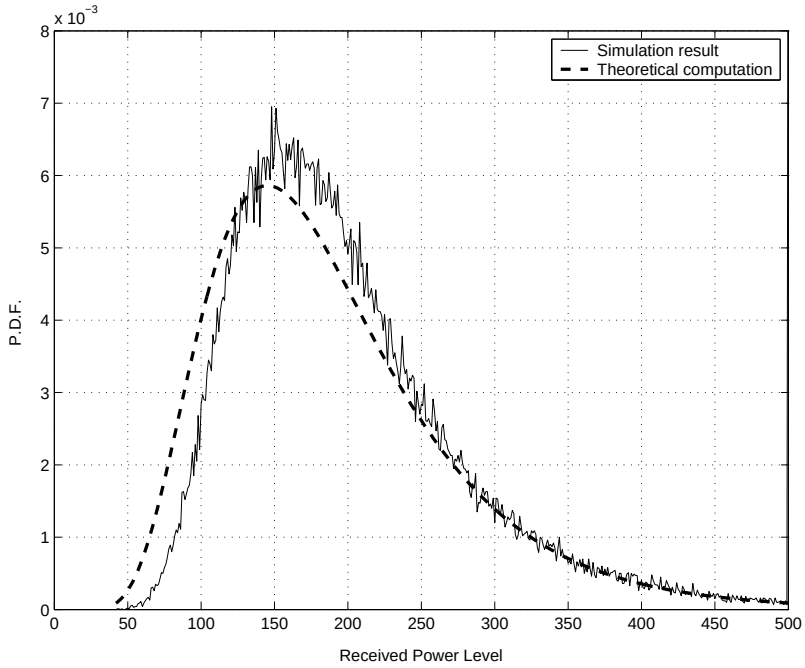

Figure 4.7: Comparison between (i) theoretical log-normal distribution and (ii) distribution of the total received power from data users subject to constrained power control obtained by simulation, with $r_{max}/R_{eq} = 0.75$ and $\delta = 2$.

The simulations are repeated for 10000 samples of random locations. The result for the power control profile with $\delta = 2$ is presented in Figure 4.7. The theoretical curve is generated using a log-normal PDF with the mean and variance computed by (4.64), where $j = 20$ is the number of data users in the cell. The simulation result matches our theory very well, therefore we conclude that the total received power from the data users subject to imperfect power control with power constraint also follows another log-normal distribution.

4.4.2 Effects of α_d and λ_d on System Performance

Unlike voice user, the activity factor α_d of data user changes with the status of the data transmission and therefore it is not a constant. With higher retransmis-

sion probability, according to Eq. (4.8), the data activity factor becomes higher, and vice versa. The retransmission probability will keep increasing until the delay threshold is met. The relationship between the retransmission probability and the data activity factor α_d in a multi-service system subject to constrained power control is illustrated in Figure 4.8, where the data arrival rate of the newly generated data packets, λ_d, is fixed to be 50 packets/s.

The effect of λ_d on the user capacity is highlighted in Figure 4.9, where we can see the maximum number of users the system could support is a decreasing function of the data arrival rate λ_d, when a constraint is imposed on the transmit power of data users. With a fixed QoS requirement of $D \leq D_{th}$, it is not difficult to see from (4.8) that with increasing λ_d, the data activity factor α_d increases. This leads to a higher retransmission probability and hence a smaller number of successfully transmitted data packets.

4.4.3 Optimal Throughput and User Capacity

In Figure 4.10 and Figure 4.11, the results for delay, outage probability, throughput and user capacity versus power control profile index are presented for the proposed power control scheme. When δ is reduced towards the negative values, the transmitted power of the data user becomes lower and lower for $r > r_{max}$. As a result, the BER of the data user is larger, and this leads to a greater retransmission probability. This in turn gives rise to the packet delay (Figure 4.10(a)) which might exceed the given delay constraint ($D_{th} = 10$ packets in this case), which implies that the number of data users shall not be increased any more. In addition, the

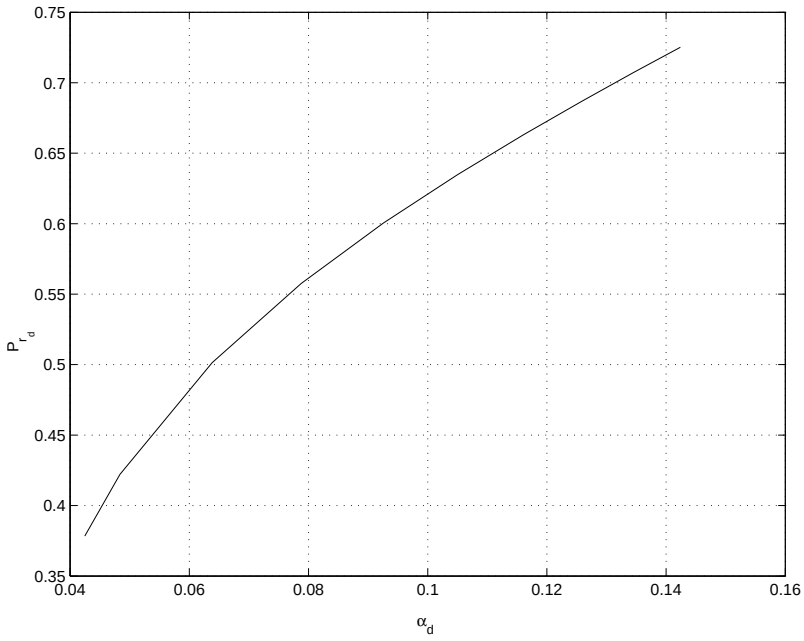

Figure 4.8: Retransmission probability versus activity factor of the data user in a cellular system with 14 users per micro cell, with $\delta = 2$, $r_{max}/R_{eq} = 0.5$, $\lambda_d = 50$ packets/s.

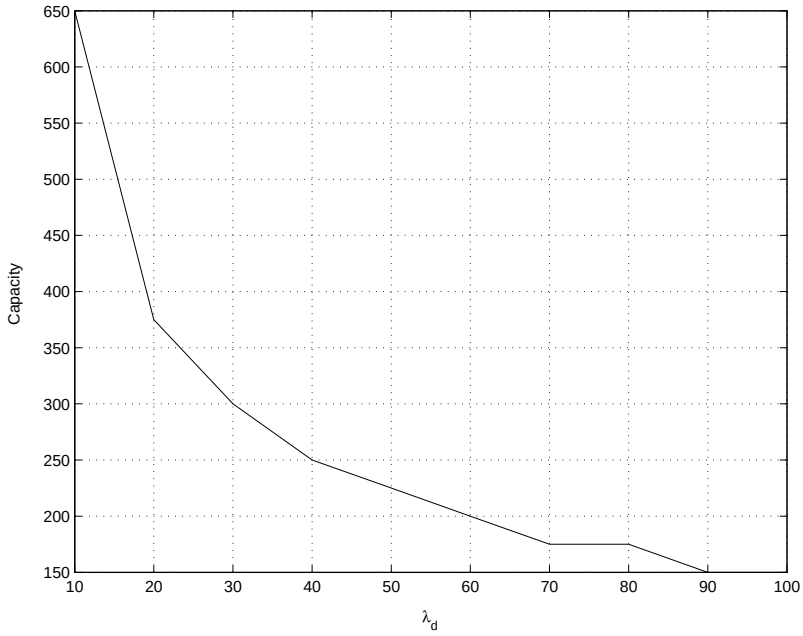

Figure 4.9: User capacity of a slotted DS-CDMA system versus data arrival rate of newly generated data packets, with $\delta = -2$, $r_{max}/R_{eq} = 0.5$.

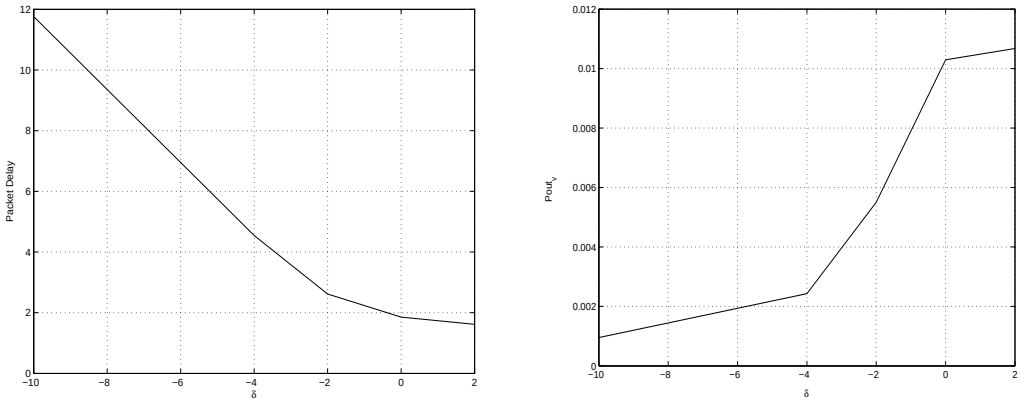

(a) Number of packet delay for data users (b) Outage Probability for voice users

Figure 4.10: Delay and outage probability as a function of power control profile index δ. $\lambda_d = 50$ packets/s, $r_{max}/R_{eq} = 0.5$, $n_v = 25$, $n_d = 50$.

smaller δ, the less the amount of interference caused by these data users outside the circle of $r = r_{max}$. Thus as shown in Figure 4.10(b), the outage probability of the voice user is greatly reduced by the constrained power control scheme. On the other hand, as discussed above, the increasing delay of the data user limits the number of feasible data users given a specific value of δ. This fact can also be used to explain the curves in Figure 4.11. In Figure 4.11(a), as δ decreases from 4 to 0, the throughput increases due to the reduced amount of interference in the system. Then, the throughput starts falling off after reaching a peak at $\delta = 0$ due to the increased delay of data packets as shown in Figure 4.10(a). The peak throughput is obtained when the user capacity reaches the maximum value, i.e. when $\delta = 0$ with $r_{max}/R_{eq} = 0.5$.

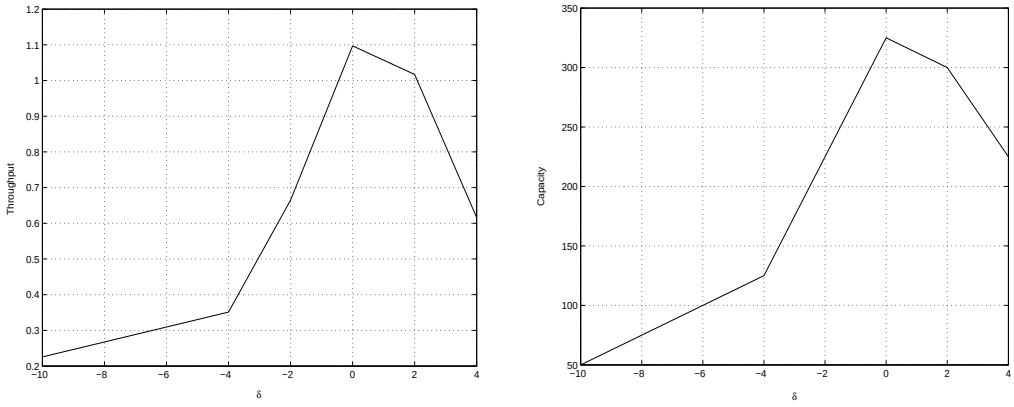

(a) Data throughput within a single cell (b) User capacity

Figure 4.11: Throughput and capacity under different power control profiles. $\lambda_d = 50$ **packets/s,** $r_{max}/R_{eq} = 0.5$**.**

4.4.4 Enhancement of User Capacity

With both outage probability and delay constraints, the maximum number of data users that can be supported by the system is different under different constrained power control profiles. As shown in Figure 4.1, the transmitted power of the data user for $r > r_{max}$ drops as δ decreases. The reduction in the interference from these data users leads to the reduction of the outage probability of voice users. However, further reduction in transmitted power of data users for $r > r_{max}$ increases their own error probability, and therefore causes larger retransmission probability and larger data packet delay. Given a fixed number of voice users, when the average delay of the data users exceeds the delay threshold D_{th}, the number of data users n_d reaches its maximum value $\hat{n}_d$. Similarly as shown in Figure 4.10(b), a larger δ results in higher transmit power of data users, thus the outage probability for the voice user increases due to higher interference power. Beyond the outage constraint

of $P_{out_v} \leq 0.01$, the maximum number of voice users $\hat{n}_v$ is reached. Due to the tradeoff between the outage probability and delay requirements, we speculate that there must be an optimum value for δ which achieves maximum capacity.

Here, user capacity of the system as defined in (4.14) is studied for different delay constraints and different constrained power control profiles. For example, the user capacity of the system with delay constraint of 10 packets and $r_{max}/R_{eq} = 0.5$ is shown in Figure 4.12. As expected, we observe the crossover between the curves for different power control profiles. When δ decreases from 4 to 0, the maximum number of data users n_d increases from 200 to 300 while the number of voice users is 25, but the n_d starts decreasing when δ is less than 0. Note that the curve of $\delta = 4$ corresponds to user capacity of the conventional power control scheme. In Figure 4.12, we observe the constrained power control scheme achieves a larger user capacity than the conventional one only if δ is no less than -2. We therefore conclude that by adjusting the transmitted power based on appropriately chosen constrained power control profiles, the overall user capacity can be enhanced.

4.4.5 Effects of δ and r_{max} on the User Capacity

The user capacity C versus different r_{max}/R_{eq} under various power control profiles is shown in Figure 4.13. With the increase of r_{max}, the user capacity of the system increases first and then decreases, due to the tradeoff between the outage probability and data packet delay. The user capacity depends on the power control profiles we use. As δ becomes smaller, the user capacity is achieved by larger value of r_{max}/R_{eq}. For a fixed r_{max}, however, there exists an optimal power control profile

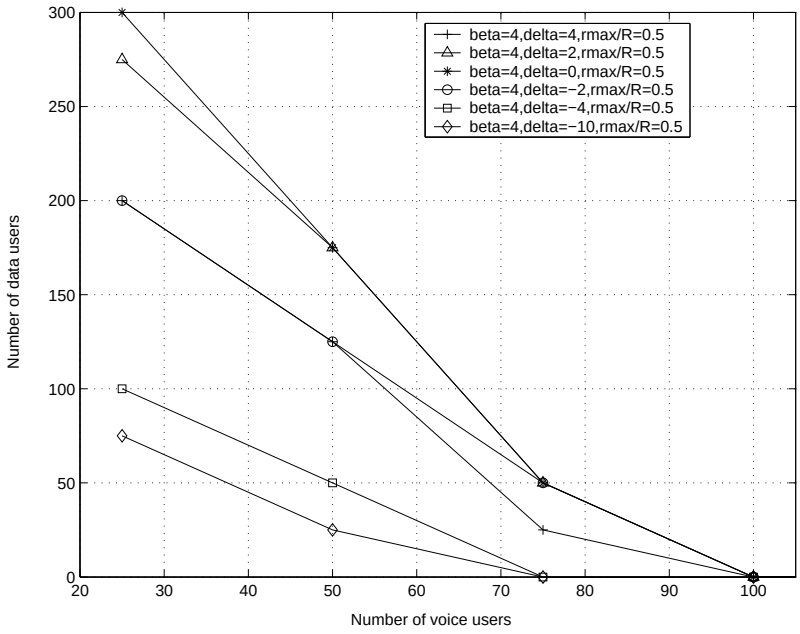

Figure 4.12: Number of data users versus number of voice users for a CDMA system under various power control profiles with service requirements of $P_{out_v} \leq 0.01$ and $D \leq 10$ packets. $\lambda_d = 50$ packets/s, $r_{max}/R_{eq} = 0.5$.

δ^* which achieves maximum user capacity. For example, at $r_{max}/R_{eq} = 0.5$, the maximum user capacity is achieved when $\delta^* = 0$; while $\delta^* = -10$ gives the maximum user capacity if $r_{max}/R_{eq} = 0.9$. If the index δ is too small, the constrained power control scheme could hardly achieve further performance improvement. This is because as the transmitted signal power of the data users drops to zero for region where $r > r_{max}$, i.e., $\delta = -\infty$, the maximum user capacity is achieved only when $r_{max} = R_{eq}$.

4.5 Summary and Contribution

We proposed a constrained power control scheme for the uplink in slotted DS-CDMA systems supporting both voice and data services. In this scheme, the

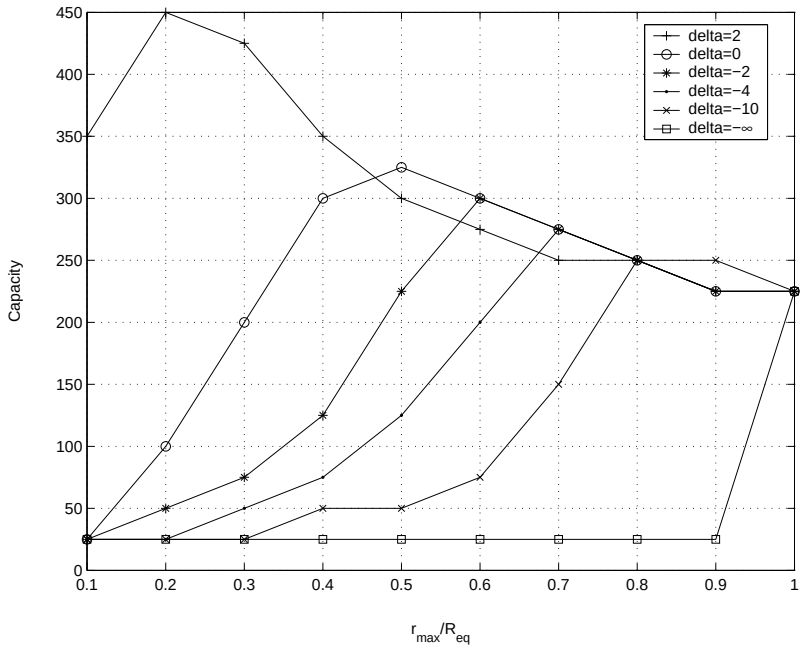

Figure 4.13: User capacity versus r_{max}/R_{eq} with different values of δ under constraints of $P_{out_v} \leq 0.01$ and $D \leq 10$ packets. $\lambda_d = 50$ **packets/s,** $m_v = 0\,\text{dB}, m_d = 2\,\text{dB}, \sigma_v = \sigma_d = 1\,\text{dB}$**.**

transmitted power of data users is constrained when the distance of the data user from the base station is greater than r_{max} $(0 < r_{max} < R_{eq})$. A profile index δ was introduced to constrain the transmitter power outside r_{max} which results in various power control profiles.

We derived a general closed form expression for the interference correction factor F_m for the constrained power control scheme. We have also shown that the PDF of the total interference power in the proposed scheme can be approximated by a log-normal PDF, and we then derived the corresponding mean and variance of the log-normal distribution to characterize the total interference in uplink of slotted DS-CDMA systems adopting the proposed scheme. The validity of this approximation has been verified by our simulation results. We also derived the

PDF of the SIR for both voice and data users and evaluated the user capacity of the system under various power control profiles subject to outage probability and delay constraints.

The proposed scheme can enhance the user capacity if appropriate power control profiles are chosen. Moreover, we found that there is an optimal δ^* which maximize the user capacity for a given range constraint r_{max}. Similarly, for power control with a given profile index δ, we can select an optimum r^*_{max} which maximize user capacity. Therefore, the constrained power control profile in terms of either δ^* or r^*_{max} can be used to optimize the user capacity.

Chapter 5

Subcarrier-and-Bit Allocation in Multiclass Multiuser OFDM Systems

In this chapter, we deal with the adaptive subcarrier-and-bit allocation (SBA) for multiuser OFDM systems supporting multiclass services. Each class has its own QoS requirements such as target data rate and BER. The purpose is to conduct a unified analysis of the constrained optimization problems and then derive their exact optimal solutions. The downlink transmission supporting two service classes is first examined. The optimized system performance is compared with the rate-adaptive scheme without multiuser diversity and a simple SBA scheme. The framework presented in this work, based on the optimal solution, can be used as a benchmark for future developed heuristic algorithm.

The optimal solution to the problem, however, is generally time consuming

due to the large number of search in the nonlinear branch and bound algorithm used [103]. Thus in the later part of this chapter, we propose two approaches to obtain the suboptimal solution. Our first approach uses a quadratic approximation to the objective function. The second approach searches for the solution in a two-step manner - the feasible set is first relaxed into real numbers, and then the integer solutions are further obtained based on the intermediate real solutions in step 1. The accuracy and complexity of these two approaches are compared with each other and also with the optimal solution.

Next, the problem is extended into a system supporting three service classes. In this case, the revenue is measured by both energy and throughput. The optimal solution to maximize the given revenue function is derived.

5.1 Optimal SBA Solution for Two Class System

5.1.1 Problem Formulation

Here we consider a rate-adaptive downlink OFDM system supporting two classes of services. Class 1 needs a constant data rate of R_1 bits/OFDM symbol and a target BER of P_{e_1}; while Class 2 needs a minimum data rate of R_2 bits/OFDM symbol and a target BER of P_{e_2}. The number of subcarriers is N, shared by K_1 Class 1 users and K_2 Class 2 users. With careful design of OFDM signal, i.e., if the length of cyclic prefix is longer than the maximum delay of the multipath channel, intersymbol interference is mitigated; hence, each subcarrier experiences only flat fading. Here we let $H_{k,n}$ denote fading gains as seen by the kth user on the nth

subcarrier. Also let N_0 denote the power spectral density (PSD) of the additive white Gaussian noise, and assume it is the same for all subcarriers and all users.

Further, we let $s_{k,n}$ denote the assignment indicator, i.e., if the nth subcarrier is assigned to the kth user, $s_{k,n} = 1$; otherwise $s_{k,n} = 0$. In our system, no subcarrier can be assigned to more than one user. Therefore, if $s_{k,n} = 1$, $s_{k',n} = 0$ for all $k' \neq k$. Let $c_{k,n}$ denote the number of bits of the kth user assigned onto the nth subcarrier. Assume that square signal constellations 4QAM, 16QAM and 64QAM are considered in our system model, so the number of bits within each symbol has three possible values: 2,4 and 6. Hence, the integer sets for $s_{k,n}$ and $c_{k,n}$ are respectively $S = \{0, 1\}$ and $C = \{0, 2, 4, 6\}$. $c_{k,n} = 0$ means that the kth user transmits no information bits on the nth subcarrier.

In [63], the function of the required received power at a given BER P_e and constellation of c bits/symbol for QAM signals is presented:

$$f(c) \approx \frac{N_0}{3}\left[Q^{-1}\left(\frac{P_e}{4}\right)\right]^2 (2^c - 1) \tag{5.1}$$

where

$$Q(x) = \frac{1}{\sqrt{2\pi}}\int_x^\infty e^{-t^2/2}\mathrm{d}t \tag{5.2}$$

Whereas, in order to maintain QoS requirements of each user, the assigned power at the transmitter for the kth user on the nth subcarrier is

$$\begin{aligned} P_{k,n} &= f(c_{k,n})/|H_{k,n}|^2 \\ &\approx \frac{N_0}{3}\left[Q^{-1}\left(\frac{P_e}{4}\right)\right]^2 (2^{c_{k,n}} - 1)/|H_{k,n}|^2 \end{aligned} \tag{5.3}$$

on the condition that the nth subcarrier is assigned to the kth user, i.e., $s_{k,n} = 1$; otherwise, $P_{k,n} = 0$.

In regard to the adaptive SBA problem concerned in this chapter, our target is to minimize the overall transmit power while satisfying all the data rate and BER constraints for both Class 1 and Class 2 users. Referring to (5.3) and its condition, the problem can be numerically formulated as below:

$$\min_{s_{k,n},c_{k,n}} \sum_{k=1}^{K_1}\sum_{n=1}^{N} \rho_1(2^{s_{k,n}c_{k,n}}-1)/|H_{k,n}|^2 + \sum_{k=K_1+1}^{K_1+K_2}\sum_{n=1}^{N} \rho_2(2^{s_{k,n}c_{k,n}}-1)/|H_{k,n}|^2 \quad (5.4)$$

subject to

$$\sum_{n=1}^{N} s_{k,n}c_{k,n} = R_1, \quad k = 1,2,\ldots,K_1 \quad (5.5)$$

$$\sum_{n=1}^{N} s_{k,n}c_{k,n} \geq R_2, \quad k = K_1+1, K_1+2, \ldots, K_1+K_2 \quad (5.6)$$

$$\sum_{k=1}^{K_1+K_2} s_{k,n} = 1, \quad n = 1,2,\ldots,N \quad (5.7)$$

and

$$s_{k,n} \in S \text{ integer}, \quad c_{k,n} \in C \text{ integer} \quad (5.8)$$

where

$$\begin{aligned} \rho_1 &= \frac{N_0}{3}\left[Q^{-1}\left(\frac{P_{e_1}}{4}\right)\right]^2 \\ \rho_2 &= \frac{N_0}{3}\left[Q^{-1}\left(\frac{P_{e_2}}{4}\right)\right]^2 \end{aligned} \quad (5.9)$$

are constants related to service category.

This formulation, as defined by (5.4)-(5.8), is a mixed-integer nonlinear programming (MINLP) problem with a nonlinear objective function (5.4) and $2(K_1+K_2)N$ integer optimization variables on discrete set. It has K_1 nonlinear equality

constraints in (5.5), K_2 nonlinear inequality constraints in (5.6) and N linear constraints in (5.7). More careful investigation reveals that the objective function is not convex, hence there is no guarantee to achieve the global optimum solution. There are cases when the algorithm is trapped at some local optimum point. In order to avoid this, and also to reduce the high complexity residing in the exponential objective function in (5.4) and the nonlinearity of the constraints in (5.5) and (5.6), we will take the following measures.

Firstly, note that the term $2^{s_{k,n}c_{k,n}}$ can only take discrete values of 1, 2^2, 2^4 and 2^6. Hence, we can replace the function $2^{s_{k,n}c_{k,n}}-1$ by a polynomial relationship $f(s_{k,n}c_{k,n})$, where $f(t)=\frac{1}{1280}t^6+\frac{59}{80}t^2$. This function was chosen because it has the lowest order among the matching polynomial functions which are convex. Thus, the objective function in (5.4) can be changed into the equivalent form:

$$\min_{s_{k,n},c_{k,n}} \sum_{k=1}^{K_1}\sum_{n=1}^{N} \rho_1 f(s_{k,n}c_{k,n})/|H_{k,n}|^2 + \sum_{k=K_1+1}^{K_1+K_2}\sum_{n=1}^{N} \rho_2 f(s_{k,n}c_{k,n})/|H_{k,n}|^2 \qquad (5.10)$$

To convert the nonlinear constraints into linear ones, we represent each integer value of $c_{k,n}$ with two binary variables:

$$c_{k,n} = 2(2d_{k,n}^{(1)} + d_{k,n}^{(0)}) \qquad (5.11)$$

where $d_{k,n}^{(1)}$ and $d_{k,n}^{(0)}$ only take 0 or 1. And this representation is equivalent to the restrictions in (5.8), i.e., $c_{k,n} \in \{0,2,4,6\}$. For example, $d_{k,n}^{(1)} = d_{k,n}^{(0)} = 1$ corresponds to $c_{k,n}=6$.

With (5.11), the product of $s_{k,n}c_{k,n}$ can be rewritten as:

$$s_{k,n}c_{k,n} = 4s_{k,n}d_{k,n}^{(1)} + 2s_{k,n}d_{k,n}^{(0)} \qquad (5.12)$$

Observing that $s_{k,n}$, $d_{k,n}^{(1)}$ and $d_{k,n}^{(0)}$ are all binary variables, their products are obviously binary as well. According to the algorithm shown in [104], (5.12) can be easily converted into the linear form with additional constraints to be given in (5.18) and (5.19). If we denote $x_{k,n} = s_{k,n}d_{k,n}^{(1)}$ and $y_{k,n} = s_{k,n}d_{k,n}^{(0)}$, the linear form of (5.12) is given by

$$s_{k,n}c_{k,n} = 4x_{k,n} + 2y_{k,n} \tag{5.13}$$

We therefore come up with the new formulation which has the same solution as the original problem given in (5.4)-(5.8).

$$\begin{aligned} \min_{\substack{x_{k,n},y_{k,n},\\ s_{k,n},d_{k,n}^{(1)},d_{k,n}^{(0)}}} \quad & \sum_{k=1}^{K_1}\sum_{n=1}^{N} \rho_1 f(4x_{k,n} + 2y_{k,n})/|H_{k,n}|^2 \\ & + \sum_{k=K_1+1}^{K_1+K_2}\sum_{n=1}^{N} \rho_2 f(4x_{k,n} + 2y_{k,n})/|H_{k,n}|^2 \end{aligned} \tag{5.14}$$

subject to

$$\sum_{n=1}^{N}(4x_{k,n} + 2y_{k,n}) = R_1, \quad k = 1, 2, \ldots, K_1 \tag{5.15}$$

$$\sum_{n=1}^{N}(4x_{k,n} + 2y_{k,n}) \geq R_2, \quad k = K_1 + 1, K_1 + 2, \ldots, K_1 + K_2 \tag{5.16}$$

$$\sum_{k=1}^{K_1+K_2} s_{k,n} = 1, \quad n = 1, 2, \ldots, N \tag{5.17}$$

$$s_{k,n} + d_{k,n}^{(1)} - 1 \leq x_{k,n} \leq 0.5(s_{k,n} + d_{k,n}^{(1)}) \tag{5.18}$$

$$s_{k,n} + d_{k,n}^{(0)} - 1 \leq y_{k,n} \leq 0.5(s_{k,n} + d_{k,n}^{(0)}) \tag{5.19}$$

and

$$x_{k,n}, y_{k,n}, s_{k,n}, d_{k,n}^{(1)}, d_{k,n}^{(0)} \in \{0, 1\} \tag{5.20}$$

Eq.(5.18) has to be added as new constraints along with the nonlinear to linear transformation in (5.13), because we need to ensure that $x_{k,n} = 1$ when $s_{k,n} = d_{k,n}^{(1)} = 1$, and zero otherwise. Likewise, the same constraints for $y_{k,n}$ as in (5.19) apply.

Thus, the newly formulated 0-1 problem has an polynomial objective function (instead of an exponential one) and all linear constraints. The price to pay, however, is the increase of the number of optimization variables. The convexity of this problem can be easily proved as in [105].

5.1.2 Solution and Results

Nonlinear branch and bound algorithm [103] is used to search for the optimum solution for our problem. This algorithm comprises of two stages, namely, branch-and-bound and sequential quadratic programming (SQP). Branch-and-bound was first proposed by Land and Doig in [106]. It is an effective way to solve integer programming (IP) problems. And recently, it is also developed to be used in conjunction with the state-of-the-art quadratic programming (QP) tools to solve non-linear programming (NLP) problems involving integer variables. The basic concept of branch-and-bound is to relax the integer constraints so that the tree search can be conducted on the real set. Once the solution is obtained, and all the integer variables happen to take integer values, the optimal solution to the original IP problem is found. If not all solutions are integer-valued, the algorithm branches on those variables who take non-integer values and solve the new problems with the additional simple bounds generated due to branching. More details of this

Table 5.1: $K_1 = K_2 = 2$,$N = 4$,$R_1 = 2$ **bits/OFDM symbol,**$R_2 = 4$ **bits/OFDM symbol,**$P_{e_1} = 10^{-5}$,$P_{e_2} = 10^{-3}$,$N_0 = 1$**.**

$s_{k,n}/c_{k,n}$	$n=1$	$n=2$	$n=3$	$n=4$
$k=1$	1/2	0/0	0/2	0/6
$k=2$	0/0	0/4	1/2	0/0
$k=3$	0/0	0/2	0/0	1/4
$k=4$	0/2	1/4	0/6	0/6

algorithm can be found in [107]. The gradient and Hessian matrix for our defined objective function and constraints are derived for the search algorithm, but the details are not shown here. No relaxations or approximations are made in our optimization process.

The optimum solution can be achieved for any given number of users and subcarriers. A simple case study is shown in Table 5.1-5.2, where the optimum solution is obtained at a snapshot of channel gains on each subcarrier for each user. The assignment results when the minimum power is achieved are presented in Table 5.1, where we can see the optimal subcarrier allocation and constellation selection on each subcarrier for each user with every constraints fulfilled. The channel gains on each subcarrier as seen by each user are also tabulated in Table 5.2 for this case. The minimized total transmit power is 56.9 unit. In order to further explain the result, if we change $c_{3,1} = 4$ and $c_{4,4} = 4$, and accordingly assign $s_{1,3}$, $s_{2,2}$, $s_{3,1}$ and $s_{4,4}$ equal to 1, the resulted total transmit power needed for the new assignment is 233.9 unit, higher than the optimal value by 6.14dB.

Table 5.2: Fading gains on each subcarrier for each user.

$\lvert H_{k,n}\rvert$	$n=1$	$n=2$	$n=3$	$n=4$
$k=1$	1.0332	0.386	0.77132	2.323
$k=2$	0.94289	1.2926	1.5579	0.92533
$k=3$	0.65558	1.1125	0.94374	2.0745
$k=4$	0.30256	2.0287	1.6813	1.1541

The performance of our optimal SBA scheme is compared with the rate-adaptive scheme without multiuser diversity as well as a simple subcarrier allocation scheme discussed in [108]. In fixed subcarrier allocation scheme like traditional FDMA scheme, subcarriers are allocated to the users according to certain predetermined mapping rule. In other words, $\{s_{k,n}\}$ are known before the optimization process. The optimal constellations on each subcarrier for each user $\{c_{k,n}\}$ are searched to achieve the minimum power. Moreover, a simple subcarrier allocation scheme is also proposed in [108] for multiuser OFDM systems, in which each subcarrier is allocated to the user who sees the highest channel gain. In this way, the subcarrier and bit allocations are decoupled. $\{s_{k,n}\}$ are firstly decided according to the ranking of channel gains, and then $\{c_{k,n}\}$ can be easily obtained to minimize the total transmit power while all the constraints are satisfied. Hereafter, we address the two schemes mentioned above FSA and BSA, respectively, for the convenience of future reference.

The transmit power of the multiclass multiuser OFDM system with different number of subcarriers is presented in Figure 5.1 for $N = 4$ and $N = 8$, where the

performance is also compared with FSA and BSA schemes. The curves are generated based on 100 observations when the channel changes and the average values are plotted against the noise spectral density N_0. The required transmit power of our presented optimal solution is always well under the other two schemes, as we can see from the gap between the optimal curve and the FSA, BSA curves in both (a) and (b). Furthermore, when the number of subcarriers increases from 4 to 8, the power difference between our optimal solution and FSA goes from 8dB to 13dB. The wider gap indicates that the performance degradation of fixed subcarrier allocation becomes worse as the system complexity increases in the multiclass multiuser environment. For BSA scheme, although the gap closes up by less than 1dB when N increases, the required transmit power is still 6dB more than that of the optimal scheme. This manifests large potential for performance enhancement of the current heuristic algorithms and imposes great need to explore more efficient suboptimal subcarrier allocation schemes to close the wide gap. Thus, the presented theoretical framework can be used as the benchmark for current and future developed heuristic SBA schemes for multiclass multiuser OFDM systems.

In order to study the power variations with changing channel conditions, the probability density distributions for the minimum required transmit power of the 3 schemes concerned in this chapter is also presented in Figure 5.2. The histograms for the minimum power at the 100 snapshots of channel gains are drawn for different SBA schemes, where we can see that not only the values of power by the optimal scheme are generally much smaller than the other two schemes, the variance of the optimal solution at different channel gains is much smaller than the other two

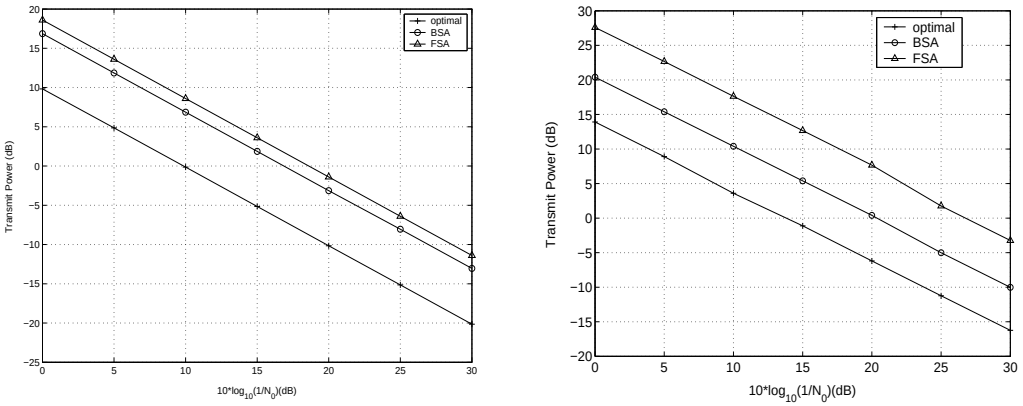

(a) $N = 4$. (b) $N = 8$.

Figure 5.1: Performance comparisons between the optimal solution and other schemes. $K_1 = 2$**,** $K_2 = 1$**,** $R_1 = 2$ **bits/OFDM symbol,** $R_2 = 6$ **bits/OFDM symbol,** $P_{e_1} = 10^{-2}$**,** $P_{e_2} = 10^{-4}$**.**

schemes. The smaller variance shows the advantage of the optimal scheme as it reduces the dynamic range of the transmit power which leads to an easier and less expensive transmitter design.

5.2 Suboptimal solution

In this section, we introduce two suboptimal approaches to further reduce the computation complexity, in order that the subcarrier-and-bit allocation can be updated according to the instantaneous channel gains in the real systems.

5.2.1 Quadratic Fitting Approach

In this approach, the objective function is replaced by a quadratic relationship which fits the first 3 points of the discrete exponential form, i.e., $(0, 0)$, $(2, 3)$ and $(4, 15)$. The resulted quadratic function is $h(t) = \frac{9}{8}t^2 - \frac{3}{4}t$. This approach

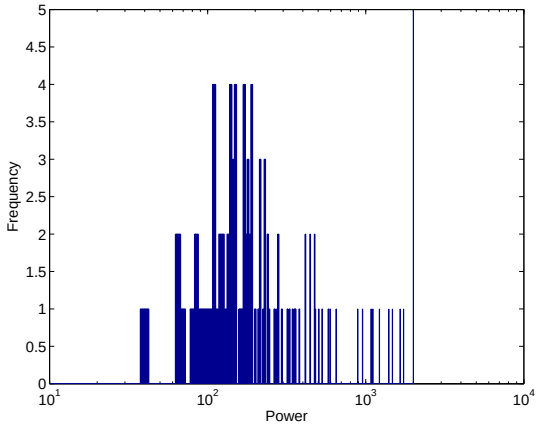

(a) FSA solution.

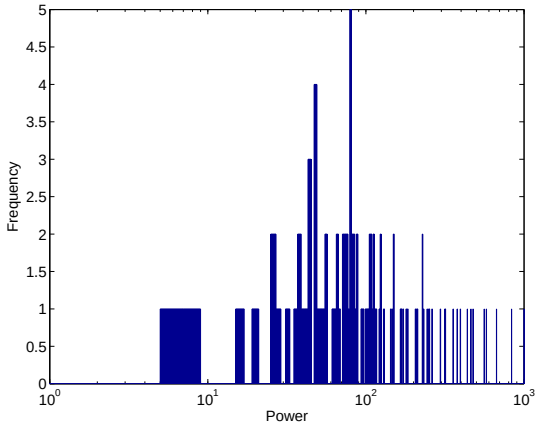

(b) BSA solution.

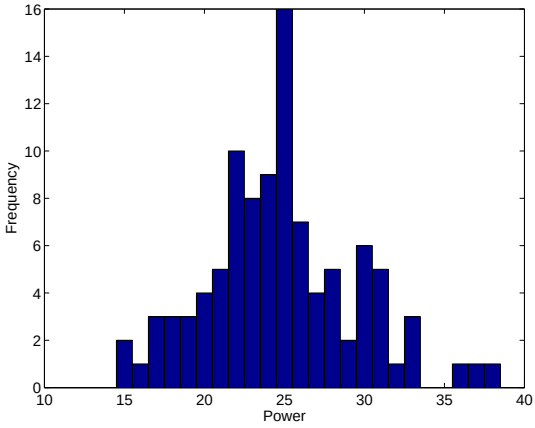

(c) Optimal Solution.

Figure 5.2: Probability density distributions for minimized transmit power of the 3 SBA schemes with a number of channel gain observations. $K_1 = 2$, $K_2 = 1$, $N = 8$, $R_1 = 2$ **bits/OFDM symbol,** $R_2 = 6$ **bits/OFDM symbol,** $P_{e_1} = 10^{-2}$, $P_{e_2} = 10^{-4}$, $N_0 = 1$.

contributes a lot to further simplify the complexity of the Gradient and Hessian Matrix of objective function and thus speed up the computation since efficient quadratic programming algorithm can be used. Again, we can use the transform in (5.13) to convert the objective function to a convex form. Then, the reformulated objective function is:

$$\min_{\substack{x_{k,n},y_{k,n},\\ s_{k,n},d_{k,n}^{(1)},d_{k,n}^{(0)}}} \quad \sum_{k=1}^{K_1}\sum_{n=1}^{N}\rho_1 h(4x_{k,n}+2y_{k,n})/|H_{k,n}|^2 + \sum_{k=K_1+1}^{K_1+K_2}\sum_{n=1}^{N}\rho_2 h(4x_{k,n}+2y_{k,n})/|H_{k,n}|^2, \tag{5.21}$$

subject to all the constraints listed in (5.15)-(5.20). The standard CPLEX solver for mixed integer quadratic programming (MIQP) was employed to find the optimum solution for the quadratic fitting formulation. However, the quadratic fitting cannot match all the 4 discrete values in the objective function, therefore, the results obtained by this scheme are only suboptimal to the original problem. Yet in the later part, we will show this scheme can achieve reliable near-optimal performance over channel variations at much reduced complexity.

5.2.2 Two-Step Approach

As the name suggests, our first step is to relax the solution of the objective function so that the variables can take real numbers. Denote $s_{k,n}c_{k,n} = \mu_{k,n}$, and then solve for $\mu_{k,n}$:

$$\min_{\mu_{k,n}} \sum_{k=1}^{K_1}\sum_{n=1}^{N}\rho_1(2^{\mu_{k,n}}-1)/|H_{k,n}|^2 + \sum_{k=K_1+1}^{K_1+K_2}\sum_{n=1}^{N}\rho_2(2^{\mu_{k,n}}-1)/|H_{k,n}|^2 \tag{5.22}$$

Table 5.3: Subcarrier and bit allocation at minimized transmit power by different algorithms. $K_1 = 2, K_2 = 1, N = 8, R_1 = 2\text{bits/OFDMsymbol}, R_2 = 6\text{bits/OFDMsymbol}, P_{e_1} = 10^{-2}, P_{e_2} = P_{e_3} = 10^{-4}$**,** $N_0 = 1$**.**

$s_{k,n}c_{k,n}$Opt	$n=1$	$n=2$	$n=3$	$n=4$	$n=5$	$n=6$	$n=7$	$n=8$
$k=1$	0	0	0	0	0	2	0	0
$k=2$	2	0	0	0	0	0	0	0
$k=3$	0	0	0	0	0	0	4	2

$s_{k,n}c_{k,n}$QF	$n=1$	$n=2$	$n=3$	$n=4$	$n=5$	$n=6$	$n=7$	$n=8$
$k=1$	0	0	0	0	0	2	0	0
$k=2$	2	0	0	0	0	0	0	0
$k=3$	0	0	0	0	0	0	4	2

$s_{k,n}c_{k,n}$TS	$n=1$	$n=2$	$n=3$	$n=4$	$n=5$	$n=6$	$n=7$	$n=8$
$k=1$	0	0	0	0	0	2	0	0
$k=2$	2	0	0	0	0	0	0	0
$k=3$	0	0	0	0	0	0	4	2

$\lvert H_{k,n}\rvert^2$	$n=1$	$n=2$	$n=3$	$n=4$	$n=5$	$n=6$	$n=7$	$n=8$
$k=1$	0.36677	0.22793	0.37622	0.36363	0.31786	0.40885	0.44364	0.47178
$k=2$	0.44852	0.12452	0.1756	0.11757	0.16514	0.26521	0.19047	0.44259
$k=3$	0.22569	0.23053	0.12987	0.19558	0.12779	0.27974	0.63145	0.55965

subject to

$$\sum_{n=1}^{N} \mu_{k,n} = R_1, \quad k = 1, 2, \ldots, K_1 \tag{5.23}$$

$$\sum_{n=1}^{N} \mu_{k,n} \geq R_2, \quad k = K_1 + 1, K_1 + 2, \ldots, K_1 + K_2 \tag{5.24}$$

Note that in (5.22), (5.23) and (5.24), the variable $\mu_{k,n}$ has been relaxed to take real solution. Moreover, the constraints corresponding to (5.7) are not included in this relaxed formulation, which physically means the subcarrier sharing is allowed in this step. Therefore, the minimum power based on the real solutions obtained here will be the lower bound for the optimized power transmission.

Based on the optimal solution obtained for the above problem, in the second step, we solve another objective function given by:

$$\min_{s_{k,n}, c_{k,n}} \quad \sum_{k=1}^{K_1+K_2} \sum_{n=1}^{N} (s_{k,n} c_{k,n} - \mu_{k,n})^2 \tag{5.25}$$

subject to

$$\sum_{n=1}^{N} s_{k,n} c_{k,n} = R_1, \quad k = 1, 2, \ldots, K_1 \tag{5.26}$$

$$\sum_{n=1}^{N} s_{k,n} c_{k,n} \geq R_2, \quad k = K_1 + 1, \ldots, K_1 + K_2 \tag{5.27}$$

$$\sum_{k=1}^{K_1+K_2} s_{k,n} = 1, \quad n = 1, 2, \ldots, N \tag{5.28}$$

$$s_{k,n} \in S \text{ integer}, \quad c_{k,n} \in C \text{ integer} \tag{5.29}$$

Also, this formulation, due to the multiplication term $s_{k,n} c_{k,n}$, is not a convex form, but we can still use (5.13) to further transfer it into a quadratic function as shown

below:

$$\min_{\substack{x_{k,n},y_{k,n},\\ s_{k,n},d_{k,n}^{(1)},d_{k,n}^{(0)}}} \sum_{k=1}^{K_1+K_2}\sum_{n=1}^{N}(4x_{k,n}+2y_{k,n}-\mu_{k,n})^2, \tag{5.30}$$

subject to all the constraints listed in (5.15)-(5.20).

The second step objective function aims to find the nearest integer solution with the least square error from the optimal real solution, with the remaining constraints fulfilled. We use a standard CPLEX solver–mixed integer quadratic programming (MIQP) to find the optimal solution in the second step. Results will show that this two-step approach can also attain a near-optimal solution, and in the sequel, its accuracy will be compared with the quadratic fitting scheme.

5.2.3 Discussions

The subcarrier and bit assignment results at one snapshot of channel gains by the optimal algorithm and the proposed two algorithms are shown in Table 5.3, where we can see the subcarrier allocation and constellation selection on each subcarrier for each user with every constraints fulfilled. The channel gains on each subcarrier as seen by each user are also tabulated, which are kept to be the same for these algorithms to facilitate a reasonable comparison. From these tables, the solutions by the two heuristic algorithms are shown to be good approximations to the optimal solution, although the assignment of subcarriers among the users might not necessarily be the same. In the tables below, "Opt" denotes the optimal scheme, "QF" is quadratic fitting for short, "TS" stands for two-step approach, and "LB" denotes the lower bound generated in the first step.

Table 5.4: Minimum power and CPU time comparisons. $K_1 = 2$**,** $K_2 = 1$**,** $N = 8$**,** $R_1 = 2$ **bits/OFDM symbol,** $R_2 = 6$ **bits/OFDM symbol,** $P_{e_1} = 10^{-2}$**,** $P_{e_2} = P_{e_3} = 10^{-4}$**,** $N_0 = 1$**.**

Algorithm	Minimized Power	CPU time
Opt	345.08	4.5h
QF	345.08	0.109s
TS	345.08	0.844s
LB	256.23	-

In Table 5.4, the minimum transmit power and the complexity of each algorithm are listed, where the complexity is manifested using the CPU time consumed by the algorithm computations. The number of Class 1 users, K_1, is 2, and there is only 1 Class 2 users, i.e., $K_2 = 1$. And the total number of subcarriers, N, is 8. The QoS requirements for both classes are also listed above Table 5.4. Hence, we can see that the complexity is greatly reduced by our proposed quadratic fitting scheme as well as two step algorithm at nearly no accuracy cost. (For the case shown in the tables, the heuristic algorithms obtain the same results as the optimal solution; yet other results do show some difference between the optimal and suboptimal approaches.)

We observed more snapshots of the channel and employed the two algorithms to perform adaptive subcarrier-and-bit allocations over each channel. In our simulations, we collected values of the minimized power in the evaluated objective function of the two suboptimal schemes over a time varying 8-path channel. The other system parameters remain the same as listed in Table 5.4. The power values

optimized by both schemes are displayed in Figure 5.3. The exact optimal integer solution, however, is highly time consuming, thus the results are not provided in this comparison. Instead, we display the minimized power based on the real solutions in the first step of two-step approach, and use it as a lower bound for the optimum power consumption. From this figure, we can see that the minimized power varies at each channel snapshot. As expected, both heuristic schemes give higher values for the solutions. Keeping in mind that the lower bound still shows significant difference from the actual optimal solution, as we can easily see from the example given in Table 5.4, we can conclude that the two heuristic algorithms give good approximations to the optimal solutions since the gaps from the actual power values to their lower bounds are not considerably large.

Further, in order to show and compare the accuracy of the two heuristic algorithms, we randomly generated 50000 multipath channels, and recorded the suboptimal solutions by the two approaches as well as the lower bound of the total transmit power. The errors from the two suboptimal solutions to their respective lower bounds are calculated as in (5.31) and (5.32),

$$\zeta_{QF} = \left(P_{QF} - P_{LB}\right)/P_{LB} \tag{5.31}$$

$$\zeta_{TS} = \left(P_{TS} - P_{LB}\right)/P_{LB} \tag{5.32}$$

and the cumulative density functions (CDF) of the normalized power errors are shown in Figure 5.4. As we can see, the quadratic fitting approach has better accuracy in a statistical sense: the errors for 60% percent of the solutions are less than 40% above the lower bound; while for two-step approach, only 44% solutions

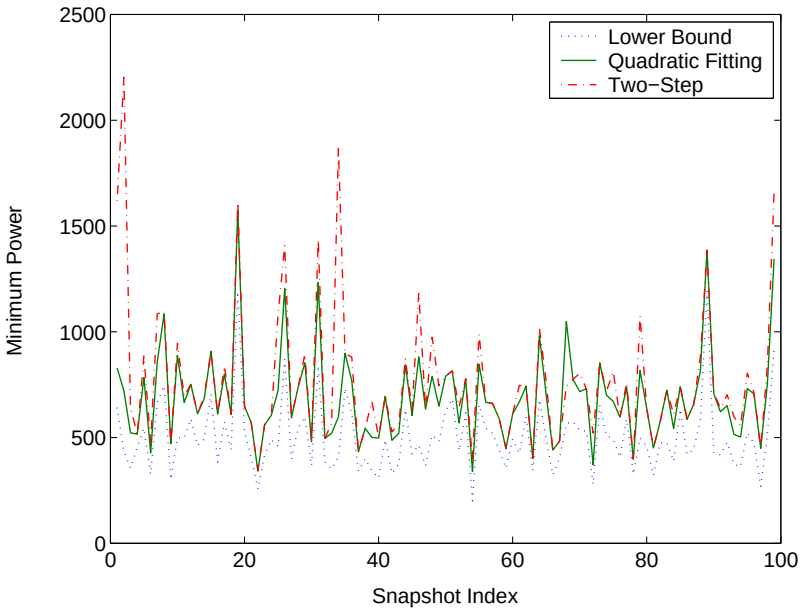

Figure 5.3: Error distribution of the two algorithms.

can guarantee errors within that range. If we consider 90% of all the samples for both schemes, a normalized error of 58% above the lower bound is guaranteed for QF, yet the error for TS goes up to 98% over the lower bound. Therefore, the quadratic fitting approach is shown to be a better approximation to the optimal result under most channel variations.

The accuracy stated in these figures gives only rough ideas for the performance of the two heuristic algorithms. The actual errors from the optimal integer solutions should be far smaller than those from the lower bound, as seen from some available data which is not systematically shown here. Therefore, in order to give more accurate and specific reference for the performance comparisons, We would carry on the effort to further speed up the computations for the optimal subcarrier-and-bit allocation scheme.

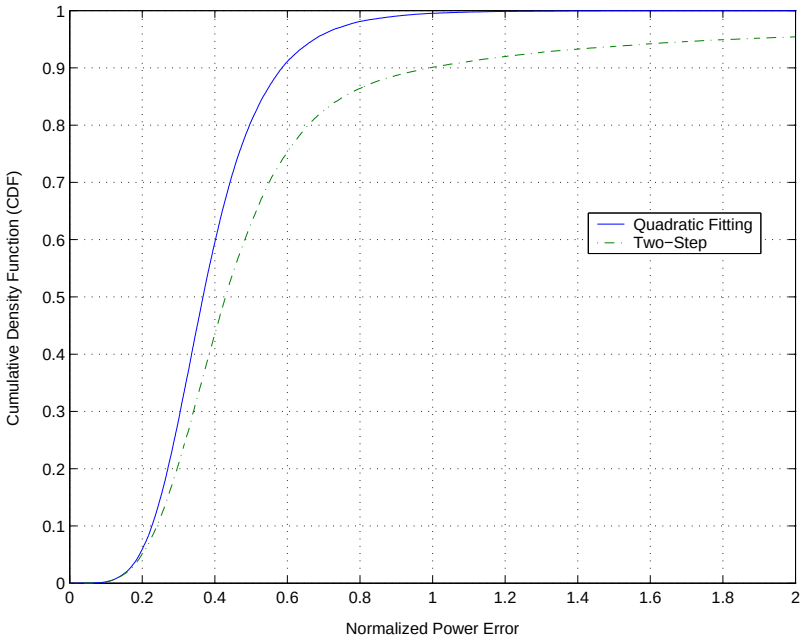

Figure 5.4: Error distribution of the two algorithms.

5.3 OFDM System Supporting Three Service Classes

5.3.1 Problem Formulation

In this section, the system model is modified by a rate-adaptive downlink OFDM system supporting *three* classes of services. Class 1 needs a constant data rate of R_1 bits/OFDM symbol and a target BER of P_{e_1}; Class 2 needs a minimum data rate of R_2 bits/OFDM symbol and a target BER of P_{e_2}; Class 3, however, is a best effort service, which has a target BER of P_{e_3}. Class 3 users are not imposed on data rate requirements; instead, they will make the best of system resources according to the instantaneous channel conditions. All the other system parameters and their respective notations remain the same as the two-class system.

With the introduction of the best effort service, Class 3, our optimization task

is different from Section 5.1, as our target here is to maximize the system revenue to achieve the maximum profit, while satisfying all the data rate and BER constraints for users from 3 classes. To this end, we have to simultaneously minimize the overall transmit power and maximize the total data throughput. Thus, we formulate the objective function as a linear combination of transmit power and data throughput.

$$\Delta = -\pi_1 P + \pi_2 U_2 + \pi_2 U_3 \tag{5.33}$$

where Δ stands for the system revenue, and P is the total transmit power to guarantee the given QoS. U_2 is the total number of bits transmitted per second, i.e., data throughput, of Class 2 users. Similarly, U_3 stands for the data throughput of Class 3 users. Three constants π_1, π_2 and π_3 are introduced for scaling and unit normalization. They are used to appropriately convert power and multiclass throughput into revenue. Their units are, respectively, /W and /bits/s and /bits/s. Note that Class 1 has constant data rate, therefore, the throughput term for Class 1 is omitted in the objective function.

Referring to (5.1), (5.3) and its condition, the total transmit power can be expressed as:

$$P = \sum_{k=1}^{K_1+K_2+K_3} \sum_{n=1}^{N} \rho(k)(2^{s_{k,n}c_{k,n}} - 1)/|H_{k,n}|^2 \tag{5.34}$$

where

$$\rho(k) = \begin{cases} \frac{N_0}{3}\left[Q^{-1}\left(\frac{P_{e_1}}{4}\right)\right]^2, & k = 1, 2, \ldots, K_1 \\ \frac{N_0}{3}\left[Q^{-1}\left(\frac{P_{e_2}}{4}\right)\right]^2, & k = K_1+1, K_1+2, \ldots, K_1+K_2 \\ \frac{N_0}{3}\left[Q^{-1}\left(\frac{P_{e_3}}{4}\right)\right]^2, & k = K_1+K_2+1, K_1+K_2+2, \ldots, K_1+K_2+K_3 \end{cases} \tag{5.35}$$

are constants related to service category.

The data throughput for Class 2 and Class 3:

$$U_2 = \sum_{k=K_1+1}^{K_1+K_2} \sum_{n=1}^{N} s_{k,n} c_{k,n} \qquad U_3 = \sum_{k=K_1+K_2+1}^{K_1+K_2+K_3} \sum_{n=1}^{N} s_{k,n} c_{k,n} \tag{5.36}$$

Thus, from (5.33)-(5.36), the problem can be numerically formulated as below:

$$\begin{aligned} \min_{s_{k,n}, c_{k,n}} \quad & \pi_1 \sum_{k=1}^{K_1+K_2+K_3} \sum_{n=1}^{N} \rho(k)(2^{s_{k,n}c_{k,n}} - 1)/|H_{k,n}|^2 - \pi_2 \sum_{k=K_1+1}^{K_1+K_2} \sum_{n=1}^{N} s_{k,n} c_{k,n} \\ & -\pi_3 \sum_{k=K_1+K_2+1}^{K_1+K_2+K_3} \sum_{n=1}^{N} s_{k,n} c_{k,n} \end{aligned} \tag{5.37}$$

subject to

$$\sum_{n=1}^{N} s_{k,n} c_{k,n} = R_1, \quad k = 1, 2, \ldots, K_1 \tag{5.38}$$

$$\sum_{n=1}^{N} s_{k,n} c_{k,n} \geq R_2, \quad k = K_1 + 1, K_1 + 2, \ldots, K_1 + K_2 \tag{5.39}$$

$$\sum_{k=1}^{K_1+K_2+K_3} s_{k,n} = 1, \quad n = 1, 2, \ldots, N \tag{5.40}$$

and

$$s_{k,n} \in \{0, 1\}, \quad c_{k,n} \in \{0, 2, 4, 6\} \tag{5.41}$$

It is easy to see that the minimization of negative revenue is equivalent to the original problem to maximize the revenue. The data rate constraints for Class 3 users are absent because they provide best effort services. As long as $s_{k,n}$ and $c_{k,n}$ get feasible solutions, the throughput for Class 3 users will take certain non-negative values.

This formulation, as defined by (5.37)-(5.41), is again a mixed-integer nonlinear programming (MINLP) problem with a nonlinear objective function (5.37) and

$2(K_1+K_2+K_3)N$ integer optimization variables on discrete set. It has K_1 nonlinear equality constraints in (5.38), K_2 nonlinear inequality constraints in (5.39) and N linear constraints in (5.40). Similarly as in Section 5.1, some transforms can be taken to ensure the convexity and at the same time linearize the constraints.

Referring to (5.10)-(5.13), we can re-formulate the 3 class optimization problem as:

$$\min_{\substack{x_{k,n},y_{k,n},\\ s_{k,n},d_{k,n}^{(1)},d_{k,n}^{(0)}}} \quad \pi_1 \sum_{k=1}^{K_1+K_2+K_3}\sum_{n=1}^{N}\rho(k)f(4x_{k,n}+2y_{k,n})/|H_{k,n}|^2 - \pi_2 \sum_{k=K_1+1}^{K_1+K_2}\sum_{n=1}^{N}(4x_{k,n}+2y_{k,n})$$
$$-\pi_3 \sum_{k=K_1+K_2+1}^{K_1+K_2+K_3}\sum_{n=1}^{N}(4x_{k,n}+2y_{k,n}) \tag{5.42}$$

subject to

$$\sum_{n=1}^{N}(4x_{k,n}+2y_{k,n}) = R_1, \quad k=1,2,\ldots,K_1 \tag{5.43}$$

$$\sum_{n=1}^{N}(4x_{k,n}+2y_{k,n}) \geq R_2, \quad k=K_1+1,K_1+2,\ldots, K_1+K_2 \tag{5.44}$$

$$\sum_{k=1}^{K_1+K_2+K_3} s_{k,n} = 1, \quad n=1,2,\ldots,N \tag{5.45}$$

$$s_{k,n}+d_{k,n}^{(1)}-1 \leq x_{k,n} \leq 0.5(s_{k,n}+d_{k,n}^{(1)}) \tag{5.46}$$

$$s_{k,n}+d_{k,n}^{(0)}-1 \leq y_{k,n} \leq 0.5(s_{k,n}+d_{k,n}^{(0)}) \tag{5.47}$$

and

$$x_{k,n}, y_{k,n}, s_{k,n}, d_{k,n}^{(1)}, d_{k,n}^{(0)} \in \{0,1\} \tag{5.48}$$

Table 5.5: Optimal subcarrier and bit allocation at maximum system revenue. $\pi_1 = 1, \pi_2 = 5, \pi_3 = 10$**,** $K_1 = K_2 = K_3 = 1$**,** $N = 8$**,** $R_1 = 2$ **bits/OFDM symbol,** $R_2 = 6$ **bits/OFDM symbol,** $P_{e_1} = 10^{-2}$**,** $P_{e_2} = P_{e_3} = 10^{-4}$**,** $N_0 = 1$**.**

$s_{k,n}c_{k,n}$	$n=1$	$n=2$	$n=3$	$n=4$	$n=5$	$n=6$	$n=7$	$n=8$
$k=1$	0	0	0	0	0	0	0	2
$k=2$	0	0	2	2	0	0	2	0
$k=3$	2	4	0	0	4	2	0	0

5.3.2 Optimal Solution

For the integer polynomial objective function, nonlinear branch and bound is employed again to search for the optimum solution for the 3 class case. The optimum solution can be achieved for any given number of users and subcarriers with predefined values for π_1, π_2 and π_3. Take $\pi_1 = 1, \pi_2 = 5, \pi_3 = 10$ and $\pi_1 = 1, \pi_2 = 8, \pi_3 = 5$ for examples. The assignment results when the maximum revenue is achieved are respectively presented in Table 5.5 and Table 5.6, where we can see the optimal subcarrier allocation and constellation selection on each subcarrier for each user with every constraints fulfilled. The channel gains on each subcarrier as seen by each user are also tabulated in Table 5.7, which are kept to be the same in Table 5.5 and Table 5.6 to facilitate a reasonable comparison.

As shown in Table 5.5 and Table 5.6, in both cases, only 1 subcarrier is assigned to User 1 to maintain its constant data rate. More subcarriers are assigned to User 2 in Table 5.6 since the throughput of Class 2 weighs higher in the revenue output as defined by (5.33). The same goes for the subcarrier allocations in Table 5.5 where U_3 plays a dominant role in the system revenue. Therefore, the constants

Table 5.6: Optimal subcarrier and bit allocation at maximum system revenue. $\pi_1 = 1, \pi_2 = 8, \pi_3 = 5$, $K_1 = K_2 = K_3 = 1$, $N = 8$, $R_1 = 2$ **bits/OFDM symbol,** $R_2 = 6$ **bits/OFDM symbol,** $P_{e_1} = 10^{-2}$, $P_{e_2} = P_{e_3} = 10^{-4}$, $N_0 = 1$.

$s_{k,n}c_{k,n}$	$n=1$	$n=2$	$n=3$	$n=4$	$n=5$	$n=6$	$n=7$	$n=8$
$k=1$	0	0	0	0	0	2	0	0
$k=2$	0	2	2	2	0	0	2	2
$k=3$	2	0	0	0	2	0	0	0

Table 5.7: Fading gains on each subcarrier for each user.

$\lvert H_{k,n}\rvert$	$n=1$	$n=2$	$n=3$	$n=4$	$n=5$	$n=6$	$n=7$	$n=8$
$k=1$	0.94003	1.1345	0.56023	1.4282	1.3371	1.5569	1.5772	1.3518
$k=2$	0.59159	1.9685	1.1348	1.8181	1.0801	0.53149	1.8736	1.2042
$k=3$	1.3577	2.0928	0.41576	0.58165	1.971	1.4944	0.9236	0.22603

π_1, π_2 and π_3 can be chosen appropriately to adjust the weight of different service classes for their respective contributions to the overall revenue, according to their priorities given by the service providers.

The performance of our optimal SBA scheme is compared with the two simplified schemes described in Section 5.1. The first is the fixed subcarrier allocation scheme, FSA, whereby subcarriers are allocated to the users according to certain predetermined mapping rule. However, users are still free to decide the modulation order in those subcarriers allocated to them. This is in principle similar to a rate-adaptive scheme without multiuser diversity. The second is the simple subcarrier allocation scheme discussed in [108], BSA, where subcarriers are allocated to user

who sees the highest channel gain in an order of service priorities. In this way, the subcarrier and bit allocations are decoupled. $\{s_{k,n}\}$ are firstly decided according to the ranking of subcarrier channel gains and priority of services. $\{c_{k,n}\}$ can then be easily obtained to maximize the system revenue while all the constraints are satisfied.

The system performance in terms of the overall revenue with different number of subcarriers is presented in Figure 5.5 and Figure 5.6 for $N = 4$ and $N = 8$, respectively, where the performance is also compared with FSA and BSA schemes. We take $N = 8$ as an example to further illustrate the two simplified allocation schemes. By FSA, the subcarriers are assigned arbitrarily by the system regardless of channel conditions: subcarriers 1-3 are allocated to user 1 (Class 1); subcarriers 4-6 to user 2 (Class 2); the rest two subcarriers 7 and 8 are allocated to user 3 (Class 3). On the other hand, by BSA, user 1 chooses the best 3 subcarriers first on which it sees the highest channel gains, and then user 2 chooses its best 3 subcarriers among the rest subcarriers; the left two subcarriers are assigned to user 3. It is much to our expectation that for each scheme, the user's revenue function becomes greater as the average SNR increases, since it is easier to fulfil the required BER with lower transmit power and higher throughput when the noise becomes smaller.

Furthermore, the performance of our presented optimal solution is always well above the other two schemes, as we can see from the revenue gap between the optimal curve and the FSA, BSA curves in both Figure 5.5 and Figure 5.6. At high SNR, the gap becomes even wider; while at the same time, the difference between

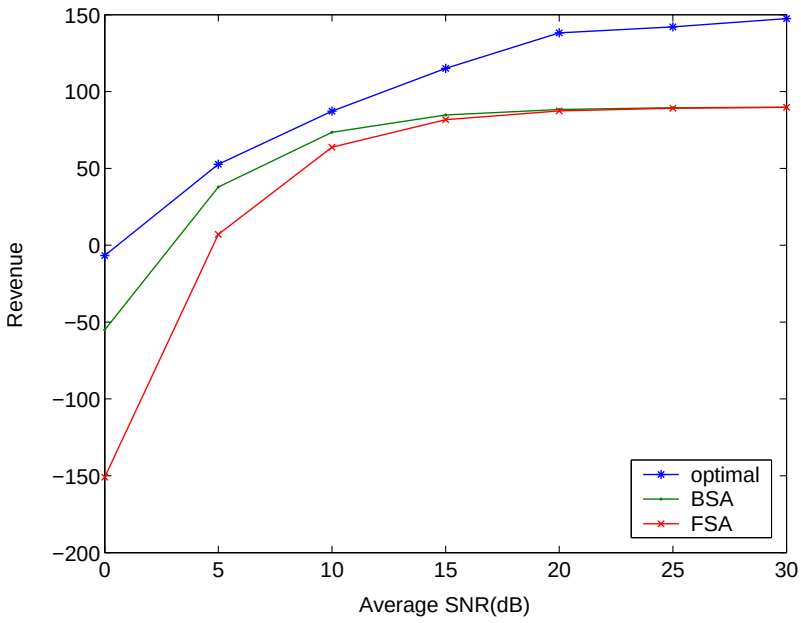

Figure 5.5: Performance comparisons between the optimal solution and other schemes. $\pi_1 = 1, \pi_2 = 5, \pi_3 = 10$**,** $K_1 = K_2 = K_3 = 1$**,** $N = 4$**,** $R_1 = 2$ **bits/OFDM symbol,** $R_2 = 6$ **bits/OFDM symbol,** $P_{e_1} = 10^{-2}$**,** $P_{e_2} = P_{e_3} = 10^{-4}$**.**

FSA and BSA is closing up, which means the simple subcarrier allocation scheme of BSA can hardly give any performance improvement over the fixed subcarrier allocation (FSA) at high SNR. This shows that rate adaptive control itself could be efficient enough in this case.

The above presented results in Figure 5.5 and Figure 5.6 are based on one channel snapshot, which means the channel was fixed over the curves. In order to show the performance comparisons upon channel variations, some channel snapshots were collected and the performance was also compared with FSA and BSA schemes, where the channel was kept to be the same at each snapshot observation. The maximum revenue and the corresponding system throughput at different channel snapshots were drawn in Figure 5.7 and Figure 5.8, where $\pi_1 = 1, \pi_2 = 5, \pi_3 = 10$ and N_0 was fixed to be 0.02. The snapshots shown in these

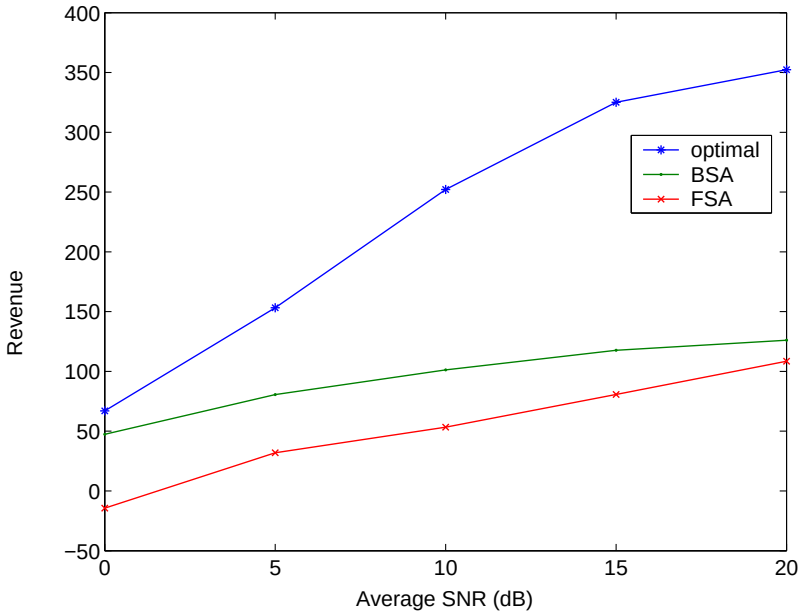

Figure 5.6: Performance comparisons between the optimal solution and other schemes. $\pi_1 = 1, \pi_2 = 5, \pi_3 = 10$**,** $K_1 = K_2 = K_3 = 1$**,** $N = 8$**,** $R_1 = 2$ **bits/OFDM symbol,** $R_2 = 6$ **bits/OFDM symbol,** $P_{e_1} = 10^{-2}$**,** $P_{e_2} = P_{e_3} = 10^{-4}$**.**

figures are numbered according to the increasing optimal revenue. From Figure 5.7, the system revenue by the optimal approach is always larger than FSA and BSA approaches, and at the same time, it has less dynamic range when the channel varies randomly. The FSA scheme, however, fluctuates greatly over the random multipath channels. When the channel suffers deep fade on certain subcarriers and those subcarriers happen to be assigned to the same user which requires high data rate at a low BER, the required transmit power soars to an extra high value which leads to a very low system revenue, as can be seen at the fifth point on the FSA performance curve in Figure 5.7. The BSA scheme appears to give higher revenue than FSA, which comes from the multiuser diversity gain brought by the subcarrier choices adapted to channel conditions of different users. The performance gain of BSA over FSA is not always remarkable, however, and it is likely due to the limited

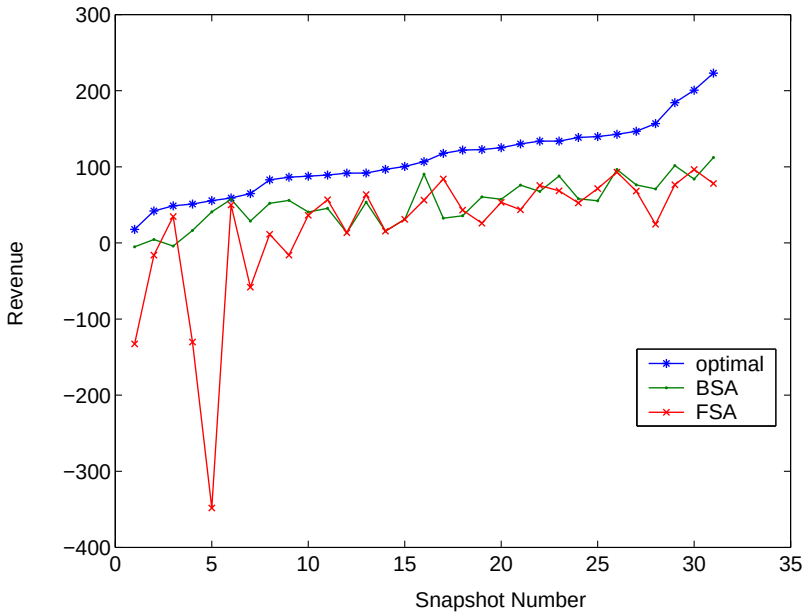

Figure 5.7: System revenues for the optimal solution and other schemes over different multipath channels. $\pi_1 = 1, \pi_2 = 5, \pi_3 = 10$,$K_1 = K_2 = K_3 = 1$,$N = 8$,$R_1 = 6$ **bits/OFDM symbol,** $R_2 = 8$ **bits/OFDM symbol,** $P_{e_1} = 10^{-2}$**,** $P_{e_2} = P_{e_3} = 10^{-4}$**,** $N_0 = 0.02$**.**

diversity potential caused by the small number of users. In addition, there is still a noticeable gap between BSA performance and that of our optimal approach, as can be seen in Figure 5.5-5.8. And according to Figure 5.8, the throughput per OFDM symbol shows significant gap between the optimal scheme and the other two. This partially results in the higher revenue generated by the optimal approach, which can be reflected from (5.33).

If we normalize the revenue by dividing it by the total throughput, the normalized revenue is displayed in Figure 5.9. Similarly in Figure 5.10, the normalized total transmit power by the optimal scheme is compared with the other two schemes. From Figure 5.10, it can be seen that the normalized transmit power is not necessarily the minimum for the optimal SBA scheme. This can be explained if

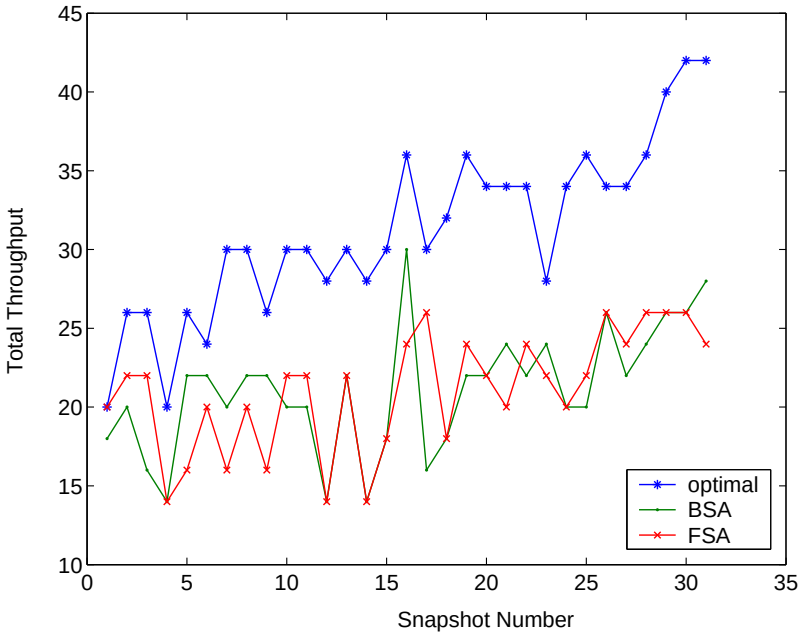

Figure 5.8: System throughput for the optimal solution and other schemes over different multipath channels. $\pi_1 = 1, \pi_2 = 5, \pi_3 = 10$**,**$K_1 = K_2 = K_3 = 1$**,**$N = 8$**,**$R_1 = 6$ **bits/OFDM symbol,** $R_2 = 8$ **bits/OFDM symbol,** $P_{e_1} = 10^{-2}$**,** $P_{e_2} = P_{e_3} = 10^{-4}$**,** $N_0 = 0.02$**.**

we bear in mind that to maximize revenue, most subcarriers transmit using higher order QAM for this specific set of constants π_1, π_2, π_3, and from (5.3), the required energy grows exponentially with the modulation order for a given BER. This also explains why the revenue per bit in Figure 5.9 is not so exciting compared with the total revenue.

The system performance is expected to obtain greater improvement over the two schemes in comparison, when we change the values of π_2 and π_3 to assign a higher weight to Class 2 users (for example, $\pi_2 = 10$, $\pi_3 = 5$). Accordingly, more extensive research on the suitable choice of π_1, π_2 and π_3 will be presented in the next section.

Besides, the suboptimal schemes which are suggested in the previous section

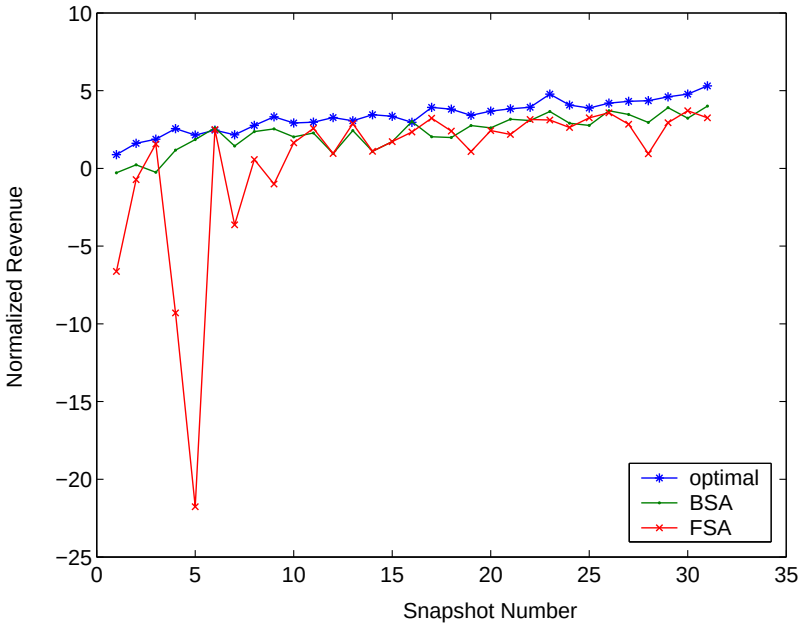

Figure 5.9: Normalized revenues for the optimal solution and other schemes over different multipath channels. $\pi_1 = 1, \pi_2 = 5, \pi_3 = 10$,$K_1 = K_2 = K_3 = 1$,$N = 8$,$R_1 = 6$ **bits/OFDM symbol,** $R_2 = 8$ **bits/OFDM symbol,** $P_{e_1} = 10^{-2}$**,** $P_{e_2} = P_{e_3} = 10^{-4}$**,** $N_0 = 0.02$**.**

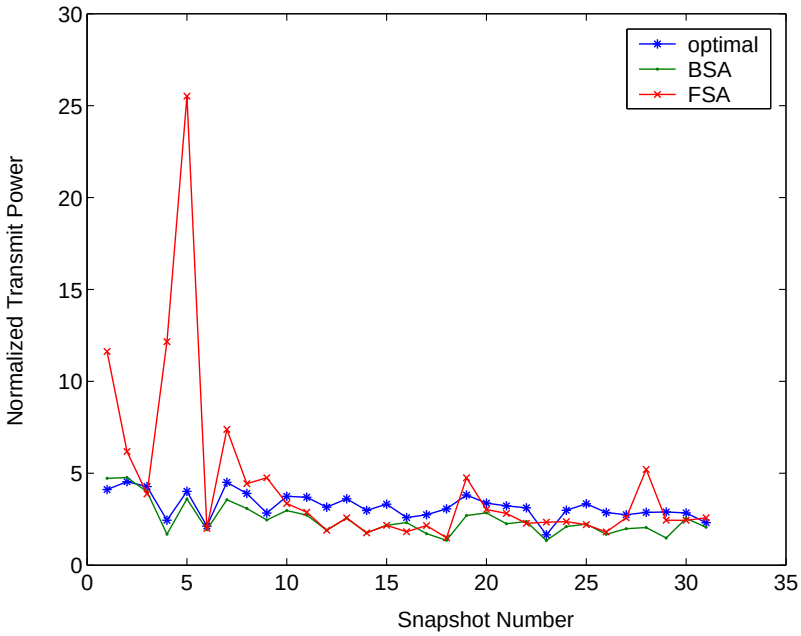

Figure 5.10: Normalized transmit power for the optimal solution and other schemes over different multipath channels. $\pi_1 = 1, \pi_2 = 5, \pi_3 = 10$,$K_1 = K_2 = K_3 = 1$,$N = 8$,$R_1 = 6$ **bits/OFDM symbol,** $R_2 = 8$ **bits/OFDM symbol,** $P_{e_1} = 10^{-2}$**,** $P_{e_2} = P_{e_3} = 10^{-4}$**,** $N_0 = 0.02$**.**

can be easily extended to the 3 class case to speed up the allocation process. And if we let $\pi_1 = 1, \pi_2 = \pi_3 = 0$, the model literally reduces to the power optimization problem for the 2 class case discussed in Section 5.1.

5.3.3 Parameter Selection and Discussion

In the previous sections, the performance of both optimal and suboptimal algorithms is discussed when the factors π_1, π_2 and π_3 are fixed. However, how to choose the values for π_1, π_2 and π_3 still needs investigation. In this section, we will study the effect of the parameters on the distribution of the "excess" radio resources among the minimum guarantee service (Class 2) and the best effort service (Class 3).

As seen in Section 5.2.3, our heuristic algorithm, quadratic fitting, can achieve better near-optimal performance than the two-step algorithm. Hence in our following simulations, the quadratic fitting approach is used to obtain the revenue. Without loss of generality, we fix $\pi_2 + \pi_3 = 1$, and then vary the value of π_2 between 0 and 1 for a given π_1 ranging from $0.05 \sim 0.25$. It is easy to see that the ratio $\pi_2/\pi_3 = \pi_2/(1 - \pi_2)$ is a monotonically increasing function in terms of π_2. 1000 samples for each set of values for π_1, π_2, π_3 were collected and averaged. Note that the throughput of Class 2 users, η_2, has a minimum data rate requirement R_2 (for this case $R_2 = 6$ bits/OFDM symbol), therefore, for Class 2 users, the choice of the parameters only affects the incremental number of bits over R_2. If we denote this incremental data rate as η_2', then $\eta_2' = \eta_2 - R_2$. In order to show the resource allocations with different parameters, we plot η_2' and η_3 against the ratio π_2/π_3,

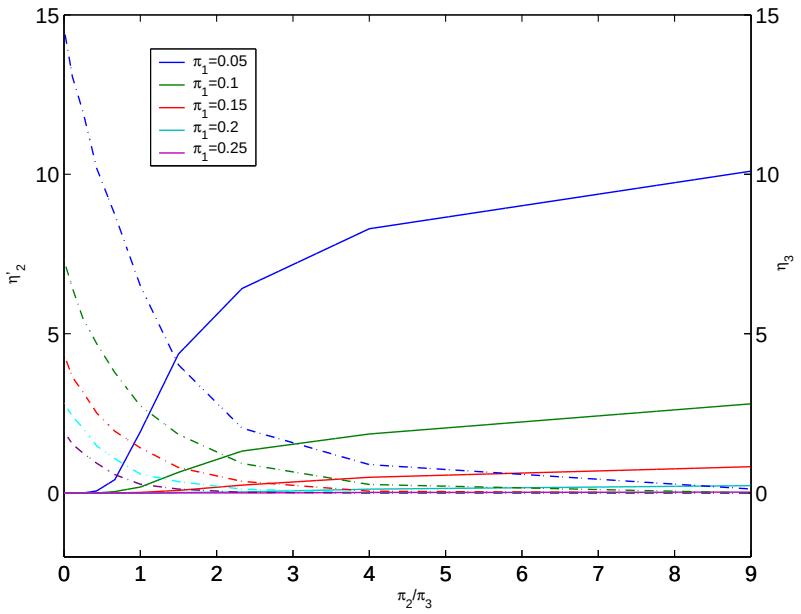

Figure 5.11: Excess throughput for Class 2 and 3 users with changing parameters π_1, π_2, π_3.

at each value of π_1 in Fig. 5.11, where η_2' were plotted in solid curves, and η_3 in dash-dotted curves. The different values of a are distinguished by colors.

As displayed in Fig. 5.11, at a constant π_2/π_3, when π_1 increases from 0.05 to 0.25, the throughput for both Class 2 and 3 is decreased. For an extreme example, when $\pi_1 = 0.25$ and $\pi_2/\pi_3 > 2.5$, both η_2' and η_3 drop to zero, which indicates that the system avoids to allocate extra power resources to Class 2 or Class 3 users. This is because the award to transmit more bits is not justified since the transmit power appears to be a more expensive resource. Therefore, the system transmits at minimum throughput, and the minimum guarantee service (Class 2) literally reduces to constant rate service. That is why η_2 is kept at 6, while Class 3 has no throughput in this case. On the other hand, for a fixed value of π_1, as π_2/π_3 increases, the throughput of Class 2 rises from 6 while that of Class 3 drops.

Hence, the results confirm that π_2/π_3 controls the resource allocations between Class 2 and 3 users. When $\pi_2 + \pi_3$ is fixed to be 1 and π_2/π_3 becomes greater, more subcarriers are allocated to Class 2 users, compared to Class 3 users, to increase their throughput so as to pursuit a higher revenue. This explains why when $\pi_2/\pi_3 = 9$, nearly no throughput can be observed for Class 3 users.

In Fig. 5.11, we can also see that for each π_1, there exists a value of π_2/π_3, where the excess throughput for Class 2 and 3 is equal, which is given by the intersections of the solid line and dash-dotted line of the same color. If we extract these intersections, the relationship of π_1 versus π_2/π_3 can be displayed in Fig. 5.12. From the results in Fig. 5.11 and 5.12, we can get rough idea about how to choose the value of π_1, π_2, π_3 so as to facilitate the allocation of radio resources according to the service needs. The system can adjust the value of π_1 to obtain certain tradeoff between power and throughput, as indicated by Fig. 5.11, and adjust π_2/π_3 at each π_1 to allocate the excess resources between the minimum guarantee and best effort services. Appropriate recommendations about the choices of π_2/π_3 at certain values of π_1 can be found in Fig. 5.12.

5.4 Summary and Contribution

Subcarrier-and-bit allocation in multicarrier transmission systems has been under extensive research as it can exploit the multiuser diversity and hence enhance the spectral efficiency of the system. Although the interest never abates to find the optimal solution for the subcarrier-and-bit allocation in OFDM systems, the

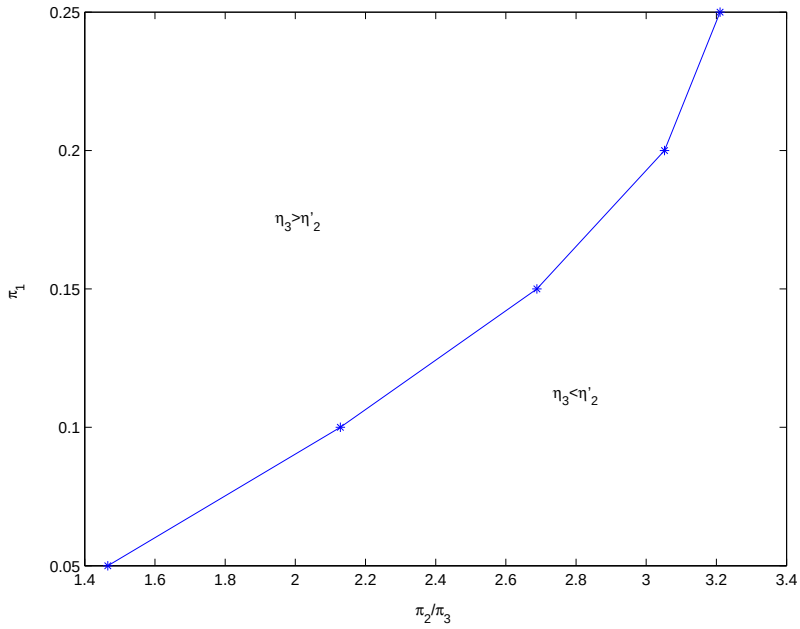

Figure 5.12: Choices of π_1, π_2, π_3 at equal excess throughput of Class 2 and 3.

computation difficulty still remains to solve the highly complicated optimization problems. Therefore, among the algorithms proposed in past literatures, some tried to make assumptions or relaxations to the original problem, or some used simplified cost functions to develop heuristic approaches, and their work was mainly for single class. For our work presented in this chapter, the optimal solutions for the concerned multiclass multiuser OFDM systems were presented.

We dealt with the subcarrier-and-bit allocations in multiclass multiuser OFDM systems. The downlink transmission was examined. Firstly, an OFDM system supporting two user classes was discussed. The overall transmit power was minimized with fulfillment of the QoS constraints of each class. The optimal scheme was formulated as a nonlinear integer programming problem, and no relaxations or assumptions were made herein. Some transformations were taken, such as polynomial fitting and linearization, to guarantee the function convexity and at the same

time reduce the complexity. Then, the *exact* optimal solution was obtained using nonlinear branch and bound algorithm. Some simple case studies were presented and the performance curves were presented. The proposed optimal scheme can provide the benchmark for the current and future research of SBA algorithms for multiclass rate-adaptive systems.

In the sequel, two suboptimal schemes were proposed, i.e., quadratic fitting and two-step, which can speed up the allocations with little accuracy penalty. The computation complexity as well as the accuracy was compared between the optimal and suboptimal schemes. The error distributions between the quadratic fitting and the two-step approaches were presented, which showed the former is more reliable and closer to the optimum. The two-step approach, though, contributes to give a lower bound to the optimal performance.

Next, we extended the subcarrier-and-bit allocation algorithms to a three class multiuser OFDM system to include best effort service. The objective was then changed to maximize the system revenue defined as a linear function of the transmit power and the throughput, with fulfillment of the QoS constraints of each class. The optimization scenario was also formulated as a nonlinear integer problem, whose optimal solution was obtained and presented in the performance curves. The parameter selection of π_1, π_2, π_3 is also discussed. π_1 controls the tradeoff between the power and throughput, and π_2/π_3 takes care of the excess resource allocation between the minimum guarantee and best effort services. Our results show that there exists a best π_2/π_3 at each π_1 where the same excess throughput can be achieved for Class 2 (minimum guarantee) and Class 3 (best effort) users.

Chapter 6

Subcarrier Allocation Schemes for MC-DS-CDMA Systems

In the last chapter, subcarrier-and-bit allocation algorithms are intensively investigated in OFDM systems. Here in this chapter, we focus on another multicarrier transmission system, MC-DS-CDMA.

Subcarrier allocation for multiuser MC-DS-CDMA systems is much more complicated when compared to OFDM systems due to the presence of MAI when multiple users transmit simultaneously on the same subcarrier. In this chapter, we present two novel suboptimal schemes to solve the subcarrier allocation problem for MC-DS-CDMA with MAI. For the convenience of future reference, we call the first proposed scheme "Proposed Scheme (Linear)" (PSL), and the second proposed scheme "Proposed Scheme (Quadratic)" (PSQ). In the first algorithm, PSL, we assume that fading gains of all users are slowly time varying and independent with each other. All subcarriers are ordered according to their respective channel gains

seen by each user at every updating stage. The subcarrier allocation coefficients of the previous updating stage together with the ordering index vector of the current updating stage are jointly used to calculate the average BER on respective subcarriers. The average BER will be used in the objective function to perform the subcarrier allocation. In the second algorithm, PSQ, we formulate the problem without using subcarrier allocation coefficients of the previous updating stage; furthermore, the actual channel gains are used instead of the ranking information in the optimizing process. Although the objective function is formulated as a QP problem, which is non-linear, we can use Kuhn-Tucker (KT) conditions to convert the problem into a solvable LP problem. The performance between our proposed algorithms, and that reported in [2] (addressed as Kim's method hereafter) are compared.

The remaining part of the chapter is organized as following: in Section 6.1, the system model is presented, which includes transmitter and receiver structure for both downlink and uplink transmissions. The two proposed algorithms are described in Section 6.2 and simulation results are given and discussed in Section 6.3. Finally, concluding remarks are drawn in Section 6.4.

6.1 System Model

The channel gain on each subcarrier is assumed to remain nearly constant within at least two updating periods and undergoes frequency non-selective fading. For simplicity, fading gains on all subcarriers are assumed to be independently and

identically distributed (i.i.d.) Rayleigh random variables. BPSK modulation is assumed.

Figure 6.1-6.4 suggest a system model for the links between mobile (MS) and base station (BS). Channel estimations are performed at receivers of both BS and MS. In the uplink, BS receiver performs channel estimation for all MS's. The obtained information is used in the uplink subcarrier allocator (USA) to compute the most suitable L_c subcarriers to each MS for uplink transmission. In the downlink, each MS feeds back its respective estimated channel information at A to downlink subcarrier allocator (DSA) located in BS for subcarrier allocation of each MS. In order to estimate the downlink channel gain, a pilot channel is used, on which the data transmitted is known at the receiver. The pilot signal is transmitted over all subcarriers in the downlink using a specific code. Whereas, in the uplink, pilot signals are only transmitted on the unused subcarriers using the user code for channel estimation, with relatively lower power to avoid excessive interference to other users. The output in USA and DSA is fed back to the uplink and downlink subcarrier selectors (USS and DSS) of MS through B and C, respectively, as illustrated in Figure 6.1-6.4. USS and DSS in MS use these information to select subcarriers for transmission and demodulation, respectively. In the following discussion, we consider downlink transmission, but our algorithm can apply to both uplink and downlink.

At the BS transmitter, the data stream of the kth user, b_k^l, is spread by the user's signature sequence, $a_k(g)$ $\{g = 0, 1, 2, \ldots, G-1\}$, with a processing gain (PG) G. The data stream of each user will be split into L_c parallel sub-streams and there

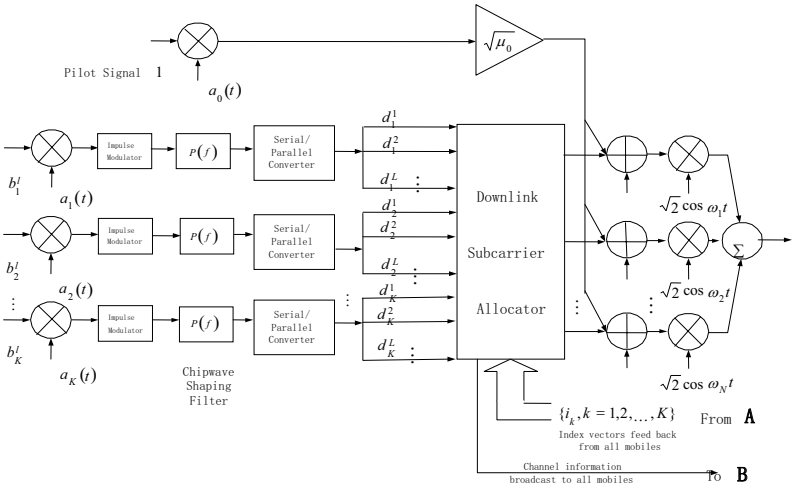

Figure 6.1: System Model of BS Transmitter.

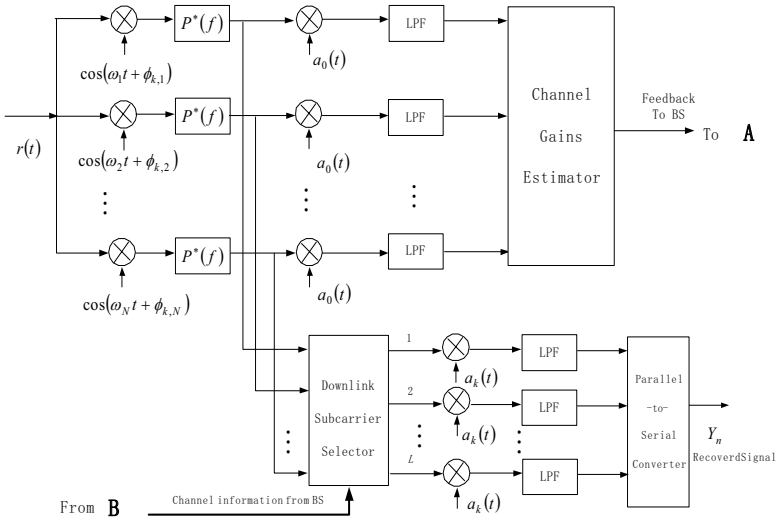

Figure 6.2: System Model of MS Receiver.

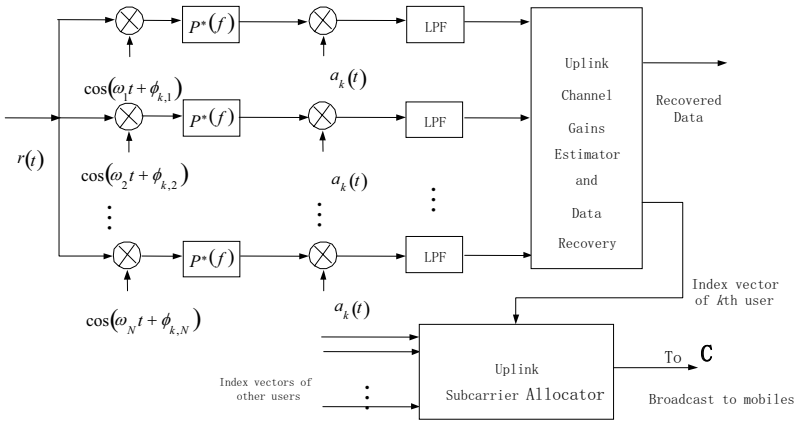

Figure 6.3: System Model of BS Receiver.

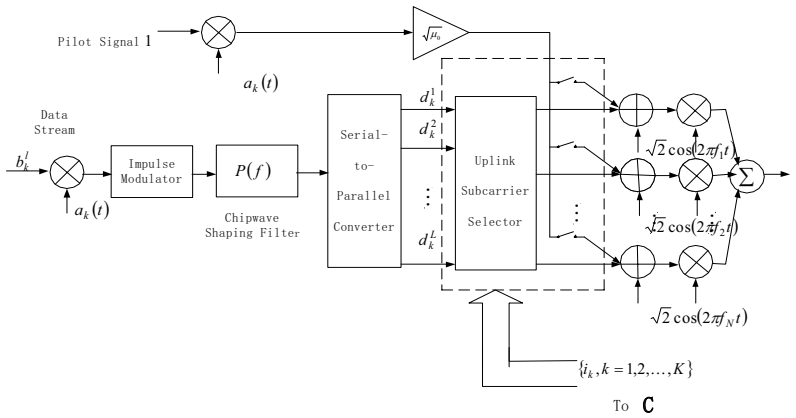

Figure 6.4: System Model of MS Transmitter.

are altogether N subcarriers. These parallel data streams will be modulated only on the corresponding subcarriers which are allocated to this user by DSA. At the MS, the received signal on each subcarrier is coherently demodulated. Furthermore, perfect phase tracking is assumed so that the random phase resulted from channel distortions will not be considered in this chapter. Let K denote the number of active users in the system and $s_{k,n}$ denote the subcarrier allocation coefficients obtained from DSA for the kth user on the nth subcarrier. The received signal at the kth MS is thus given as

$$\begin{aligned} r_k(t) &= \sum_{k=1}^{K} \sqrt{2E_{c_k}} \sum_{l=-\infty}^{\infty} b_k^l a_k(t-lT) \sum_{n=1}^{N} s_{k,n}\alpha_{k,n}\cos(\omega_n t + \phi_{k,n}) \\ &\quad + \sqrt{\frac{2E_{c_k}\mu_0}{N}} \sum_{l=-\infty}^{\infty} a_0(t-lT) \sum_{n=1}^{N} \alpha_{k,n}\cos(\omega_n t + \phi_{k,n}) + w(t), \end{aligned} \quad (6.1)$$

where

$$s_{k,n} = \begin{cases} 1 & \text{if } k\text{th subcarrier is selected} \\ 0 & \text{if } k\text{th subcarrier is not selected} \end{cases}, \quad (6.2)$$

and $a_k(t)$ is given by

$$a_k(t) = \sum_{g=0}^{G-1} a_k(g)p(t-gT_c), \quad (6.3)$$

where $\{a_k(g), g = 0, 1, 2, \ldots, G-1\}$ is a short random code sequence for MS k, consisting of G chips that take values $\{\pm 1\}$. E_{c_k} is the received energy per chip for MS k, $\mu_0(> 1)$ is the additional energy gain allocated to pilot signal where code $a_0(g)\,\{g = 0, 1, 2, \ldots, G-1\}$ is used, T and T_c are the symbol and chip period, respectively, with $T = GT_c$. $\alpha_{k,n}$ is the amplitude of channel gain on the nth subcarrier seen by the kth MS. ω_n is the carrier angular frequency of the nth subcarrier, and $\phi_{k,n}$ denotes the phase shift as a result of Doppler effect.

The frequency response of the chip waveform $p(t)$ is bandlimited to B_s and satisfies Nyquist criterion. $w(t)$ is AWGN with zero mean and variance η_0. Eq. 6.1 needs to be modified for uplink transmission, taking into the consideration of the difference in pilot channel transmission.

The output of the wave-shaping filter on the nth subcarrier is given by

$$\begin{aligned} y_k(t) &= \sum_{k\in U_n} \sqrt{E_{c_k}}\alpha_{k,n} \sum_{l=-\infty}^{\infty} b_k^l \sum_{g=0}^{G-1} a_k(g) h\left[t-(lG+g)T_c\right] \\ &\quad + \sqrt{\frac{E_{c_k}\mu_0}{N}}\alpha_{k,n} \sum_{l=-\infty}^{\infty} \sum_{g=0}^{G-1} a_0(g) h\left[t-(lG+g)T_c\right] + \tilde{w}(t), \end{aligned} \tag{6.4}$$

where U_n is the set of the active users who share the nth subcarrier among the total K active users. $h(t)$ denotes the matched filter impulse response, where its frequency response $H(f) = |P(f)|^2$ and satisfies Nyquist criterion. $\tilde{w}(t)$ is the filtered AWGN. The output signal of the correlator for the lth bit can be written as

$$Y_n = \sum_{g'=0}^{G-1} a_k(g') y[(g'+lG)T_c] = S_n + I_n + W_n, \tag{6.5}$$

where

$$S_n = G\sqrt{E_c}\alpha_{k,n} b_k^l, \tag{6.6}$$

$$I_n = G\sqrt{E_c}\alpha_{k,n} \times \left[\sum_{j\in U_n, j\neq k} C_{k,j}(0) b_j^l + \sqrt{\frac{\mu_0}{N}} C_{k,0}(0) \right], \tag{6.7}$$

and

$$W_n = \sum_{g'=0}^{G-1} a_k(g') \tilde{w}\left[(g'+lG)T_c\right]. \tag{6.8}$$

are respectively the desired signal, the interference resulted from other users sharing the same subcarrier and the noise term. $C_{k,j}(0)$ is the cross-correlation coefficient

between the kth and jth user signature sequences defined by

$$C_{k,j}(0) = \frac{1}{G}\sum_{g=0}^{G-1} a_k(g)a_j(g). \tag{6.9}$$

Note that $h[(g'-g)T_c] = 0$ for $g' \neq g$, since it satisfies Nyquist Criterion.

For simplicity, we assume $E_{c_i} = E_{c_j}\, \forall i \neq j$. The accurate and in-time estimation of channel gains is important since the allocation is adapted to instantaneous channel conditions. In this chapter, we assume the channels are perfectly estimated.

6.2 Algorithm Description

6.2.1 PSL Algorithm

In PSL, the objective is to minimize the BER of respective users, rather than minimizing the overall BER of all users, by properly assigning subcarriers among users. Since our scheme considers MAI when minimizing each user's BER performance, the solution is expected to approach the optimal value of the real system.

Problem Formulation

Here, let $s_{k,n}$ denote the subcarrier allocation coefficients and $P_{e,k,n}$ denotes average BER of the kth user on the nth subcarrier. The objective function for the allocation process can then be expressed as

$$\min \sum_{n=1}^{N} s_{k,n} P_{e,k,n|\kappa_n} \quad \forall k = 1, 2, \ldots, K, \tag{6.10}$$

subject to

$$\sum_{n=1}^{N} s_{k,n} = L_c \quad \forall k = 1, 2, \ldots, K, \tag{6.11}$$

where

$$\mathbf{S} = \begin{bmatrix} s_{11} & s_{12} & \dots & s_{1N} \\ s_{21} & s_{22} & \dots & s_{2N} \\ \vdots & \vdots & \vdots & \vdots \\ s_{K1} & s_{K2} & \dots & s_{KN} \end{bmatrix}. \tag{6.12}$$

This formulation does not guarantee minimum overall BER performance. Instead, the respective BERs for each user are given in the K objective functions in (6.10). However, since each user chooses L_c subcarriers to minimize its BER, the total system BER will hopefully also be at the minimum. By separately considering BER of respective users, solving the problem iteratively becomes possible. In the following, we will show how to obtain the average BER on a subcarrier as needed in the objective function 6.10.

BER Computation on a Given Subcarrier under MAI

Assume fading gains on the N subcarriers are given as $\{\alpha_1^2, \alpha_2^2, \dots, \alpha_N^2\}$, at a certain updating stage. If we order these gains and let $r_1 = \max(\{\alpha_1^2, \alpha_2^2, \dots, \alpha_N^2\})$, $r_2 = \max(\{\alpha_1^2, \alpha_2^2, \dots, \alpha_N^2\} - r_1)$, ..., $r_N = \max(\{\alpha_1^2, \alpha_2^2, \dots, \alpha_N^2\} - r_1 - r_2 - \dots - r_{N-1})$, we will have $r_1 \geq r_2 \geq \dots \geq r_N$. The p.d.f. of $r_p, p = 1, 2, \dots, N$ can be found in [2]. The BER on this subcarrier for user k which has the pth largest channel gain, conditioned on the number of users simultaneously allocated to subcarrier

n, κ_n, is given by [2]

$$P_{e,k,p|\kappa_n} = \frac{1}{2} + \frac{N!}{(N-p)!(p-1)!}\sum_{t=0}^{N-p}\begin{pmatrix} N-p \\ t \end{pmatrix}\frac{(-1)^{t+1}}{t+p}\frac{1}{\sqrt{2\pi\sigma^2_{\xi(\kappa_n)}}} \times \int_0^\infty \sqrt{\frac{x^2}{x^2+(t+p)/\bar{\gamma}}}\exp\left(-\frac{x^2+1}{2\sigma^2_{\xi(\kappa_n)}}\right)\sinh\left(\frac{x}{\sigma^2_{\xi(\kappa_n)}}\right)\mathrm{d}x \quad (6.13)$$

where $\bar{\gamma} = \mathbf{E}\{\alpha_k^2 E_b/\eta_0\}$, $E_b = GE_c$. The variable ξ is defined as

$$\xi(\kappa_n) = \sum_{j\in U_n, j\neq k} C_{k,j}(0)b_j^l + \sqrt{\frac{\mu_0}{N}}C_{k,0}(0), \quad (6.14)$$

and the interference is given by $I_n = G\sqrt{E_c}\alpha_{k,n}\xi(\kappa_n)$ as defined in (6.7). Here we assume that $\mathbf{E}\left\{c^2_{k,j}(0)\right\} = \mathbf{E}\left\{c^2_{k,0}(0)\right\} = 1/G$. $\xi(\kappa_n)$ can be assumed to be Gaussian if G is large enough by Central Limit Theorem (CLT). If the data symbols b_k^l of all users and the chips of random signature sequences are equally distributed, the mean of the interference term $\xi(\kappa_n)$ is zero and its variance is given by

$$\sigma^2_{\xi(\kappa_n)} = \mathbf{E}\left\{c^2_{k,j}(0)\right\} + \frac{\mu_0}{N}\mathbf{E}\left\{c^2_{k,0}(0)\right\} = \frac{\kappa_n - 1}{G} + \frac{\mu_0}{GN}. \quad (6.15)$$

If the subcarriers for different users fade independently, the probability of choosing one subcarrier among N subcarriers will be equal in the long run. Therefore, the average BER can be calculated using

$$P_{e,k,p} = \sum_{\kappa_n=1}^{K}\begin{pmatrix} K \\ \kappa_n \end{pmatrix}\left(\frac{1}{N}\right)^{\kappa_n}\left(1-\frac{1}{N}\right)^{K-\kappa_n}P_{e,k,p|\kappa_n}, \quad (6.16)$$

Eq. (6.16) is further used by the objective function (6.10) to select subcarriers for each user.

The Algorithm

The problem formulated in (6.10) and (6.11) is mathematically quite difficult to solve, and that is our motivation to propose this algorithm to make the allocation process easier. Each user estimates channel gains of all subcarriers based on the pilot signals received and generates an index vector according to the order of subcarrier channel gains. The index vector of every user is fed back to BS so that it has the order of subcarrier channel gains of all users. For example, for user k, the channel gain of each subcarrier is given in the set $\{\alpha_{k,1}^2, \alpha_{k,2}^2, \ldots, \alpha_{k,N}^2\}$. If $\alpha_{k,1}^2$ is the second largest in the set, $\alpha_{k,2}^2$ is the Nth largest in the set (i.e. the smallest in the set), ..., and $\alpha_{k,N}^2$ is the largest in the set, the index vector of user k $\{2, N, \ldots, 1\}$ is fed back to the BS. When calculating BER $P_{e,k,p}$, the index vectors of all users are used. The subcarrier allocation coefficients of the previous updating stage $\mathbf{S}_{i-1}$ are also used to compute the average BER. We use the objective function together with the constraints defined respectively in (6.10) and (6.11) to obtain the subcarrier allocation coefficients of the current updating stage $\mathbf{S}_i$. Similarly, the subcarrier allocation coefficients $\mathbf{S}_i$ will also be used to decide the subcarrier allocation coefficients of the next updating stage $\mathbf{S}_{i+1}$.

The basis of the algorithm is the assumption that each subcarrier channel gain is slowly varying; therefore, we can assume the subcarriers allocated to the other users in the previous updating stage remain almost unchanged when computing the BER of a certain user at the current updating stage. This assumption allows us to make use of the previous subcarrier allocation coefficients to make it much easier

to find the solution, when subcarrier allocation and BER minimization for each user are intertwined to each other, and moreover, search in a large solution space is expected. The allocation process begins with $\mathbf{S}_0$ which is obtained by assuming that each user selects its best L_c subcarriers regardless of other users' channel conditions. Then $\mathbf{S}_i 0$ and the index vectors fed back to BS will be used to generate $\mathbf{S}_1$ which denotes the subcarrier allocation coefficients at the first updating stage. $\mathbf{S}_1$ and the index vectors generated at the second updating stage will be used to decide subcarrier allocation coefficients $\mathbf{S}_2$, and so on. The generation of $\mathbf{S}_i$ from $\mathbf{S}_{i-1}$ is not to be completed in one step, but rather an iterative process.

More specifically, each iteration is summarized in the following five steps:

1) Each MS orders all subcarriers according to the greatness of their channel gains and generates an index vector. The generated index vectors are fed back to the BS. The BS has a $K \times N$ matrix consisting of index information from all MS's.

2) BS selects subcarriers for each MS according to (6.10) and (6.11) iteratively. For each user, L_c subcarriers which give minimum average BER are selected. The BER, however, is computed using the index vector obtained by the user and subcarrier allocation coefficients of the other users in $\mathbf{S}_{i-1}$. Note that in the computation of the BER of a MS in the current updating stage, we assume all the other MS's still use previous allocated subcarriers.

3) Repeat step (2) for all MS's.

4) The matrix of subcarrier allocation coefficients of the current updating stage $\mathbf{S}_i^{(1)}$ is then obtained, which completes the first iteration. The jth iteration can be completed the same way using step (2) and (3).

5) To check whether $\mathbf{S}_i^{(1)}$ is the solution, we assume $\mathbf{S}_i^{(0)} = \mathbf{S}_{i-1}$. If $\mathbf{S}_i^{(1)} = \mathbf{S}_i^{(0)}$, then the subcarrier allocation coefficients of the ith updating stage is given as $\mathbf{S}_i = \mathbf{S}_i^{(1)}$ and the process stops. If $\mathbf{S}_i^{(1)} \neq \mathbf{S}_i^{(0)}$, repeat step (2) - (4) to obtain $\mathbf{S}_i^{(2)}$, and compare whether $\mathbf{S}_i^{(2)} = \mathbf{S}_i^{(1)}$. In general, the jth iteration can be examined the same way by checking whether $\mathbf{S}_i^{(j)} = \mathbf{S}_i^{(j-1)}$. If they are equal, the iteration stops and $\mathbf{S}_i = \mathbf{S}_i^{(j)}$.

In our simulation, we found that generally only 4-6 iterations are needed for the solution to converge, for a system with four subcarriers and 16 users. Hence, the algorithm is a promising technique for real-time implementation.

6.2.2 PSQ Algorithm

In PSL, the use of the previous allocation coefficients can reduce the computational complexity. This is reasonable if the channel is slowly time-varying. However, only using the ranking of the subcarrier channel gains and not the actual channel gains in the optimization process may not necessarily produce accurate results. Besides, once a decision error is generated, it will be propagated to the next decision. In this section, another method will be proposed to avoid such discrepancies caused by the incomplete knowledge in channel information.

Problem Formulation

We formulate the objective function to allocate subcarriers according to the actual values of channel gains while considering the MAI. In this method, it is speculated that a user should select the subcarrier on which the fading gain for this user is

maximized after excluding the interference to other users. In this way, we include allocation coefficients and interference terms in one objective function as follows:

$$\max f(s_{k,n}) = \max \sum_{k=1}^{K} \sum_{n=1}^{N} \left[H_{k,n} s_{k,n} - s_{k,n} \sum_{g=1}^{K} [C_{k,g}(0) H_{g,n} s_{g,n}] \right], \; g \neq k, \quad (6.17)$$

subject to

$$\sum_{n=1}^{N} s_{k,n} = L_c \quad \forall k = 1, 2, \ldots, K, \quad (6.18)$$

$$0 \leq s_{k,n} \leq 1, \quad s_{k,n} \in \{0, 1\} \quad (6.19)$$

The constraint defined in (6.18) is the same as (6.11) which means each user is allocated with the same number of subcarriers. The value of L_c depends on the data rate to be supported. $\mathbf{H}$ is a $K \times N$ matrix consisting of all subcarrier channel gains for all users, and $\mathbf{C}$ is a $K \times K$ matrix consisting of all the cross correlations between signature sequences. Their elements are respectively denoted as $H_{k,n}$ and $C_{k,g}(0)$. $H_{k,n}$ represents the kth user's channel gain on the nth subcarrier. $C_{k,g}(0)$ gives the cross-correlation between the kth and gth user's random sequences which is proportional to the interference power introduced by user g, if user g is also using the same subcarrier n for transmission (i.e., $s_{g,n} = 1$). Without the second term in the objective function, it is similar to what has been proposed, for example in [76]. Adding this term is to introduce penalty when multiple users are sharing the same subcarrier for transmission. Although its impact on BER may not be so straightforward, our results show that such approximation is sufficient to obtain good BER performance.

This scheme is not as simple as PSL in terms of complexity, since the objective function is formulated as a QP problem. The coefficient of the quadratic term is

given by the multiplication of the channel gain and the cross correlation between the desired user k and the "interference" user g ($g \neq k$). Under the assumption that all users are allocated identical power on each subcarrier, if the channel gain of the gth user ($g \neq k$) is large, this means the gth user's channel is in good condition. It may, on the other hand, cause great interference to the other users who are using the same subcarrier. The amount of interference has been defined in many publications using the channel gains [109]- [110]. Similarly, if the signature sequences between the desired user k and the interference users are highly correlated, great interference power and poor system performance are also expected for user k.

The QP problem, however, can be rewritten in a linear form if KT conditions are applied. We first have to rewrite the matrix $\mathbf{S}$ given in (6.12) into a vector form. The $K \times N$ variables $s_{k,n}$ are rearranged as $\mathbf{t}$=$\{s_{1,1}, s_{1,2}, \ldots,$

$s_{1,N}, s_{2,1}, s_{2,2}, \ldots, s_{2,N}, \ldots, s_{K,N}\}$ =$\{t_1, t_2, \ldots, t_\xi, \ldots, t_{K\times N}\}$. We now use ξ to represent the index of vector $\mathbf{t}$. We define ξ_c = ceil(ξ/N) as the nearest integer towards infinity of ξ/N and ξ_m = mod(ξ/N) as the modulus of ξ/N. Then, we obtain $\xi = (\xi_c - 1) \times N + \xi_m$. We should notice that if we substitute $k = \xi_c$, $n = \xi_m$ into (6.17)-(6.19), we have the following form

$$\begin{aligned} \max f(t_\xi) &= \max \sum_{\xi=1}^{K\times N} \left[t_\xi H_{\xi_c,\xi_m} - t_\xi \sum_{g=1}^{K} \left[C_{\xi_c,g}(0) H_{g,\xi_m} t_{(g-1)N+\xi_m} \right] \right] \\ &= \max \sum_{\xi=1}^{K\times N} t_\xi H_{\xi_c,\xi_m} - \sum_{\xi=1}^{K\times N} \sum_{g=1}^{K} \left[C_{\xi_c,g}(0) H_{g,\xi_m} t_\xi t_{(g-1)N+\xi_m} \right], \; g \neq \xi_c, \end{aligned} \tag{6.20}$$

subject to

$$\sum_{\xi_c=j} t_\xi = L_c \quad \forall j = 1, 2, \ldots, K,\ \xi = 1, 2, \ldots, K \times N, \tag{6.21}$$

$$0 \le t_\xi \le 1, \quad t_\xi \in \{0, 1\} \tag{6.22}$$

In the above expressions, we change the two-dimensional indices k and n to a one-dimensional index $\xi\,\{\xi = 1, 2, \ldots, K \times N\}$. After the substitution and convert the problem from maximization to minimization, we can find (6.20)-(6.22) form a general quadratic problem. By replacing c_i by $-H_{\xi_c,\xi_m}$, x_i by t_ξ, b_j by L_c, $H_{\xi,(g-1)N+\xi_m}$ by $C_{\xi_c,k}(0)H_{k,\xi_m}$ and letting $K \times N = I$, we can get the standard QP form given by (A-7)-(A-9) in Appendix C. The double summation part of (6.20) totally has $K \times K \times N$ terms, but (A-7) has $K^2 \times N^2$ terms. Those absent terms will be padded by 0. Finally, in order to maintain the symmetry property of $H_{\xi,(g-1)N+\xi_m}$ given in (A-9), the coefficients for both $t_\xi t_{(g-1)N+\xi_m}$ and $t_{(g-1)N+\xi_m} t_\alpha$ will each take the value $\frac{1}{2}\left[C_{\xi_c,g}(0)H_{g,\xi_m} + C_{g,\xi_c}(0)H_{\xi_c,\xi_m}\right]$.

Assuming that Lagrangian multipliers are given by $\mathbf{u} = (u_1, u_2, \ldots, u_j, \ldots, u_K)^T$, $\mathbf{v}_1 = (v_1, v_2, \ldots, v_\xi, \ldots, v_{K\times N})^T$ and $\mathbf{v}_2 = (v_{1+K\times N}, v_{2+K\times N}, \ldots, v_{\xi+K\times N}, \ldots, v_{2K\times N})^T$, we use KT conditions to convert the original QP problem in (6.20)-(6.22) into the following LP problem:

$$\text{Minimize} \quad \varphi(z) = \sum_{\xi=1}^{K\times N} z_\xi, \tag{6.23}$$

Subject to

$$\begin{aligned} \textstyle\sum_{g=1}^{K} \quad & \left[C_{\xi_c,g}(0)H_{g,\xi_m} + C_{g,\xi_c}(0)H_{\xi_c,\xi_m}\right] s_{(g-1)N+\xi_m} \\ & + u_j - v_\xi + v_{k\times N+\xi} + \operatorname{sgn}(H_{\xi_c,\xi_m}) z_\xi = H_{\xi_c,\xi_m}, \end{aligned} \tag{6.24}$$

$$\sum_{\xi_c=j} t_\xi = L_c \quad \forall j = 1, 2, \ldots, K,\ \xi = 1, 2, \ldots, K \times N, \tag{6.25}$$

$$u_j \geq 0,\ v_\xi \geq 0,\ v_{K\times N+\xi} \geq 0,\ z_\xi \geq 0,\ \xi = 1, 2, \ldots, K \times N, j = 1, 2, \ldots, K, \tag{6.26}$$

$$t_\xi v_\xi = 0, \tag{6.27}$$

$$t_\xi v_{K\times N+\xi} = 0. \tag{6.28}$$

Eqs. (6.23)-(6.26) define a solvable LP problem. Besides, they should also satisfy constraints (6.27) and (6.28), which can be realized by ensuring that t_ξ and v_ξ, and also t_ξ and $v_{K\times N+\xi}$ cannot be the basic variables simultaneously when simplex method is used. The solution to these equations will be the same as the original formulated QP problem described in (6.17)-(6.19). Since the slack variables for (6.21) are all zeros, KT conditions (A-16) do not appear in the LP problem formulation.

This subcarrier allocation algorithm does not use the allocation coefficients of the previous updating stage; therefore, it can avoid discrepancy propagations across different stages. Furthermore, since the subcarrier allocation coefficients of the previous stage $\mathbf{S}_{i-1}$ are not needed, it is can be applied to a slightly less slowly time-varying channel. Another advantage of this algorithm is that it ensures an easier implementation by the conversion from the original QP problem to a solvable LP problem, for which many efficient and robust algorithms and softwares have been developed [111–113].

6.3 Simulation Results

In this section, the performance of the proposed schemes is evaluated using computer simulation over Rayleigh fading channel. We compare the performance of our

schemes with that of Kim's method proposed in [2] without MAI considerations.

The channel is assumed to experience only slow fading. A Doppler frequency of 30Hz is used in our simulation for generation of channel gains on the subcarriers. The updating period is 1.0 ms so that the channels only made reasonable changes over each updating period. Accordingly, for a transmission rate of 1M symbols per second per subcarrier, 1000 symbols are transmitted on each subcarrier over each updating period. It was found from our simulations that the initial subcarrier allocation can be arbitrarily assigned (such as select the best L_c subcarriers without considering MAI), and only a few iterations are needed for the algorithm to converge.

Figure 6.5 shows the performance comparison between PSL and Kim's method where the number of users is chosen to be 16 or 30. The total number of subcarriers available for all users is 4 and each user selects one subcarrier to transmit data. In Figure 6.5, we can see that when SNR is low, our allocation scheme has almost the same performance as Kim's method. However, with the increase in SNR, the BER performance improves significantly for our scheme.

To further compare PSL with Kim's method, we simulate it when each user selects two subcarriers to transmit data. For a fair comparison, we modify Kim's scheme so that each user also selects two subcarriers with largest channel gains. Figure 6.6 shows the simulation results where the number of user is equal to 16 or 30. The total number of subcarriers is 4 and each user is allocated 2 subcarriers. From these curves, we can see that PSL has better BER performance even if SNR is low. At the higher end of SNR, our algorithm shows an even greater performance

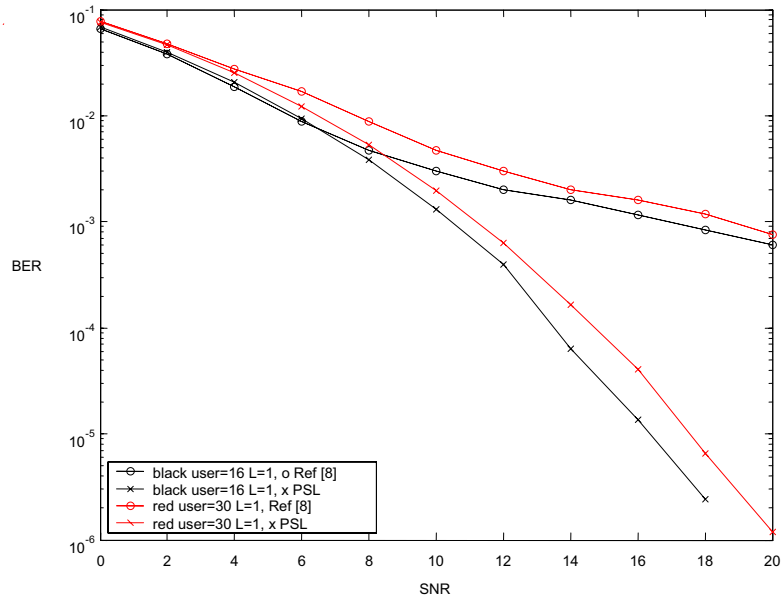

Figure 6.5: PSL compare with Kim's method, User=16 and 30, $L_c = 1$.

gain.

However, PSL works well only when either a large number of users are present or each user uses more than one subcarrier for its data transmission. For further investigation, we make comparisons for the BER performance between PSL and Kim's scheme when the total number of subcarriers is 4 and the number of active users is 8. Each user can choose up to 1 subcarrier from all the 4 subcarriers. As shown in Figure 6.7, PSL shows worse performance than Kim's. Our scheme takes into consideration of the interference from other users using the same subcarrier, yet the interference is not large enough to see the advantage when the number of users is small. On the other hand, the decision at current stage is based on the subcarrier allocation at previous stage; this will inevitably generate inaccuracy and cause discrepancy propagations in the allocation process. Therefore, under such circumstances as in Figure 6.7, it is sufficient to simply use the method described

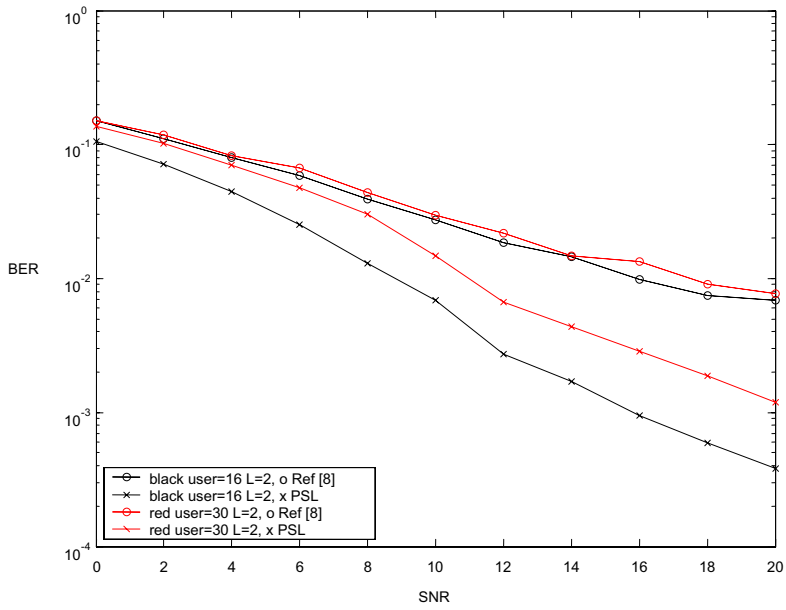

Figure 6.6: PSL compare with Kim's method, User=16 and 30, $L_c = 2$.

in [2] for subcarrier allocation.

When up to two subcarriers can be selected for each user, the possibility is high for one subcarrier to accommodate more users, compared with the case where each user only selects one subcarrier. This high possibility of subcarrier sharing, in turn, increases the level of interference. Figure 6.7 shows the BER performance when the number of users is also 8 but we can select up to two subcarriers for each user. In this case, PSL has better BER performance compared with Kim's scheme. Thus, we can see that when the system has reasonable large number of users or when each user demands many subcarriers for transmission, our scheme shows significant BER improvement.

From the simulation results presented above, we show that in general there is an improvement in the BER performance of PSL, compared with Kim's method. The main reason is that we jointly consider the effect of MAI when we allocate

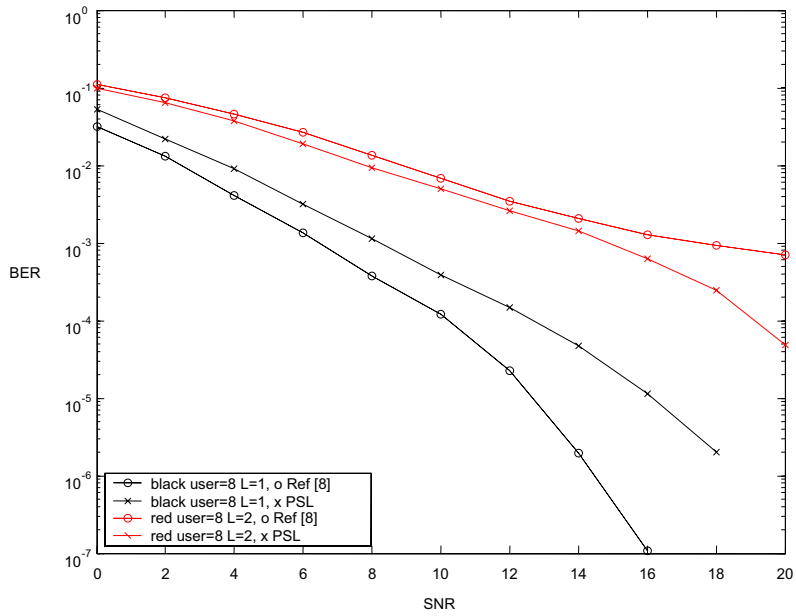

Figure 6.7: PSL compare with Kim's method, User=8, $L_c = 1$ and 2.

subcarriers to users. When the number of users or subcarriers is large, PSL shows greater improvement.

In the following, we compare our second scheme, PSQ, with Kim's scheme in [2] as well as PSL through simulations. In the simulations, we use Jakes Model to generate fading channel and the Doppler shift of the channel is set to 30Hz. The duration of updating period is 1ms. Given a transmit data rate of 1M symbols per second per subcarrier, 1000 symbols will be transmitted over each updating period.

Figure 6.8 shows the simulation results of the system with 8 active users. Each user selects 1 subcarrier to transmit data. As we can see from Figure 6.8, this new scheme PSQ has BER improvement compared to both the PSL and Kim's method. In this case, however, the performance of PSL is worse than Kim's, as we have explained above.

Figure 6.9 is the simulation results with 8 active users, each of which selects two

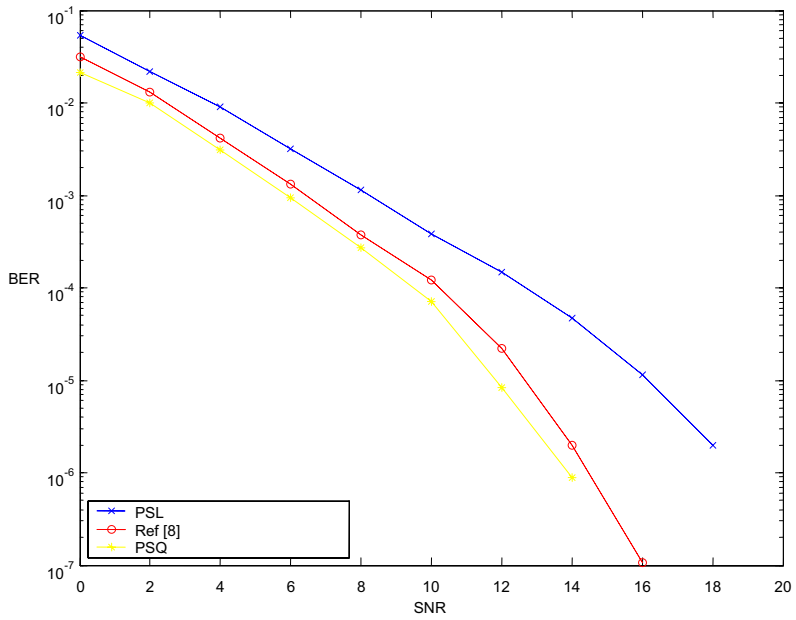

Figure 6.8: PSQ compare with PSL and Kim's method, User=8, $L_c = 1$.

subcarriers for data transmission. From this figure, we can see that both PSL and PSQ show some improvement on BER performance compared to Kim's method. In this case, PSL improves the system performance with the surging effect of MAI due to greater number of subcarriers each user selects than in Figure 6.8. As for PSQ, it shows even better BER performance than PSL, because it does not base the allocation decisions on the previous allocation coefficients, which can avoid discrepancy propagation. Thus, PSQ gives more accurate subcarrier allocation results than PSL.

The simulation results with 16 users are shown in Figure 6.10 and Figure 6.11, in which each user selects one and two subcarriers, respectively. The conclusion is similar to what we have drawn from Figure 6.9.

To sum up, PSQ show BER improvement compared with Kim's method. PSL

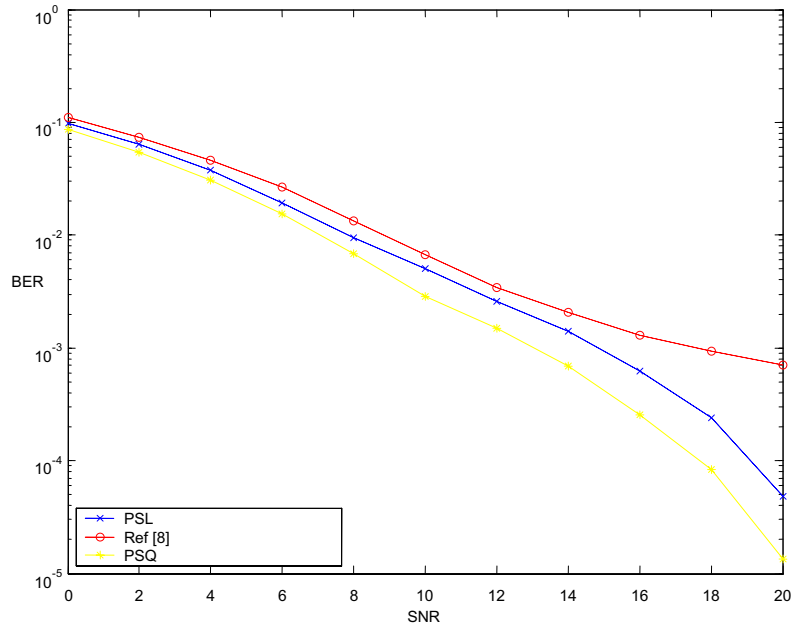

Figure 6.9: PSQ compare with PSL and Kim's method, User=8, $L_c = 2$.

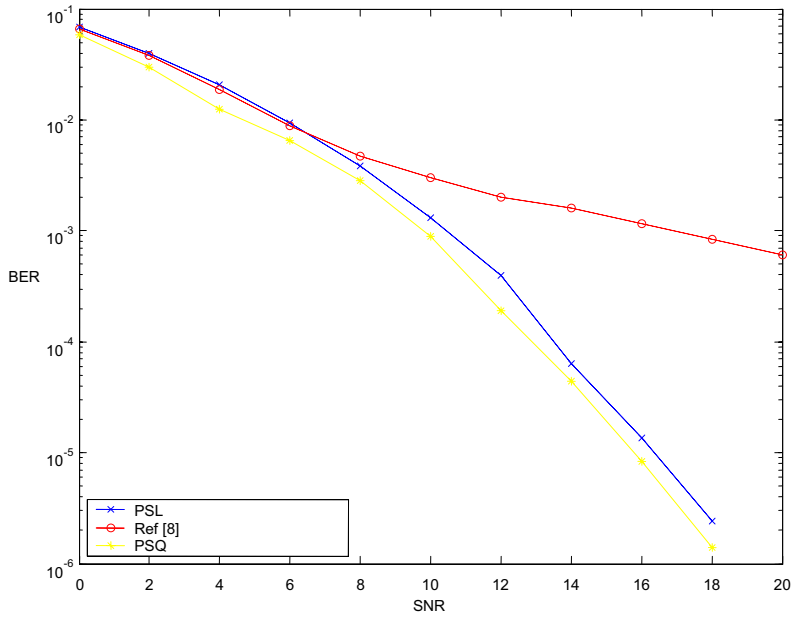

Figure 6.10: PSQ compare with PSL and Kim's method, User=16, $L_c = 1$.

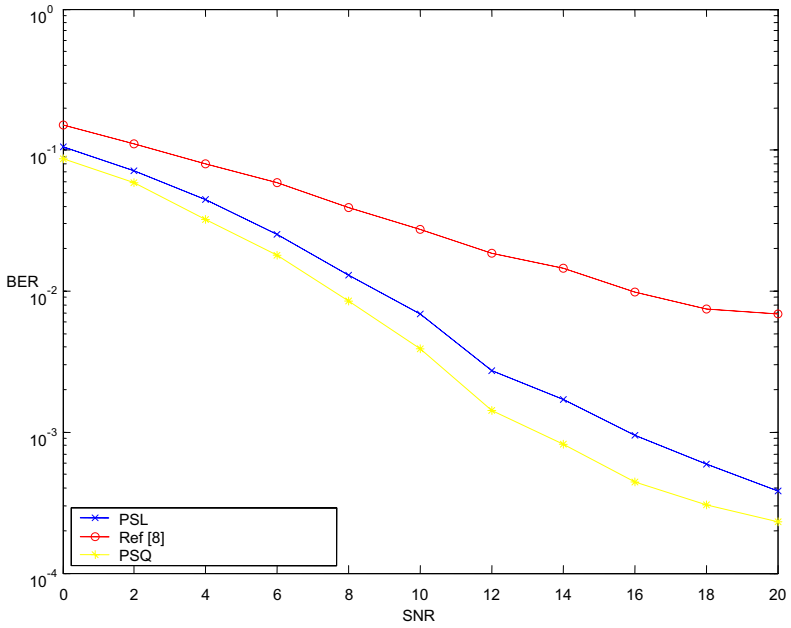

Figure 6.11: PSQ compare with PSL and Kim's method, User=30, $L_c = 1$.

also generally shows improvement over Kim's method except when subcarrier sharing rate is low. Among the three schemes, PSQ shows the best performance. With these results, we get some idea of the advantage to take into consideration of the effect of MAI in the process of subcarrier allocations. If we compare the two proposed schemes, namely, PSL and PSQ, PSQ turns out to provide even better performance. This is because the scheme uses the instantaneous channel information instead of only ranking index and it needs no information about previous allocation coefficients. This can result in an improved accuracy compared with the other schemes. As for PSL, it performs well when the interference from other users sharing the same subcarrier has a strong effect on the allocation coefficients. Generally, the BER performance of PSL improves with the increase of interference.

6.4 Summary and Contribution

The difficulty of subcarrier allocations in MC-DS-CDMA systems is that the effect of MAI has to be taken into consideration to obtain the optimal solution. This complicates the optimization process and is probably why no optimal solution is provided so far. In this chapter, we proposed two suboptimal subcarrier allocation schemes for MC-DS-CDMA systems in the presence of MAI. For the first algorithm, we formulated the objective function to minimize each user's BER performance with considerations of MAI. From the simulation results, our first method generally shows BER performance improvement compared to the conventional method in [2] (Kim's method) and those without adaptive subcarrier allocation. The performance improvement increases with the increase of SNR. When SNR is low (usually below 8dB), our method is quite similar to Kim's scheme; when SNR increases, the SNR improvement can be 4-10 dB with various number of users or subcarriers selected. However, our method performs well when either a large number of users are present or when each user uses more subcarriers to transmit data. The decision based on previous subcarrier allocation may generate discrepancy to the allocation process, and this discrepancy may result in some performance degradation if the effect due to MAI is small.

In order to overcome the limitation of the first method, we defined a new objective function using the instantaneous channel gains and cross-correlation coefficients, which appeared to be a QP problem. Such a scheme is not as simple as the first one, but this scheme can improve the system performance even more

significantly. This is because the method allocates subcarriers while considering the MAI effect. Further, the decisions were made according to the actual values of channel gains without using the previous allocation coefficients. We used Kuhn-Tucker conditions to convert our objective function to a solvable linear problem without changing the solution to the original problem. From the simulation results, this method outperforms all the schemes mentioned in this chapter and shows improved accuracy compared with our first method. Continual effort should be put into obtaining the optimal solution to the subcarrier allocation problem in MC-DS-CDMA systems.

Chapter 7

Cognitive Radio

In the previous chapters, our research focused on systems employing OFDM, DS-CDMA and MC-CDMA technologies which occupy a given system bandwidth. We aimed to improve the spectral efficiency through subcarrier and bit allocation for multicarrier systems, and power control profile for DS-CDMA systems. Most of these technologies have their own technical merits. DS-CDMA is the technology adopted for current deployed 2G/3G system and it is believed that the technology will continue to be there for another decade. On the other hand, standardization activities on 3GPP, WiFi and WiMax (check reference for this) have made OFDM as the candidate for beyond 3G systems and wireless local area networks. Despite the popularity of the OFDM technologies, they still have some technical challenges to overcome such as high PAPR, high inter-cell interference because the reuse factor is 1, etc.

It is no doubt that in the future there is going to be radio systems using different technologies. The current scenario is that different radio systems use their

allocated frequency bands for transmission. This, of course, will impose some limitations in making efficient use of spectrum. For example, some radio systems may have used up the spectrum allocated to them and thus encounter congestion, but at the same time, other spectrum could be under-utilized. As a countermeasure for such spectrum usage limitations, the idea of dynamic spectrum allocation for various radio systems, which is also known as cognitive radio, has been brought up as mentioned in Chapter 3. It is believed that spectrum can be more efficiently used although there are still many technical difficulties to overcome, such as reconfigurability of terminal stations and base stations.

From another point of view, with the coexistence of these technologies, the users are expected to choose the radio system and the spectrum they are operating on according to their QoS requirements. Furthermore, the coding and modulation techniques and parameters are also adapted to the transmission link conditions. On the other hand, the users or the base stations also need to take care of the interference imposed on other users sharing the same spectrum. Appropriate measures should be taken to alleviate this impairment in order to optimize the overall system performance.

This chapter takes a very simple treatment on cognitive radio. We foresee that the future base stations have reconfigurable capability, whereby a wide spectrum can be partitioned into many small bands of different bandwidth at any instant of time. Each band can support a radio system and the partition is made to optimize its usage. The cognitive radios look into the allocation of unused frequency bands to secondary users. We propose a centralized cognitive radio model. An example

is a powerful base station which can communicate with multiple users using systems of different technologies, and the base station is capable of assigning suitable frequency bands to users. We study the adaptive frequency bands' allocation algorithms, in the situation either with or without primary users. Integer programming techniques are used to perform the frequency band allocation so that the defined utility function is maximized. A suboptimal heuristic algorithm is also presented to speed up the allocation process. In the heuristic approach, the frequency bands of the OFDM users are assigned first, and then the CDMA users choose their transmission bands among the remaining spectrum. As the utility function is divided into two parts and maximized in a two-step manner, the results deviate from the optimal results, yet with only negligible loss in the utility function.

7.1 System Model

The total available spectrum is divided into N_T frequency bins. Assuming that there are two groups of secondary users with their frequency bands for transmission to be allocated: (a) An OFDM user requires a continuous spectrum equal to L frequency bins, and no sharing of any of these frequency bins with other users is allowed (b) K narrow-band CDMA users of processing gain G. Each occupies only one frequency bin, but can share the same frequency bin for transmission with other CDMA users. The cross correlation between two CDMA users k and j is given by $C_{k,j}$, which is proportional to the amount of interference between the two users. We assume that the base station has the intelligence to compute and assign

the frequency band to each user. The target of the design is to make optimal use of precious radio spectrum based on an objective (utility) function to be defined shortly.

Assuming that channel frequency response between the base station and each user over the specified spectrum can be correctly sensed and fed back to the base station for decision. For simplicity, we assume each frequency bin takes one of the discrete number of channel states. By doing so, we can actually reduce the amount of information feedback to the base station. We assume that channel state has a higher value at higher channel gain or lower level of interference. Notably, although the channel states are assigned in a way related to the channel gain, it is not necessarily a linear relationship. This relationship, however, is defined so that the channel state is linearly related to the revenue if the frequency bin is in use. Denote the channel states as $\{H_{0,n}\}_{n=1}^{N_T}$ for OFDM user and $\{H_{k,n}\}_{n=1}^{N_T}$ for the kth CDMA users where $k = 1, \ldots, K$. Finally, let $s_{k,n}$ denote the assignment indicator, i.e., if the nth frequency bin is assigned to the kth user, $s_{k,n} = 1$; otherwise $s_{k,n} = 0$, for all $k = 0, 1, \ldots, K$ where $k = 0$ indicates the OFDM user.

7.1.1 No Primary Users

If there is no primary user in the cognitive radio, the whole spectrum which comprises of the N_T frequency bins can all be used by the OFDM and CDMA users. The objective here is to allocate the spectrum among these users according to their respective channel conditions so that the overall spectrum usage is optimized. The

problem is thus formulated as below:

$$\max_{s_{k,n}} \quad \sum_{k=0}^{K}\sum_{n=1}^{N_T} s_{k,n}H_{k,n} - \sum_{n=1}^{N_T}\sum_{k=1}^{K}\sum_{\substack{j=1\\ j\neq k}}^{K} s_{k,n}s_{j,n}\frac{C_{k,j}H_{j,n}}{GH_{k,n}} \tag{7.1}$$

subject to

$$\sum_{n=1}^{N_T-L+1} s_{0,n}s_{0,n+1}\ldots s_{0,n+L-1} = 1 \tag{7.2}$$

$$\sum_{n=1}^{N_T} s_{0,n} = L \tag{7.3}$$

$$\sum_{k=1}^{K} s_{0,n}s_{k,n} = 0, \quad n = 1, 2, \ldots, N_T \tag{7.4}$$

$$\sum_{n=1}^{N_T} s_{k,n} = 1, \quad k = 1, 2, \ldots, K \tag{7.5}$$

and

$$s_{k,n} \in \{0, 1\} \quad k = 0, 1, 2, \ldots, K; n = 1, 2, \ldots, N_T \tag{7.6}$$

Note that we formulate the objective function in (7.1) to allocate frequency bands according to the channel states of the frequency bins of all users. The first term of the objective function explains the fact that the higher the channel state value, the better the channel gain is, therefore, the higher priority should that frequency bin be assigned to the corresponding user. The second term accounts for the MAI if the same frequency bin is shared among CDMA users, and the negative sign is an indication of its penalty to the cognitive radio. This amount of interference is proportional to the cross-correlation between the two codes used and the channel state of the interferer. Conversely, a higher processing gain G means higher interference rejection capability and hence shall result in lower penalty.

By this utility function, the system tries to allocate subcarriers to those users who see the highest gain, and at the same time prevents these subcarriers to be

simultaneously assigned to users who will therefore suffer from excessive interference. For example, if $H_{k,n} = 16$, $H_{j,n} = 1$, $H_{l,n} = 14$ and we are to assign two users to this subcarrier, since $\frac{H_{j,n}}{H_{k,n}} = \frac{1}{16}$, $\frac{H_{l,n}}{H_{k,n}} = \frac{14}{16}$ and $\frac{H_{k,n}}{H_{j,n}} = 16$, $\frac{H_{k,n}}{H_{l,n}} = \frac{16}{14}$, through the maximization of the objective function, it is more probable that subcarrier n will be assigned to user k and l, but not to user j, as the interference from user k on user j seems to be detrimental. On the other hand, the use of G and C are also needed to distinguish systems operating under different processing gain and codes of different orthogonality. With higher processing gain and better orthogonality, the effect of interference is much less significant.

The constraint defined in (7.2) is to ensure that the frequency bins assigned to the OFDM user is continuous in frequency. Moreover, the total number of the frequency bins assigned to OFDM user is equal to L, as indicated in (7.3). And those constraints in (7.4) ensure that once the frequency bin is assigned to OFDM user, no other users can share the same frequency bin for transmission. For simplicity, we also assume that each CDMA user only takes one frequency bin, as shown by the constraints in (7.5).

7.1.2 With Primary Users

If the presence of primary users is detected, those frequency bins occupied by the primary users have to be blocked from being allocated to any of the OFDM or CDMA users which are the secondary users. The vector $\mathbf{v}$ is used to indicate the frequency bins which have been taken by the primary users. Take $N_T = 16$ as an example: if frequency bins 4−8,10,16 are occupied, $\mathbf{v} = \{0\,0\,0\,1\,1\,1\,1\,1\,0\,1\,0\,0\,0\,0\,0\,1\}$.

v is sensed, stored and updated at the base stations according to the locations and spectrum sensed by the secondary users.

The spectrum allocation in this case can be formulated as:

$$\max_{s_{k,n}} \quad \sum_{k=0}^{K}\sum_{n=1}^{N_T} s_{k,n}H_{k,n} - \sum_{n=1}^{N_T}\sum_{k=1}^{K}\sum_{\substack{j=1\\ j\neq k}}^{K} s_{k,n}s_{j,n}\frac{C_{k,j}H_{j,n}}{GH_{k,n}} \tag{7.7}$$

subject to

$$v_n \sum_{k=0}^{K} s_{k,n} = 0, \quad n = 1, 2, \ldots, N_T \tag{7.8}$$

$$\sum_{n=1}^{N_T-L+1} s_{0,n}s_{0,n+1}\ldots s_{0,n+L-1} = 1 \tag{7.9}$$

$$\sum_{n=1}^{N_T} s_{0,n} = L \tag{7.10}$$

$$\sum_{k=1}^{K} s_{0,n}s_{k,n} = 0, \quad n = 1, 2, \ldots, N_T \tag{7.11}$$

$$\sum_{n=1}^{N_T} s_{k,n} = 1, \quad k = 1, 2, \ldots, K \tag{7.12}$$

and

$$s_{k,n} \in \{0, 1\} \quad k = 0, 1, 2, \ldots, K; n = 1, 2, \ldots, N_T \tag{7.13}$$

In (7.8), v_n is the nth element of **v**, and is the added constraint to ensure no OFDM or CDMA system should be allocated these frequency bins which have been taken by the primary users. The objective function and other constraints are similar to the case without primary users.

In the next section, we will show how we transform the nonlinear constrained integer problem into a quadratic integer problem with only linear constraints. Also, we will present the optimal solutions obtained in the two cases.

7.2 The Optimal Solution

The formulation defined by (7.1)-(7.6) is a nonlinear binary programming problem. The objective function can be expressed in quadratic form. The nonlinear constraints in (7.2), however, can be converted into a linear expression through some simple transforms. More specifically, if we denote $y_n = s_{0,n}s_{0,n+1}\ldots s_{0,n+L-1}$, we can easily see that y_n is also a binary variable. Further, $y_n = 1$ if and only if $s_{0,n} = s_{0,n+1} = \ldots s_{0,n+L-1} = 1$ and zero elsewhere, which can be ensured by (7.15) and (7.16). Hence, the constraints in (7.2) can be replaced by

$$\sum_{n=1}^{N_T-L+1} y_n = 1 \tag{7.14}$$

subject to the following two added constraints

$$y_n \geq \sum_{p=n}^{n+L-1} s_{0,p} - (L-1), \quad n = 1, 2, \ldots, N_T - L + 1 \tag{7.15}$$

$$y_n \leq \frac{1}{L}\sum_{p=n}^{n+L-1} s_{0,p}, \quad n = 1, 2, \ldots, N_T - L + 1 \tag{7.16}$$

Similarly, (7.4) can be converted into linear, if we let $z_{k,n} = s_{0,n}s_{k,n}$ and then rewrite it as:

$$\sum_{k=1}^{K} z_{k,n} = 0, \quad n = 1, 2, \ldots, N_T \tag{7.17}$$

$$z_{k,n} \geq s_{0,n} + s_{k,n} - 1, \quad k = 1, 2, \ldots, K; n = 1, 2, \ldots, N_T \tag{7.18}$$

$$z_{k,n} \leq 0.5\left(s_{0,n} + s_{k,n}\right), \quad k = 1, 2, \ldots, K; n = 1, 2, \ldots, N_T \tag{7.19}$$

where (7.18) and (7.19) are the constraints added to ensure $z_{k,n} = 1$ when $s_{0,n} = s_{k,n} = 1$ and zero otherwise.

After converting all the constraints into linear form, we will next convert the problem into the standard quadratic form. We rearrange all the optimization variables into a vector denoted by $\mathbf{t}$, i.e. $\mathbf{t}=\{s_{0,1} \quad s_{0,2} \ldots s_{0,N_T} \quad s_{1,1} \ldots s_{1,N_T} \ldots s_{K,N_T} \quad z_{1,1} \quad z_{1,2} \ldots z_{1,N_T} \ldots z_{K,N_T} \quad y_1 \quad y_2 \quad \ldots \quad y_{N_T-L+1}\}$. Therefore, $\mathbf{t}$ includes all the variables used in the objective function and the constraints, and its length is $2(K+1)N_T - L + 1$. In the following, we will use i as the index for the optimization vector where $i = 1, 2, \ldots, 2(K+1)N_T - L + 1$. Further, let $i_c = \text{ceil}(i/N_T)$ denote the nearest integer greater than i/N_T, and also $i_m = \text{mod}(i/N_T)$ is the modulus of i/N_T. Thus, the objective function can be rewritten as

$$\min_{\mathbf{t}} \quad \sum_{i=N_T+1}^{(K+1)N_T} \sum_{\substack{j=2 \\ j\neq i+1}}^{K+1} t_i t_{(j-1)N_T+i_m} \frac{C_{i_c-1,j-1} H_{(j-1)N_T+i_m}}{G H_i} - \sum_{i=1}^{(K+1)N_T} t_i H_i \tag{7.20}$$

Note that to maximize the original function is equivalent to minimize the negative function. All the constraints in (7.3), (7.5) and (7.14)-(7.19) can also be modified in a similar way,

$$\sum_{n=1}^{N_T-L+1} t_{(2K+1)N_T+n} = 1 \tag{7.21}$$

$$t_{(2K+1)N_T+n} \geq \sum_{p=n}^{n+L-1} t_p - (L-1), \quad n = 1, 2, \ldots, N_T - L + 1 \tag{7.22}$$

$$t_{(2K+1)N_T+n} \leq \frac{1}{L} \sum_{p=n}^{n+L-1} t_p, \quad n = 1, 2, \ldots, N_T - L + 1 \tag{7.23}$$

$$\sum_{n=1}^{N_T} t_n = L \tag{7.24}$$

$$\sum_{k=1}^{K} t_{(K+k)N_T+n} = 0, \quad n = 1, 2, \ldots, N_T \tag{7.25}$$

$$t_{(K+k)N_T+n} \geq t_n + t_{kN+n} - 1, \quad k = 1, 2, \ldots, K; n = 1, 2, \ldots, N_T \quad (7.26)$$

$$t_{(K+k)N_T+n} \leq 0.5\left(t_n + t_{kN+n}\right), \quad k = 1, 2, \ldots, K; n = 1, 2, \ldots, N_T \quad (7.27)$$

$$\sum_{n=1}^{N_T} t_{kN+n} = 1, \quad k = 1, 2, \ldots, K \quad (7.28)$$

$$t_i \in \{0, 1\}, \quad i = 1, 2, \ldots, 2(K+1)N_T - L + 1 \quad (7.29)$$

The standard CPLEX solver mixed-integer quadratic programming (MIQP) can be used to find the optimal solution for the dynamic spectrum allocation after all these transformation. For cognitive radio with primary users, the additional constraints in (7.8) are rewritten likewise, i.e., $v_n \sum_{k=0}^{K} t_{kN+n} = 0, n = 1, 2, \ldots, N_T$.

7.3 Illustration and Discussion

7.3.1 Spectrum Allocation with no Primary users

We simulated a scenario containing an OFDM user demanding 16 frequency bins and 16 CDMA users. All these users share the available 32 frequency bins, i.e., $L = 16, K = 16, N_T = 32$. The channel states for all the users are independent from each other. A snapshot of all the channel states for the OFDM user ($k = 0$) and the 16 CDMA users ($k = 1, 2, \ldots, K$) can be found in Figure 7.1, assuming 16 possible states taking integer values from 1 to 16. In order to show the channel more clearly, we plot the channel states for the OFDM user over the defined spectrum in Figure 7.2. The cross correlations between any two CDMA users can be found in Figure 7.3.

We obtained the solution for the spectrum allocation defined in (7.20)-(7.29)

Freq bin no. / User no.	1	2	3	4	5	6	7	8	9	10	11	12	13	14	15	16	17	18	19	20	21	22	23	24	25	26	27	28	29	30	31	32
OFDM	6	14	6	3	15	13	11	3	2	15	3	9	2	4	6	1	12	6	6	1	14	2	11	5	7	10	7	5	11	1	16	6
1	12	3	1	5	10	15	16	8	11	7	1	14	6	14	16	12	4	5	16	7	15	15	16	8	4	16	8	5	1	6	8	16
2	8	14	3	1	12	7	1	10	13	11	4	4	3	12	10	7	11	1	16	1	15	3	1	9	7	8	16	12	16	12	12	9
3	10	4	14	7	16	8	14	11	13	3	14	7	2	2	11	7	9	6	7	11	16	7	14	12	3	13	14	8	7	13	13	12
4	2	2	11	11	8	2	12	9	13	13	12	1	3	14	8	15	10	5	15	6	13	8	4	4	2	7	3	1	6	7	9	15
5	6	6	6	14	3	15	16	4	9	6	12	5	2	6	14	16	5	7	8	9	6	13	16	5	2	4	14	4	11	7	9	16
6	10	10	1	13	10	11	2	11	8	13	7	14	9	3	14	8	15	1	16	7	2	7	5	15	1	11	13	12	8	5	13	15
7	15	3	6	3	9	11	1	4	8	6	8	11	13	9	9	1	2	5	16	3	2	13	4	4	14	6	6	16	14	2	4	7
8	16	14	12	9	6	16	12	12	11	13	16	15	7	15	2	14	5	4	12	2	15	1	9	3	7	7	12	12	9	10	16	11
9	1	6	5	9	13	8	14	7	2	3	13	2	14	7	5	1	14	10	11	10	9	16	9	7	13	5	1	13	5	14	2	7
10	2	8	3	15	14	7	5	7	9	3	7	8	13	9	10	2	16	14	14	11	4	14	14	11	14	7	9	4	3	5	9	14
11	7	7	7	8	6	14	12	7	4	11	16	7	1	12	3	12	2	5	1	3	7	16	5	3	7	12	13	13	9	8	15	9
12	2	5	14	1	10	2	5	3	5	2	4	6	11	1	12	3	16	10	6	7	14	5	5	7	14	9	3	14	16	1	14	13
13	5	16	10	16	13	10	2	15	5	15	9	15	2	14	9	1	15	9	2	12	3	8	4	12	6	16	9	13	16	2	11	7
14	11	16	1	1	1	4	15	1	14	8	9	3	4	15	3	2	16	3	6	7	6	6	9	6	4	3	4	13	12	9	5	16
15	16	16	7	9	14	7	2	15	7	3	8	7	15	1	15	12	10	1	1	4	14	1	4	15	9	9	14	15	4	12	7	1
16	7	8	5	15	11	5	12	11	9	5	7	16	3	2	4	1	16	6	14	10	5	5	11	13	4	8	5	7	8	1	6	16

Figure 7.1: Channel states for all users. $N_T = 32, K = 16, L = 16$.

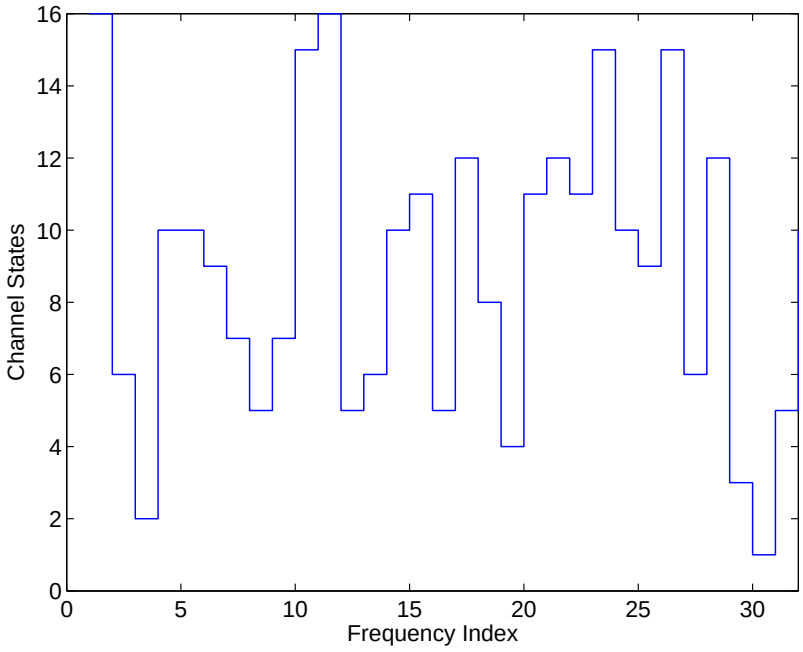

Figure 7.2: Channel states for the OFDM user. $N_T = 32, K = 16, L = 16$.

User i / User j	1	2	3	4	5	6	7	8	9	10	11	12	13	14	15	16
1	1	0.0713	0.0867	0.0742	0.0995	0.0867	0.0486	0.0903	0.0020	0.0637	0.0944	0.0041	0.0286	0.0677	0.0586	0.0065
2	0.0713	1	0.0879	0.0488	0.0891	0.0762	0.0655	0.0971	0.0171	0.0136	0.0755	0.0313	0.0463	0.0339	0.00096	0.0334
3	0.0867	0.0879	1	0.0247	0.0994	0.0906	0.0350	0.0278	0.0093	0.0241	0.0902	0.0324	0.0573	0.0185	0.0738	0.0112
4	0.0742	0.0488	0.0247	1	0.0384	0.0862	0.0857	0.0819	0.0246	0.0898	0.0604	0.0140	0.0161	0.0883	0.0979	0.0601
5	0.0995	0.0891	0.0994	0.0384	1	0.0362	0.0231	0.0450	0.0643	0.0245	0.0468	0.0497	0.0075	0.0767	0.0045	0.0165
6	0.0867	0.0762	0.0906	0.0862	0.0362	1	0.0777	0.0208	0.0252	0.0397	0.0481	0.0509	0.0625	0.0626	0.0991	0.0359
7	0.0486	0.0655	0.0350	0.0857	0.0231	0.0777	1	0.0276	0.0678	0.0509	0.0277	0.0579	0.0823	0.0941	0.0444	0.0423
8	0.0903	0.0971	0.0278	0.0819	0.0450	0.0208	0.0276	1	0.0996	0.0614	0.0944	0.0912	0.0815	0.0690	0.0309	0.0558
9	0.0020	0.0171	0.0093	0.0245	0.0643	0.0252	0.0678	0.0996	1	0.0637	0.0769	0.0054	0.0115	0.0846	0.0172	0.0037
10	0.0637	0.0136	0.0241	0.0898	0.0245	0.0397	0.0509	0.0614	0.0637	1	0.0313	0.0817	0.0235	0.0587	0.0924	0.0330
11	0.0944	0.0755	0.0902	0.0604	0.0468	0.0481	0.0277	0.0944	0.0769	0.0313	1	0.0206	0.0364	0.0976	0.0717	0.0643
12	0.0040	0.0313	0.0324	0.0140	0.0497	0.0509	0.0579	0.0912	0.0054	0.0817	0.0206	1	0.0783	0.0466	0.0232	0.0318
13	0.0286	0.0463	0.0573	0.0161	0.0075	0.0625	0.0823	0.0815	0.0115	0.0235	0.0364	0.0783	1	0.0789	0.0634	0.0660
14	0.0677	0.0339	0.0185	0.0883	0.0767	0.0626	0.0941	0.0690	0.0846	0.0587	0.0976	0.0466	0.0789	1	0.0538	0.0919
15	0.0586	0.0001	0.0738	0.0979	0.0045	0.0991	0.0444	0.0309	0.0172	0.0924	0.0717	0.0232	0.0634	0.0538	1	0.0781
16	0.0064	0.0334	0.0112	0.0601	0.0165	0.0359	0.0423	0.0558	0.0037	0.0330	0.0643	0.0318	0.0660	0.0919	0.0781	1

Figure 7.3: Correlation coefficients between any two CDMA users. $K = 16$**.**

for the channel states listed in Figure 7.1. The assignments of the frequency bins among the $K + 1$ users are shown in Figure 7.4. The continuous 16 bins No. 2-17 are assigned to the OFDM user, and they are not allowed to be shared by any other users. Moreover, the frequency allocation to each CDMA user ($k = 1, 2, \ldots, 16$) is also highlighted. For example, both user 14 and user 16 are assigned to use the 32th frequency bin for transmission. The reason is easy to explain, if we look back onto the chart for the channel states in Figure 7.1: Excluding those frequency bins which are allocated to the OFDM user ($N_T = 2 \sim 17$), the 32th frequency bin is the best choice for user 14 and user 16, at which both of them show the highest possible values for the channel states 16. However, this explanation is just a glimpse into the channel states' perspective. In the actual allocation process, the decision is also based on the impact of multiple access interference so that the overall utility function in (7.1) is maximized.

What can also be observed in Figure 7.4 is that not every frequency bin will be finally allocated to the users. Some bins are not used, like $N_T = 20, 24, 25, 30$.

Freq bin no.	1	2	3	4	5	6	7	8	9	10	11	12	13	14	15	16	17	18	19	20	21	22	23	24	25	26	27	28	29	30	31	32
User no.																																
OFDM	0	1	1	1	1	1	1	1	1	1	1	1	1	1	1	1	1	0	0	0	0	0	0	0	0	0	0	0	0	0	0	0
1	0	0	0	0	0	0	0	0	0	0	0	0	0	0	0	0	0	0	0	0	0	0	0	0	1	0	0	0	0	0	0	0
2	0	0	0	0	0	0	0	0	0	0	0	0	0	0	0	0	0	0	0	0	0	0	0	0	0	1	0	0	0	0	0	0
3	0	0	0	0	0	0	0	0	0	0	0	0	0	0	0	0	0	0	0	1	0	0	0	0	0	0	0	0	0	0	0	0
4	0	0	0	0	0	0	0	0	0	0	0	0	0	0	0	0	0	1	0	0	0	0	0	0	0	0	0	0	0	0	0	0
5	0	0	0	0	0	0	0	0	0	0	0	0	0	0	0	0	0	0	0	0	0	1	0	0	0	0	0	0	0	0	0	0
6	0	0	0	0	0	0	0	0	0	0	0	0	0	0	0	0	0	1	0	0	0	0	0	0	0	0	0	0	0	0	0	0
7	0	0	0	0	0	0	0	0	0	0	0	0	0	0	0	0	0	0	0	0	0	0	0	0	0	0	0	1	0	0	0	0
8	0	0	0	0	0	0	0	0	0	0	0	0	0	0	0	0	0	0	0	0	0	0	0	0	0	0	0	0	0	1	0	0
9	0	0	0	0	0	0	0	0	0	0	0	0	0	0	0	0	0	0	0	0	0	1	0	0	0	0	0	0	0	0	0	0
10	0	0	0	0	0	0	0	0	0	0	0	0	0	0	0	0	0	1	0	0	0	0	0	0	0	0	0	0	0	0	0	0
11	0	0	0	0	0	0	0	0	0	0	0	0	0	0	0	0	0	0	0	0	0	1	0	0	0	0	0	0	0	0	0	0
12	0	0	0	0	0	0	0	0	0	0	0	0	0	0	0	0	0	0	0	0	0	0	0	0	0	0	0	0	1	0	0	0
13	0	0	0	0	0	0	0	0	0	0	0	0	0	0	0	0	0	0	0	0	0	0	0	0	1	0	0	0	0	0	0	0
14	0	0	0	0	0	0	0	0	0	0	0	0	0	0	0	0	0	0	0	0	0	0	0	0	0	0	0	0	0	0	0	1
15	1	0	0	0	0	0	0	0	0	0	0	0	0	0	0	0	0	0	0	0	0	0	0	0	0	0	0	0	0	0	0	0
16	0	0	0	0	0	0	0	0	0	0	0	0	0	0	0	0	0	0	0	0	0	0	0	0	0	0	0	0	0	0	0	1

Figure 7.4: Optimal spectrum allocation for OFDM and CDMA users without primary users. $N_T = 32, K = 16, L = 16$**.**

That is because our goal is to optimize the overall system performance, they do not provide favorable channel conditions seen by the users in consideration.

7.3.2 Spectrum Allocation with Primary users

Figure 7.5 shows the final frequency allocation chart for the OFDM and 16 CDMA users, given the conditions that frequency bin 2, 3,21-23 and 32 are blocked by primary users. The channel states remain the same as listed in Figure 7.1. As less frequency bins are available for the secondary OFDM and CDMA users, more subcarrier sharing among the CDMA users is observed in the assignment. Taking the 4th bin as an example, 5 CDMA users ($K = 4, 5, 10, 13, 16$) are allocated to simultaneously transmit on it. Frequency bin 25 remains unused.

Due to the blocking of certain frequency bins by the primary users, the constraint of continuous L frequency bins in (7.10) may not be satisfied. As a result, the optimal solution may not exist. In this case, the solver at the base station will show that no solution exists, and the OFDM user's spectrum allocation cannot be

Freq bin no.	1	2	3	4	5	6	7	8	9	10	11	12	13	14	15	16	17	18	19	20	21	22	23	24	25	26	27	28	29	30	31	32
User no.																																
OFDM	0	0	0	0	1	1	1	1	1	1	1	1	1	1	1	1	1	1	1	1	0	0	0	0	0	0	0	0	0	0	0	0
1	0	0	0	0	0	0	0	0	0	0	0	0	0	0	0	0	0	0	0	0	0	0	0	0	0	1	0	0	0	0	0	0
2	0	0	0	0	0	0	0	0	0	0	0	0	0	0	0	0	0	0	0	0	0	0	0	0	0	0	0	0	1	0	0	0
3	0	0	0	0	0	0	0	0	0	0	0	0	0	0	0	0	0	0	0	0	0	0	0	0	0	0	1	0	0	0	0	0
4	0	0	0	1	0	0	0	0	0	0	0	0	0	0	0	0	0	0	0	0	0	0	0	0	0	0	0	0	0	0	0	0
5	0	0	0	1	0	0	0	0	0	0	0	0	0	0	0	0	0	0	0	0	0	0	0	0	0	0	0	0	0	0	0	0
6	0	0	0	0	0	0	0	0	0	0	0	0	0	0	0	0	0	0	0	0	0	0	0	1	0	0	0	0	0	0	0	0
7	0	0	0	0	0	0	0	0	0	0	0	0	0	0	0	0	0	0	0	0	0	0	0	0	0	0	0	1	0	0	0	0
8	1	0	0	0	0	0	0	0	0	0	0	0	0	0	0	0	0	0	0	0	0	0	0	0	0	0	0	0	0	0	0	0
9	0	0	0	0	0	0	0	0	0	0	0	0	0	0	0	0	0	0	0	0	0	0	0	0	0	0	0	0	0	1	0	0
10	0	0	0	1	0	0	0	0	0	0	0	0	0	0	0	0	0	0	0	0	0	0	0	0	0	0	0	0	0	0	0	0
11	0	0	0	0	0	0	0	0	0	0	0	0	0	0	0	0	0	0	0	0	0	0	0	0	0	0	0	0	0	0	1	0
12	0	0	0	0	0	0	0	0	0	0	0	0	0	0	0	0	0	0	0	0	0	0	0	0	0	0	0	0	1	0	0	0
13	0	0	0	1	0	0	0	0	0	0	0	0	0	0	0	0	0	0	0	0	0	0	0	0	0	0	0	0	0	0	0	0
14	0	0	0	0	0	0	0	0	0	0	0	0	0	0	0	0	0	0	0	0	0	0	0	0	0	0	0	1	0	0	0	0
15	1	0	0	0	0	0	0	0	0	0	0	0	0	0	0	0	0	0	0	0	0	0	0	0	0	0	0	0	0	0	0	0
16	0	0	0	1	0	0	0	0	0	0	0	0	0	0	0	0	0	0	0	0	0	0	0	0	0	0	0	0	0	0	0	0

Figure 7.5: Optimal spectrum allocation for OFDM and CDMA systems in the presence of primary users. $N_T = 32, K = 16, L = 16$,**v** = $\{0110000000000000000001110000000001\}$**.**

granted.

7.4 Heuristic Approach

The optimal solution assigns the spectrum for OFDM and CDMA users simultaneously, thus, when the number of users or the number of available frequency bins increases, the computation is slowed down due to the increase in the number of optimization variables. In order to speed up the optimization process, a heuristic approach is proposed. In our approach, we try to perform the spectrum allocation for OFDM user first, since it requires continuous frequency bins for transmission and hence constraints are more stringent. Then we proceed to assign the remaining spectrum among the CDMA users. Since the optimization is not all-at-once computation, but conducted in a consecutive order, the solution obtained by this approach is only suboptimal. However, our results show that the complexity is greatly reduced by this approach without much cost of accuracy. In fact, our sim-

ulation results show there are many cases where optimal solutions can be obtained using the heuristic approach.

The proposed heuristic approach is a two-step approach. Firstly, we choose the best frequency bins for the OFDM user. This is equivalent to solving the problem:

$$\max_{s_{0,n}} \quad \sum_{n=1}^{N_T} s_{0,n} H_{0,n} \tag{7.30}$$

subject to

$$\sum_{n=1}^{N_T-L+1} s_{0,n} s_{0,n+1} \ldots s_{0,n+L-1} = 1 \tag{7.31}$$

$$\sum_{n=1}^{N_T} s_{0,n} = L \tag{7.32}$$

$$s_{0,n} \in \{0,1\} \quad n = 1, 2, \ldots, N_T \tag{7.33}$$

By this, the most favorable L bins are selected, which are continuous in frequency.

After the allocation for OFDM user, the remaining $N_T - L$ frequency bins (if no blocking) are assigned to the K CDMA users, in the way that the following objective function is attained,

$$\max_{s_{k,n}} \quad \sum_{k=1}^{K} \sum_{n=1}^{N_T} s_{k,n} H_{k,n} - \sum_{n=1}^{N_T} \sum_{k=1}^{K} \sum_{\substack{j=1 \\ j \neq k}}^{K} s_{k,n} s_{j,n} \frac{C_{k,j} H_{j,n}}{G H_{k,n}} \tag{7.34}$$

subject to

$$s_{0,n} \sum_{k=1}^{K} s_{k,n} = 0, \quad n = 1, 2, \ldots, N_T \tag{7.35}$$

$$\sum_{n=1}^{N_T} s_{k,n} = 1, \quad k = 1, 2, \ldots, K \tag{7.36}$$

$$s_{k,n} \in \{0,1\} \quad k = 1, 2, \ldots, K; n = 1, 2, \ldots, N_T \tag{7.37}$$

Note that in (7.35), $s_{0,n}$ has been decided by the solution to the problem defined in (7.30)-(7.33) and hence the constraints are all in linear form. The constraints in (7.35) avoid the frequency sharing between the CDMA users and the OFDM user.

Freq bin no. / User no.	1	2	3	4	5	6	7	8	9	10	11	12	13	14	15	16	17	18	19	20	21	22	23	24	25	26	27	28	29	30	31	32
OFDM	0	0	0	0	0	0	0	0	0	0	0	0	0	0	0	0	1	1	1	1	1	1	1	1	1	1	1	1	1	1	1	1
1	0	0	0	0	0	0	0	0	0	0	0	0	0	0	1	0	0	0	0	0	0	0	0	0	0	0	0	0	0	0	0	0
2	0	1	0	0	0	0	0	0	0	0	0	0	0	0	0	0	0	0	0	0	0	0	0	0	0	0	0	0	0	0	0	0
3	0	0	0	0	1	0	0	0	0	0	0	0	0	0	0	0	0	0	0	0	0	0	0	0	0	0	0	0	0	0	0	0
4	0	0	0	0	0	0	0	0	0	0	0	0	0	0	0	1	0	0	0	0	0	0	0	0	0	0	0	0	0	0	0	0
5	0	0	0	0	0	0	1	0	0	0	0	0	0	0	0	0	0	0	0	0	0	0	0	0	0	0	0	0	0	0	0	0
6	0	0	0	0	0	0	0	0	0	0	0	1	0	0	0	0	0	0	0	0	0	0	0	0	0	0	0	0	0	0	0	0
7	1	0	0	0	0	0	0	0	0	0	0	0	0	0	0	0	0	0	0	0	0	0	0	0	0	0	0	0	0	0	0	0
8	0	0	0	0	0	1	0	0	0	0	0	0	0	0	0	0	0	0	0	0	0	0	0	0	0	0	0	0	0	0	0	0
9	0	0	0	0	0	0	0	0	0	0	0	0	1	0	0	0	0	0	0	0	0	0	0	0	0	0	0	0	0	0	0	0
10	0	0	0	1	0	0	0	0	0	0	0	0	0	0	0	0	0	0	0	0	0	0	0	0	0	0	0	0	0	0	0	0
11	0	0	0	0	0	0	0	0	0	0	1	0	0	0	0	0	0	0	0	0	0	0	0	0	0	0	0	0	0	0	0	0
12	0	0	1	0	0	0	0	0	0	0	0	0	0	0	0	0	0	0	0	0	0	0	0	0	0	0	0	0	0	0	0	0
13	0	0	0	1	0	0	0	0	0	0	0	0	0	0	0	0	0	0	0	0	0	0	0	0	0	0	0	0	0	0	0	0
14	0	1	0	0	0	0	0	0	0	0	0	0	0	0	0	0	0	0	0	0	0	0	0	0	0	0	0	0	0	0	0	0
15	1	0	0	0	0	0	0	0	0	0	0	0	0	0	0	0	0	0	0	0	0	0	0	0	0	0	0	0	0	0	0	0
16	0	0	0	0	0	0	0	0	0	0	0	1	0	0	0	0	0	0	0	0	0	0	0	0	0	0	0	0	0	0	0	0

Figure 7.6: Heuristic solution without primary users. $N_T = 32, K = 16, L = 16$**.**

Based on the formulation in (7.30)-(7.33) (OFDM assignments) and (7.34)-(7.37) (CDMA assignments), linear programming and quadratic programming can be used, respectively, to obtain the solutions for both OFDM and CDMA users. Some performance degradation is expected occasionally as the solution is suboptimal. Figure 7.6 illustrates the solution obtained for the previous example where no primary users are present. Although it appears that the frequency band assignments are distinctively different, the error between the values of the objective function is only 1.88% (371.74 by optimal versus 364.75 by suboptimal). Meanwhile, the computation time of the heuristic approach is reduced to 0.188s from the original 1.172s.

For the case with primary users, similar algorithm is used and the problem definitions for the two-step scheme are listed below:

Step 1- OFDM assignment:

$$\max_{s_{0,n}} \quad \sum_{n=1}^{N_T} s_{0,n} H_{0,n} \tag{7.38}$$

subject to

$$v_n s_{0,n} = 0, \quad n = 1, 2, \ldots, N_T \tag{7.39}$$

$$\sum_{n=1}^{N_T-L+1} s_{0,n} s_{0,n+1} \ldots s_{0,n+L-1} = 1 \tag{7.40}$$

$$\sum_{n=1}^{N_T} s_{0,n} = L \tag{7.41}$$

$$s_{0,n} \in \{0, 1\} \quad n = 1, 2, \ldots, N_T \tag{7.42}$$

where (7.39) blocks the assignments of the primary users' spectrum to OFDM user by the vector $\mathbf{v}$ defined above.

Step 2- CDMA assignment:

$$\max_{s_{k,n}} \quad \sum_{k=1}^{K} \sum_{n=1}^{N_T} s_{k,n} H_{k,n} - \sum_{n=1}^{N_T} \sum_{k=1}^{K} \sum_{\substack{j=1 \\ j \neq k}}^{K} s_{k,n} s_{j,n} \frac{C_{k,j} H_{j,n}}{G H_{k,n}} \tag{7.43}$$

subject to

$$v_n \sum_{k=1}^{K} s_{k,n} = 0, \quad n = 1, 2, \ldots, N_T \tag{7.44}$$

$$s_{0,n} \sum_{k=1}^{K} s_{k,n} = 0, \quad n = 1, 2, \ldots, N_T \tag{7.45}$$

$$\sum_{n=1}^{N_T} s_{k,n} = 1, \quad k = 1, 2, \ldots, K \tag{7.46}$$

$$s_{k,n} \in \{0, 1\} \quad k = 1, 2, \ldots, K; n = 1, 2, \ldots, N_T \tag{7.47}$$

where (7.44) ensures that the spectrum used by the primary users will not be assigned to any of the CDMA users.

The allocation result by the suboptimal algorithm in presence of primary users is displayed in Figure 7.7. Again, in this case, the two-step approach only shows negligible error from the optimal result: the maximum values of the utility function for both algorithms are, respectively, 346.733 and 343.74.

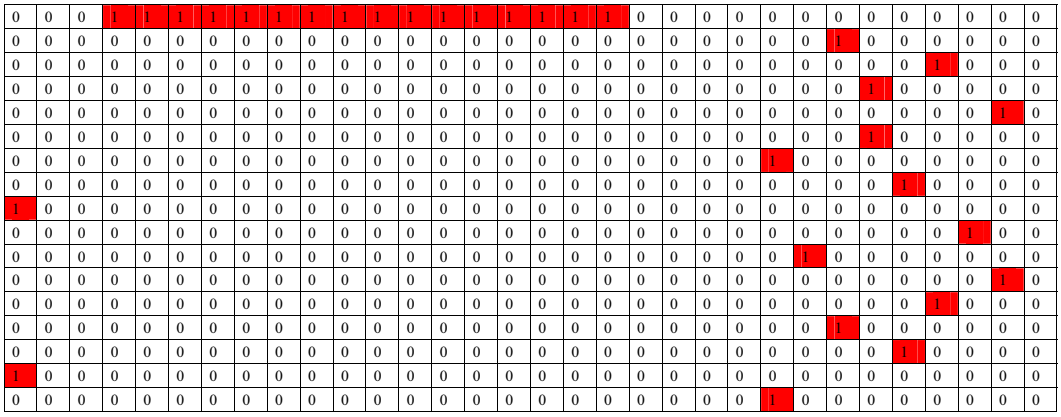

Figure 7.7: Heuristic solution in presence of primary users. $N_T = 32, K = 16, L = 16$,**v** $= \{0\,1\,1\,0\,0\,0\,0\,0\,0\,0\,0\,0\,0\,0\,0\,0\,0\,0\,0\,0\,0\,1\,1\,1\,0\,0\,0\,0\,0\,0\,0\,0\,1\}$**.**

7.5 Summary and Contribution

We made some assumptions on the future systems, such as the reconfigurability of base station and mobile devices. And the base station is also assumed to be able to support multiple radio systems. We then proposed a centralized model, where a powerful base station can support users having different types of communication systems such as OFDM and CDMA, and the frequency bins assigned to each user can be dynamically assigned. We set up a nonlinear binary integer programming algorithm to perform the allocation of frequency bins to all the users, both in the presence or absence of primary users. We demonstrated how it can be converted into an equivalent linearly constrained quadratic programming problem and presented the optimal solutions in both cases with and without the consideration of primary users. Finally, a two-step suboptimal heuristic approach was proposed to speed up the spectrum allocation process with little penalty in the utility.

Chapter 8

Conclusions

This thesis focused on the high capacity high spectral efficiency transmission techniques in the wireless broadband system. We reviewed the key techniques attractive for NextG, and introduced the 3 promising systems, i.e., OFDM, CDMA and MC-CDMA. Their technical considerations were discussed and performance enhancement in these systems was explored.

We studied the ICI effect in OFDM system, and concluded from the theoretical derivations that ICI remains the same with increasing system bandwidth. But the subcarrier bandwidth is fixed to ensure time nonselective fading for a given mobility group. Further investigation in this scenario showed that there is a maximum bandwidth for each channel condition beyond which the transmission will degrade, in both uncoded and coded OFDM systems. These results showed that there could be a limit in OFDM system bandwidth which would be a barrier to achieve high transmission rate while trying to support a given mobility group.

Next, power control in a DS-CDMA system was investigated and a constrained

power control profile was proposed. Data users are subject to the imposed power constraints associated with their distance from the base station, yet the voice users follows the same power profile as in the conventional scheme. A profile index was suggested to define different power profiles. The validity of the log-normal approximation for the total received power was verified under the new power control scheme. The interference correction factor was also derived for the proposed profiles, and the values were shown to be different from the commonly adopted value for the conventional power control. The PDFs for the SIR for both voice and data users were then derived which was followed by the theoretical user capacity. Notably, in our approach, the retransmission rate is successfully introduced to the evaluation of outage probability and thus enables the evaluation of theoretical capacity. The results showed that the proposed power control scheme causes larger delay and higher retransmission rate for the data users, but at the same time it decreases the average interference level and can eventually increase the total number of users the system could accommodate, if appropriate control parameters are chosen. For our proposed power control scheme, the optimum profile index can be chosen to maximize the capacity, subject to certain delay and outage constraints.

Subcarrier-and-bit allocation problems were extensively investigated. The focus was first on OFDM systems. The achievable gain by the use of optimal subcarrier-and-bit allocation is quantified using spectral flatness measurement (SFM), RMS delay spread and subcarrier correlation coefficient. The empirical functions manifesting the relationship between the power gain and those parameters are presented for a special case, and it was shown that the minimum transmit power

can be achieved on a certain RMS delay spread for a given number of users and subcarriers.

Later the subcarrier-and-bit allocation was studied in multiclass multiuser OFDM system. The constrained power minimization problem was firstly formulated and then converted into a convex nonlinear integer problem, so that the optimal solution can be derived. It is noteworthy that our solution is the *exact* optimal solution without any assumption or relaxation, which is novel in the literature. Thus, the theoretical framework and the optimal solution can be used as a benchmark for the suboptimal approaches. In order to further simplify the computation, two suboptimal schemes were proposed which showed good approximation to the optimal solution. At the same time, a lower bound for the minimum transmit power was also obtained from the suboptimal scheme. While in a three class case, best effort service was also included and the system revenue was maximized subject to all the constraints imposed by all the users.

The subcarrier allocation was further investigated in MC-DS-CDMA system. Two novel suboptimal subcarrier allocation algorithms were proposed to improve the spectral efficiency of the system, with the consideration of the MAI. The first algorithm was developed to iteratively search for the optimal subcarrier allocations so as to simultaneously minimize the average BER over each subcarrier. The second one aimed to maximize the overall system utility, and the objective function was formulated as a quadratic programming (QP) problem, which was then converted into a solvable linear programming (LP) problem through Kuhn-Tucker (KT) conditions. The performance of these two schemes were presented and compared with

Kim's method [2]. It was shown that with MAI taken account of, our second approach gives general BER improvement over the other two schemes, while the first approach also performs well above the Kim's method except when the subcarrier sharing rate is low.

Finally, a simple model of cognitive radio was proposed. The spectrum was dynamically allocated to OFDM and CDMA users in the proposed centralized model, subject to their individual spectrum requirements. The optimal solution to maximize the spectrum usage was presented, with or without the presence of primary users. Further, a heuristic approach was proposed, and it was observed that this approach only gives minimal penalty from the optimal scheme, if it does not provide the optimum.

Bibliography

[1] T. Summers and S. Wilson, "Snr mismatch and online estimation in turbo decoding," *IEEE Trans. Commun.*, vol. 46, no. 4, pp. 421–423, April 1998.

[2] Y. Kim, I. Song, S. Yoon, and R. P. S, "A multicarrier cdma system with adaptive subchannel allocation for forward links," *IEEE Trans. Veh. Technol.*, vol. 48, no. 5, pp. 1428–1436, September 1999.

[3] E. Dinan and B. Jabbari, "Spreading codes for direct sequence cdma and wideband cdma cellular networks," *IEEE Commun. Magazine*, pp. 48–54, September 1998.

[4] P. Bello, "Selective fading limitations of the kathryn modem and some system design considerations," *IEEE Trans. Commun. Technol.*, vol. COM-13, pp. 320–333, September 1965.

[5] M. Zimmermann and A. Kirsch, "The an/gsc-10/kathryn variable rate data modem for hf radio," *IEEE Trans. Commun. Technol.*, vol. COM-15, pp. 197–205, April 1967.

[6] E. Powers and M. Zimmermann, "A digital implementation of a multichannel data modem," in *Proc. IEEE Int. Conf. Commun.*, Philadelphia, PA, 1968.

[7] R. Chang, "Synthesis of band-limited orthogonal signals for multichannel data transmission," *Bell Syst. Tech. J.*, vol. 45, pp. 1775–1796, December 1966.

[8] R. Chang and R. Gibby, "A theoretical study of performance of an orthogonal multiplexing data transmission scheme," *IEEE Trans. Commun. Technol.*, vol. COM-16, pp. 529–540, August 1968.

[9] S. Weinstein and P. Ebert, "Data transmission by frequency division multiplexing using the discrete fourier transform," *IEEE Trans. Commun. Technol.*, vol. COM-19, no. 5, pp. 628–634, October 1971.

[10] L. Cimini, "Analysis and simulation of a digital mobile channel using orthogonal frequency division multiplexing," *IEEE Trans. Commun.*, vol. COM-33, pp. 665–675, July 1985.

[11] T. de Couasnon and et. al., "Ofdm for digital tv broadcasting," *signal processing*, vol. 39, pp. 1–32, 1994.

[12] K. Fazel and G. Fettweis, *Multi-Carrier Spread-Spectrum.* Kluwer Academic Publishers, 1997.

[13] M. Russell and G. L. Stuber, "Interchannel interference analysis of ofdm in a mobile environment," in *Proc. VTC'95*, 1995, pp. 820–824.

[14] P. Robertson and S. Kaiser, "The effects of doppler spreads in ofdm(a) mobile radio systems," in *Proc. VTC'99-Fall*, 1999, pp. 329–333.

[15] N. Yee, J. P. Linnartz, and G. Fettweis, "Multi-carrier cdma in indoor wireless radio networks," in *Proceedings PIMRC'93*, Yokohama, Japan, 1993, pp. 109–113.

[16] A. Chouly, A. Brajel, and S. Jourdan, "Orthogonal multicarrier techniques applied to direct sequence spread spectrum cdma systems," in *Proc. IEEE Globecom '93*, Houston, TX, November 1993, pp. 1723–1728.

[17] G. Fettweis, A. Bahai, and K. Anvari, "On multicarrier code division multiple access (mc-cdma) modem design," in *Proc. IEEE VTC*, 1994, pp. 1670–1674.

[18] K. Fazel and L. Papke, "On the performance of convolutionally-coded cdma/ofdm for mobile communication system," in *Proc. PIMRC'93*, 1993, pp. 468–472.

[19] S. Hara and R. Prasad, "Overview of multicarrier cdma," *IEEE Commun. Mag.*, pp. 126–133, December 1997.

[20] V. M. DaSilva and E. S. Sousa, "Performance of orthogonal cdma codes for quasi-synchronous communication systems," in *Proc. of IEEE ICUPC'93*, Ottawa, Canada, October 1993, pp. 995–999.

[21] S. Kondo and L. B. Milstein, "Performance of multicarrier ds-cdma systems," *IEEE Trans. Commun.*, vol. 44, no. 2, pp. 238–246, February 1996.

[22] L. Vandendorpe, "Multitone direct sequence cdma system in an indoor wireless environment," in *Proc. of IEEE First Symposium of Communications and Vehicular Technology*, Delft, Netherlands, October 1993, pp. 4.1.1–4.1.8.

[23] C. Berrou, A. Glavieux, and P. Thitimajshima, "Near shannon limit error-correcting coding and decoding: Turbo-codes," in *ICC'93, Conf. Rec.*, Geneva, May 1993, pp. 1064–1070.

[24] S. L. Goff, A. Glavieux, and C. Berrou, "Turbo-codes and high spectral efficiency modulation," in *IEEE International Conference on Communications ICC'94*, New Orleans, LA, May 1994, pp. 645–649.

[25] A. Worm, P. Hoeher, and N. Wehn, "Turbo-decoding without snr estimation," *IEEE Commun. Lett.*, vol. 4, no. 6, June 2000.

[26] J. L. Massey, "Coding and modulation in digital communications," in *International Zurich Seminar on Digital Communications*, Zurich, Switzerland, March 1974, pp. E2 (1)–E2 (4).

[27] G. Ungerboeck, "Channel coding with multilevel/phase signals," *IEEE Trans. Inform. Theory*, vol. IT-28, pp. 55–67, January 1982.

[28] ——, "Trellis-coded modulation with redundant signal sets," *IEEE Commun. Mag.*, vol. 25, pp. 5–21, February 1987.

[29] E. Biglieri, D. Divsalar, P. J. McLane, and M. K. Simon, *Introduction to Trellis-Coded Modulation with Applications.* New York: Macmillan, 1991.

[30] B. Sklar, "Rayleigh fading channels in mobile digital communication systems part ii: Mitigation," *IEEE Commun. Mag.*, pp. 148–155, September 1997.

[31] D. Divsalar and M. K. Simon, "Multiple trellis coded modulation (mtcm)," *IEEE Trans. Commun.*, vol. 36, pp. 410– 419, April 1988.

[32] M. K. Simon and D. Divsalar, "The performance of trellis coded multilevel dpsk on a fading mobile satellite channel," *IEEE Trans. Veh. Technol.*, vol. 37, no. 2, pp. 78–91, May 1988.

[33] E. Zehavi, "8-psk trellis codes for a rayleigh channel," *IEEE Trans. Commun.*, vol. 40, no. 5, pp. 873–884, May 1992.

[34] G. Caire, G. Taricco, and E.Biglieri, "Bit-interleaved coded modulation," *IEEE Trans. Inform. Theory*, vol. 44, no. 3, pp. 927–946, May 1998.

[35] P. Robertson and T. Worz, "Bandwidth-efficient turbo trellis-coded modulation using punctured component codes," *IEEE J. Select. Areas Commun.*, vol. 16, no. 2, pp. 206–218, February 1998.

[36] S. L. Goff, "Performance of bit-interleaved turbo-coded modulations on rayleigh fading channels," *Electron. Lett.*, vol. 36, no. 8, pp. 731–733, April 2000.

[37] P. Hoeher, "New iterative turbo decoding algorithms," in *Proc. Int. Symp. Turbo Codes and Related Topics*, 1997, pp. 63–67.

[38] P. Robertson, E. Villebrun, and P. Hoeher, "A comparison of optimal and suboptimal map decoding algorithms operating in the log domain," in *Proc. Int. Conf. Communications*, 1995, pp. 1009–1013.

[39] P. Jung, "Novel low complexity decoder for turbo codes," *Electron. Lett.*, pp. 86–87, January 1995.

[40] X. Li, B. Vucetic, and Y. Sato, "Optimum soft-output detection for channels with intersymbol interference," *IEEE Trans. Inform. Theory*, vol. 41, no. 3, pp. 704–713, May 1995.

[41] C. Doulillard, M. J'ez'equel, and C. Berrou, "Iterative correction of intersymbol interference," *Eur. Trans. Telecommun.*, vol. 6, no. 3, pp. 507–511, 1995.

[42] A. Elosery and C. Abdallah, "Distributed power control in cdma cellular systems," *IEEE Antennas and Propagation Magazine*, vol. 42, no. 4, pp. 152–159, August 2000.

[43] F. C. M. Lau and W. M. Tam, "Novel sir-estimation-based power control in a cdma mobile radio system under multi-path environment," *IEEE Trans. Veh. Technol.*, vol. 50, no. 1, pp. 314–320, January 2001.

[44] J. Wang and A. Yu, "Open-loop power control error in cellular cdma overlay systems," *IEEE J. Select. Areas Commun.*, vol. 19, no. 7, pp. 1246–1254, July 2001.

[45] T. Nagatsu, T. Tsuruhara, and M. Sakamoto, "Transmitter power control for cellular land mobile radio," in *Proc. IEEE GLOBECOM*, 1983, pp. 1430–1434.

[46] T. Fujii and M. Sakamoto, "Reduction of cochannel interference in cellular systems by intra-zone channel reassignment and adaptive transmitter power control," in *Proc. IEEE Veh. Technol. Conf.* VTC-98, 1998.

[47] J. Zander, "Performance of optimum transmitter power control in cellular radio systems," *IEEE Trans. Veh. Technol.*, vol. 41, no. 1, pp. 57–62, February 1992.

[48] ——, "Distributed cochannel interference control in cellular radio systems," *IEEE Trans. Veh. Technol.*, vol. 41, no. 3, pp. 305–311, August 1992.

[49] S. A. Grandhi, R. Vijayan, D. J. Goodman, and J. Zander, "Centralized power control in cellular radio systems," *IEEE Trans. Veh. Technol.*, vol. 42, no. 4, pp. 466–468, November 1993.

[50] Q. Wu, "Performance of transmitter power control in cdma cellular mobile systems," *IEEE Trans. Veh. Technol.*, vol. 48, no. 2, pp. 571–575, March 1999.

[51] R. D. Yates and C.-Y. Huang, "Integrated power control and base station assignment," *IEEE Trans. Veh. Technol.*, vol. 44, no. 3, pp. 638–644, August 1995.

[52] R. D. Yates, "A framework for uplink power control in cellular radio systems," *IEEE J. Select. Areas Commun.*, vol. 13, no. 7, pp. 1341–1347, September 1995.

[53] S. V. Hanly, "An algorithm for combined cell-site selection and power control to maximize cellular spread spectrum capacity," *IEEE J. Select. Areas Commun.*, vol. 13, no. 7, pp. 1332–1340, September 1995.

[54] ——, "Capacity and power control in spread spectrum macrodiversity radio networks," *IEEE Trans. Commun.*, vol. 44, no. 2, pp. 247–256, February 1996.

[55] S. Grandhi and J. Zander, "Constrained power control in cellular radio systems," in *Proc. IEEE Veh. Technol. Conf.* VTC-94, 1994.

[56] R.Yates and C. Y. Huang, "Constrained power control and base station assignment in cellular radio systems," in *IEEE/ACM Trans. Network*, 1995.

[57] T. Wong, J. Mark, and K. Chua, "Resource allocation in mobile cellular networks with qos constraints," in *Pro. Wireless Communications and Networking Conf.*, March 2002.

[58] W. Kumwilaisak and et. al., "A cross-layer quality-of service mapping architecture for video delivery in wireless networks," *IEEE J. Select. Areas Commun.*, vol. 21, no. 10, pp. 1685–1698, December 2003.

[59] L. Alonso and R. Agusti, "Automatic rate adaptation and energy-saving mechanisms based on cross-layer information for packet-switched data networks," *IEEE Radio Communications*, pp. S15–S20, March 2004.

[60] J. Yao, J. Mark, T. Wong, and e. a. Y.H. Chew, "Virtual partitioning resource allocation for multiclass traffic in cellular systems with qos constraints," *IEEE Trans. Veh. Technol.*, vol. 53, no. 3, May 2004.

[61] M. Bozinovski, P. Popovski, and L. Gavrilovska, "Qos-based policy for call admission control in mobile cellular network," in *Proc. Wireless Communications and Networking Conf.*, vol. 2, 2000, pp. 502–506.

[62] C. Comaniciu and H. Poor, "Jointly optimal power and admission control for delay sensitive traffic in cdma networks with lmmse receivers," *IEEE Trans. Signal Processing*, vol. 51, pp. 2032–2042, August 2003.

[63] C. Wong, R. Cheng, K. Letaief, and R. Murch, "Multiuser ofdm with adaptive subcarrier, bit, and power allocation," *IEEE J. Select. Areas commun.*, vol. 17, no. 10, pp. 1747–1758, October 1999.

[64] C. Wong, C. Tsui, R. Cheng, and K. Letaief, "A real-time subcarrier allocation scheme for multiple access downlink ofdm transmission," in *IEEE Proc. VTC'99*, vol. 2, 1999, pp. 1124–1128.

[65] Y. Zhang and K. Letaief, "Multiuser adaptive subcarrier-and-bit allocation with adaptive cell selection for ofdm systems," *IEEE Trans. Wireless Commun.*, vol. 3, no. 5, pp. 1566–1575, September 2004.

[66] X. Liang and J. Zhu, "An adaptive subcarrier allocation algorithm for multiuser ofdm system," in *IEEE Proc. VTC'2003-Fall*, 2003, pp. 1502–1506.

[67] T. Alen, A. Madhukumar, and F. Chin, "Capacity enhancement of a multiuser ofdm system using dynamic frequency allocation," *IEEE Trans. Broadcasting*, vol. 49, no. 4, pp. 344–353, December 2003.

[68] Y. Kim, H. Nam, and B. Womack, "An adaptive grouped-subcarrier allocation algorithm using comparative superiority," in *IEEE Proc. MILCOM'2005*, 2005, pp. 1–7.

[69] W. Rhee and J. Cioffi, "Increase in capacity of multiuser ofdm system using dynamic subchannel allocation," in *IEEE Proc. VTC'2000*, 2000, pp. 1085–1089.

[70] H. Yin and H. Liu, "An efficient multiuser loading algorithm for ofdm-based broadband wireless sytem," in *IEEE Global Telecommunications Conference*, vol. 1, 2000, pp. 103–107.

[71] Z. Shen, J. Andrews, and B. Evans, "Adaptive resource allocation in multiuser ofdm systems with proportional rate constraints," *IEEE Trans. Wireless Commun.*, vol. 4, no. 6, pp. 2726 – 2737, November 2005.

[72] Q. Chen, E. Sousa, and S. Pasupathy, "Multicarrier cdma with adaptive frequency hopping for mobile radio systems," *IEEE J. Select Areas Commun.*, vol. 14, no. 9, pp. 1852–1858, December 1996.

[73] P. Fan, J. Li, and Z. Cao, "A near optimal subchannel allocation policy in forward links for multicarrier cdma system," in *Proc. VTC 2001 Spring*, vol. 2, 2001, pp. 896 – 900.

[74] J. Kim, N. G. C, and G. Huang, "Adaptive data transmission based on band-selection for mc-cdma systems," in *Proc. GLOBECOM'01*, vol. 5, 2001, pp. 3125–3129.

[75] M. Tabulo, D. Laurenson, S. Mclaughlin, and E. Al-Susa, "A linear programming algorithm for a grouped mc-cdma system," in *Proc. VTC 2003 Fall*, vol. 3, 2003, pp. 1463–1467.

[76] E. Al-susa, D. Cruickshank, and S. Mclaughlin, "Practical algorithm for adaptive subcarrier-hopping multicarrier multiple access transmission," *Electronics Letters*, vol. 39, no. 21, pp. 1544–1546, October 2003.

[77] C. Wong, R. Cheng, K. Letaief, and R. Murch, "Multiuser ofdm with adaptive subcarrier, bit, and power allocation," *IEEE J. Select. Areas Commun.*, vol. 17, no. 10, pp. 1747–1758, October 1999.

[78] D. Statovci and T. Nordstrom, "Adaptive subcarrier allocation, power control and power allocation for multiuser fdd-dmt systems," in *Proc. ICC*, vol. 1, 2004, pp. 11–15.

[79] H. E. Levin, "A complete and optimal data allocation method for practical discrete multitone systems," in *Proc. GLOBECOM'01*, vol. 1, 2001, pp. 369–374.

[80] K. Witrisal, Y. Kim, R. Prasad, and L. Ligthart, "Antenna diversity for ofdm using cyclic delays," in *Proc. IEEE 8th Symposium on Communications and Vehicular Technology in the Benelux, SCVT-2001*, October 2001.

[81] F. S. H. H. M.Bossert, A. Huebner and E. Costa, "On cyclic delay diversity in ofdm based transmission schemes," in *Proc. 7th International OFDM Workshop*, September 2002.

[82] W. Jakes and et.al., *Microwave mobile communications.* New York: Wiley, 1974.

[83] B. Kim, Y. Fang, and T. Wong, "Rate-adaptive mac protocol in high rate personal area networks," in *Proc. IEEE Wireless Communications and Networking Conference (WCNC'04)*, Atlanta, Georgia, 2004.

[84] A. Hoang and M. Motani, "Buffer and channel adaptive modulation for transmission over fading channels," in *Proc. IEEE International Conferrence on Communications (ICC'03)*, Anchorage, 2003.

[85] T. Elbatt and A. Ephremides, "Joint scheduling and power contol for wireless *ad hoc* networks," *IEEE. Trans. Wireless Commun.*, vol. 3, no. 1, pp. 74–85, January 2004.

[86] M. Chiang, "Balancing transport and physical layers in wireless multihop networks: jointly optimal congestion control and power control," *IEEE J. Select. Areas Commun.*, vol. 23, no. 1, pp. 104–116, January 2005.

[87] FCC, "Spectrum policy task force report," vol. ET Docket 02-155, Nov 2002.

[88] S. Haykin, "Cognitive radio: brain-empowered wireless communications," *IEEE J. Select. Areas Commun.*, vol. 23, no. 2, pp. 201–220, February 2005.

[89] D. Cabric, S. Mishra, and R. Brodersen, "Implementation issues in spectrum sensing for cognitive radios," in *Proc. Asilomar Conference on Signals and Systems and Computers*, 2004.

[90] W. Horne, "Adaptive spectrum access: using the full spectrum space," in *Proc. Telecommunications Policy Research Conference (TPRC)*, 2003.

[91] V. Chakravarthy, A. Shaw., M. Temple, and J. Stephens, "Cognitive radio - an adaptive waveform with spectral sharing capability," in *Proc. WCNC'05*, 2005.

[92] C. Rieser, T. Rondeau, C. Bostian, and T. Gallagher, "Cognitive radio testbed: further details and testing of a distributed genetic algorithm based cognitive engine for programmable radios," in *Proc. MILCOM*, vol. 3, October 2004.

[93] T. Rondeau, B. Le, C. Rieser, and C. Bosstian, "Cognitive radios with genetic algorithms: an intelligent control of software defined radios," in *SDR Forum Technical Conference*, November 2004, pp. C–3–C–8.

[94] S. Shankar, C. Chou, K. Challapali, and S. Mangold, "Spectrum agile radio: capacity and qos implications of dynamic spectrum assignment," in *Proc. Globecom*, 2005.

[95] S. Mangold, A. Jarosch, and C. Monney, "Cognitive radio - trends and research challenges," in *Proc. Swisscom Innovations*, June 2005.

[96] A. Hulber, "Spectrum sharing through beacons," in *Proc. PIMRC'05*, 2005.

[97] L. Fenton, "The sum of a log-normal probability distribution in scattered trasmission systems," *IRE Trans.*, vol. C5-8, pp. 57–67, March 1960.

[98] W. Huang and V. Bhargava, "Performance evaluation of a ds/cdma cellular system with voice and data services," in *Proc. IEEE Personal, Indoor and Mobile Radio Communications, Seventh IEEE International Symposium on.*, vol. 2, 1996, pp. 588–592.

[99] M. Jansen and R. Prasad, "Capacity, throughput, and delay analysis of a cellular ds cdma system with imperfect power control and imperfect sectorization," *IEEE Trans. Veh. Technol.*, vol. 44, no. 1, pp. 57–75, February 1994.

[100] J. Kim and M. Honig, "Resource allocation for multiple calsses of ds-cdma traffic," *IEEE Trans. Veh. Technol.*, vol. 49, no. 2, March 2000.

[101] L. Kleinrock and F. Tobagi, "Packet switching in radio channels: Part i-carrier sense multiple access modes and their throughput-delay characteristics," *IEEE Trans. Commun.*, vol. com-23, no. 12, December 1975.

[102] C. Chai, Y. Chew, Y. Zhao, , and K. Li, "Constrained power control scheme to increase capacity of multi-service systems," in *Proc. ICICS*, 2003.

[103] H. Yin and H. Liu, "An efficient multiuser loading algorithm for ofdm-based broadband wireless sytem," in *IEEE Global Telecommunications Conference*, vol. 1, 2000, pp. 103–107.

[104] S. Rao, *Engineering Optimization: Theory and Practice*, 3rd ed. John Wiley & Sons, 1996.

[105] K. Zhou and Y. Chew, "Exact solution to adaptive subcarrier-and-bit allocation in multiclass multiuser ofdm systems," *submitted to IEEE Trans. Veh. Technol.*, September 2005.

[106] A. Land and A. Doig, "An automatic method for solving discrete programming problems," *Econometrica*, pp. 28:497–520, 1960.

[107] S. Leyffer, "Integrating sqp and branch-and-bound for mixed integer nonlinear programming," *Computational Optimization and Applications*, August 1998.

[108] J. Jang and K. Lee, "Transmit power adaptation for multiuser ofdm systems," *IEEE J. Select. Areas Commun.*, vol. 21, no. 2, pp. 171–178, Feburary 2003.

[109] X. Gui and T. Ng, "Performance of asynchronous orthogonal multicarrier cdma system in frequency selective fading channel," *IEEE Trans. Commun.*, vol. 47, no. 7, pp. 1084–1091, July 1999.

[110] S. Kondo and L. Milstein, "Multicarrier cdma system with cochannel interference cancellation," in *Proc. VTC*, vol. 3, June 1994, pp. 1640–1644.

[111] O. R. text book group, *Operational Research*. Tsing Hua University Publishing House, 2002.

[112] P. Venkataraman, *Applied Optimization with Matlab Programming*. John Wiley & Sons, 2001.

[113] E. Nering and W. Albert, *Linear programs and related problems*, united kingdom ed. Academic press limited, 1999.

[114] M. Bazaraa, H. Sherali, and C. Shetty, *Nonlinear Programming: theory and algorithms*, 2nd ed. John Wiley & Sons, 1993.

List of Publications

[1] K. Zhou and Y.H. Chew, "Heuristic algorithms to adaptive subcarrier-and-bit allocation in multiclass multiuser OFDM system", in *Proc. VTC'06 Spring*, to be held in May 2006.

[2] K. Zhou and Y.H. Chew, "Adaptive subcarrier-and-bit allocation in multiclass multiuser OFDM system", in *Proc. Asilomar'05*, Oct 2005, pp. 1456 - 1460.

[3] K. Zhou, Y.H. Chew and Y. Wu, "Optimal solution to adaptive subcarrier-and-bit allocation in multiclass multiuser OFDM system", in *Proc. the 5th international worshop on Multi-Carrier Spread-Spectrum (MC-SS'05)*, Sep 2005, pp. 345-352.

[4] K. Zhou and Y.H. Chew, "Performance of 2D FFT modulated signal over multipath fading channels", in *Proc. PIMRC'04*, Sep, 2004, pp. 1337 - 1341.

[5] K. Zhou and Y.H. Chew, "Maximum bandwidth of orthogonal frequency division multiplex (OFDM) over Multipath fading channel", in *Proc. ICCCAS'04*, Jun, 2004, pp. 57-61.

[6] K. Zhou and Y.H. Chew, "Exact solution to adaptive subcarrier-and-bit allocation in multiclass multiuser OFDM system", submitted to *IEEE Trans. Veh. Technol.*, currently under second review.

[7] H. Long, K. Zhou and Y.H. Chew, "Two subcarrier allocation schemes for MC-DS-CDMA systems in the presence of multiple access interference", submitted to *IEEE Trans. Veh. Technol.*

[8] K. Zhou and Y.H. Chew, "Cognitive radios with centralized spectrum allocation capacity", submitted to *IEEE Commun. Lett.*

[9] C.C. Chai, K. Zhou and Y.H. Chew, "Constrained power control scheme to enhance capacity of slotted DS-CDMA cellular systems", submitted to *IEEE Trans. Veh. Technol.*

[10] K. Zhou and Y.H. Chew, "On the allocation of frequency bands in cognitive radio", submitted to *GLOBECOM'06*.

[11] K. Zhou and Y.H. Chew, "On quantifying the achievable performance gain by optimal subcarrier-and-bit allocation algorithm in multiuser OFDM systems", submitted to *MILCOM'06*.

Appendix A

Functions G for Different Power Control Profiles

In Section III, we derived the interference correction factor for the data users F_{m_d} for the proposed scheme. The expression for F_{m_d} is in terms of the summation of the $G(L, d_{n,i})$ functions which are tabulated in Table 4.1, where L and $d_{n,i}$ are defined in (4.35) and (4.33), respectively. For the constrained power control profiles

indicated by different δ, the functions G are listed below,

$$G_{\delta=2}(L,d_{n,i}) = 4d_{n,i}\ln\left(\frac{Ld_{n,i}}{Ld_{n,i}-1}\right) - \frac{1}{L}\left[\frac{4L^2d_{n,i}^2-6Ld_{n,i}+1}{(Ld_{n,i}-1)^2} + \frac{(L-1)\left(3+Ld_{n,i}^2-2Ld_{n,i}-2d_{n,i}\right)d_{n,i}}{(d_{n,i}-1)^2(Ld_{n,i}-1)^2} + \ln\left(\frac{Ld_{n,i}-L}{Ld_{n,i}-1}\right)\right] \quad (A.1)$$

$$G_{\delta=0}(L,d_{n,i}) = 4d_{n,i}\ln\left(\frac{Ld_{n,i}}{Ld_{n,i}-1}\right) + \frac{6Ld_{n,i}-4L^2d_{n,i}^2-2}{L(Ld_{n,i}-1)^2} + \frac{1}{L^2(d_{n,i}-1)^2} \quad (A.2)$$

$$G_{\delta=-2}(L,d_{n,i}) = 4d_{n,i}\ln\left(\frac{Ld_{n,i}}{Ld_{n,i}-1}\right) + \frac{6Ld_{n,i}-4L^2d_{n,i}^2-1}{L(Ld_{n,i}-1)^2} + \frac{(L-1)\left(3Ld_{n,i}^2-2Ld_{n,i}-2d_{n,i}+1\right)}{L^3d_{n,i}(d_{n,i}-1)^2(Ld_{n,i}-1)^2} + \frac{1}{L^3d_{n,i}^2}\ln\left(\frac{Ld_{n,i}-1}{d_{n,i}-1}\right) \quad (A.3)$$

$$G_{\delta=-4}(L,d_{n,i}) = 4d_{n,i}\ln\left(\frac{Ld_{n,i}}{Ld_{n,i}-1}\right) + \frac{6Ld_{n,i}-4L^2d_{n,i}^2-1}{L(Ld_{n,i}-1)^2} + \frac{4}{L^4d_{n,i}^3}\ln\left(\frac{Ld_{n,i}-1}{d_{n,i}-1}\right) + \frac{(L-1)\left[L^2d_{n,i}^4+4-2(L+1)d_{n,i}\left(Ld_{n,i}^2+3\right)+d_{n,i}^2(L^2+9L+1)\right]}{L^4d_{n,i}^2(d_{n,i}-1)^2(Ld_{n,i}-1)^2} \quad (A.4)$$

$$G_{\delta=-10}(L,d_{n,i}) = 4d_{n,i}\ln\left(\frac{Ld_{n,i}}{Ld_{n,i}-1}\right) + \frac{6Ld_{n,i}-4L^2d_{n,i}^2-1}{L(Ld_{n,i}-1)^2} + \frac{25}{L^7d_{n,i}^6}\ln\left(\frac{Ld_{n,i}-1}{d_{n,i}-1}\right) + \frac{1-L^{-4}}{4L^3d_{n,i}^2} + \frac{4(1-L^{-3})}{3L^4d_{n,i}^3} + \frac{9(1-L^{-2})}{2L^5d_{n,i}^4} + \frac{16(1-L^{-1})}{L^6d_{n,i}^5} + \frac{1}{L^5d_{n,i}^4}\left[\frac{1}{L^2(d_{n,i}-1)^2} - \frac{1}{(Ld_{n,i}-1)^2}\right] + \frac{9}{L^6d_{n,i}^5}\left[\frac{1}{L(d_{n,i}-1)} - \frac{1}{(Ld_{n,i}-1)}\right] \quad (A.5)$$

Appendix B

KT Conditions

For a NLP problem given by

$$\text{Minimize} \qquad f(x_1, x_2, \ldots, x_i, \ldots, x_I), \tag{B.1}$$

Subject to

$$w_j(x_1, , x_2, \ldots, x_i, \ldots, x_I) + y_j = 0, \quad j = 1, 2, \ldots, P, \tag{B.2}$$

$$y_j \geq 0, \quad i = 1, 2, \ldots, I. \tag{B.3}$$

where $y_j \, (j = 1, 2, P)$ are slack variables. If the objective function $f(x)$ and the constraints $w_j(x)$ are differentiable at $\mathbf{x}_0$ where $\mathbf{x}_0$ denotes a feasible solution, then there exist scalars $\mathbf{u} = (u_1, u_2, \ldots, u_j, \ldots, u_P)^T$ such that [113] [114]:

$$\nabla f(\mathbf{x}_0) + \sum_{j=1}^{P} u_j \nabla w_j(\mathbf{x}_0) = 0, \tag{B.4}$$

$$u_j w_j(\mathbf{x}_0) = 0, \quad j = 1, 2, \ldots, P, \tag{B.5}$$

$$u_j \geq 0. \tag{B.6}$$

The vector $\mathbf{u} = (u_1, u_2, \ldots, u_j, \ldots, u_P)^T$ is defined as Lagrangian multiplier and (B.4)-(B.6) are known as the Kuhn-Tucker (KT) conditions.

QP is a special class of NLP in which the objective function is quadratic and the constraints are linear. The QP problem is given by:

$$\text{Minimize} \quad f(\mathbf{x}) = \sum_{i=1}^{I} c_i x_i + \frac{1}{2} \sum_{i=1}^{I} \sum_{k=1}^{I} H_{i,k} x_i x_k, \tag{B.7}$$

Subject to

$$\sum_{i=1}^{I} a_{j,i} x_i + y_j = b_j, \quad j = 1, 2, \ldots, P+Q, \tag{B.8}$$

$$0 \leq x_i \leq 1,\ i = 1, 2, \ldots, I,\ x_i \in \{0, 1\},\ H_{i,k} = H_{k,i}. \tag{B.9}$$

where $\mathbf{x} = (x_1, x_2, \ldots, x_I)^T$, c_i is the element of $\mathbf{c} = (c_1, c_2, \ldots, c_I)^T$, $a_{j,i}$ and b_j are constants and $H_{i,k}$ is the element of a symmetric $I \times I$ matrix $\mathbf{H}$, which is positive definite. Eq. (B.9) can be re-written as $-x_i \leq 0$ and $x_i - 1 \leq 0$. By adding slack variables e_i and $e_{i+I}\,(i = 1, 2, \ldots, I)$, (B.9) can be expressed as

$$-x_i + e_i = 0 \quad i = 1, 2, \ldots, I, \tag{B.10}$$

$$x_i - 1 + e_{I+i} = 0 \quad i = 1, 2, \ldots, I, \tag{B.11}$$

$$e_i, e_{I+i} \geq 0 \tag{B.12}$$

If the Lagrangian multiplier vectors of (B.8), (B.10) and (B.11) are denoted as $\mathbf{u} = (u_1, u_2, \ldots, u_j, \ldots, u_{P+Q})^T$, $\mathbf{v}_1 = (v_1, v_2, \ldots, v_i, \ldots, v_I)^T$, $\mathbf{v}_2 = (v_{I+1}, v_{I+2}, \ldots, v_{I+i}, \ldots, v_{2I})^T$, respectively, applying the KT conditions, we have

$$-\sum_{k=1}^{I} H_{i,k} x_k - \sum_{j=1}^{P+Q} u_j a_{j,i} + v_i - v_{I+i} = c_i \quad i = 1, 2, \ldots, I, \tag{B.13}$$

$$x_i v_i = 0 \quad i = 1, 2, \ldots, I, \tag{B.14}$$

$$x_i v_{I+i} = 0 \quad i = 1, 2, \ldots, I, \tag{B.15}$$

$$u_j y_j = 0 \quad j = 1, 2, \ldots, P+Q, \tag{B.16}$$

$$x_i, v_i, v_{I+i}, u_j, y_j \neq 0 \quad H_{i,k} = H_{k,i}. \tag{B.17}$$

The solution to (B.13)-(B.17) gives the optimal solution to problem (B.7)-(B.9). By introducing an artificial scalar $\mathbf{z} = (z_1, z_2, \ldots, z_I)^T$, and define

$$\begin{cases} \text{sgn}(c_i) = 1 & \text{if} \quad c_i \geq 0 \\ \text{sgn}(c_i) = -1 & \text{if} \quad c_i < 0 \end{cases} \tag{B.18}$$

We next modify (B.13) into

$$\text{Minimize} \quad \varphi(z) = \sum_{i=1}^{I} z_i, \tag{B.19}$$

Subject to ,

$$-\sum_{k=1}^{I} H_{i,k} x_k - \sum_{j=1}^{P+Q} u_j a_{j,i} + v_i - v_{I+i} + \text{sgn}(c_i) z_i = c_i \tag{B.20}$$

The solution to (B.19)-(B.20) will be the same to (B.13) when $z_i = 0, (i = 1, 2, \ldots, I)$. Note that the constraints given in (B.14)-(B.16) still need to be satisfied. These relationships will be satisfied by avoiding putting x_i and v_i, x_i and v_{I+i}, u_j and v_j as the basic variables simultaneously.